Evaluation of Lightweight Aggregate Concrete
For Precast, Prestressed Driven Piles

by

Neill Allen Belk

A dissertation submitted to the Graduate Faculty of
Auburn University
in partial fulfillment of the
requirements for the Degree of
Doctor of Philosophy

Auburn, Alabama
August 3, 2013

Keywords: durability, driveability, stress limits

Approved by

J. Brian Anderson, Chair, Associate Professor of Civil Engineering
Anton K. Schindler, Professor and Director of the Highway Research Center
David J. Elton, Professor of Civil Engineering

ABSTRACT

Driven piles, specifically, precast, prestressed (PCPS) piles are concrete foundation elements used to transmit heavy structural loads and moments to an adequate bearing layer and reduce total settlement. Lightweight concrete has been used in many applications including floor slabs, bridge decks and girders, and precast façade elements to reduce the structural dead load. Current literature of driven piles and lightweight concrete showed a lack of research done on the union of these two concepts. The goal of this research was to evaluate the use of lightweight aggregate concrete in PCPS driven piles.

Laboratory trial mixtures were evaluated based on a typical normalweight concrete (NW) mixture design for the Charleston, SC area. The normalweight coarse aggregate was systematically replaced with commercially available expanded slate at 50 % (LW50) and 100 % replacement (LW100) levels. Laboratory made concrete was accelerated cured to mimic steam curing beds for PCPS pile applications.

Preliminary modeling of axial resistance and driveability were performed based on existing soil data in Charleston and laboratory measured concrete modulus and density values. NW, LW50, and LW100 piles were cast and driven in Charleston, SC. Hardened concrete behavior was evaluated based on standard-cured and field-cured specimens. The piles were driven 7 days after casting and monitored with Pile Driving

Analyzer® (PDA). All measured driving stresses were well below the stress limits set forth by the American Association of State Highway Transportation Officials (AASHTO) (2010). Restrike estimates of soil resistance after one day showed the NW pile was 99 % of the predicted ultimate resistance, while the LW50 and LW100 piles had achieved approximately 75 and 80 percent of the predicted ultimate resistance. Driveability models were then adjusted based on PDA measured data to improve the accuracy of comparisons between measured and predicted driving stresses with the driving stress limits.

Laboratory and field concrete specimens showed that an increase in coarse aggregate replacement with lightweight aggregate does not significantly affect the compressive strength; whereas, the modulus of elasticity linearly decreases. Laboratory prepared specimens showed moderate chloride ion penetration. The field specimens showed high chloride ion penetrability due to inadequate concrete consolidation from a loss in workability. Pile concrete with 50 and 100 % lightweight coarse aggregate can be cast, handled, and driven with the same effort as normalweight concrete piles.

ACKNOWLEDGEMENTS

I would like to thank God for His perfect will. I thank Dr. Brian Anderson for taking a chance on me and affording me the opportunity to come to Auburn. I appreciate his help as both a technical advisor and a friend. I would also like to thank Dr. Anton Schindler and Dr. David Elton for their guidance and contribution to this dissertation. Thanks are given to Auburn University for allowing me to use laboratory facilities, equipment, and providing me with financial assistance.

I want to thank Steve Hall of the Pile Driving Contractors Association (PDCA). I appreciate the help from members of the PDCA of South Carolina, without which, this project would never have happened. Thanks to John Parker, Marty Swain, and the crew at Parker Marine Contracting Corp. for their help and patience placing the instrumentation and casting the test piles. I want to thank John King, Mike McCormick, and the crew from Pile Drivers Inc. for driving the test piles. Thanks to Gerald Smeltzer and Van-Smith Concrete for providing the concrete used in the test piles. I want to thank Greg Canivan, Heath Forbes, and Telford Wood at S&ME in Charleston for providing technical assistance, pile testing services, and laboratory space.

I would also like to express my gratitude to Dr. Joseph Coe, former faculty at The Citadel and currently at Temple University, for arranging pile driving activities to occur at The Citadel Geotechnical Experimentation Site.

Thanks to Reid Castrodale, formerly with Stalite Inc., and Charles Freeman and Jody Wall of Stalite Inc. for providing the lightweight aggregate, technical assistance, and help during pile concrete placement. I would also like to thank the Expanded Shale, Clay, and Slate Institute for financial support.

I would also like to thank Billy Wilson and those that helped with laboratory concrete mixing and my roommate Kevin Kane, for providing immeasurable help in the field. I want to thank Jon Honeycutt for helping me understand PDA traces.

Finally, I want to express my sincerest gratitude to my parents, Allen and Angie Belk, for their endless love and support, without which, I would not have become the man I am today.

TABLE OF CONTENTS

LIST OF TABLES

LIST OF FIGURES

1.0 INTRODUCTION

Deep foundations have been used for centuries to transmit large axial and/or lateral loads to the surrounding soil. The primary deep foundation elements are drilled shafts and driven piles. Piles are prefabricated foundations typically made of concrete or steel. Drilled shafts are concrete columnar elements formed in the ground that can be used in a variety of soil conditions and locations. Driven piles come in many types, shapes, and sizes which makes them quite versatile in different soil conditions. The research presented herein is for square precast, prestressed concrete driven piles.

1.1 Statement of Need

Driven concrete piles have many applications; however, concrete piles are used due to their economic design and inherent ability to withstand severe environments. These precast, prestressed (PCPS) elements endure many driving conditions and also provide adequate structural stability as foundations. Lightweight concrete has been used for decades to reduce dead loads within structures; however, it is gaining popularity as lightweight aggregates can provide internal curing which provides higher performing structural elements with respect to strength and durability while still providing a lighter structure.

There exists a gap within the literature from a lack of research between driven concrete piles and lightweight concrete. A new technology provided to the concrete pile contractors allows growth and helps move the industry forward. There may be reduced

cost in the transportation of reduced weight PCPS elements due to either lighter loads per truck which reduces the fuel demand per truck thereby lowering fuel costs.

1.2 Proposal of Work

The proposed research to investigate of the use of lightweight concrete in driven piles was presented to members of the Pile Driving Contractors Association (PDCA) of South Carolina. The potential benefits included strength gain, enhanced durability, and truck load reductions. Concerns over the driveability were voiced by the manufacturers and contractors including potential hammer rebound from a reduced concrete modulus. The Auburn University research team agreed that all of these issues would be addressed in the research. The stakeholders, including the pile contractors, consultants, and material suppliers, agreed with the idea of casting full-scale test piles, driving the piles, and testing the piles in Charleston, SC. The data from the research would then be presented to the PDCA for their assessment, as well as the deep foundation industry.

1.3 Research Objectives

The primary objective of this project was to evaluate the use of lightweight aggregate (LWA) concrete in driven PCPS piles. The specific objectives of the project included the following:

- Develop lightweight concrete mixtures for driven pile concrete that represents 50 % and 100 % replacement of coarse aggregates
- Develop and calibrate a driveability model for lightweight concrete piles including stresses and blows per foot based on parameters developed from laboratory mixtures
- Cast and install full-scale test piles to determine:

a) if the piles can be handled and driven without damage

b) if the piles experience rebound

c) if hammer performance is reduced

d) if there is any significant difference in tension and compression stresses between lightweight and normalweight concrete piles

Once these objectives were achieved, preliminary recommendations were made to the PDCA for use of lightweight concrete to be used in concrete piles.

1.4 Research Approach and Scope of Work

The scope of work to meet the above objectives included a review of current literature with regards to driven pile design and lightweight concrete. A review of the geotechnical and structural design was presented, as well as the typical development of a concrete pile from casting to driving. The mechanical properties of strength and modulus of elasticity of lightweight concrete were reviewed. The durability of lightweight concrete was reviewed along with its dimensional stability and its performance in current PCPS applications. Pile driving and stresses were evaluated for normalweight and lightweight concrete mixtures.

The laboratory testing plan included an evaluation of lightweight concrete mixtures with respect to fresh and hardened concrete properties. The laboratory mixtures were used to set acceptable criteria for field testing, as well as provide concrete data for preliminary modeling for driveability and soil resistance.

The field testing plan included developing a casting and driving plan for the full-scale test piles. Existing subsurface data were used to select pile driving locations. Dynamic testing data were collected and compared to driveability models to develop

criteria for lightweight concrete driving stresses. A comparative study of fresh and hardened concrete properties of field and lab cured concrete specimens was implemented.

Pre-driving and field-calibrated computer modeling were used to evaluate critical stresses within the pile to determine its survivability during driving. The culmination of these three project aspects were used to make recommendations on the use of LWA concrete in driven piles.

1.5 Dissertation Outline

Chapter 1: Introduction

Chapter 2: Background and Literature Review

Chapter 3: Research Methodology

Chapter 4: Presentation and Analysis of Data

Chapter 5: Discussion of Results

Chapter 6: Conclusions and Recommendations

2.0 BACKGROUND AND LITERATURE REVIEW

Literature reviewed pertaining to pile foundations with respect to design, manufacturing, and driving is presented in this chapter. Concrete material is evaluated, as well as literature pertaining to lightweight concrete strength, dimensional stability, durability, and current PCPS applications.

2.1 Pile Background

Deep foundations are used to carry large structural loads and reducing settlement when surface soils are insufficient. There are several types of deep foundations including ,but not limited to, driven piles, drilled shafts, continuous flight auger cast-in-place piles, and caissons. Driven piles are simply prefabricated columns driven into the ground using an impact hammer, vibratory hammer, or direct push. Drilled shafts are columnar elements formed within the ground by placing concrete and reinforcing steel in a drilled open hole. In all cases, the foundation type is used to shed the structural load through side friction and base resistance.

Driven piles have many useful applications including bridge and building foundations, slope stabilization, and retaining walls. Piles date back to the Han Dynasty where timber piles were used in bridge construction from 200 BC to AD 200 (Tomlinson 1994). Vitruvius in the first century B.C. suggested alder piles be driven below foundations in swampy places because of their ability to take in water which keeps them from decay and support structures of enormous weight. This material is worthless above ground and easily can endure for a long time when covered with moisture (Morgan

1960). Vitruvius also specified driven piles to be machine driven at closely spaced intervals for temples built upon loose earth or marsh areas. Timber piles may be made of charred alder, olive wood, or oak (Morgan 1960).

Piles are typically timber, steel, or concrete . Timber piles are basically treated tree trunks with carefully removed branches and bark that range from 30 to 65 ft (9 to 20 m) in length and not containing significant defects (Das 2011). Timber piles are shoed or pointed to protect the tip as presented in Figure 2.1 while the top of the pile is typically banded or confined to prevent "brooming" of the pile head as depicted in Figure 2.2. The American Society of Civil Engineers' *Manual of Practice,* No. 17 (1959) classify timber piles based on certain pile diameters' ability to carry a certain load ranging from 12 to 14 in. (30.5 to 35.5 cm). Timber piles should have a diameter greater than 6 in. (15 cm) (Das 2011).

Figure 2.1. Pile toe protection devices (Hannigan et al. 2006)

Steel piles are manufactured in several cross sections; however, the H-pile and pipe piles tend to be the standard ranging in size from 8 to 24 in. (204 to 610 mm) (Das 2011). Steel sheet piles can also be driven or vibrated into the ground. Steel H-piles with a driving shoe are depicted in Figure 2.3 along with a closed-end pipe pile in Figure 2.4.

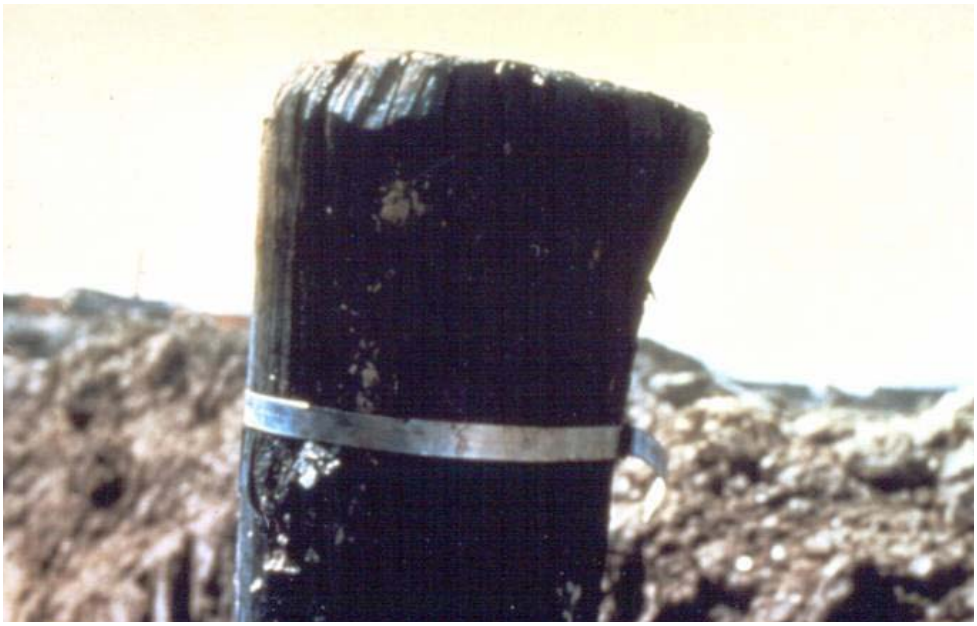

Figure 2.2. Banded timber pile to prevent brooming (Hannigan et al. 2006)

Figure 2.3. Steel H-pile sections with driving shoes (Hannigan et al. 2006)

Figure 2.4. Closed-end steel pipe pile (Hannigan 2011)

Sheet piles are used in shoring of earth and water. Steel piles can be easily spliced together with a weld; therefore, they can be driven to deep elevations. Steel piles also have the advantage of withstanding high driving stresses for both compression and tension through difficult driving (compressive) or through weak soils or voids (tensile). Steel piles are subject to corrosion; therefore, should only be temporary when used in marine environments. H-piles may be shoed for protection, but they may be damaged or deflected beyond vertical during hard driving (Das 2011).

Concrete piles are versatile in cross section, strength, and driving conditions. Cross sections can vary from circular to triangular and just about any geometry formwork that can be made; however, manufacturing and handling of unique cross sections limits driven concrete piles to square and spun-cast cylindrical piles as depicted in Figure 2.5 and Figure 2.6, respectively.

Figure 2.5. Square PCPS piles

Figure 2.6. Spun-cast PCPS piles (Hannigan et al. 2006)

Square piles are the easiest to form and handle, whereas spun-cast piles are a special pile in which the pile is formed by a rotating formwork that creates a concrete "tube" with a thickness of approximately 6 in. (15 cm) and can reach outside diameters of up to 70 in. (178 cm). Driven piles are typically precast, prestressed concrete; however, the American Association of State Highway Transportation Officials (AASHTO) also contains driving specifications for normally reinforced concrete piles along with piles of other materials. Advantages to prestressed concrete are its inherent durability characteristics; whereby, as long as the permeability is not too high, chloride and sulfate ions, and exterior water cannot penetrate to the reinforcement level. Prestressed concrete can withstand handling stresses and difficult driving; however, the tensile limits are not as high as steel piles. The cost of concrete on a whole tends to be cheaper than steel. Unlike steel, concrete can be quite difficult to splice; therefore, length of pile foundations are typically governed by the length of a truck bed, but may be longer if transported on barges to waterway construction sites or cast on site.

2.1.1 Pile Design

Piles are designed based on geotechnical and structural provisions. A thorough site investigation is required from a geotechnical aspect which includes collection of subsurface information. Geotechnical resistance is a function of soil strength. Strength is typically correlated from the standard penetration test (SPT) and/or the cone penetration test (CPT), or other approved subsurface testing methods. The SPT provides blow counts or "N–values" which is are standard measures of soil resistance dating back to Charles Gow as early as 1922 of the Raymond Concrete Pile Company (Davidson et al. 1999).

The SPT N–value is a measure of the number of blow counts a 140 lb (63.5 kg) hammer falls 30 in. (76 cm) and drives a split-spoon sampler through a distance of 12 in. (30.5 cm). The SPT provides an analog to the pile driving process. The test was developed to measure the density of soil formations (Davidson et al. 1999). Widespread empirical correlations have been developed relating the penetration resistance to various engineering properties of soil. The most commonly developed correlations relate soil resistance to bearing capacity, shear strength parameters, soil modulus, and liquefaction potential (Davidson et al. 1999). The CPT cone also provides an analog to soil resistance. Cone tip resistance is an indication of end bearing; and sleeve friction provides side resistance data. Tests are used in pile capacity design which will be outlined later in this section. Soil samples may also be gathered within certain soil strata during drilling, and lab strength testing may be performed on "undisturbed" samples from the ground.

The FHWA has published a manual on the design and construction of driven pile foundations (Hannigan et al. 2006). Pile selection and evaluation are outlined in the FHWA pile manual where appropriate selection of pile types should consider pile characteristics, subsurface conditions, and performance criteria (Hannigan et al. 2006). Project location and topography are also key factors when determining which pile type to choose due to steep terrain or vibration concerns of surrounding structures during pile driving (Hannigan et al. 2006).

Once a trial size is selected, the axial and lateral resistance of the pile foundation must be determined. There are several methods, and not all are alike; therefore, it is up to the engineer to choose the most suitable method and apply appropriate design factors for

safety. Engineering judgement and local experience generally dictates if the piles will gain resistance from side or base resistance or a combination of the two. Piles may be used as individual elements or placed in pile groups "held" together with a pile cap to distribute the structural load. Piles are designed for cohesionless and/or cohesive soils or possibly for bearing on to rock.

The ultimate axial resitance of a pile, Q_u, is calculated using Equation 2.1 where f_s is the unit side resistance, A_s is the pile surface area, q_b is the unit base resitance of the bearing layer, and A_b is the cross-sectional area of the pile. When piles are driven through multiple soil layers of varying strength, the side resistance of each layer is calculated, summed over the length of the pile, and added to the base resistance to obtain the ultimate value.

$$Q_u = f_s A_s + q_b A_b \tag{2.1}$$

Several methods exists for determining side and base resistance of piles from different soil types and pile types. The "alpha" and "beta" methods presented in Das (2011) are just one way for determining unit side resistance of piles within clays and sands, respectively as presented in Equations 2.2 and 2.3 where α is an empirical adhesion factor, s_u is the undrained shear strength of clay, K is the earth pressure coefficient, σ'_v is the effective stress along the length of the pile, and δ' is the effective friction angle between the soil and the pile.

$$f_s = \alpha \cdot s_u \tag{2.2}$$

$$f_s = \beta \cdot \tan\delta = K\sigma'_v \tan\delta' \tag{2.3}$$

The unit base resistance may be estimated for piles bearing in clay and sand using Equations 2.4 and 2.5 also presented in Das (2011), respectively where N^*_c and N^*_q are

bearing capacity factors and *q'* is the effective vertical stress at the base of the pile. N^*_c is taken as 9 for saturated clays, and N^*_q is based on the effective friction angle of the sand.

$$q_b = N^*_c \cdot s_u = 9 \cdot s_u \quad (2.4)$$

$$q_b = N^*_q \cdot q' \quad (2.5)$$

An iterative process develops when choosing the correct pile type, size, and length based on a multitude of factors including structural requirements, driveability, and cost. Axial resistance methods have been developed for piles in simple idealized sand and clay soil profiles. More rational methods exist based on SPT N-values and CPT cone and sleeve resistance due to soil variability.

Several programs have been developed that incorporate these design methods into their software. Three of the most common axial resistance programs for piles are FB – Deep (Schmertmann 1967; Florida Bridge Software Institute 2002), DRIVEN (Mathias and Cribbs 1998) and UniPile (Fellenius and Goudreault 2002). These programs use either SPT N-values, CPT cone tip resistances, or user provided strength of soils to determine axial capacity values. These methods have been developed and calibrated from load testing case studies. Unit side and base resistances are estimated and then used in GRL WEAP to model the driveability of the pile.

Upon choosing the pile size and length of pile from axial and lateral resistance calculations, the pile must be installed. Piles can be installed by several methods including vibration, jetting, and impact driving. Impact driving is the most common, especially for structural steel and concrete piles. Driving is a vigorous process and tends to be the most critical time for the pile during its lifetime; therefore, AASHTO has set guidelines, at least for transportation and bridge structures, on the driving compression

and tensile stresses for piles. The tensile and compressive driving stress limits (TSL and CSL) are outlined in the 2010 AASHTO LRFD Bridge Design Code and presented in Equation 2.6a and b and Equation 2.7 for precast, prestressed concrete piles where f'_c is the 28-day compressive strength and f_{pe} is the effective prestress applied over the gross cross-section. Equations 2.1a and 2.1b are for normal environments and severe corrosive environments, respectively. The tensile driving stress equation for a normal environment in SI units is presented in parenthesis where strength and effective prestress are in MPa. The other equations remain the same with psi instead of MPa units.

$$TSL < 3\left(f'_c\right)^{1/2} + f_{pe} \qquad \left(< 0.25\left(f'_c\right)^{1/2} + f_{pe}\right) \tag{2.6a}$$

$$TSL = f_{pe} \tag{2.6b}$$

$$CSL = 0.85 f'_c - f_{pe} \tag{2.7}$$

ACI 543 (2005) mentions that typical minimum effective prestress after losses is normally 700 to 800 psi (4.8 to 5.5 MPa) but may reach upwards of 1,000 to 1,200 psi (6.7 to 8.3 MPa) for longer piles that may encounter alternating dense and soft layers. IBC (2006) Section 1809.2.3.2 stipulates that effective prestress in piles shall not be less than 700 psi (4.8 MPa) for piles greater than 50 ft (15.2 m) in length. PCI (1993) shares the same compression limit as the 2010 AASHTO LRFD Bridge Design Manual; however, the allowable tension limit is not as strict providing a tension stress limit (TSL_{PCI}) presented in Equation 2.8; therefore AASHTO (2010) stress limits are the only stress limits presented herein.

$$TSL_{PCI} = 6 \cdot \left(f'_c\right)^{1/2} + f_{pe} \tag{2.8}$$

2.1.2 Structural Design

The design and implementation of precast, prestressed concrete piles are governed by several industry codes. The American Concrete Institute (ACI) and AASHTO provide different design codes for non-transportation and transporation structure foundations, respectively. The Precast, Prestressed Concrete Institute (PCI) has also set design criteria for pile design. The International Buiding Code (IBC) specifies certain structural and geotechnical design considerations for non-transportation structures.

The IBC (2006) is used for construction purposes and provides guidance on the design, handling, and driving of precast concrete piles. IBC (2006) tends to set minimum and maximum limits and typically refers to more specific design codes for detail and commentary. IBC (2006) refers to ACI (318) for the structural design of the pile which sets design specifications for non – transportation structures. ACI develops recommendations from several committees including ACI 211 (1991), ACI 318 (2011), and ACI 543 (2005) which addresses the standard practice of selecting and proportioning concrete, the standard practice for structural concrete design (strength and durability), and the standard practice for design, manufacture, and installation of concrete piles, respectively. AASHTO (2010) addresses all of these internally for bridge and highway related structures. PCI has also compiled a committee report for recommended practice of prestressed concrete piles titled PCI Committee on Prestressed Concrete Piling (1993). In the report, PCI (1993) refers to standards within ACI and ASTM International (ASTM) with regard to pile material and testing of pile materials.

2.1.3 Prestressed Concrete Pile Development

The life of a pile is complex and has several critical stages. Prestressed concrete piles are cast, cured, stored, hoisted, transported, and driven. Once a pile has survived the driving process, it then must withstand the design loads from the structure and do so while not degrading over time in the ground.

Prestressed concrete piles are typically cast in the pile driving contractor's work yard. Metal formwork is set up in a prestressing bed. The beds stretch over a distance that can accommodate several piles to be cast in one bed. Dividers are placed within the bed to separate each pile. Once the formwork is set up, prestressing strands are outstretched the distance of the bed across all piles and tensioned to the jacking stress before concrete placement. Spiral or tie transverse reinforcment is then added to provide confinement to the concrete, as well as provide shear reinforcement as depicted in Figure 2.7.

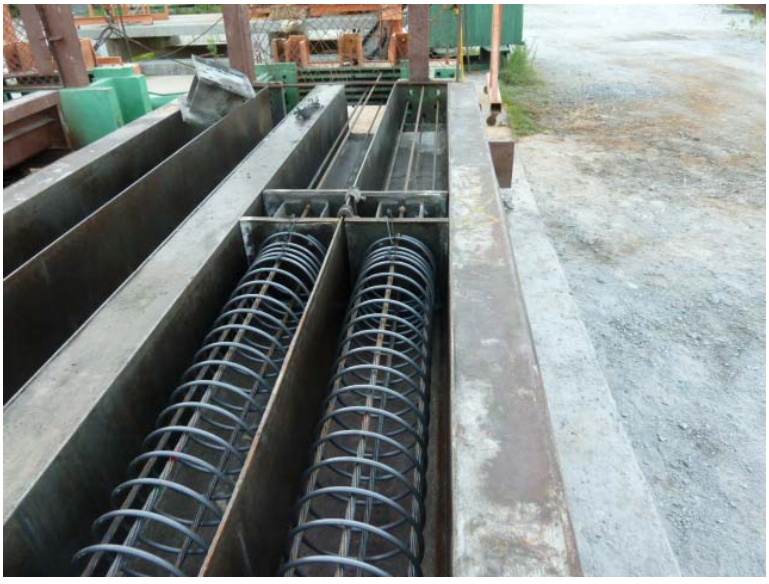

Figure 2.7. Prestressing beds prior to concrete placement

Concrete is then placed into the forms and then consolidated in the forms. Once placed, the concrete is typically cured between 18 and 24 hours under accelerated curing conditions during which heat is applied to the concrete formwork for rapid strength development. ACI 543 (2005) specifies a preset period of 2 to 4 hours before heat is applied to the concrete piles, and then the maximum curing temperature should not exceed 165°F (74 °C) with the rate of temperature increase not to exceed 60°F/hr (33.3 °C/hr) (ACI 543 2005). Steam is typically used to heat the space between the tarp and form, which thereby heats the concrete. After approximately 18 to 24 hours, the are "cut" with a torch in a particular pattern so as not to over-stress the pile or place any unwanted eccentric loading on it. Release is the time that tension from the prestressing strands is released and transferred to the concrete pile thereby precompressing the pile, thereby locking in compressive stresses. The minimum strength of concrete at time of transfer must be 3,500 psi (24 MPa) (ACI 543 2005).

The pile is then removed from the prestressing bed and stored in the yard until time of transporting to the job site and driven. IBC (2006) specifies that prestressed concrete piles must achieve a minimum concrete compressive strength of at least 75% of the 28-day design compressive strength before being driven, but not less than the strength capable of withstanding handling and driving forces. The minimum 28-day concrete compressive strength must be 5,000 psi (34.5 MPa) (IBC 2006). Once the piles have reached an appropriate strength, they are placed on flat-bed tractor trailers or barges, if working over water.

ACI (543) and AASHTO (2010) have set tensile and compressive stress limits for the extreme tension and compression fiber of concrete elements under precompression.

Limits are set at critical times for prestressed members immediately after release; however under concentric prestressing, there will only be compression after transfer on all faces. Bending stresses will develop during hoisting and handling of the member and tensile stress should not exceed the modulus of rupture (f_r) as set in ACI 318 (2011) or AASHTO LRFD (2010), depending on the structure type. These codes also set compressive stress limits for after transfer and also for long-term after prestress losses.

2.1.4 Pile Driving System

2.1.4.1 Pile Hammers

Once a pile has attained sufficient strength to withstand driving, it is hammered into the ground through brute force. Piles are placed in pile "leads" which hold the piles at the proper alignment during the driving process. There are several hammer types ranging from drop hammers to vibratory hammers. The oldest method is the a drop hammer. The technology has not changed, but the manner of which the hammer is raised and lowered has. Drop hammers have evolved from manually pulling the weight by hand with many people to a crane hoisting the weight and dropping it as depicted in Figure 2.8.

Figure 2.8. Crane hoisted drop hammer (Likins 2005)

Drop hammers have a low range of energy delivery into the pile system with low productivity between 4 to 8 blows per minute (bpm). These hammers are not recommended for concrete piles due to high dynamic forces and potential for pile head damage.

External-combustion type hammers (ECH) include single and double acting air, steam, and hydraulic hammers. Air and steam hammers require an air compressor or steam plant to produce the pressure to raise and/or drop the weight for single and double acting hammers, respectively. Air and steam hammers have a wide range of rated energies depending on the ram weight and stroke of a particular hammer. Similar to air and steam hammers are single- and double-acting hydraulic hammers that have a fully adjustable stroke and can be adjusted during driving to protect the pile during critical driving. Hydraulic hammers are the most complex of all ECH and require more complex

maintenance and higher initial costs (Hannigan et al. 2006). Three different external combustion hammers are presented in Figure 2.9.

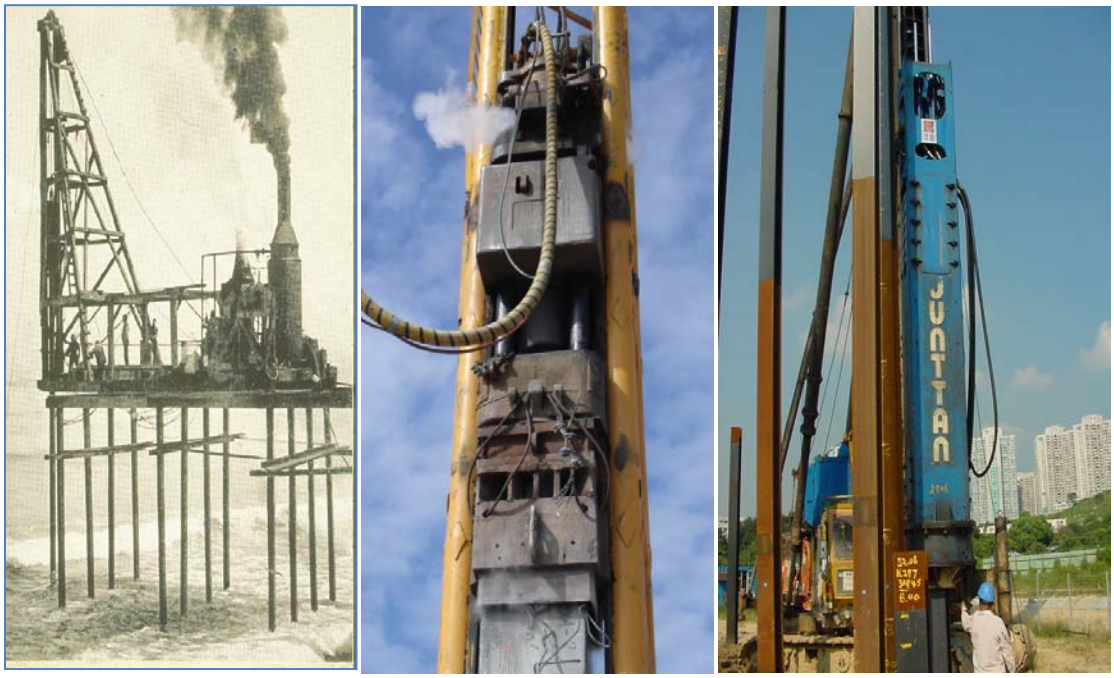

a b c

Figure 2.9. External combustion hammers a) steam b) air and c) hydraulic (Likins 2005)

Diesel hammers also come in single- and double-acting types; however, compression and combustion of "on-board" diesel fuel provides pressure to raise the ram. Single-acting hammers are tripped by manually raising the ram, and then the compression of diesel fuel causes the ram to raise and deliver energy into the pile. Diesel hammers will run continuously until the diesel-engine hammer is deprived of fuel. The stroke is variable for open-ended hammers due to the varying resistance the pile encounters from the soil. An open-ended diesel hammer is depicted in Figure 2.10. Diesel hammers may be used on all pile types; however, the use of diesel hammers causes air pollution by its exhaust gasses (Hannigan et al. 2006).

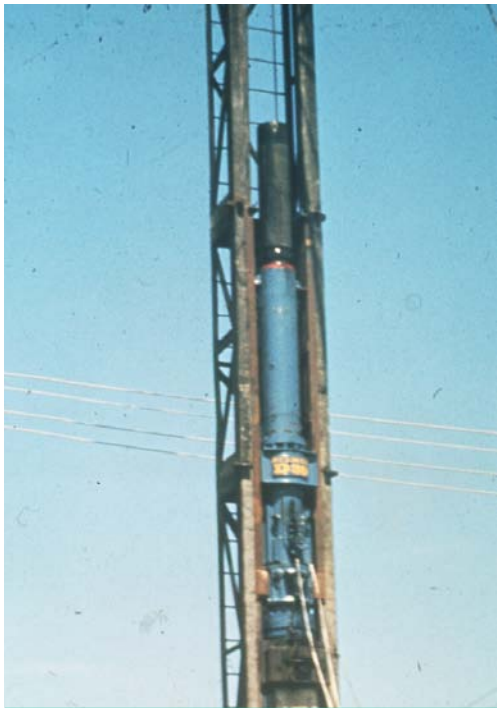

Figure 2.10. Open-ended diesel hammer (Likins 2005)

Finally, vibratory hammers are only suitable for steel H-piles or pipe piles. Vibratory hammers tend to be used for rapid installation of base resistance piles in granular soils. They can also be used to remove piles, and are very popular when working over water to help set up pile driving templates. Vibratory hammers carry the highest investment and maintenance costs of all hammer types. A vibratory hammer is presented in Figure 2.11. The eccentric weights are spun at a high rate to produce the a vibrating axial force to the pile where the horizontal components of the rotating weights cancels out (Hannigan et al. 2006).

Figure 2.11. Vibratory hammer installing sheet piles (Likins 2005)

2.1.4.2 Hammer Impact

The hammer system consists of several elements that are used in energy delivery and dissipation for pile driving and protection. The basics are simple, a ram of mass (*M*) and acceleration (*a*) produce a force (*F*). This force or weight of the ram falls a distance (*d*) to produce energy (*E)*. That energy is delivered to the pile through a system of anvils and cushions to prevent pile head damage as presented in Figure 2.12. The hammer first strikes the anvil or striker plate which equally distributes the energy into the hammer cushion. This cushion assembly is designed to protect the hammer while also transmitting the delivered energy. The hammer cushion is held by an adapter which seats within the pile helmet or driving head. The helmet sits atop the pile and helps guide the pile within the leads. The leads are used to maintain alignment of the hammer-pile system to ensure a concentric blow is delivered to the pile and presented in Figure 2.12

(Hannigan et al. 2006). Multiple adapters are used within the helmet so it can be used with different pile types and sizes. In the presence of concrete piles, a pile cushion is required to protect the pile head.

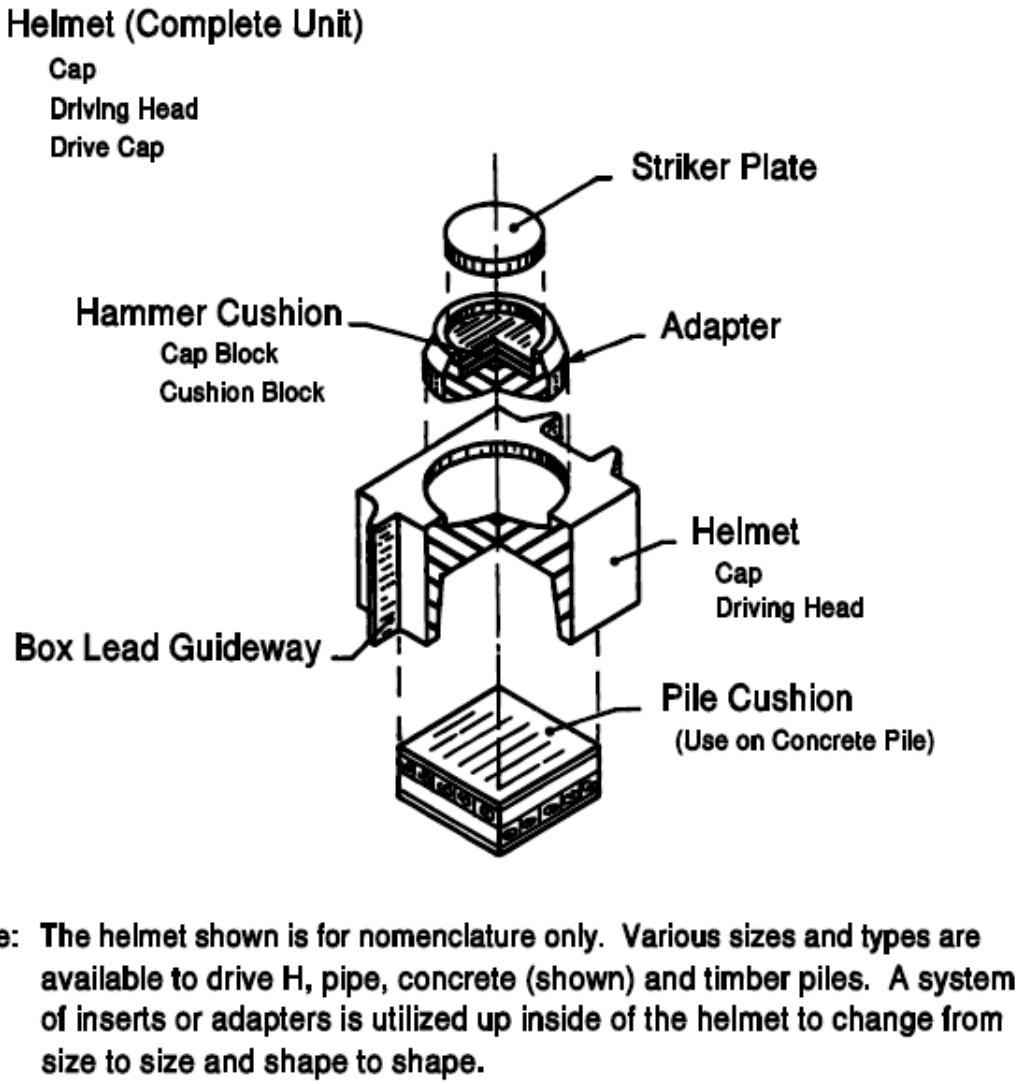

Figure 2.12. Pile helmet assembly configuration
(adapted from Hannigan et al. 2006)

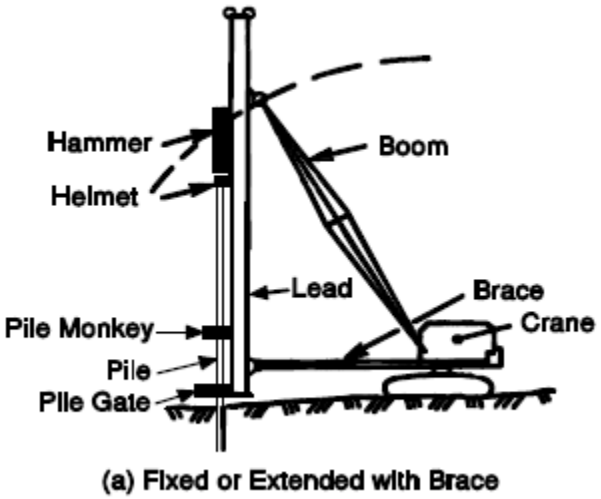

Figure 2.13. Crane with attached leads
(adapted from Hannigan et al. 2006)

2.1.4.3 Pile Mechanics and Behavior

When a hammer strikes a pile, a shear wave travels down the pile. As soil fails in base resistance, the pile settles into its design bearing elevation. The induced compression wave travels down the length of the pile and reflects as a compression or tension wave depending on the presence of soil resistance. The impact of the hammer causes a compression wave to travel down the pile and reflect back as a tension wave after a time (t) of $2L/c$ if there is no soil resistance where L is the length of the pile and c is the speed of the traveling wave. The reflected wave is reduced if side friction and/or end bearing are generated due to the resistance compression wave (Hussein and Goble 2000). The wave may also be reduced due to early reflection from damage within the pile. Figure 2.14 presents a visual respresentation of the induced stress waves within a pile during driving.

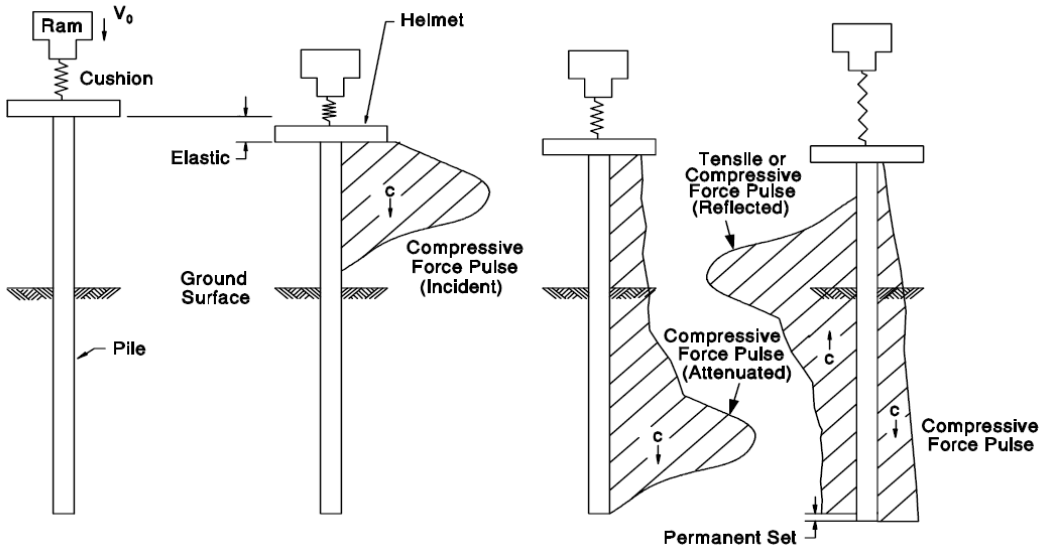

Figure 2.14. Induced stress wave travel during pile driving
(adapted Hannigan et al. 2006)

The first few feet of pile driving may be critical because sufficient resistance has not developed to reduce the tension wave. This is particularly critical for concrete piles due to poor tensile strength of concrete (Hussein and Goble 1987). There also exists critical times during driving that must be monitored which include hard driving, driving through voids, or pile damage. Induced compressive stresses are monitored to prevent crushing of the material and tension stresses are monitored to prevent pile yielding or pulling apart (Hussein and Goble 2000). In the event of hard driving, compressive stresses can nearly double the impact stress and damage the pile toe (Hussein and Goble 2000). If driving through voids, the exact opposite occurs in which no resistance is available, and a tension wave develops just like driving at the ground surface. If waves reflect too soon, then a change in impedence has occurred in essence means a change in cross-secion due to damage within the pile or decreased modulus (Hussein and Goble 2000).

Several methods are employed to ensure that the proper installation and performance criteria have been achieved. Simple observations are made during pile

driving to assess the hammer and pile performance (Hussein and Goble 1987). The number of blows to drive the pile into the ground has been used to determine the pile base resistance; while, hammer stroke and blows per minute are measures to evaluate the hammer performance (Hussein and Goble 1987). More rigourous methods are used to determine the structural integrity of the pile and soil resistance required for design.

As the pile is driven, permanent displacement must take place to ensure the pile does not "bounce." Smith (1960) introduced two terms to consider when driving piles including quake and set depicted in Figure 2.15.

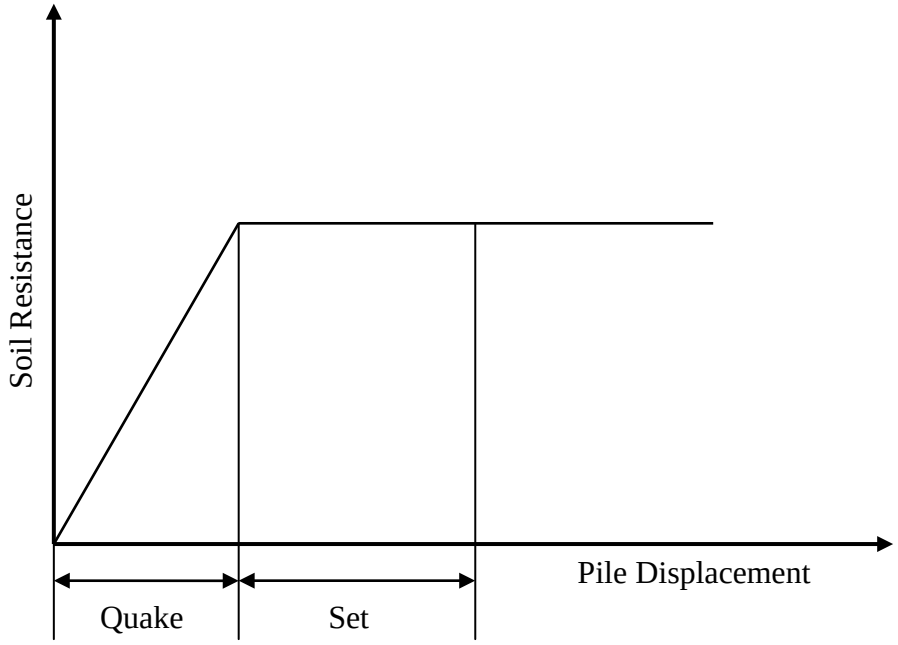

Figure 2.15. Quake and set during pile driving (adapted from Smith 1960)

The quake is the amount of displacement that must be overcome to fully mobilize the side and base resistance (Smith 1960). If the quake is not overcome, the pile will move down and then bounce up and not set. Once the pile has displaced through the required quake, the pile sets, which is measured to ensure the driving criteria is met.

2.1.5 Pile Driveability Modeling

Driveability modeling is a means of quantifying and predicting pile and hammer performance. GRL Wave Equation Analysis of Pile Driving (WEAP) is a commercially available software that is used to simulate motions and forces in due to impact or vibratory hammers (Pile Dynamics Incorporated 2010). The blow count, axial stresses, transferred energy, pile velocity, and residual stresses are calculated based on soil, hammer, and pile properties (Pile Dynamics Incorporated 2010).

GRL WEAP contains a database of different manufacturers' hammers to choose from to model including ECH, diesel, drop, and vibratory hammers. The driveability analysis requires the static unit side and base resistance values for each soil layer encountered in a given profile soil profile in addition to the estimated quake and damping values for varying soil types (Pile Dynamics Incorporated 2010).

2.1.6 Pile Testing

Driven piles can be tested in several ways which include dynamic and static tests. The Pile Driving Analyzer® (PDA) is used to verify geotechnical resistance and monitor the structural health during driving. PDA is a useful tool to estimate stresses that develop within a pile due to driving from accelerometers and strain gages mounted to the top of piles before driving as depicted in Figure 2.16. Gage measurements are recorded with a PDA computer as depicted in Figure 2.17.

Figure 2.16. PDA gage being installed at the top of the pile

Figure 2.17. PDA computer

ASTM D4945 (2008) provides the standard testing method for PDA testing. The concept for the PDA is to measure the top force and velocity of stress waves within the pile. Using stress wave theory for a uniform, elastic rod impacted at one end, the force (F) along a uniform pile length can be determined using Equation 2.3 where E is the modulus of elasticity, A is the cross-sectional area, c is the particle wave velocity, and V is the wave speed of the travelling compression/tension wave. The force and velocity are proportional to one another by the impedence (Z) which is the term in parenthesis of Equation 2.9. Wherever there is a change in the pile impdence along the length of the pile, then the stress waves will reflect at this point. This is usually due to a reduction in the cross-sectional area due to pile damage (Husseini and Rausche 1991)

$$F = \left(\frac{E \cdot A}{c} \right) \cdot V \tag{2.9}$$

The force and velocity are calculated based on measured strain and acceleration of the pile from the bolted on transducers. Hammer strikes are recorded (traces) during pile driving are depictions of the force and velocity at the top of the pile. These traces are used to evaluate pile installation behavior. Figure 2.18 presents a hammer trace of normal driving with side and base resistance developed along the pile and the same pile with damage. Horizontal axis is in terms of L/c, and the vertical is Force and Velocity depending on the measurement. The green bar represents the full lenngth of the pile within each trace depicted below. Damage is indicated by the wave reflecting prior to $2L/c$ and depicted by the red bar in Figure 2.18b. Figure 2.19 depicts the damaged PCPS pile exhumed for visual examination. The numbers in parenthesis on a wave trace indicate the maximum value on the vertical scale. The two solid gray lines indicate the initial time the wave starts and then the time it takes for the wave to travel down and back

to the top of the pile. The dashed gray in Figure 2.16b indicates the reflected wave time to reach the damaged portion of the pile and back. The velocity trace in Figure 2.16a indicates the pile moved up or rebounded because the velocity fell below the horizontal axis prior to the second vertical line corresponding to *2L/c*.

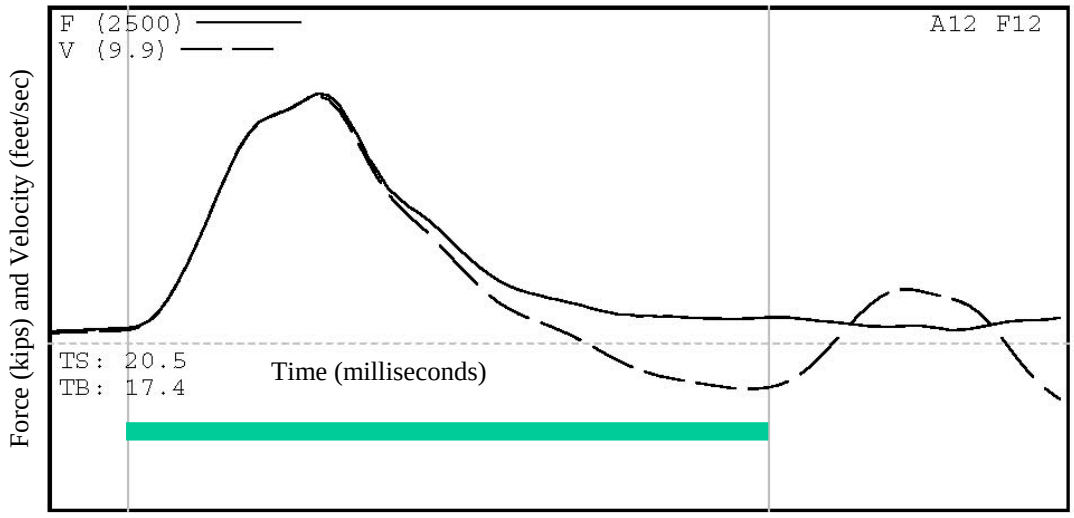

a

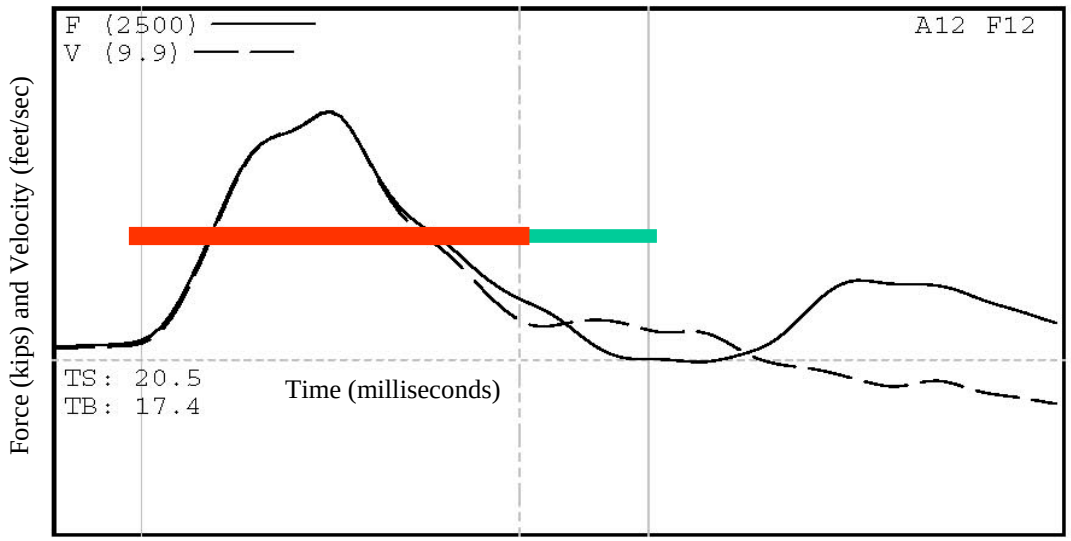

b

Figure 2.18. PDA traces of a PCPS pile a) good and b) damaged (adapted from Likins 2011)

Figure 2.19. Damaged PCPS pile (adapted from Likins 2011)

Figure 2.20 presents additional PDA wave traces of damaged piles. Convergence of velocity and force curves shows potential of pile damage, and when there is a velocity peak corresponding to a force trough, it is an indication that the pile is damaged (Webster and Teferra 1996).

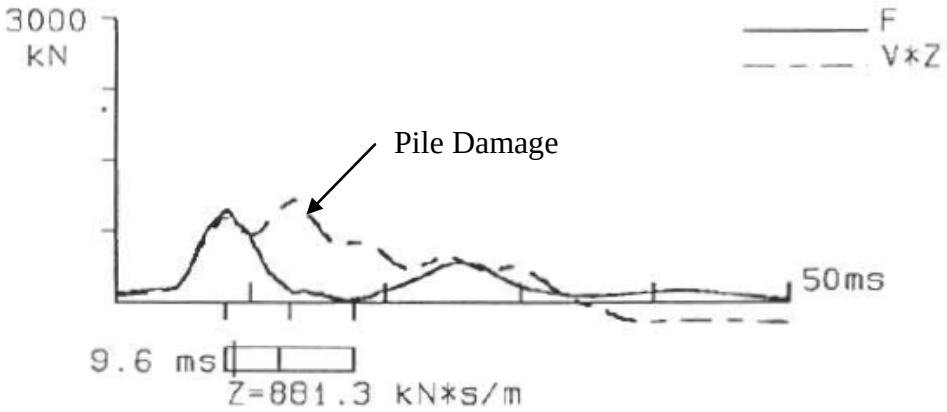

a

(adapted from Webster and Teferra 1996)

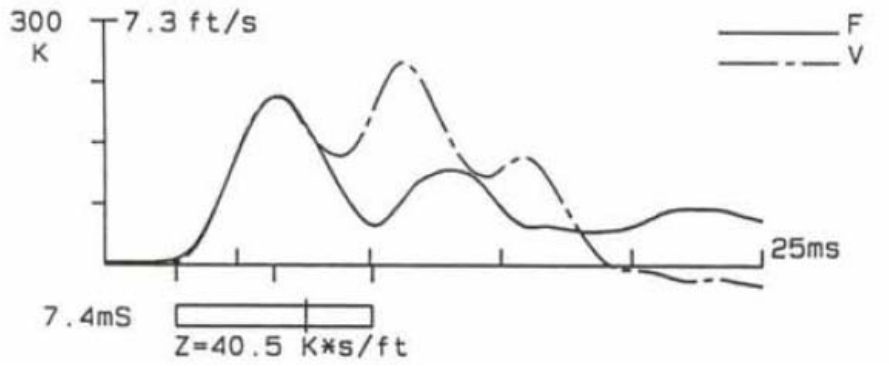

b

(adapted from Hussein and Goble 2000 with permission from ASCE)

Figure 2.20 Wave traces depicting pile damage

In addition to pile damage, it is necessary to address potential upward movement of piles or rebound. This upward movement can occur before or after the pile has permanently set. PDA traces show this upward movement when the velocity curve dips below the horizontal axis. If the velocity curve dips below the horizontal axis prior to *2L/c*, the pile is not setting; therefore, it is not overcoming the quake needed to permanently set. When the velocity curve dips below the horizontal axis after a time *2L/c*, then the pile moves up, but it has already set meaning the pile is driving deeper. Figure 2.21 presents wave traces of the top displacement with time. The rebound is measured as the maxium displacement minus the set.

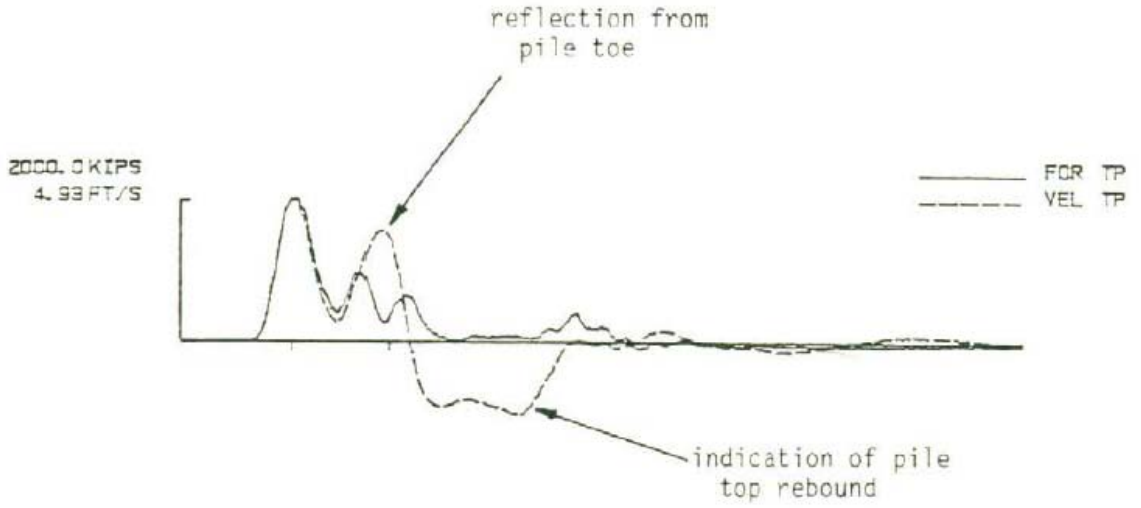

Figure 2.21. PDA wave trace indicating pile rebound
(adapted from Hussein and Goble 1987 with permission from ASCE)

A refined estimate of the pile resistance uses the CAse Pile Wave Analysis Program® (CAPWAP) which is a PDA signal matching technique. The force output from PDA is input, and using assumed soil resistance, quake, and pile properties, the program iterates and calculates a velocity wave which is compared to the measured wave velocity from PDA. The solution is non-unique; however, the total overall resistance is typcally within 10 percent of the actual pile resistance (Likins, CAPWAP 2011).

Dynamic tests are reasonably cheap, especially when testing a large number of piles. Dynamic tests are quite useful when calibrated against a static load test at the site.

Static load testing has been around for decades and is the most accurate method for determining pile resistance. Static load tests consist of axial compression, axial tension, and lateral loading. There are two primary reasons for conducting a load test which include 1) developing information for use in the design and/or construction of pile foundations and 2) confirming the suitabiltiy of the pile-soil system to support the design load with an appropriate factor of safety. Axial compression tests are the most common

of the static load test and is outlined in ASTM D1143 (1994) in which a vertical load is applied either by dead weight across a kentledge beam or a load actuator against a reaction beam. The pile is typically instrumented with strain gages or telltales to determine soil resistance with depth and vertical displacement measuring devices at the pile head for settlement. Telltales are unstrained rods placed in open ducts or sleeves within the concrete that measure the displacement with respect to the pile head.

The use of static load tests also allows the designer to determine, during the project design stage, a more accurate pile length to be manufactured due to the complicated nature of splicing PCPS piles. Steel piles can be welded; however, timber and concrete tends to be more intricate and are typically not performed.

2.2 Concrete Background

2.2.1 Concrete Microstructure

Concrete has become a universal building material because of its versatility and economy. It is comprised of three phases which include the aggregate, hydrated cement paste (hcp), and the interfacial transition zone (ITZ) (Mehta and Monteiro 2006). Concrete is economical due to locally available aggregates that are used for concrete production. Aggregates come in all shapes, sizes, and strengths. Physical aggregate properties that affect concrete properties include gradation, shape, texture, and density (Mehta and Monteiro 2006). Aggregates typically are either crushed stone or rounded river gravel. Crushed stone tends to have elongated sides and rougher faces; whereas, naturally weathered gravel typically has rounded sides and smoother surfaces (Mehta and Monteiro 2006).

The hcp is comprised of solid cement particles, void space, and water (Neville 2011). Due to hydration of cement, water within the concrete exothermically reacts with the cement particles creating four primary hydration products including calcium silicate hydrate (C-S-H), calcium hydroxide (CH), calcium sulfoaluminate hydrates (sulfates) (Neville 2011). These hydration products comprise the cement matrix for which the aggregate are a part. The cement matrix acts as a glue to hold the aggregates in place. The C-S-H formed from hydration is a very strong and dense amorphous structure that comprises 50 to 60 % of the solids (Mehta and Monteiro 2006). CH formed from hydration comprises 20 to 25% of the solids in the hcp (Mehta and Monteiro 2006). CH crystals are plate like prisms and are weak compared to C-S-H and is the weak link in hcp. These plates have preferred orientations that are attracted to the surface of aggregates which creates a plane of weakness along the aggregate surface. Sulfates formed from cement hydration include needle-shaped ettringite crystals and plate like monosulfate hydrate crystals. Sulfates comprise 15 to 20% of the hcp solids; however, they affect setting, rate of hardening, and long-term stability (Mehta and Monteiro 2006). Finally, unhydrated cement particles are left from incomplete hydration due to cement particles being too close together or not enough water available for hydration (Mehta and Monteiro 2006).

Voids within the hardened cement paste include interlayer space within the C-S-H structure, capillary voids (space not filled by hcp solids), and air voids either entrapped and/or entrained air voids (Mehta and Monteiro 2006). The interlayer voids are very small openings between “sheets” of C-S-H. These small voids are too small to affect strength and permeability of the concrete; however, if water within these voids were ever

removed, major creep and shrinkage would occur (Mehta and Monteiro 2006). Capillary voids are voids not filled by solid components of hcp (Mehta and Monteiro 2006). Capillary voids along with air voids are equal to the porosity within concrete. Decreasing the porosity increases the concrete strength and lowers the permeability (Mehta and Monteiro 2006). Large, irregular entrapped air and perfect spheroid shaped entrained air comprise the total air content of concrete. Entrapped air is left by incomplete consolidation (Neville 2011). Entrained air is formed from chemical admixtures. Aggregate size and construction methods affect entrapped air content which impacts strength and permeability. Air entraining admixtures are used to create a perfectly round and evenly distributed air void system for freezing and thawing durability resistance (Neville 2011).

The final phase of hydrated cement paste is water which is classified by four categories including capillary water, adsorbed water, interlayer water, and chemically bound water (Mehta and Monteiro 2006). Capillary water is water within voids larger than 5 nm (Mehta and Monteiro 2006). As the relative humidity (RH) decreases from 100 to 95%, free water is removed and does not cause volume change within the concrete. RH of 95% causes water in the smallest capillary voids to escape which will begin to cause drying shrinkage. As RH decreases from 95 to 30%, the adsorbed water close to solid surfaces is lost causing significant shrinkage within the hcp. In the event of extreme heat, significant drying shrinkage will occur from a further decrease in relative humidity. Finally, chemically bound water found in hydration products can only be lost due to hydration (Mehta and Monteiro 2006).

The final phase of concrete is the interfacial transition zone found between the aggregate face and hardened cement matrix. The ITZ develops due to water films around the coarse aggregates as bleed water tends to move upward as presented in Figure 2.22.

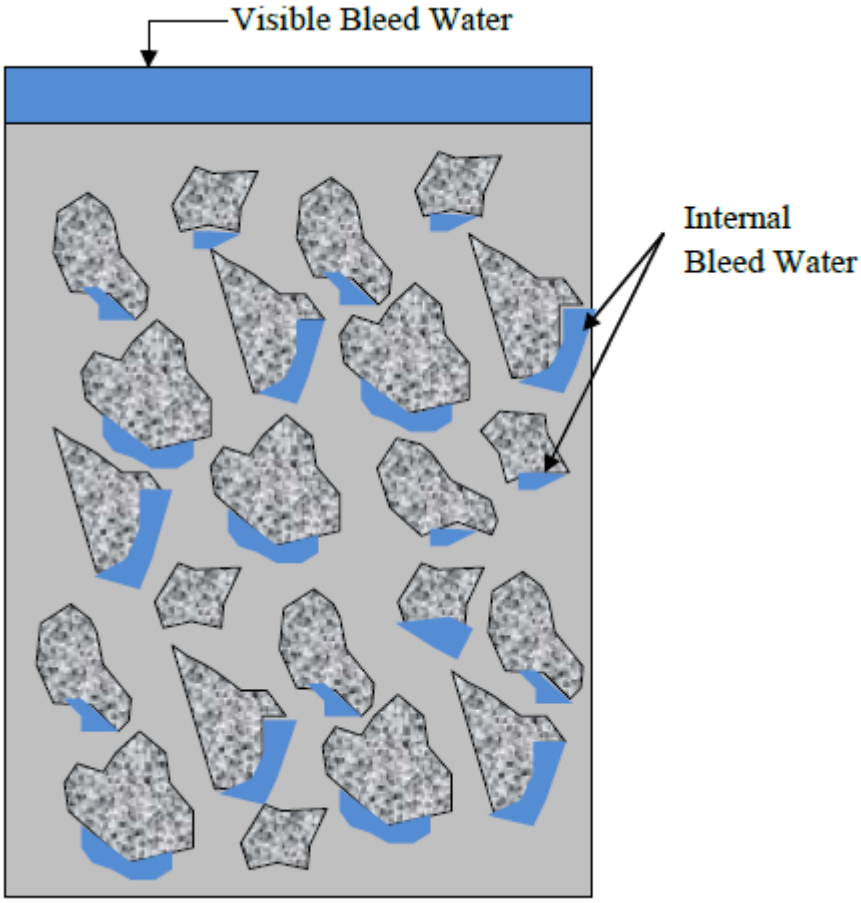

Figure 2.22. Schematic of bleed water trapped beneath coarse aggregates (adapted from Mehta and Monteiro 2006)

This moisture around the aggregate increases the *w/c* ratio relative to the cement matrix (Mehta and Monteiro 2006). Higher *w/c* also increases the CH crystals forming along the aggregate face (Neville 2011). Concrete failures initiate within the ITZ due to being weaker than the bulk paste (Mehta and Monteiro 2006). Microcracks form due to varying degrees of thermal expansion during hydration and propagate from the ITZ to within the cement matrix and then on through the concrete specimen.

Improving/decreasing the ITZ improves the concrete properties. Pozzolans can be used within concrete to react with the bad CH which forms in the ITZ and forms the good C-S-H. Reducing the size of coarse aggregate reduces the size of the ITZ therefore increasing the relative strength and decreasing the permeability.

2.2.2 Factors Affecting Hardened Concrete Properties

There are numerous factors which affect the modulus, strength, and permeability of concrete. Most of these factors work together and changing one thing will affect the manner in which the other factors allow the concrete to behave. The most significant factor is the *w/c* ratio, whereby a decrease in the *w/c* generally increases the strength (Neville 2011). The air content and the volume of all voids inversely affects the strength of concrete (Neville 2011). In addition to *w/c* ratio, the actual cement used produces varying concrete strengths due to cement processing. Cement clinker is crushed to different sizes and is characterized by Blaine fineness which is a measure of cement surface area per unit volume. The finer the cement (i.e. higher Blaine) the more rapidly it will react and affect the concrete strength (Mehta and Monteiro 2006). Cement composition also affects the strength by rate of hydration. Cement hydration is a time dependent reaction as well; therefore, concrete strength and modulus is provided in terms of concrete age. Water is directly proportional in cement hydration; therefore, an increase in water will cause an increase in the *w/c* ratio causing a decrease in strength (Neville 2011).

Aggregate type, roughness, and size all play roles on concrete strength. The type of aggregate significantly affects the tensile and flexural strength due to the shape and texture. Concretes made with crushed aggregates tend to have higher tensile and flexural

strength due to angularity and roughness of crushed aggregates; whereas, smooth, rounded sides of river gravel will tend to decrease these strengths. The better the bond with aggregate and cement also reduces the ITZ which decrease the permeability. In addition to aggregate type, as mentioned earlier, aggregate size affects hardened properties. As maximum nominal aggregate size increases, the ITZ increases which decreases strength and and increases the permeability (Mehta and Monteiro 2006).

Mineral admixtures or supplementary cementing materials (SCMs) are typically added in large amounts to reduce concrete costs (cement reduction) and enhancement of fresh and hardened concrete properties (Mehta and Monteiro 2006). The most common types of SCMs are fly ash, iron blast-furnace slag, and silica fume which are used to increase workability and produce high-performance concretes (Mehta and Monteiro 2006). Chemical admixtures are used to affect early and long term properties of concrete. Accelerators and retarders are used to adjust the setting times of concrete and speed up or delay the rate of hydration. Accelerators are used to provide higher early strengths and in low concrete placement temperatures to increase the rate of hydration (Neville 2011). Likewise, retarders tend to lower the early age strengths and increase the long-term concrete strength while slowing down the rate of hydration (Mehta and Monteiro 2006). Water reducing admixtures are used to increase the workability for a given *w/c* ratio or allow for a reduction of in *w/c* while maintaining adequate workability (Neville 2011). Air entrainment admixtures are used not only to provide a proper freezing and thawing air system, but also used to provide a better workability (Neville 2011).

Curing conditions are a significant factor affecting hardened concrete properties. Curing conditions must consider time, temperature, and humidity (Mehta and Monteiro

2006). Higher curing temperatures will cause the concrete to mature much faster than standard curing [T ≈ 73 °F (23 °C)]. Higher temperatures will increase early concrete strength while decreasing the long-term strength and vice versa for cooler concrete placement and curing (Mehta and Monteiro 2006).

Neville (2011) states that not only does high ambient temperature cause an increase in water demand, but also an increase in fresh concrete temperature. The high ambient temperature also increases slump loss and rapid hydration, thereby, decreasing the long-term strength (Neville 2011). In hot weather concreting, there is a loss in workability (slump) and admixtures tend not to work properly (ACI 305 1999). The hardened concrete properties of hot weather placed concrete are also adversely affected. Long-term strength is reduced and permeability is increased due to rapid hydration of cement particles (ACI 305 1999). Verbeck and Helmuth (1968) showed an approximate decrease of 1,500 psi in compressive strength from specimens cured at 120 °F (49 °C) compared to those cured at room temperature as presented in Figure 2.23. Brooks et al. (2007) showed that Type I cement cured at 104 °F (40 °C) has a compressive strength reduction of approximately 1,450 psi (10 MPa) as compared to the same cement cured at 73 °F (23 °C) as depicted in Figure 5.24.

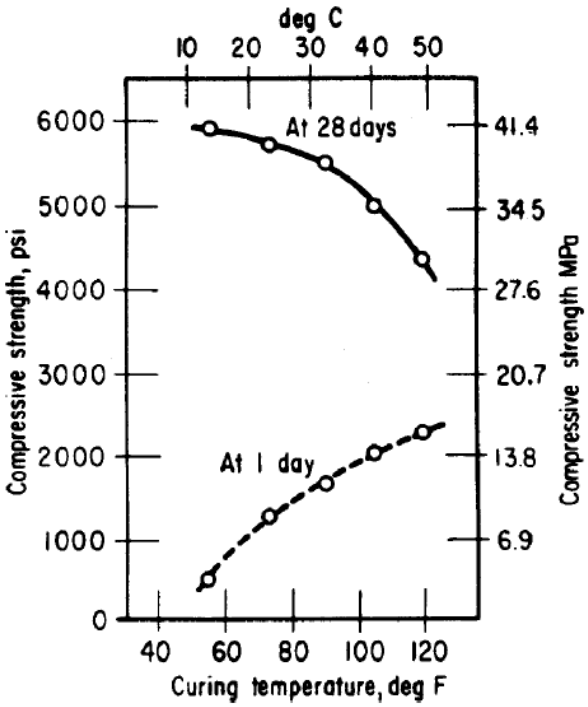

Figure 2.23. Curing temperature on compressive strength
(adapted Verbeck and Helmuth 1968)

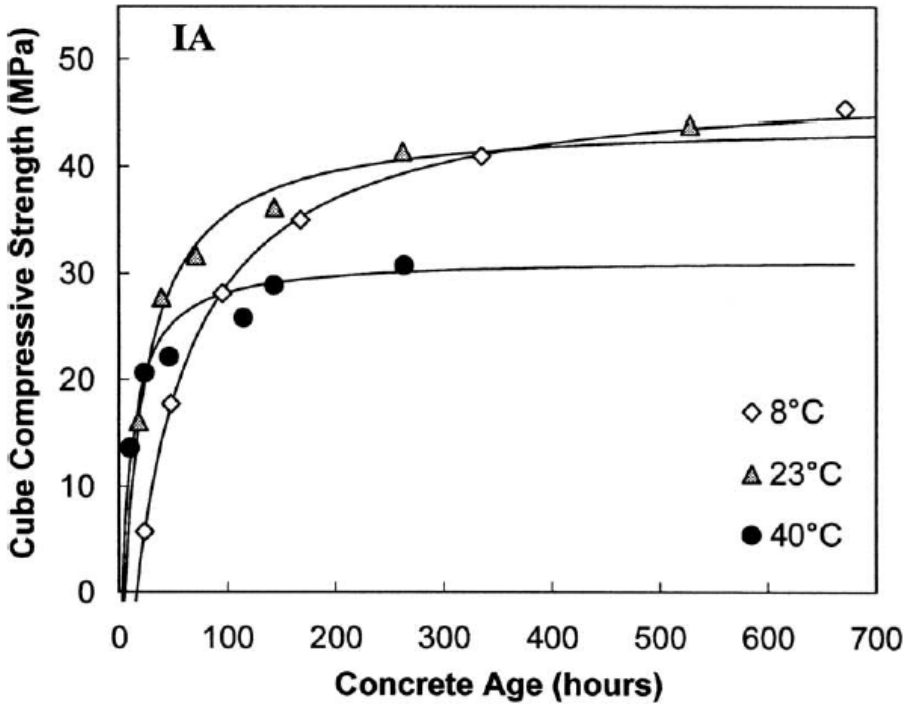

Note: 1 psi = 0.0069 MPa; F° = 1.8C° + 32

Figure 2.24. Compressive strength development of Type I cement
(adapted from Brooks et al. 2007 with permission from ASCE)

Mehta and Monteiro (2006) show the effect of high ambient temperature on the slump with the use of ASTM C494 Type D admixtures. Concrete placed at an ambient temperature of 109°F (43°C) with the use ASTM C494 Type D admixture exhibited a slump loss of approximately 2.25 in. (5.7 cm) within the first hour of mixing and another 1.75 in. (4.4 cm) within the second hour (Mehta and Monteiro 2006).

In conjunction with temperature, humidity of the concrete and curing area plays a significant role in strength gain/loss and permeability reduction. The rate of . As water is removed, drying shrinkage increases which leads to the formation of more microcracks and decreases the strength of the concrete. Initial stage curing to ensure proper moisture to concrete is typically provided between 7 and 14 days (Mehta and Monteiro 2006).

Concrete testing conditions, while not a part of the concrete mixture, play a role in measured strength, modulus, and permeability. Testing conditions include specimen size, rate of loading, capping method, consolidation, and curing methods. All of these conditions are covered in ASTM and AASHTO testing guidelines.

Specimen size, for instance, whether it be diameter or length to diameter ratio (L/D) can show a significant difference in strength. A 4x8 in. (10x20 cm) concrete cylinder can test 5 to 10 % higher strength than a 6x12 in. cylinder of the same concrete (Neville 2011, Day 1994). 6x12 in. (15x30 cm) cylinders are the standard for strength measurement and relative strengths decreases as the diameter increases to approximately 24 in. (61 cm) when the height of the cylinder is maintained at twice the diameter (Mehta and Monteiro 2006). The rate of testing in compression will also affect the compressive strength which is the reason ASTM C39 limits the load rate to approximately 30,000 and 60,000 lb/min. (13,600 and 27,200 kg/min) for 4x8 in. (10x20 cm) and 6x12 in. (15x30

cm) cylinder specimens, respectively. Higher loading rates tend to increase the apparent strength (Mehta and Monteiro 2006).

Concrete specimens must also be prepared so that the ends are perpendicular and planar. Load concentrations may develop if ends are not planar (Neville 2011). Several methods exist to properly cap cylindrical specimens which include sawing, grinding, or capping (bonded or unbounded). Most common end capping methods are sulfur capping and neoprene padding.

2.3 Literature Review

2.3.1 Lightweight Concrete

Lightweight aggregates have been used in structural concrete for centuries that date back to early Roman construction of the Pantheon dome and the Coliseum (ACI 213 2003). Use of lightweight aggregate concrete (LWAC) has not been readily available until the advent of manufactured lightweight shale aggregates in the 20th Century (ACI 213 2003). LWAC has been used to reduce the weight of high rise structures within slabs and columns and on bridge decks. LWAC has not been used in major infrastructure due to poor performance in strength and durability; however, newer aggregates have minute, unconnected voids (Iwanami et al. 2005). The unconnected voids allows for a lower permeability than in previous lightweight concrete research which means improved durability and performance.

Lightweight concrete takes its form by several means; however, the most common way to produce lightweight concrete is to replace normalweight aggregates with aggregates that are lighter in weight that produce a concrete unit weight less than approximately 135 pcf (2,160 kg/m^3). Lightweight concrete can be manufactured in

many ways which include full replacement of normalweight coarse and fine aggregates with lightweight equivalents (full lightweight) or more typically replacing a portion of the coarse aggregate and using normal weight fine aggregate (sand-lightweight).

Lightweight aggregates are classified in several different ways which include structural, insulating, or a combination of the two (Holm and Ries 2006). Structural lightweight aggregates used in concrete must adhere to ASTM C330 (2009) and include a variety of sources and manufacturing processes including rotary kiln expanded clay, shale, and slate, sintered grate expanded shale and slates, pelletized or extruded fly ash, and expanded slag (Kosmatka et al. 2002). The most common process involves extensively heating clay, shale, or slate in a kiln. The cooled product is then crushed and separated into aggregate sizes similar to conventional aggregate sizes. The final product is a very hard, lightweight, and porous material with various concrete applications. Natural pumice and scoria can also be processed to produce lightweight aggregate (Kosmatka et al. 2002). All lightweight aggregates have a different shape and texture based on the locally available source and manufacturing method (Holm 1983). Lightweight aggregates are typically chosen based on local availability and different physical properties.

2.3.2 Fresh Concrete Properties

Lightweight aggregate properties vary predominantly in absorption capacity, bulk density, and strength. Each aggregate property affects the fresh and hardened concrete properties. Holm and Ries (2006) discussed the absorption rate and capacity of lightweight aggregates used in concrete mixing as depicted in Figure 2.25. Due to the high quantity of readily available voids, most water is absorbed within a few hours, and

upon 24 hours of preconditioning. LWA concrete mixtures can achieve precise *w/c* due to the low continued rate of absorption beyond 24 hours (Holm and Ries 2006). Absorption rate also has a bearing on proportioning and placing of concrete because absorbed water within the lightweight pores are not readily available as mixing water (ACI 213 2003). Lightweight aggregate will absorb between 5 to 25% by dry weight compared to approximately 2% for normal weight aggregates (Holm and Ries 2006).

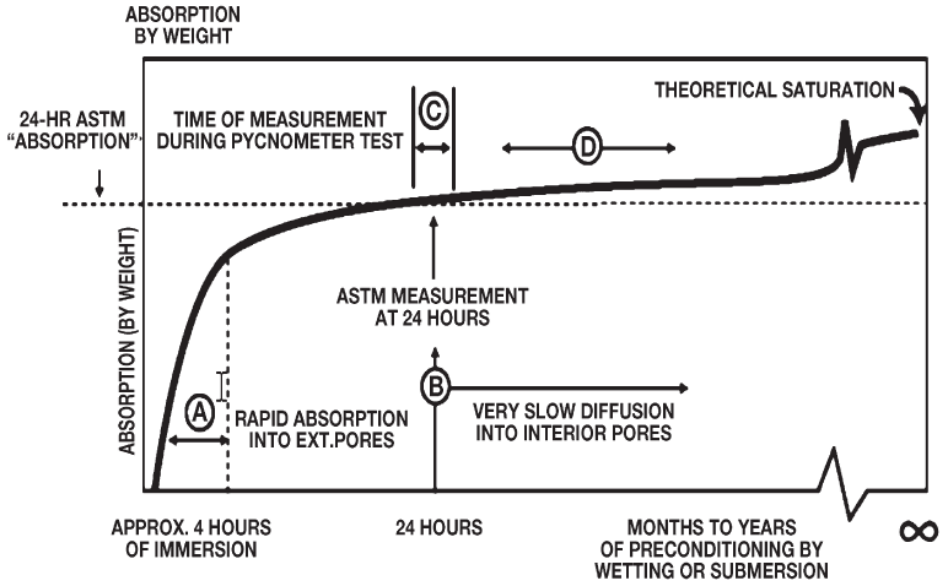

Figure 2.25. Absorption rate of lightweight aggregates
(adapted from Holm and Ries 2006, Reprinted, with permission, from STP169D-Significance of Tests and Properties of Concrete and Concrete Making Materials, copyright ASTM International, 100 Barr Harbor Drive, West Conshohocken, PA 19428)

Lightweight aggregate concrete can be produced, placed, and finished in the same manner as normalweight concrete; however, it is necessary to ensure the lightweight aggregates have been readily prewetted to ensure the lightweight aggregates do not soak up the mixing water thereby increasing slump loss and decreasing the workability. Lo et al. (1999) studied the effects of aggregate pre-wetting and showed that an increase in pre-

wetting time increased the strength and workability of the concrete. The expanded clay was mixed after zero, 30-minute, and 1-hour pre-wetting and provided slumps between 2.5 and 3.5 in. (63.5 and 89 mm) without significant segregation of aggregates (Lo et al. 1999).

2.3.3 Concrete Strength

Lightweight aggregates are used to partially or fully replace normalweight aggregates in concrete to make lightweight concrete. The lightweight aggregate used for replacement also affects the concrete strength in the same aspects as normalweight aggregates, but also provides additional factors which affect the strength.

Just like normalweight aggregates used in concrete, local availability is a primary factor. Not all lightweight aggregates are created the same. Some have higher strength, some have more absorption capacity, and some are natural or artificially manufactured. With this variability comes variability in concrete strength. It is necessary to clarify that research presented in this literature review is based on a variety of lightweight aggregates with different strengths, densities, and absorptions characteristics.

Lightweight aggregate concretes have strength ceilings based on aggregate strength. Once this ceiling is reached, further addition of cementitious material does not appreciably increase the strength (Holm 1983). The strength ceiling can be increased by reducing the maximum aggregate size (ACI 213 2003). Normalweight concrete develops elastic incompatibility due to significantly different stiffness values of the aggregate and cement matrix (Bremner and Holm 1986). Due to the inelastic mismatch of stiffness, failure will occur within the mortar prior to reaching the normalweight strength ceiling (Holm 1983). However, the inclusion of lightweight aggregates with similar stiffness to

the cement matrix will decrease stress concentrations and microcracking (Bremner and Holm 1986). Lo et al. (2007) studied the effects of aggregate strength of expanded clay on concrete strength. With a *w/c* of 0.4, the compressive cube strength was 5,500 psi (38 MPa) at 7 days and 6,400 psi (44 MPa) at 28 days and increased to 6,700 psi (46 MPa) at 56 days indicating the strength ceiling had still not been reached (Lo et al. 2007). Chi et al. (2003) studied the effects of cold-bonded pelletized aggregates used in concrete mixtures and showed a direct relationship of higher density and higher strength lightweight aggregates provide higher compressive strength and modulus. In addition, a decrease in strength and modulus of elasticity occurred as the lightweight coarse aggregate volume increased (Chi et al. 2003).

Current lightweight aggregates now have minute, unconnected voids allowing for higher strength and lower permeability as compared to concretes in the past made with lightweight aggregate (Iwanami et al. 2005). The biggest contributor to concrete strength is the microstructure which is adversely affected by the ITZ. High-performance concretes that have high strength or high durability due to a particularly dense hydrated cement paste structure (Neville 2011).

Unlike normalweight aggregates, lightweight aggregates have much larger surface pores. Lo et al. (2007) studied the effects of aggregate strength, pore distribution, and the ITZ on concrete strength. Aggregate sizes of 0.2 in (0.1 cm) and 1 in. (2.54 cm) both showed increasing pores with increasing *w/c*; however, the 0.6 in. (1.5 cm) aggregate concrete showed exceptionally high porosity due in part to the stronger aggregate having a lower absorption and less surface pores where the ITZ interlock can take place (Lo et al. 2007). This interlock can be seen from a scanning electron microscope (SEM) image

depicted in Figure 2.26. SEM images clearly show a continuous and tight ITZ without large pores (Lo et al. 1999). Wasserman and Bentur (1996) noticed that the surfaces of the aggregate were fuzzy due to hydration products penetrating into the aggregates surface pores.

Figure 2.26. SEM image of lightweight aggregate interlock with cement matrix (adapted from Lo and Cui 2004, Reprinted from Materials Letters, Vol. 58, T.Y.Lo and H.Z. Cui, Effect of porous lightweight aggregate on strength of concrete, 916-919, 2004, with permission from Elsevier)

Lo and Cui (2004) examined the ITZ and its effect on the compressive strength of lightweight concrete. The mechanical interlock between the aggregate and the bulk cement paste reduces the "wall effect" from CH crystals forming on the surface of the aggregates as they do with normal weight aggregates (Lo and Cui 2004). Compressive strengths for LWAC were 6,700 psi (46.5 MPa) and 7,400 psi (51 MPa) at 7 and 28 days showing 91% of strength gain was within 7 days. Normalweight concrete typically achieves 70 to 80% of its 28-day strength at 7 days (Lo and Cui 2004). The higher bond

within the ITZ is credited with the rate increase of strength (Lo and Cui 2004). The absorbed water in lightweight aggregates is not necessarily available for mixing water; however, it does provide a marked advantage over normalweight concrete with low *w/c*. High cementitious concretes perform well with lightweight aggregates that contain internal curing water (Holm and Ries 2006). This absorbed water is used for internal curing which extends the curing cycle of in-place structures. Campbell and Tobin (1967) showed that job-cured specimens were about 91% and 98% of ASTM cured compressive strengths for normal and lightweight concretes, respectively. Lightweight aggregates contain internal curing water and tend to be more forgiving in unfavorable ambient conditions and curing practices (Al-Khaiat and Haque 1998; Holm and Ries 2006).

Al-Khaiat and Haque (1998) studied the long-term strength development in severe hot and dry, salt laden environments. Commercially available Lytag was used as the lightweight aggregate to produce a 4 in. (100 mm) slump concrete with a fresh unit weight of approximately 112 pcf (1,790 kg/m^3). Specimens were initially water cured at 1 to 7 days and then placed in seaside conditions and on a rooftop. Compressive cube strength at 28 days was higher for specimens placed in seaside conditions after 1 to 7 days moist curing as opposed to water cured and rooftop samples with the same initial curing regime (Al-Khaiat and Haque 1998). The 28-day strength seemed to be less sensitive to a lack of curing as compared to normalweight concrete; however, beyond one month of exposure, the long-term strength development of the lightweight concrete seems to behave in a similar manner to that of normalweight concrete (Al-Khaiat and Haque 1998).

Weber and Reinhardt (1997) studied the effects of replacing 25 percent of the coarse aggregate with lightweight aggregate. This mixture produced a unit weight of approximately 140 pcf (2,250 kg/m^3) which is considered a normalweight concrete according to the German standard (Weber and Reinhardt 1997). A rapid hardening portland cement was used with silica fume to produce a water/(cement + silica fume) ratio of 0.3. Compressive cubes were prepared and soaked for 6 days in water then placed in air at a relative humidity of 65%, air at 65%, air varying in temperature and relative humidity, and sealed in aluminum foil. Testing showed no significant change in compressive strength of the cubes. X-ray diffraction showed C-S-H, ettringite, and CH which only form if water is available; therefore, according to curing conditions, water was only supplied from the lightweight aggregate (Weber and Reinhardt 1997).

This internal curing water mentioned also provides an internal source for long-term pozzolanic activity either with the use of pozzolans or the use of alkali/silica rich lightweight aggregates. Later age strength increases of about 20% can occur due to pozzolanic reaction between aggregates and alkaline pore solution with the CH deposited in surface pores (Wasserman and Bentur 1996). ACI 213 (2003) states that a long-term pozzolanic activity exists due to the silica-rich expanded aggregates reacting with liberated calcium hydroxide during hydration. Zhang and Gjorv (1990) studied the use of different lightweight aggregates with varying densities and outer shell thicknesses. The study showed that lightweight aggregates with less dense outer shells behaved similarly to normalweight aggregates including developing the “wall effect” from calcium hydroxide (Zhang and Gjorv 1990). Less dense outer shells that tended to be more porous hardly showed a trace of a CH-rich zone as accompanied with normalweight

aggregates (Zhang and Gjorv 1990). It is possible the long-term internal curing effects allowed for thorough hydration of the cement at the porous aggregate interface due to pozzolanic activity.

2.3.4 Concrete Modulus of Elasticity

Factors affecting the lightweight concrete strength typically affect the elastic modulus; however, a lower density aggregate will invariably lower the modulus. ACI 318 (2011) allows designers to estimate the static modulus of elasticity with Equation 2.10 where f'_c is the 28-day compressive strength; w_c is the concrete density for normalweight concrete and the calculated equilibrium density as determined in ASTM 567 (2005). The calculated equilibrium density represents the long-term density of lightweight concrete after exposure to a relative humidity of 50 ± 5 % and a temperature of 73.5 ± 3.5 °F (23 ± 2 °C) for a period of time to achieve constant mass (ASTM 567 2005).

$$E_c = 33 \cdot w_c^{1.5} \cdot \sqrt{f'_c} \qquad (2.10)$$

Mehta and Monteiro (2006) define the dynamic modulus of elasticity as the tangent portion from the origin of a stress-strain curve which corresponds to small, instantaneous strain. The dynamic modulus may be 20 to 40 percent higher than the static modulus of elasticity (Mehta and Monteiro 2006).

Swamy and Bandyopadhyay (1975) and Lydon and Baldendron (1986) provide the static modulus of elasticity as a function of the dynamic modulus (E_d) with units of GPa. Equation 2.11 and 2.12 present their formulas rearranged with E_d in terms of E_c for comparative purposes, respectively.

$$E_d = \frac{(E_c + 4.1)}{1.04} \qquad (2.11)$$

$$E_d = \frac{E_c}{0.83} \tag{2.12}$$

Ke et al. (2009) studied expanded clay and shale used in lightweight concrete mixtures and showed that an increase in lightweight coarse aggregate volume would produce a decrease in modulus and strength. They also showed that the decrease was not as severe with the use of lower absorption capacity lightweight aggregates. The reduction of Young's modulus with an increased LWA volume fraction showed less for expanded shale aggregates (Ke et al. 2009). For the expanded clay aggregate concrete, the strength decreased with increasing volume fraction; however, the increase in the two expanded shale fractions did not show a reduction in strength, and even showed an increase for one mix (Ke et al. 2009). Weber and Reinhardt (1997) studied concrete with 25% replacement of coarse aggregate only and provided a modulus of 4,900 ksi (34 GPa), whereas, Al-Khaiat and Haque (1998) replaced all coarse and fine aggregate with lightweight equivalents which produced a concrete modulus of 3,800 ksi (26 GPa). The modulus of elasticity measured was all more than the ACI code, British Standard, and Norwegian Standard (Al-Khaiat and Haque 1998). Holm and Ries (2005) in an industry report showed a linear reduction as the percentage of coarse aggregate is replaced with structural lightweight aggregate as presented in Figure 2.27. Similarly, Chi et al. (2003) showed as lightweight aggregate volume fraction increased, the elastic modulus decreases in a linear fashion.

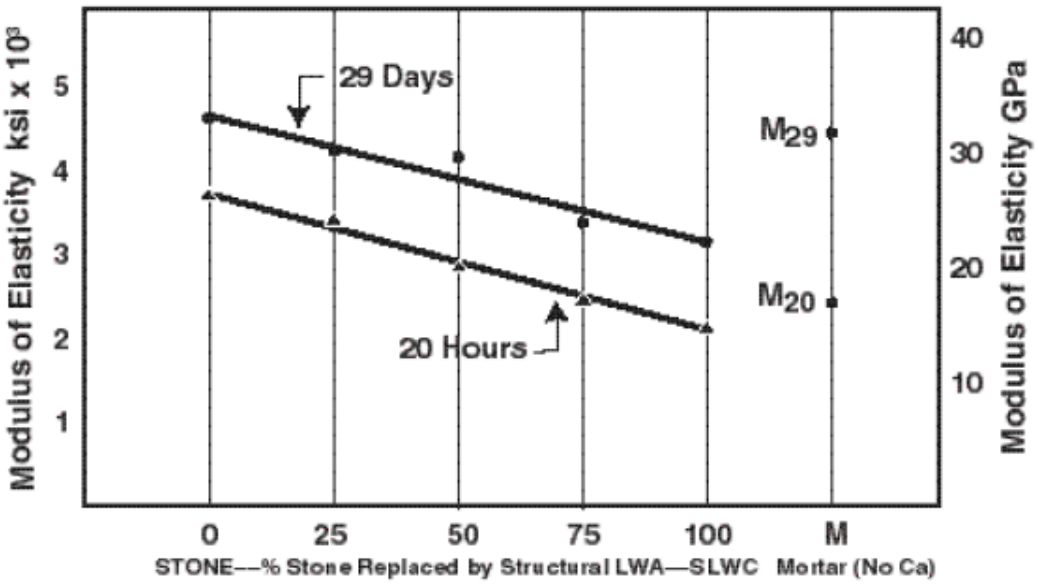

Figure 2.27. Effect of lightweight replacement on modulus of elasticity (adapted Holm and Ries 2005 with permission from ESCSI)

2.3.5 Dimensional Stability

The introduction of lightweight aggregate in concrete has shown a decrease in the overall concrete modulus. Does this reduction in modulus affect the concrete's dimensional stability? Lura et al. (2007) studied the use of internal curing water and its consequences. Experimental methods showed that the relative humidity (RH) remains close to 100 % within lightweight concrete mixtures which was maintained above 95% after 15 days. During the same time period, the RH of the normal weight specimens fell below 90 %. Autogenous shrinkage was reduced with the use of internal curing water from LWA which in turn lowers self-induced internal stresses while being restrained and shows a reduced cracking tendency of structures with low *w/c* (Lura et al. 2007).

Similarly, Cleary and Delatte (2008) agree that lowering the *w/c* increases the tendency for autogenous shrinkage (AS); however, AS can be mitigated with proper moisture. This becomes difficult with $w/c < 0.45$ as the reduction in permeability hinders

the movement of external curing moisture into concrete specimens. High performance concrete was cracking early in Ohio DOT (ODOT) structures possibly due to the difference in absorption capacities of the LWA uses; however, field test data showed possible improvement in cracking potential due to internal curing (Cleary and Delatte 2008). LWA substitution improved early and ultimate strength and reduced the cracking tendency. LWA with an AC of at least 2% provided an additional 27 pcy (16 kg/m^3) of moisture as opposed to an AC equal to 1% which could potentially change the *w/c* approximately 0.056 (Cleary and Delatte 2008). Generally all mixtures met or exceeded ODOT strength specifications and with even a partial replacement of fine aggregate with LWAC will allow for internal curing. It may be higher cost for material; however, these costs are most likely to be outweighed by reducing the life-cycle costs due to reduced cracking (Cleary and Delatte 2008).

Several studies investigated the use of aggregates with varying moisture conditions. Zhutovsky et al. (2002) showed that using saturated lightweight aggregate was effective in eliminating AS. Natural pumice was used with absorption capacities ranging from 13 to 27 %. The study showed that larger lightweight aggregates with higher absorption proved to be better at eliminating autogenous shrinkage which was opposite of the initial hypothesis that smaller aggregate would be better (Zhutovsky et al. 2002). Similarly, Kohno et al. (1999) evaluated aggregate type and moisture content. Expanded shale, two high-performance pelletized aggregates, and a control NWA were used in which moisture varied from 4.42% for the high-performance aggregate to 35.4 % for the expanded shale. The expanded shale with the highest moisture content rapidly expanded until it stabilized at 180 microns after 1 day. The high-performance pelletized

aggregate increased to 300 microns after 90 days, and the normalweight control increased to 430 microns after 90 shows. The varying moisture contents showed that as moisture content of the lightweight aggregate increases, the AS decreases (Kohno et al. 1999).

Bentur et al. (2001) showed that AS can be effectively mitigated with approximately 25 % partial replacement by volume. Dry and SSD lightweight coarse aggregates were used. Normalweight concrete showed shrinkage strains while the LWA concrete experienced expansion based on the initial moisture state. The SSD lightweight aggregate concrete never showed shrinkage while the air-dried aggregate specimens began to shrink after 24 hours with small shrinkage strains after 5 days. Slight compressive stresses developed in both the SSD and air-dried LWA concretes; however, the air-dried specimen developed tensile stresses after 40 hours. The SSD LWA concrete developed slight tensile stresses after 5 days, while the normalweight concrete specimen developed tensile stresses at the onset of curing. Shrinkage was significantly reduced with the use of lightweight aggregates in SSD conditions as compared to air dry aggregates. The difference in moisture content of the aggregates did not affect the strength of the lightweight specimens (Bentur et al. 2001).

2.3.6 Concrete Durability

Durability has been questioned with lightweight aggregate concrete for decades. It is necessary to address the multiple durability concerns with concrete in which the key to them all is concrete permeability. As discussed earlier, the permeability of concrete is a function of the integrity of the ITZ. In addition to permeability, lightweight's ability to resist chloride ion penetration, freezing and thawing, alkali-silica reactivity, and sulfate attack are presented.

2.3.6.1 Permeability

Permeability is measured and presented in a couple of ways, either directly or indirectly, including the salt ponding test and the rapid chloride ion penetration test (RCPT) outlined in ASTM C 1543 (2010) and C 1202 (2010), respectively. The salt ponding test measures the penetration of chloride ions into concrete specimens, whereas, the RCPT test measures the current which passes through a concrete specimen. The measured current passed (Coulombs) is an indication of the concrete's ability to resist chloride ions which relates to its permeability. The water permeability can also be determined by use of a falling-head permeability test on a concrete specimen with an induced pressure head allowing the water to flow from higher pressure head to a lower pressure head.

Lightweight aggregate concrete shows a low permeability due to several factors including low *w/c* of the paste, improved ITZ, and decrease in microcracking due to elastic compatibility of aggregate and cement matrix (Neville 2011). Keeton (1970) performed falling head permeability tests on normalweight and lightweight concrete specimens with varying strengths, thicknesses, and relative humidity. The all lightweight showed concrete producing a 5,000 psi (34.5 MPa) 28-day strength showed to have the lowest permeability of the normal- and lightweight concretes (Keeton 1970). Bamforth (1987) determined the water permeability and gas permeability of concrete specimens under an induced pressure. Cylindrical specimens were tested in a jig that confined the specimen to prevent leaks, as well as "short circuiting" which kept water and gas from going around the concrete specimens. The lightweight concrete contained air entrainment. The permeability measured for the lightweight concrete from both water

and nitrogen gas testing showed to be at or less than the normal weight concretes tested (Bamforth 1987). Similarly, Emiko et al. (2010) tested several lightweight aggregate concretes with varying *w/c*, absorptions and pre-soak times and showed that the penetrability properties for LWA concrete are significantly affected by the *w/c*. The water permeability was determined, and showed increases in the *w/c* would increase the penetrability, whereas, an increase in cement paste content would decrease the penetrability (Emiko et al. 2010). The water permeability was shown to be of the same magnitude as normalweight values under an induced pressure of 5,800 psi (40 MPa) (Emiko et al. 2010). ACI 213 (2003) states that the using certain lightweight aggregates create a pozzolanic reaction thereby decreasing the permeability of the concrete which minimizes the leaching of soluble compounds and possibly reduce the occurrence of sulfate attack. High-quality, structural lightweight concrete should be used to reach desired long-term performance in resisting intrusion of chloride ions and carbonation (ACI 213 2003).

2.3.6.2 Chloride Ion Penetration and Carbonation

Initial curing has shown to be a contributing factor to lightweight durability. In the same study by Al-Khaiat and Haque (1998), salt ponding tests showed durability is much more sensitive to lack of curing as opposed to compressive strength, and results establish a need for initial curing of coastal structures where durability is a concern. It is possible that the high temperature and humidity accelerated hydration lead to less uniformity in hydration products (Al-Khaiat and Haque 1998). Haque et al. (2004) also studied sand-lightweight mixes compared with normalweight concrete. With an increase in initial curing from 1 day to 7 days, the sand-lightweight mixture showed comparable

results to that of the normalweight mixture for water penetration, carbonation depth, and chloride penetration. An increase in initial curing produced negligible carbonation depths for the sand-lightweight concrete (Haque et al. 2004). Lo et al. (2006) studied the effects of entrained air on strength, surface absorptions, and chloride permeability. RCPT was used to measure the chloride penetration of *w/c* = 0.4 mixtures with 13.5 and 31.9% air contents. The charge in Coulombs decreased with decreasing air content; however, the current passed measured was more than the acceptable limit for high chloride ion penetrability of >4000 Coulombs. RCPT may not be the ideal test for LWA concrete permeability with such high air content (Lo et al. 2006). Ke-feng and Gjorv (2003) studied different normalweight and lightweight concretes with silica fume. Specimens were tested similar to the ASTM C1202 RCPT; however, instead of 60 V maintained on the specimen, 12 V were used. High-strength lightweight concrete with silica fume showed to have the lowest permeability (Ke-feng and Gjorv 2003). Haque et al. (2004) showed partial sand-lightweight mixtures were comparable in terms of depth of water penetration when compared to similar strength normalweight concrete.

It is necessary to prevent the penetration of chloride ions and carbonation within reinforced concrete to prevent corrosion of the reinforcing steel. Kayali and Zhu (2005) studied the ingress of chloride ions in moderate-strength (MS), high-strength (HS) normalweight, and high-strength lightweight (HSLW) concrete. The compressive strength at 35 days for each concrete was approximately 4,700 psi (32 MPa), 10,500 psi (72 MPa), and 10,000 psi (69 MPa) for the MS, HS, and HSLW concretes, respectively. Silica fume and fly ash were added to produce high-strength lightweight concrete slabs. Slab surfaces were exposed to 20,000 ppm chloride solution on one surface and tested

every week for the chloride concentration in the cementitious material. Lightweight slabs showed low concentration of chloride ions beyond 0.2 in. (5 mm). The lightweight slabs showed to have the lowest concentration of chloride ions at 0.2 in. (5 mm) compared to the MS and HS normal weight mixtures as depicted in Figure 2.28. It is possible that the low concentration of chloride ions after long exposure times may have been due to highly absorptive LWA and a dense matrix with disconnected pores (Kayali and Zhu 2005).

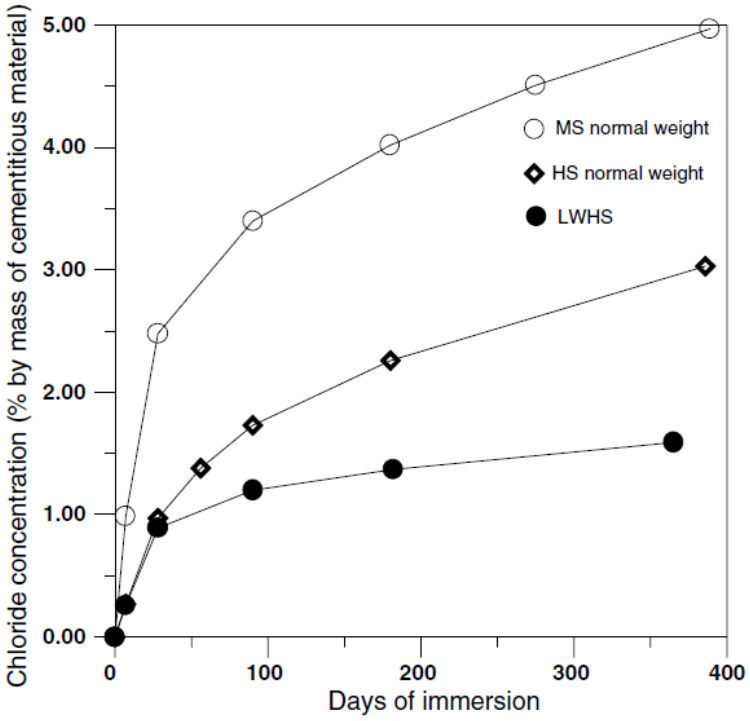

Figure 2.28. Chloride ion concentration at 0.2 in. depth
(adopted from Kayali and Zhu 2005, Reprinted from Construction and Building Materials, Vol. 19, O. Kayali and B. Zhu, Chloride induced reinforcement corrosion in lightweight aggregate high-strength fly ash concrete, 327-336, 2005, with permission from Elsevier)

Chia and Zhang (2002) tested moderate and high-strength normalweight and lightweight concrete for water permeability and chloride penetrability. They also tested some mixtures with silica fume. Expanded clay was used with absorptions of 5, 7, and 9% at 1 hr, 24 hr, and 7 days of soaking beyond the 7.3% initial moisture content,

respectively. Several testing methods were used for durability testing including the water permeability test, immersion test, salt ponding test, and RCPT. At normal-strength levels of approximately 4,400 psi (30 MPa) to 5,800 psi (40 MPa), the lightweight specimens showed lower permeability than the normalweight concrete specimens; however, the high-strength lightweight specimens (compressive strength > 7,200 psi (50 MPa)) tested with a permeability of the same order of magnitude as the normalweight specimens (Chia and Zhang 2002). In addition to water permeability, the chloride penetrability of lightweight to normalweight concrete at each strength level was very similar. There did not seem to be a correlation between water permeability of concrete mixtures and chloride penetrability; however, RCPT showed relationships with the immersion and salt ponding tests (Chia and Zhang 2002).

Of particular interest are the effects of elevated curing temperatures on the durability of concrete such as in high-strength applications and/or prestress concrete curing. Gjorv et al. (1994) exposed high-strength lightweight aggregate concretes to elevated maximum curing temperatures of 122, 149, and 176 °F (50, 65, and 80 °C). Concrete specimens made with expanded clay aggregate were accelerated chloride tested. Dry aggregate concrete compressive strength was not significantly affected with curing temperatures up to 176 °F (80 °C) as depicted in Figure 2.29; however, at 122 °F (50 °C) the compressive strength of the wet aggregate concrete was reduced (Sandvik and Gjorv 1992; Gjorv et al. 1994). Both the wet and dry aggregate concretes showed a chloride permeability increase with increased maximum curing temperature over 149 °F (65 °C) (Gjorv et al. 1994).

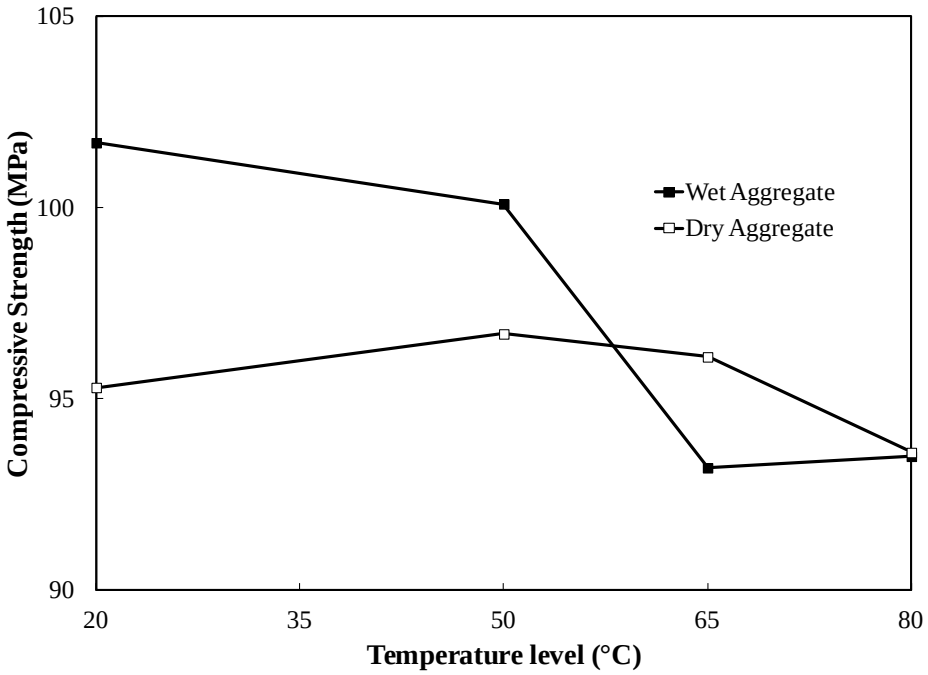

Figure 2.29. Compressive strength development of wet and dry aggregate concrete (adapated from Gjorv et al. 1994)

2.3.6.3 Freezing and Thawing Durability

Another issue pertaining to concrete durability is the ability to resist freezing and thawing conditions in colder climate areas. Mao and Ayuta (2008) investigated several parameters such as aggregate density, water content, crushing strength, and pore structure, as well as different freezing rates to evaluate freezing and thawing resistance of lightweight concrete. Lightweight concrete specimens of two different aggregate densities (0.85 and 1.24 g/cm^3) were subjected to ASTM C666 (2008), Standard Method for Resistance of Concrete to Rapid Freezing and Thawing. The lightweight concrete mixed with the higher-density aggregate showed superior freezing and thawing resistance. The lower-density aggregate did provide better resistance during low freezing rates (Mao and Ayuta 2008). The pore structure proved to be the most fundamental factor influencing freezing and thawing resistance where lower pore volume aggregates

with smaller pores showing good resistance (Mao and Ayuta 2008). Gao et al. (2002) evaluated different water reducing admixtures to improve the frost resistance of lightweight concrete. With development of microcracks being the major factor leading to lower frost resistance in high performance LWA concrete, the Gao et al. (2002) showed that a more complete hydration of cement due to admixtures created a filling material within the pores creating a mechanical interlock and either stopped or suppressed the propagation of microcracks. Contrary to Mao and Ayuta (2008), Gao et al. (2002) stated that the LWA concrete exhibited higher frost resistance due to the 20 to 50 % of voids provided by the aggregate (Gao et al. 2002).

Several studies have evaluated freezing and thawing durability with respect to the dynamic modulus after freezing and thawing cycles. Cleary and Delatte (2008) subjected several lightweight mixtures with varying replacement percentages of coarse aggregate to 300 freezing and thawing cycles. Specimens were cast with and without lightweight aggregate. The normalweight specimen's relative dynamic modulus was within the mid to high 90 percent with the lightweight slightly lower. All specimens were still shown to be freezing and thawing resistant (Cleary and Delatte 2008). Mao and Ayuta (2008) also showed LWA can be used in regular and rapid freezing and thawing cycles with most mixes having a relative dynamic modulus greater than 80 percent. The lower density proved highly resistant with 100 % relative dynamic modulus through both regular and rapid freezing and thawing cycles. The higher density aggregate concrete subjected to 6 cycles/day dropped below the ASTM limit of 60 percent at approximately 150 cycles (Mao and Ayuta 2008).

2.3.6.4 Alkali-Silica Reaction

An area not showing much research is investigation of alkali-silica reaction (ASR) with respect to lightweight aggregates. Mladenovic et al. (2004) noticed the lack of research and that the European standard for LWA acknowledged that ASR may be possible and offers preventative measures such as using low-alkali materials in concrete; however, the standard does not address any test methods or limits of expansion for LWA. Normalweight concrete testing procedures were validated and then applied to LWA concrete (Mladenovic et al. 2004). Four common LWA used in Slovenia were evaluated including expanded vermiculite, clay, glass, and perlite. Concrete mixtures with these aggregates were tested using ASTM C 1260 (2007) (accelerated mortar bar test), ASTM C 289 (2007) (rapid chemical test), and combined scanning electron microscope-energy dispersive X-ray. The accelerated mortar bar test showed no expansion of the aggregates and only 0.13 % for the perlite which is still below the ASTM C 1260 (2007) limit of 0.20 % expansion. Chemical tests showed that expanded glass and perlite were highly reactive; however, the accelerated mortar bar test showed no visible expansion possibly due to the porous texture of the aggregate which may have accommodated the ASR expansive gel and any other reaction products (Mladenovic et al. 2004).

Collins and Bareham (1987) studied the effects of using lightweight porous aggregate to reduce ASR expansion. Results showed that when using low reactivity aggregates, the lightweight aggregates performed much better when compared to normalweight concrete for expansion suppression. Thin section examinations show that expansive gel was reduced; however, it was not expanded into the lightweight pores

showing it is possible that potassium rich pore water reduced the reaction process (Collins and Bareham 1987).

2.3.6.5 Sulfate Attack

Sulfate can be a concern both from exposed sulfate attack and delayed ettringite formation (DEF). Several studies have evaluated lightweight concrete resistance to internal and external sulfate attacks. Use of silica-rich expanded aggregates providing long-term pozzolanic effects will decrease the permeability and reduce the possibility of external sulfate attack (ACI 213 2003). Maltais et al. (2006) studied the feasibility of using LWA concrete to achieve 100-year design life of modular hybrid piers (MHP). Long-term behavior was both evaluated using laboratory concrete mixtures and numerical modeling. Three different concrete producers provided lightweight concrete all with Class F fly ash with one manufacturer providing ultra-fine fly ash which were used to validate the numerical models. Models showed that expansive gypsum would reach a depth of approximately 1.5 in. (3.8 cm) after 100 years showing the good performance (Maltais et al. 2006). Al-Khaiat and Haque (1999) and Haque et al. (2004) showed that lightweight concrete, when properly cured performs comparable to normalweight strength equivalents in addition to having a much lower sulfate ion concentration than the 5 % limit listed in ACI 318 (2011) after one year.

An issue of particular importance is the elevated curing temperatures used in precast, prestressed applications. High temperatures either from high hydration temperatures or applied heat may cause delayed ettringite formation when the internal concrete temperature reaches between 158 °F and 176 °F (70 °C and 80 °C) (Neville 2011). Upon concrete cooling along with adequate humidity, delayed ettringite may form

which is an expansive substance that causes microcracks which attacks the concrete mortar from the inside (Mehta and Monteiro 2006). Ronne and Hammer (1999) discuss the influence of maximum curing temperature, moisture condition through both external and internal water supply, and chemical composition on DEF of structural concrete. Expanded clay LWA showed lower expansion compared to normal weight concrete specimens. The lightweight concrete specimens also showed a higher critical curing temperature of approximately 160°F (71 °C); whereas, the normal weight threshold temperature was between 150 and 160°F (66 and 71 °C) (Ronne and Hammer 1999). An addition of 5% silica fume showed to prevent or at least delay the reaction of ettringite formation with a critical temperature between approximately 140 and 195 °F (60 and 91 °C) (Ronne and Hammer 1999).

2.3.7 Precast/Prestressed Concrete Applications

Lightweight concrete has been used successfully in many precast/prestress applications including girders, slabs, and precast exterior panels to reduce the dead load of structures. Precast manufacturers have been able to maximize the reduction in dead load weights of lightweight elements and accommodate shipping trucks, which lowers transportation and project costs, as well as environmental consequences (Holm and Ries 2006). Lightweight concrete has even been specified for higher strength in precast applications and for offshore members (Holm and Ries 2006). Prestress applications require adequate concrete strength and stiffness so as not to deflect too much and withstand creep due to prestress force. Kahn and Lopez (2005) researched the time dependent behavior of LWA concrete with expanded slate used in AASHTO bridge girders. The concrete investigated was considered high-performance mixtures due to

high compressive strengths of 8,000 and 10,000 psi with unit weights less than 120 pcf (1,920 kg/m^3). The lightweight specimens were shown to have a 620-day creep that was substantially less than that of previous studies (Kahn and Lopez 2005). Industry models including the AASHTO refined and lump sum model, PCI, and ACI 209 models were used to estimate the elastic shortening, shrinkage, and creep and compared to the measured values. All methods were shown to overestimate the prestress losses for the 10,000 psi (69 MPa) girders, whereas, the AASHTO refined and ACI 209 overestimated the prestress losses for the 8,000 psi (55 MPa) strength girders. Initial research showed that these two methods may be used to conservatively predict losses in high strength elements (Kahn and Lopez 2005).

Another concern for lightweight concrete in prestress conditions is the transfer length and development flexural length. Waldron et al. (2005) evaluated the use of LWA concrete in AASHTO Type II and IV bridge girders. The transfer length measured in the Type IV girders was determined to be 33 bar diameters (d_b) without any cracking which is significantly shorter than 50 d_b and 60 d_b used in the AASHTO (2010) LRFD specifications. Considering the lightweight modifying factor (λ) of 0.85, the calculated development lengths increase by 18%; however, the lengths measured from the Type II girders was determined to be quite close to the AASHTO specification which may or may not have been conservative (Waldron et al. 2005).

2.3.8 Ductility

Adequate ductility of concrete allows structural concrete members to deform more prior to failure. Piles are axially loaded elements during driving; however, recalling from earlier, pile elements are used to also withstand large lateral loads. Piles behave as

a rotated cantilever “beam” when subjected to lateral loads. Several studies have evaluated the use of LWA concrete and its ductility.

Sin et al. (2011) investigated the flexural response of lightweight concrete as it compares to normalweight concrete with respect to cracking, deflection, strength, and ductility. Strength showed to be quite similar between the two; however, there were significant differences in other design areas. LWA concrete showed to have an increased number of cracks; however, the crack widths were much smaller than the normalweight concrete (Sin et al. 2011). Depending on the LWA used, the ductility index showed to either be slightly lower or slightly higher at crushing (Sin et al. 2011). Rossignolo et al. (2003) showed the strain for the high-performance lightweight mixtures was higher than the strain typically observed for normalweight concrete at the same compressive strength level showing ductile behavior.

LWA concrete has shown to require more lateral and confining steel to reach its increased ductility (Shah et al. 1983; Basset and Uzumeri 1986; Sin et al. 2011). Basset and Uzumeri (1986) investigated the effects of confining steel, both transverse and longitudinal, within lightweight concrete. Three standard column reinforcing details were used along with a detail of no confinement. The unconfined LWA concrete columns exhibited very brittle behavior; therefore, a minimum steel requirement is necessary to provide adequate ductility (Basset and Uzumeri 1986). Sin et al (2011) showed closer spacing of transverse reinforcment helps prevent disintegraton of concrete by confining the compressive zone concrete and increases the failure ductility; however, confinement did not improve the crushing ductility.

2.3.9 Dynamic Performance of Structural Lightweight Concrete

Pile driving is dynamic process in which a concrete pile will feel both compressive and tensile stresses. Several factors must be considered when evaluating dynamic resistance of lightweight concrete. Due to the lack of literature on lightweight piles, lightweight beams and columns are evaluated to determine lightweight dynamic resistance. Chen et al. (2010) evaluated the use of dry lightweight aggregate concrete in reinforced lightweight concrete beams. An increase in concrete strength was the most efficient means of increasing the lightweight concrete stiffness. Porous LWA has the ability to enhance the damping behavior by increasing the damping ratio by 13 to 30 % as compared to the normalweight control beams (Chen et al. 2010). An increase in steel, necessary for ductility, showed to decrease the damping ratio; however, the decrease was similar in both the lightweight and normalweight beams. The LWA reinforced concrete beams showed to be more favorable in seismic resistance of a structure (Chen et al. 2010).

Jensen and Hoiseth (1983) studied the effects of fallen objects on LWAC used in offshore oil production platforms. Different impact loading heads were examined. A mass of 240 lb (109 kg) was dropped from varying heights and at varying velocities. Testing showed that penetration, impact time, and impact forces strongly depend on the concrete material properties along with mass, velocity, and shape of the loading head (Jensen and Hoiseth 1983). Impact loadings on the specimens showed more crater like depressions in the LWAC as opposed to spalling of NWC under the same loading conditions. The impact stress may exceed the crushing strength of the concrete; however,

confinement and consolidation are factors that may improve these results (Jensen and Hoiseth, 1983).

2.3.10 Lightweight Concrete Piles

It is possible for LWA concrete to be used in prestressed driven piles. The piles must first be fabricated, and research shows that LWA concrete performs, as well as normalweight concrete. There is also promise in its ability to withstand the impact of a driving hammer. Research by Jensen and Hoiseth (1983) applied a rather heavy load over a small area across the concrete specimens; however, a pile hammer applies the load across the entire cross section. Pile installation also uses hammer cushions and pile cushions to reduce the initial impact of the hammer on the concrete to prevent damage to the pile head.

While there is no literature available, Gerwick (1968) mentioned the successful use of LWA concrete in bearing, sheet, and fender piles. Gerwick's (1968) experience indicated greater flexibility with lightweight piles; however, the pile head was more susceptible to spalling that could be mitigated with increased sprial confinement as mentioned with previous lightweight ductility studies. In addition to adequate ductile behavior, the lower LWA concrete modulus reduces the stress wave velocity to approximately 9,800 ft/s (2,985 m/s). The maximum compressive and tensile stresses during driving are reduced by 18 to 22% due to an apparent internal damping which partially offsets the lower tensile strength of the concrete (Gerwick 1968).

2.3.11 Modified Concrete Piles

Concrete designs across all spectra have not only been concerned with strength, but are also transitioning into a strength and durability design as outlined in ACI 211

(1991). Strength of concrete is still a large factor in structural design, but more and more designers are incorporating long-term performance. Concrete durability issues affect the structural resistance which means additional monies spent on long-term maintenance and upgrade costs of structures. Concrete mixture designs are now developed for high strength, enhanced durability, and a combination of both. Mixtures are also developed for enhanced workability. These mixtures are now known as high-performance concretes (HPC).

Suleiman et al. (2010) studied ultra-high-performance concrete (UHPC) H-piles. Concrete compressive strengths ranged from 26 to 32 ksi (180 to 220 MPa) which allowed the contractors to use larger hammers for larger penetration rates and reduced construction time (Suleiman et al. 2010). The concrete H-pile was designed to have the approximate surface area and weight of a HP 10x57. The high-strength concrete allowed the section to be designed without shear reinforcement and decreased the required cover from 1.25 in. (3.2 cm) to 0.75 in. (1.9 cm) (Suleiman et al. 2010). The UHPC also showed enhanced durability due to its low porosity with a chloride ion penetration resistance that is 28 times smaller than normal concrete and a corrosion rate 120 times slower than normal concrete (Vande Voort et al. 2008). No other cases were found of modified concrete piles.

2.4 Summary of Literature

Precast, prestressed driven piles are a new topic of discussion with respect to structural applications. Literature showed a lack of research and a need to implement and verify the use of lightweight concrete as a viable material in deep foundation pile elements. A summary of pile applications has been presented along with benefits and

constraints of lightweight aggregate concrete. LWA has been shown to enhance the performance of structural concrete through long-term strength gain and increased durability due to an inherent internal curing.

Not all lightweight aggregates are created equal; therefore, it is necessary to include quality aggregates with lighter density and higher strength and surface pores to provide the benefits presented above. Lightweight concrete has become a form of another high-performance concrete due to enhanced properties of lighter-weight and enhanced long-term strength and durability. LWA concrete has been used successfully in other strucutral applications such as beams, slabs, and columns. Lightweight concrete has shown similar or enhanced dynamic performance in these applications which should carry over to strucutral pile applications. Lightweight concrete has been used in pile applications successfully; however, there is an absence of literature which fully documents these uses. The aim of this work is to bridge the gap between structural lightweight concrete and deep foundation technologies.

3.0 RESEARCH METHODOLOGY

The research and investigative study consisted of several aspects including laboratory mixing, curing, and testing of trial concrete mixtures. Preliminary pile models were developed prior to field implementation. Full-scale test piles were cast and driven then modeled to verify insitu conditions.

3.1 Laboratory Study

3.1.1 Laboratory Concrete Mixing

The approach was to start from scratch with laboratory concrete evaluation and build up to a full-scale test pile to be driven and dynamically tested. The first step was to determine adequate concrete mixtures that met a minimum of 3,500 psi (24 MPa) release strength and a 28-day specified compressive strength (f'_c) of 5,000 psi (34.5 MPa) (ACI 543 2005; IBC 2006). Initially, ACI 211 (1991) was used to determine initial trial batch proportions for concrete until the "standard" normalweight concrete mixture for concrete piles in Charleston, SC was obtained. Concrete pile manufacturers in Charleston typically use the same ready mixed concrete producer for their piles which varies due to project need. The primary ingredients typically remain the same. The Charleston mixture was then used with modifications to proportions to achieve workability with a slump of 2 to 4 in. (50 to 100 mm) and required hardened properties and is presented in Table 3.1. Weights presented are in saturated-surface dry (SSD) moisture state.

Table 3.1 – Charleston, SC concrete pile mixture proportions

Item	NW
Cement Content (pcy)	752
Water Content (pcy)	293
SSD Normalweight Coarse Aggregate (pcy)	1875
SSD Fine Aggregate (pcy)	1157
Water-Reducing Admixture (oz/yd^3)	30

Note: 1 pcy = 0.6 kg/m^3; 1oz/yd^3 = 1.31 oz/m^3

The above mixture proportions provide a concrete with a water to cement ratio (*w/c*) of 0.38 which equates to a compressive strength of 6,375 psi (44 MPa) which is well beyond f'_c of 5,000 psi (34.5 MPa) (ACI 211 1991). Materials available at Auburn University were similar to that of Charleston, SC, and these were used for all applicable concrete trial mixes. Table 3.2 presents the material comparison between Charleston and Auburn.

Table 3.2 – Concrete material comparison

Item	Charleston, SC	Auburn University
Cement	Type II Lafarge	Type I/II Lafarge
Coarse Aggregate	#67 Granite, Martin Marietta	#67 Limestone, Calera
Fine Aggregate	Palmetto sand	Shorter sand
Fineness Modulus (FM)	2.42	2.45
SSD BSG Coarse Aggregate	2.67	2.76
SSD BSG Fine Aggregate	2.65	2.64
AC Coarse Aggregate (%)	0.5	0.2
AC Fine Aggregate (%)	0.1	0.5
Water-Reducing Admixture	WRDA Grace 35	WRDA Grace 64

Three-quarter in. (1.9 cm) expanded slate (supplied by Stalite) coarse aggregate was used in the 50 % and 100 % replacement mixes of normalweight coarse aggregate, and its material properties are presented in Appendix A. The lightweight aggregate was

placed in special 55-gallon (0.2 m^3) barrels depicted in Figure 3.1 with a valve at the bottom so the aggregate could be soaked for no less than 7 days as suggested by the supplier.

Figure 3.1. 55-gallon lightweight aggregate soaking barrels

After at least 7 days of soaking, the water in the barrel was drained out one day prior to mixing with the aggregate to reach as close to SSD moisture condition as possible. In the event of unequal moisture distribution upon draining, aggregate to be used in mixing that day were taken out and placed on a clean swept concrete surface in the lab and mixed thoroughly and placed in to 5-gallon (0.02 m^3) buckets prior to mixing. Moisture corrections were then taken on the newly mixed aggregate so as to obtain a more uniform reading.

Multiple trial mixtures were evaluated primarily to achieve adequate workability and desired fresh unit weight of the mix. The primary adjustment for each trial mixture was the paste volume (volume of cement and water). A slump of 2 to 4 in. (5 to 10 cm) was taken as acceptable values for structural lightweight concrete according to Kosmatka

et al. (2002). Materials were batched at and then mixed at room temperature. Concrete mixing followed ASTM C 192 (2002) for machine mixing with slight variations. The mixer was "buttered" with cement, fine aggregate, and water to reduce friction of the mixer and absorption of mixing water into the mixer. With the mixer off, the coarse aggregate was added (50 % mixture alternated normal weight and lightweight aggregate addition). With the mixer running, approximately 20 % of the mixing water was added to the aggregate, as it tended to be within 10 percent of its absorption capacity. The fine aggregate was added along with 40 % of the mixing water. The liquid W.R. Grace WRDA 64 was then added to the mixture and allowed to mix for 10 to 15 seconds to allow for full incorporation. The mixer was then stopped to add the cement. The mouth of the mixer was then covered for a few revolutions so as to keep the cement from escaping before adhering to the mixture. The remaining 40% of the mixing water was added slowly to the mix. Once all ingredients were added, the entire mixture was allowed to mix for 3 minutes, then rest 3 minutes covered (to prevent evaporation of mixing water), and then mixed for an additional 2 minutes per ASTM C192.

Trial mixtures were developed for different coarse aggregate replacements. The mixtures developed were for an all normalweight aggregate mix (0% replacement), a 50 % replacement of coarse aggregate mix, and a 100 % replacement of coarse aggregate replacement. Table 3.3 presents the representative proportions of these mixtures. These values were used as targets due so that concrete behavior could be bracketed in these limits. The *w/c* for each mixture was taken to be 0.4 as set as the maximum for pile applications exposed to salt water or potentially corrosive ground water (ACI 543 2005).

Table 3.3 – Mixture proportions from laboratory phase

Item	NW	LW50	LW100
Cement Content (pcy)	717	717	717
Water Content (pcy)	290	290	284
SSD Normalweight Coarse Aggregate (pcy)	1703	853	0
SSD Lightweight Coarse Aggregate (pcy)	0	460	992
SSD Fine Aggregate (pcy)	1361	1330	1216
Water-Reducing Admixture (oz/yd^3)	43	43	36
Total Air Content (%)	2	3	3.5
w/c	0.4	0.4	0.4

Note: 1 pcy = 0.6 kg/m^3; 1oz/yd^3 = 1.31 oz/m^3

3.1.2 Laboratory Curing

All cylinders were allowed to cure under accelerated conditions for the first 18 hours to mimic prestressing bed conditions. A typical accelerated curing profile for Charleston, SC is presented in Figure 3.2 which shows a holding period at the fresh temperature followed by a 10 °F/hr (5.6 °C/hr) increase in temperature to a maximum temperature of 160 °F (71 °C). The maximum temperature is then held for 6 hours until the prestress force is transferred or "released" to the concrete. At this time, the concrete must have achieved 3,500 psi (24 MPa). In the laboratory, the holding period was set at 3 hours which allowed the "release" time to be 18 hours. The SURE CURE ™ system manufactured by Products Engineering was used to heat the concrete test cylinders to the desired temperature profile in Figure 3.2. The SURE CURE ™ system contains 8 – 4x8 in. (10x20 cm) heated molds. Of the 8 molds, 3 cylinders were used for the 3-day tests, 3 cylinders were used for the 7-day tests, and 2 cylinders were used as "Master" cylinders in which thermocouples were inserted from the 6x12 in. (15x30 cm) match curing sleeves. The 18-hour, 1-day, 14-day, and the 28-day breaks were cured under match

curing conditions with 6x12 in. (15x30 cm) insulated sleeves that were heated along with the same temperature given to the SURE CURE ™ system as depicted in Figure 3.3.

With the SURE CURE ™ system, a curing profile as depicted in Figure 3.2 is programmed into a computer. The microprocessor then "tells" the 4x8 in. (10x20 cm) insulated molds to heat up through a thermocouple. Power/heat is then sent from the microprocessor unit to heat the insulated mold. The 6x12 in. (15x30 cm) molds are then "slaved" to the smaller SURE CURE ™ molds through a thermocouple measuring the heat supplied to the smaller mold and telling the match cure sleeves to heat at the same programmed profile.

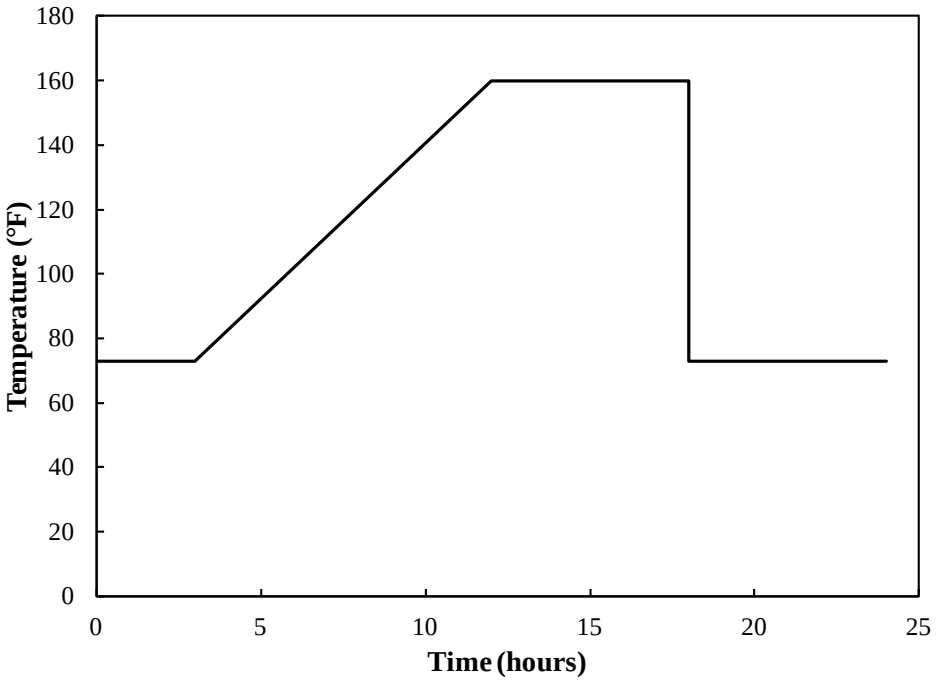

Figure 3.2. Typical pile curing profile from Charleston, SC used for laboratory curing

After initial accelerated curing, all cylinders were moved to the moist curing room with constant temperature and humidity. Cylinders remained under standard curing until time of testing.

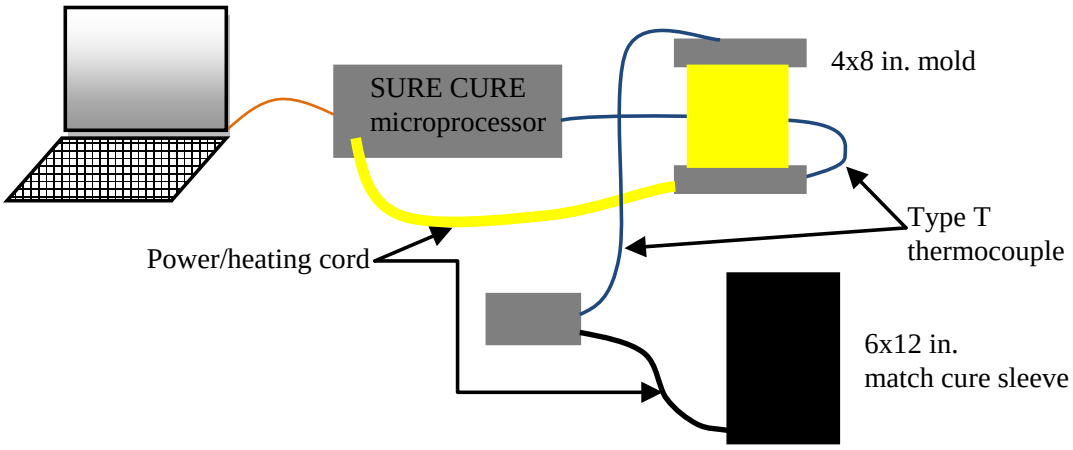

Figure 3.3. Schematic of SURE CURE ™ system

3.1.3 Concrete Laboratory Testing

Concrete testing included both fresh and hardened concrete properties. Fresh properties including the slump (ASTM C143), yield (ASTM C138), air content (ASTM C173), and fresh temperature were measured immediately after mixing. Upon fresh concrete testing, compression cylinders were made for hardened concrete testing.

Compression cylinders were then prepared for testing of modulus of elasticity and compressive strength. Standard 6x12 in. (15x30 cm) compression cylinders were prepared for 18-hour, 1-day, 14-day, and 28-day testing ages. Cylinders of 4x8 in. (10x20 cm) diameter were prepared for the 3-day and 7-day tests due to equipment availability. The 3-day and 7-day cylinders strengths were reduced 5% as mentioned earlier from Day (1994) and Neville (2011) due to several reasons pertaining to the

specimen size. The smaller size allows better consolidation of the concrete. In addition to better consolidation, the smaller size prevents certain failure planes from developing as they wood within a larger 6x12 in. (15x30 cm). The modulus of elasticity was measured in accordance with ASTM C 469 (2002) with a compressometer immediately prior to compressive strength testing. Upon completion of modulus testing, the cylinders were loaded to compressive failure according to ASTM C 39 (2009). Three 6x12 in. (15x30 cm) splitting tensile strength cylinders were prepared and tested at 28 days for the NW, LW50, and LW100 mixes according to ASTM C 496 (2004).

Additional 4x8 in. (10x20 cm) cylinders made for each concrete mixture were also tested for chloride-ion penetrability; however, the RCPT mostly gives an indication of the permeability of the concrete specimen as opposed to chloride ion penetration. Specimens of 2 in. (5 cm) thickness were cut from the cylinders using a water-cooled diamond bladed saw and tested according to ASTM C 1202 (2010). Figure 3.4 depicts the PROVE'it RCPT set up with and RLC Instrument Co. Model 164 readout. Specimens were tested at 56 days to provide a long term measure of durability.

Figure 3.4. RCPT setup

3.2 Pre-driving Modeling

3.2.1 Soil Model Development

Once the concrete was developed to show adequate fresh and hardened concrete properties from laboratory mixing, numerical models were developed to estimate the side and base resistance, as well as estimate the driveability performance. The soil model was developed from insitu testing data gathered from The Citadel Geotechnical Experimentation Site (CGES). The SPT boring from 2004 presented in Appendix B was used as it was within 100 ft (30.5 m) of an existing H-pile depicted in Figure 3.5. An idealized profile is presented in Table 3.4 along with the average SPT N-values.

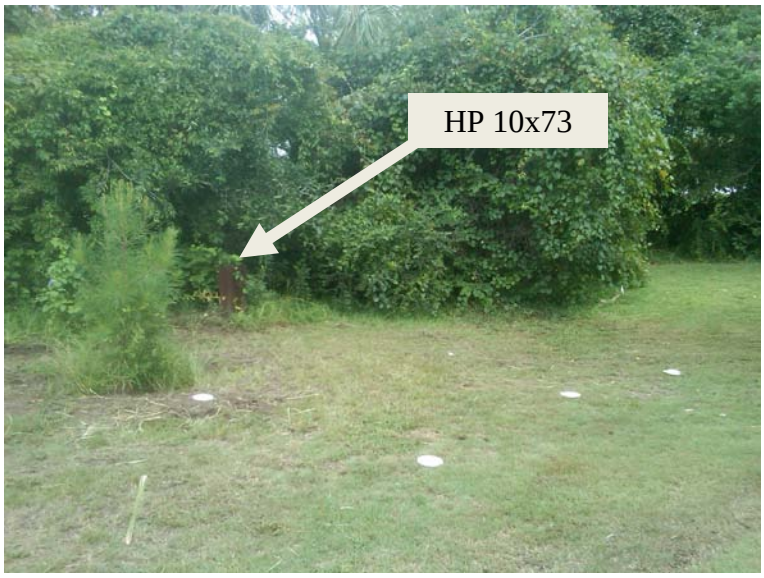

Figure 3.5. CGES existing HP 10x73 location (looking west)

Table 3.4 - Idealized soil profile of 2004 SPT CGES boring
(Soil Consultants Inc. 2004)

Layer	Depth to Bottom (ft)	Material Encountered	Average SPT N-value
Stratum 1	23	Loose Sand	6
Stratum 2	28	Soft Clay	3
Stratum 3	37	Soft to Medium Stiff Clayey Silt	8
Stratum 4	46 [1]	Soft to Medium Stiff Clayey Silt [2]	6

1. Boring terminated
2. Cooper Marl

The test piles were chosen to be driven offset from the existing H-pile. Additional insitu data for the CGES were also collected and considered, which include additional SPT data, CPT testing, and driving logs and PDA data from the existing HP 10x73 (H-pile nominal width by pile weight/linear foot). SPT N-values for the Cooper Marl (Marl) generally range from 10 to 20 blows/ft (blow/0.3 m); however, over the last

few years, CPT testing has become the predominant insitu soil investigation tool for characterizing soils in Charleston (Camp 2004). Due to the availability of SPT data at the "exact" location of the future pile driving, the SPT borings were chosen for soil models. The additional soil data are also provided in Appendix B.

Deep foundations in Charleston, SC are typically designed to bear into the Cooper Marl formation due to the weak overlain coastal plain soils. The overburden material ranges to a depth of approximately 30 to 45 ft (9 to 14 m) consisting of very soft clays and loose sands (Camp 2004). The Marl is a massive calcium rich marine deposit typically encountered from approximately 30 to 60 ft (9 to 18 m) and is generally 100 ft (30 m) thick or more (Camp and Parmar 1999). Cooper Marl typically classifies as a firm to stiff, highly plastic sandy clay or sandy silt (SC-SM) according to the Unified Soil Classification System (USCS) (Camp and Parmar 1999). The Marl is a thixotropic behaving soil which refers to the time-dependent process by which the soil is softened due to remolding followed by a return of the original, harder state (McCarthy 2002). This thixotropic behavior is also termed "pile freeze" or "pile set-up." This freeze occurs due to pile installation and the displacement and shearing of the cemented soil structure. The shearing of the soil matrix causes large excess pore pressures to develop which causes the strength of the soil to decrease due to effective stress. Over time, these excess pore pressures dissipate and return to steady state conditions causing the soil strength to increase, thereby, considerably increasing the side and base resistance of driven piles after time of driving. End of driving in non-thixotropic soils typically represents ultimate soil resistance; however, piles driven into thixotropic soils such as the Cooper Marl are typically restruck some time after the end of driving to verify the ultimate resistance.

3.2.2 Axial Resistance Model

Static axial resistance was estimated for the concrete piles using FB-Deep as mentioned in Chapter 2 (Schmertmann 1967). Piles were modeled with 50 ft (15 m) embedment. This length was chosen to achieve at least 5 to 20 ft (1.5 to 6 m) of embedment into the Cooper Marl based on borings and CPT soundings. Square PCPS piles with a width of 12 in. (30.5 cm) were modeled, and this pile size was used for field testing.

The Cooper Marl typically provides an ultimate side resistance of 2.6 ksf (125 kPa) and an ultimate base resistance of 26 ksf (1,250 kPa) for concrete pile foundations (Camp 2004). The ultimate resistance of the pile was determined using the FB-Deep estimate for side resistance above the bearing Marl. FB-Deep does not account for pile freeze; therefore, typical side and base resistance within the Marl was determined from typical unit resistance for the portion of pile embedded in the Marl.

3.2.3 Driveability Performance

In addition to determining the axial resistance of the pile, it was necessary to determine if all of the piles would drive successfully in the field. A driveability model was developed in GRL WEAP to evaluate the driving stresses and capacity predictions. Unit side and base resistances from the axial model were used as soil inputs and are located in Appendix C. Using the average SPT N-value from each layer from Table 3.4 the ultimate unit side resistance and base resistance was determined using equations found in Tables 3.5 and Table 3.6, respectively. The ultimate resistance of the piles was determined with Equation 2.1. Soil types 1 and 2 are representative of the soils within the boring, and they are the only ones presented here.

Table 3.5 – Unit side resistance for concrete piles
(Florida Bridge Software Institute 2002)

Soil Type	Description	Ultimate Unit Side Resistance (tsf)
1	Plastic-clay	2.0N(110-N)/4006.6
2	Clay-silt sand mixtures, very silty sand, silts and marls	2.0N(110-N)/4583.3

Note: 1 tsf = 95.8 kPa

Table 3.6 – Unit base resistance for concrete piles
(Florida Bridge Software Institute 2002)

Soil Type	Description	Ultimate Unit Base Resistance (tsf)
1	Plastic-clay	0.7N
2	Clay-silt sand mixtures, very silty sand, silts and marls	1.6N

Note: 1 tsf = 95.8 kPa

Unit base resistances are required for the GRL WEAP models due to the fact that, as piles are driven, their ultimate base and side resistances are overcome to penetrate deeper into the soil strata Piles are driven through different soil types with varying density or consistency, and as such, pile stresses develop within the pile and must be monitored accordingly to prevent the pile from breaking.

The estimated axial resistance was computed from FB-Deep for the overburden material and industry practice for the Marl. The resistance must also be adjusted accordingly for the Marl in the WEAP analysis. Based on conversations with local consultants, standard practice in Charleston assumes approximately $1/6^{th}$ the ultimate unit side and base resistance for the Marl in driveability models; therefore, 0.433 ksf (21 kPa)

and 4.33 ksf (210 kPa) were used for "ultimate" side and base resistance, respectively during pile driving. The piles were the modeled with the ultimate side and base resistance for the Cooper Marl to estimate the pile behavior during hard driving in which large compressive stresses can develop within the pile.

Preliminary lab testing values for the static modulus and unit weight were used depending on the replacement percentage of coarse aggregate. Table 3.7 presents preliminary pile inputs into the WEAP model. The static modulus (E_s) for the normal weight pile was selected as the default within GRL WEAP. E_s was selected for the 50 % and 100 % replacement piles based on 7-day age breaks because it was agreed that the piles would be driven at 7 days after casting. The density provided was the average fresh unit weight from the laboratory trial batches.

Table 3.7 – Pre-driving pile inputs for GRL WEAP

Input	Coarse Agg. Replacement		
	0%	50%	100%
E_s (ksi)	5000	3800	3350
Density (pcf)	150	135	120

Note: 1 ksi = 0.0069 GPa; 1 pcf = 16 kg/m^3

The pile hammer information is the final input required for a WEAP analysis. The contractor used a Junttan HHK 4A fully adjustable stroke, hydraulic hammer. Manufacturer hammer cushion information was used and a 6 in. (15 cm) thick plywood pile cushion was used. Piles were modeled with different strokes ranging from 6 in. (15 cm) to 18 in. (46 cm) with 12 in. (30.5 cm) being used to monitor the pile performance and ensure stresses were within acceptable driving stress limits along with acceptable driving times and hammer blows/ft (blows/m).

3.3 Field Work Study

Upon completion of laboratory mixing and preliminary modeling, a plan was devised to cast, drive, and test full-scale test piles in Charleston, SC. Research monies and donations by the stakeholders were the driving force of what was planned and completed. The pile manufacturer agreed to produce two piles per coarse aggregate replacement mixture; therefore, there were 6 total piles of 55 ft (17 m) in length. An additional 5 ft (1.5 m) of stick up length was added to what was modeled to ensure enough clearance for instrumentation cables and future static load testing. While placing the instrumentation, it was observed that the contractor used ½ inch diameter special strands and not ½ inch diameter prestressing strands. The cross-sectional area of ½ inch diameter special strands is 0.167 in^2 (4.24 mm^2) as opposed to ½ inch diameter stands which is 0.153 in^2 (3.89 mm^2) which will affect the effective prestress within the pile.

3.3.1 Load Test Instrumentation Plan

Certain static load testing and thermal instrumentation was selected in the event of a future static and lateral load test. Monies limited the amount of instrumentation to be placed in the piles. The 50 % NW replacement pile was chosen to be the representative mixture to be axial load tested, while the 100 % replacement pile was chosen to be laterally load tested. The normalweight piles were not instrumented for any static load test. Sister-bar strain gages depicted in Figure 3.6 were placed in the 50 % NW replacement mixture for a future static axial load test. Two strain gages were placed at three different levels within the pile. Two were placed towards the top of the pile within the overburden material.

Figure 3.6. No. 4 sister-bar strain gages

These gages were intended to measure the pile response within the overburden material. Two gages were placed at the anticipated layer change between the overburden and the Marl. The final two strain gages were placed at the expected mid-point of embedment within the Marl to measure the resistance provided by the Marl. All lead wires daylighted approximately 2.5 ft (0.76 m) from the top of the pile. Figure 3.7 presents the layout plan for strain gages within the 50 % NW replacement pile. Strain gages were tied to the outer prestressing strands as shown in Figure 3.8.

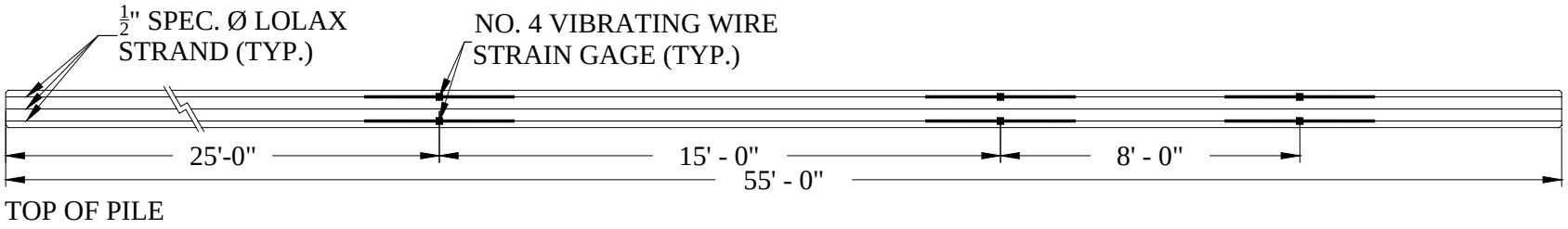

Note: 1 ft = 0.3028 m

Figure 3.7. Sister-bar strain gage layout plan

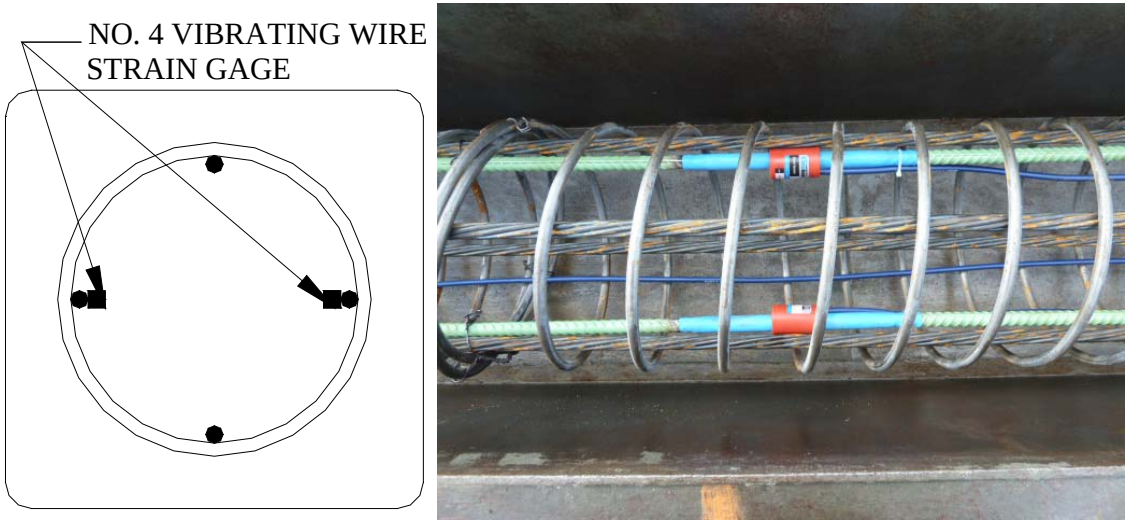

Figure 3.8. Sister-bar attachment

One of the 100 % coarse aggregate replacement piles was instrumented with 50 ft (15 m) of inclinometer casing as depicted in Figure 3.9. The casing was installed 0.5 in. (1.3 cm) from the top of the pile. The casing was installed to measure the horizontal displacement profile during a lateral load test using an inclinometer.

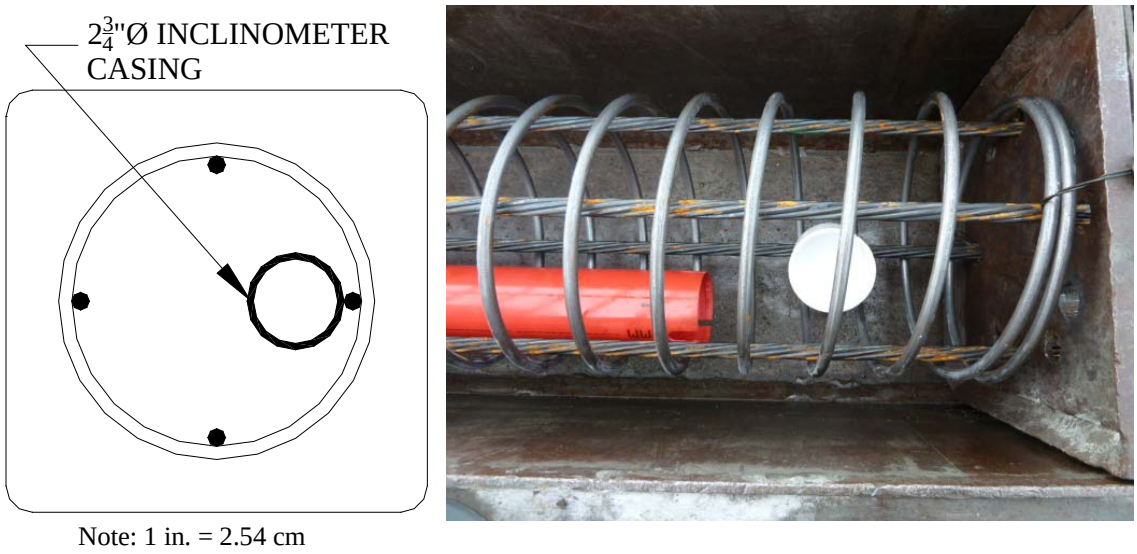

Note: 1 in. = 2.54 cm

Figure 3.9. Inclinometer casing prior to attachment

3.3.2 Heat of Hydration Thermal Instrumentation

In addition to instrumentation for the static load testing, thermocouples were placed within one of the piles from each concrete mixture to obtain a temperature profile of the piles during accelerated curing conditions. Thermocouples were also placed in a representative compressive cylinder for each mixture to measure the temperature profile closer to what the field cured cylinders would experience. Finally, thermocouples were placed in a representative cylinder to monitor the temperature profile of the standard cured specimens. The temperature profile for the standard cured specimens was used to determine a strength-maturity curve.

The thermocouples within the piles were placed at approximately the third points of the length. Figure 3.10 presents the layout of the thermocouples. These were used to

monitor the internal concrete temperature and verify how much heat was generated in the hot conditions for summer in Charleston, SC. Thermocouples were placed within the middle core of the concrete pile. Zip ties were tied in a crossing fashion as depicted in Figure 3.11 to provide a means of tying and stabilizing the thermocouple during placement and consolidation of concrete.

A Campbell Scientific® CR 1000 datalogger was used to record the thermocouple measurements. Two systems were used. One system was used in conjunction with an AM16/32B multiplexer to measure the nine thermocouples in the piles and the three field-cured cylinders and depicted in Figure 3.12. The other system only contained a datalogger to measure the temperature of the three standard-cured cylinders. These cylinders were moved with the standard cured cylinders to a moist curing room and recorded the constant concrete temperature. The programs used in recording the thermocouple measurements were set to record the temperature every five minutes for the first 24 hours and then every 15 minutes until recording was ended. Thermocouples were disconnected after 6 days from the piles and field cured specimens, because the piles were driven the following morning, and the temperature oscillated consistently along with the change in the ambient temperature. The standard-cured thermocouple cylinders were disconnected at 8 days when cylinders were to be transported back to Auburn University.

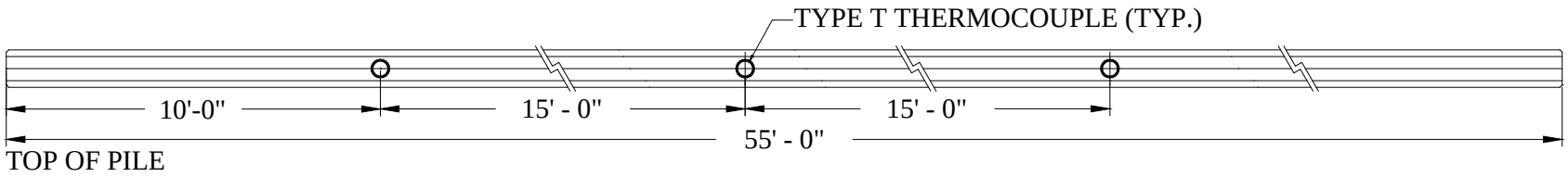

Note: 1 ft = 0.3028 m

Figure 3.10. Thermocouple layout plan

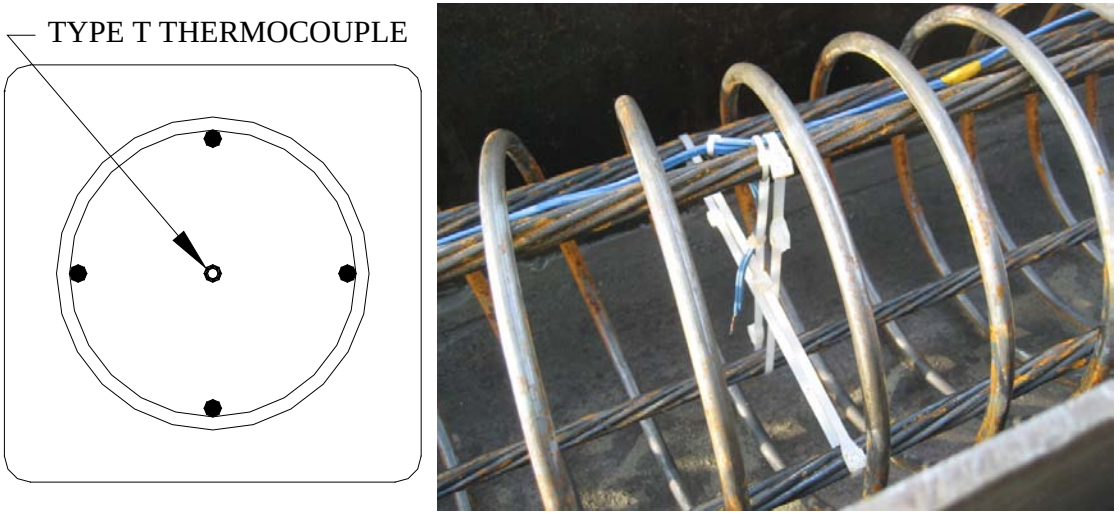

Figure 3.11. Thermocouple attachment

Figure 3.12. Datalogger with multiplexer for field cure thermocouples

3.3.3 Pile Casting and Fresh Concrete Testing

Piles were cast in successive placements along the steam curing bed. Two piles for each mix were cast side by side as shown in Figure 3.13. One ready-mixed truck was sent for each concrete mixture. Casting began at 10:00 am with air temperatures already reaching into the low 90's °F (32's °C). Concrete was sampled for fresh concrete testing from each truck after 10 ft (3 m) of pile had been placed. Concrete was then taken from the truck as necessary to fill the cylinder molds set aside for each mixture as shown in Figure 3.13. Standard fresh concrete tests were performed as was performed in the laboratory (slump, density, temperature, air).

Standard 6x12 in. (15x30 cm) cylinders were prepared for the modulus of elasticity and compressive strength and for splitting tensile strength testing. Compressive cylinder molds were prepared for 12-hr, "release", 1-day, 3-day, 7-day, 14-day, 28-day, and 91-day ages. Two cylinders were made for each age break, for each mixture, and for standard and field curing temperature cycles.

Figure 3.13. Placement of concrete in pile beds

The total number of compressive cylinder molds prepared was 96. Three 6x12 in. (15x30 cm) cylinder molds were prepared for splitting tensile strength testing for each mix bringing the total number 6x12 in. (15x30 cm) cylinders to 105 cylinders. Six additional 6x12 in. (15x30 cm) cylinders were prepared to measure concrete temperature for the strength-maturity study. Three were made for standard curing conditions, and three were prepared for field curing conditions. The total number of 6x12 in. (15x30 cm) cylinder molds prepared was 111.

All prepared cylinders were prepared for the NW and LW50 concrete mixtures. The cylinder molds for the LW100 were prepared and set out to receive concrete. Five cylinders were not prepared in error. To ensure the 28-day strength was tested, two of the cylinders designated for splitting tensile strength were reassigned to be 28-day standard cured cylinders. The 3rd designated splitting tensile cylinder was prepared and field-cured instead of standard-cured in error. The 91-day standard-cured cylinders were not

prepared; therefore, there is no indication of the long-term compressive strength under standard curing conditions. The 12-hour field-cured cylinders were not tested.

In addition to compressive cylinders, nine 4x8 in. (10x20 cm) cylinders were prepared (3 per mix) for rapid chloride-ion penetration test (RCPT). These cylinders were standard cured.

Upon prestress release at approximately 20 hours after placement, the piles were removed from the bed and placed in outside storage on the contractor's pile yard until pile driving. The pile thermocouples were disconnected at this time to handle the piles and were reconnected as soon as all the piles were set aside. The thermocouples within the field-cured cylinders were not disconnected and taken directly to the storage area. The temperature cylinders sat next to the piles until time of driving. The outside storage of piles and thermocouple cylinders is depicted in Figure 3.14. The standard-cured cylinders were all transported to the Soils and Materials Engineers (S&ME) lab in Mt. Pleasant, SC, stripped from the molds, and placed into the moist curing room until they were transported to Auburn University. The field-cured cylinders were stripped from the molds at the time of release and placed in an outside storage area on the contractor's pile casting yard.

Figure 3.14. Outside storage of piles with temperature cylinders

3.3.4 Hardened Concrete Testing of Field Specimens

The plan for hardened concrete testing was similar to testing of laboratory prepared specimens with a few exceptions. It was intended to test the modulus of elasticity and compressive strength at each age break; however, time constraints required changes to be made. While in Charleston, S&ME Inc. provided their laboratory testing facilities for compression testing. Due to the quantity of cylinders needing to be tested, it was decided that the modulus of elasticity would only be tested at "release," 7 days and 28 days. Release was approximately 20 hours. These ages were chosen because they are critical ages for the concrete within the pile. Release modulus is critical in the determination of elastic shortening. Testing at 7 days provided a modulus at the time of driving and was used in driveability models. Twenty-eight days was chosen because ACI allows designers to estimate the modulus based on 28-day strengths; therefore, this value would provide a reasonable comparison made to this predicted value.

The compressive strength was tested at every age. The 12-hour standard-cured cylinders were all tested at approximately the same time. This is noted because the 50 % replacement mixture was placed approximately an hour after the normalweight mixture, and the 100 % replacement mixture was likewise placed 2 hours after the normalweight mixture.

The splitting tensile strength was tested on three normalweight and three 50 % NW replacement mixture standard-cured cylinders at 28 days. A mix up caused the lone 100 % NW replacement mixture cylinder to be field cured as opposed to standard curing conditions. It was still tested at 28 days to provide a ball-park estimate of tensile strength.

The 4x8 in. (10x20 cm) cylinders made for each concrete mixture were also tested for chloride-ion penetrability

3.3.5 Pile Driving

Piles were driven on the campus of The Citadel in Charleston, SC at the CGES. Piles were driven in the layout depicted in Figure 3.15 with an approximate orientation of North. This layout was chosen for multiple reasons. All piles were driven in relative proximity to the existing HP 10x73 because of existing soil data and to reduce the footprint depicted in Figure 3.4. The NW piles were driven on either side of the LW50 pile to possibly be used as anchor reaction piles; however, after consulting the contractor, a dead weight axial load test was agreed to be more economical and safe. This setup also provides a normal weight pile as a reaction pile for a lateral load test of the LW100 pile.

The spacing of the piles was optimized based on the minimum specified in ASTM D1143 (1994). The minimum clear distance for a static axial load test should be at least

five times the maximum diameter of the largest test pile but not less than 7 ft (2.1 m); therefore, the clear spacing was set to be 7 ft (2.1 m) with a center-to-center spacing of 8 ft (2.4 m) (ASTM D1143).

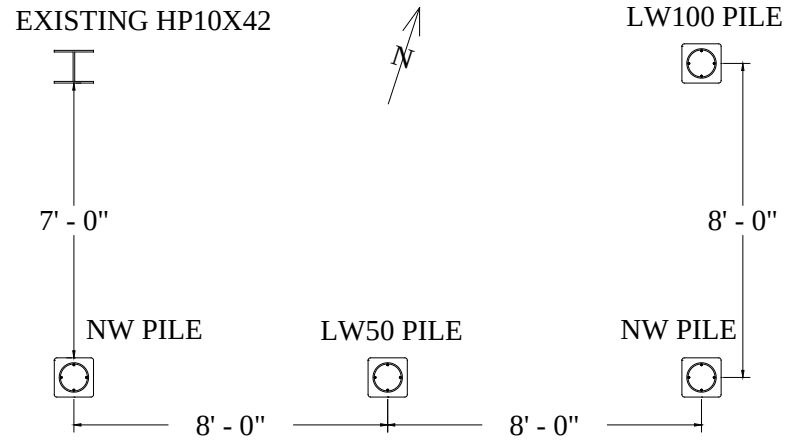

Note: 1 ft = 0.3028 m

Figure 3.15. Pile layout plan

The contractor decided to pre-drill to a depth of 10 ft (3 m). This is typical practice for pile drivers in Charleston, SC so as to get through poor, low resistance soils to begin driving. The piles would have most likely "run" or sink after the first hammer strike to this depth. This method of installation also reduces potentially harmful and high tensile stresses that develop in low and no resistance soil horizons. The contractor used a Junttan PM 16 track-mounted pile driving rig with a Junttan HHK 4A hydraulic hammer as depicted in Figure 3.16. The hammer stroke was set to 12 in. (30.5 cm) for approximately the first 30 ft (10 m) of driving (actual depth of 40 ft (12 m)) and then increased to 18 in. (46 cm) for the final 10 ft (3 m) of driving in the Marl.

Figure 3.16. Junttan PM16 with HHK 4A pile hammer

As modeled, a 6 in. (15 cm) thick plywood pile cushion was used for each pile as depicted in Figure 3.17. Each pile used a new cushion to ensure stresses within each type of concrete pile could be compared. The piles were dynamically tested for each hammer blow with the use of Pile Driving Analyzer® (PDA). The stresses within the pile were monitored in real time. In addition to monitored stresses, the hammer blows per foot (bpf) were recorded to give an indication of driving performance and resistance. A PDA estimate of the capacity after initial driving was also recorded.

Figure 3.17. 6 in. (15 cm) plywood pile cushions

The piles were restruck the following morning to obtain an idea of the resistance gain due to the pile setup within the Marl. Typically, contractors in Charleston wait 5 to 7 days to restrike the piles to obtain a long-term resistance estimate from pile setup; however, the contractor only agreed to restrike the next morning. The used pile cushions from the previous day were used during restrike. PDA was used again for stress monitoring and estimate restrike resistance of the piles. Hammer blows per inch (bpi) were recorded for restrike due to the increased capacity over time. The stroke was set at 18 in. (46 cm) which was the final stroke at end of driving. The driving was monitored for 6 in. (15 cm) of movement. After the restrike of the LW50 pile, it was driven an additional 2.5 ft (0.76 m), thereby leaving 2.5 ft (0.76 m) of stick up. This was done for

the axial load test which would be safer and more efficient. The contractor suggested adding dead weight loads.

3.3.7 Transportation and Final Curing of Cylinders

All remaining field and standard cured cylinders were brought back to Auburn University for hardened concrete testing. Remaining cylinders included the compressive test cylinders for 14, 28, and 91 days, as well as the splitting tensile strength cylinders and the 4x8 in. (10x20 cm) cylinders for RCPT testing. Four, 50-gallon (0.2-m^3) capacity plastic utility totes were used to transport the cylinders back to Auburn University. A base layer of moist sand was placed in the bottom of each tote. Cylinders were then placed in totes, and moist sand was then packed around the cylinders and on top of the cylinders. The moist sand was used to provide both a buffer between cylinders to prevent beating against one another and to prevent moisture from escaping the standard-cured cylinders. The lid of each tote was then securely fastened to the tote by use of zip ties. The cylinders were driven straight back to Auburn and placed in to the moist curing room. Field cured specimens were also placed in the moist room at this time because the piles at this point were driven into the ground which has relative constant humidity and temperature.

3.3.8 Instrumentation Baseline Readings

Strain gage readings were taken directly after casting, 2 days after release, and immediately following restrike. These readings were taken to ensure survivability of the gages from casting and driving. Baseline inclinometer readings were taken immediately after restrike of the piles.

3.4 Field-Calibrated Modeling

3.4.1 Axial Resistance

The pre-driving models were adjusted to match driving and field testing conditions encountered. Input values in FB-Deep were changed including soil thicknesses and SPT N-values based the SPT boring performed in 2002 as compared to the driving conditions incurred. The soil conditions were different than what was expected; therefore, new side resistance values were determined. The blow counts observed from pile driving were compared with the 2002 CGES SPT boring N-values to best match the field conditions. An idealized profile is presented in Table 3.8 along with the average SPT N-values.

Table 3.8 – Idealized soil profile of 2002 SPT CGES boring
(Soil Consultants Inc. 2002)

Layer	Depth to Bottom (ft)	Material Encountered	Average SPT N-value
Stratum 1	1.5	Loose Sand	2
Stratum 2	17	Medium Dense to Very Dense Sand	30
Stratum 3	29	Soft Clay	2
Stratum 4	34	Medium Dense Sand	17
Stratum 5	39	Stiff Clayey Silt	11
Stratum 6	47 [1]	Very Stiff Clayey Silt [2]	24

1. Boring terminated
2. Cooper Marl

3.4.2 Driveability

Using the adjusted axial model, more precise resistances were used in GRL WEAP to model the driving of each pile. Driving logs, internal stresses, and axial

resistance estimates were then compared with values from PDA records and axial load test data. An estimated dynamic modulus was then used in the WEAP models based on the measured wave speed from pile driving. The dynamic modulus (E_d) was estimated using Equation 3.1 where w_c is the fresh density of the normal weight concrete or the calculated equilibrium density of lightweight concrete as determined from ASTM C 567 (2005), g is the acceleration due to gravity, and c is the measured wave speed from the PDA.

$$E_d = \frac{w_c}{g} \cdot c^2 \tag{3.1}$$

3.5 Concrete Made to Simulate Charleston Temperature Conditions

Upon testing the 28-day compressive strength of cylinders prepared in Charleston, it was observed that the strengths were lower than expected for a *w/c* between 0.36 and 0.38. In an effort to understand these lower strengths; concrete batches were mixed in the laboratory with heated materials. A possible explanation of the low strengths was the high fresh concrete temperature and high ambient temperature at the time of concrete placement and field curing as mentioned in Neville (2011), Brooks et al. (2007), and Verbeck and Helmuth (1968).

An attempt to recreate Charleston concrete batch proportions was unsuccessful due to a variety of reasons including differences in aggregates between Charleston and Auburn. It was thought better to show that increased placing temperature decreases the long-term strength; therefore, the batch proportions used in preliminary laboratory mixing was used, but with heated materials.

All materials including the “butter” materials for laboratory mixing were placed in an environmental chamber for a minimum of 24 hours and set to approximately 108°F

(42°C) which was the maximum temperature that could be achieved. The lightweight aggregate was not placed in the heated environmental chamber. An attempt to heat the lightweight aggregate was unsuccessful. The lightweight aggregate "sweats" when in closed 5-gallon (0.02-m^3) buckets causing moisture to evaporate out of the lightweight aggregate pores and condense thereby changing the moisture state of the aggregate from when first batched. It was decided to batch the lightweight aggregate at room temperature expecting the other heated materials to sufficiently increase the fresh concrete temperature. The concrete temperature over time for the standard-cured cylinders was measured as in the field with a thermocouple and recorded with a datalogger. Standard cured cylinders were placed in an insulated box until the approximate time of "set" so as to prevent excessive heat loss. The temperature of the field-cured specimens was taken as the heat applied to the SURE CURE™.

At 20 hours, which represented release time in the field, the standard cured cylinders were moved to the moist curing room. The field cured cylinders were then moved into an environmental chamber set to 85 °F (29 °C) which represents the average daily ambient temperature from Charleston, SC during field concrete placement. Each cylinder was placed into an individual 5-gallon (0.02 m^3) bucket treated with lime to prevent leaching of calcium hydroxide from the hydrated cement paste. Each field-cured cylinder was allowed to cure for six additional days and then moved into the moist curing room to represent when all cylinders were transported back to Auburn and placed in the moist curing room.

4.0 PRESENTATION AND ANALYSIS OF DATA

The results from laboratory work, preliminary and final modeling, and field work are presented herein.

4.1 Laboratory Concrete Results

4.1.1 Fresh Concrete Testing Data from Laboratory Phase

Trial concrete mixtures for all normalweight aggregates, 50 % lightweight coarse aggregates, and 100 % lightweight coarse aggregates were developed based on achieving acceptable slump, density, and compressive strength data. Laboratory fresh concrete testing provided the slump, fresh density, fresh temperature, and total air content, and these results are presented in Table 4.1.

Table 4.1 – Fresh concrete testing values of lab mixtures

Fresh Test	NW	LW50	LW100
Slump (in.)	1.5	3.5	2.5
Fresh Density (pcf)	149	135	119
Fresh Temperature (°F)	73	73	74
Total Air Content (%)	3.5	4	3.5

Note: 1 in. = 2.54 cm; 1 pcf = 16 kg/m^3; F° = 1.8C° + 32

4.1.2 Hardened Concrete Properties

The modulus of elasticity and compressive strength were calculated from testing records according to ASTM C 469 (2002) and C 39 (2009), respectively. The development of compressive strength with time for all laboratory phase mixtures is presented in Figure 4.1 and Figure 4.2 presents the measured and predicted modulus of

elasticity. The predicted modulus of elasticity was determined from an equation in ACI 318 (2011) and presented in Equation 2.10. The normalweight concrete's fresh density of 149 (2,384 kg/m^3) was used; while the calculated equilibrium density of 132 pcf (2,112 kg/m^3) and 114 pcf (1,824 kg/m^3) was used for the LW50 and LW100, respectively, as determined using ASTM C 567 (2005).

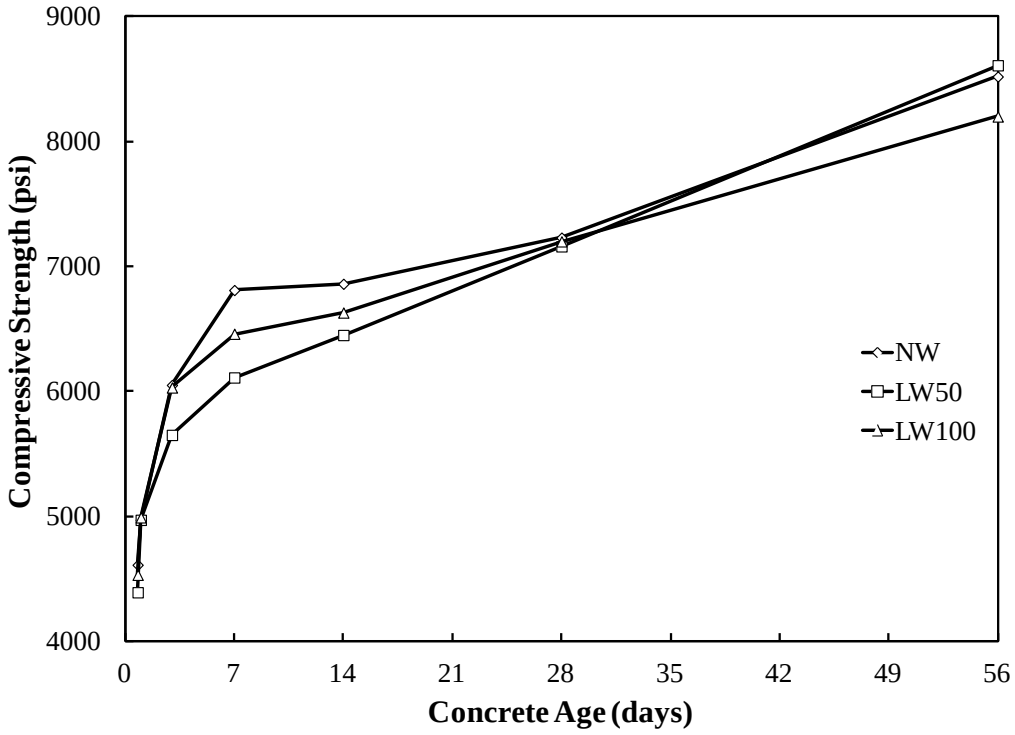

Note: 1 psi = 0.0069 MPa

Figure 4.1. Lab compressive strength versus concrete age

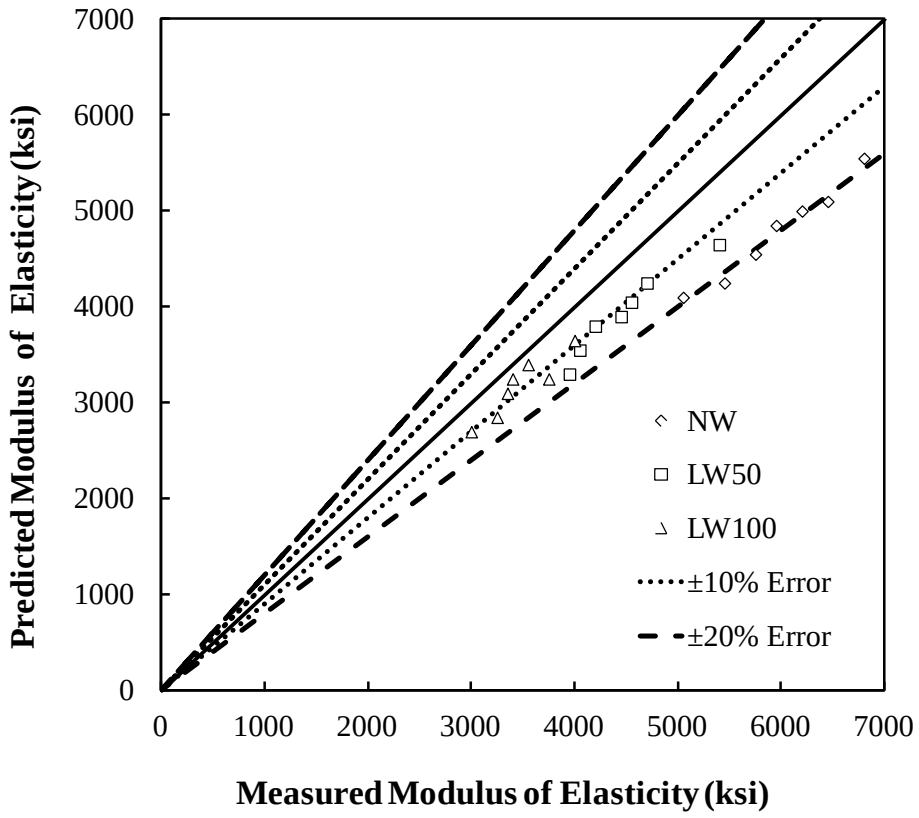

Note: 1 ksi = 0.0069 GPa

Figure 4.2. Lab predicted versus measured static modulus of elasticity

An alternative way of presenting the data above was to plot the compressive strength and static modulus with respect to coarse aggregate replacement percentage for each age and are presented in Figure 4.3 and Figure 4.4 for compressive strength and modulus of elasticity, respectively. The concrete ages presented are release at 18 hr., expected time of pile driving at 7 days, and standard pay age strength at 28 days. The measured splitting tensile strength at 28 days was 630 psi (4.3 MPa), 585 psi (4 MPa), and 590 psi (4.1 MPa) for the NW, LW50, and LW100 mixes, respectively.

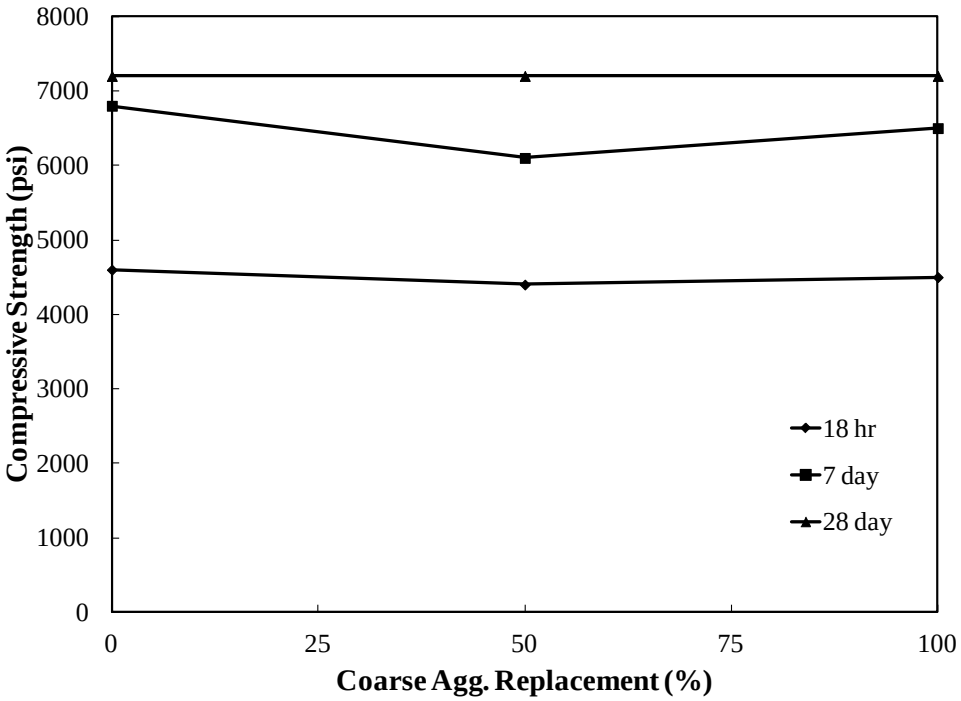

Note: 1 psi = 0.0069 MPa

Figure 4.3. Laboratory-cured compressive strength versus coarse replacement

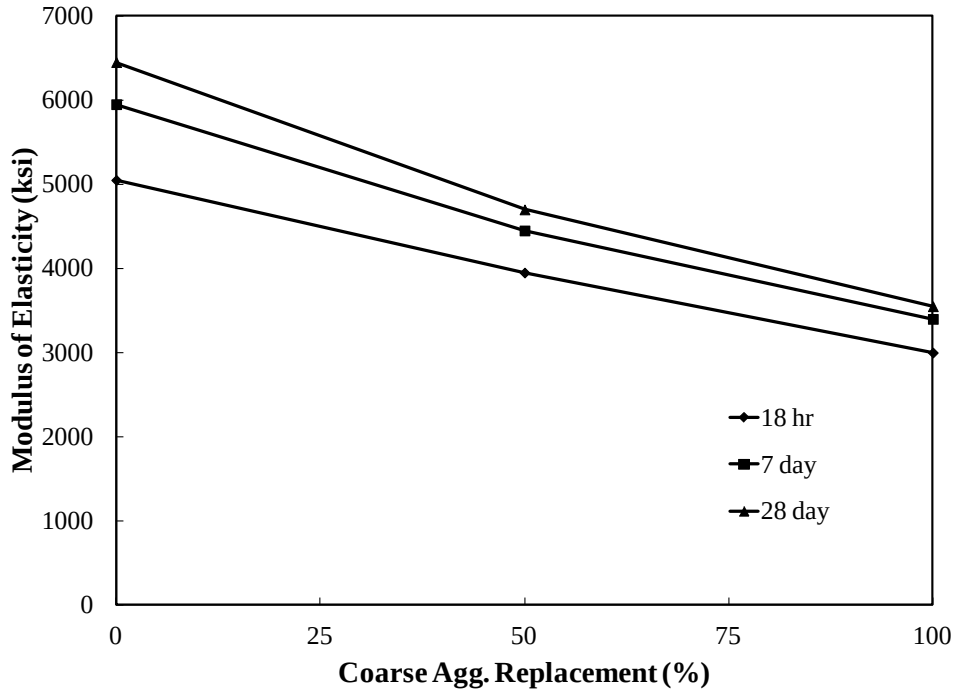

Note: 1 ksi = 0.0069 GPa

Figure 4.4. Laboratory-cured modulus of elasticity versus coarse replacement

In addition to mechanical properties, the durability of the concrete was evaluated using the RCPT, and the current passed over time (Coulombs) is presented in Table 4.2 along with the ASTM C 1202 (2010) designation for the chloride ion penetrability.

Table 4.2 – Lab RCPT values and chloride ion penetrability

Concrete Mixture	Charge Passed (Coulombs)	Cl^- Penetrability
NW	2307	Moderate
LW 50	3002	Moderate
LW 100	3081	Moderate

4.2 Pre-driving Modeling Results

4.2.1 Axial Resistance Model

FB-Deep estimated the pile to be embedded 19 ft (5.8 m) into the bearing layer; therefore, with 19 ft (5.8 m) of embedment within the Marl, the resistance from the Cooper Marl was estimated to have 198 kips (881 kN) and 26 kips (116 kN) for side and base resistance, respectively. Due to the uniqueness of the Cooper Marl and its time dependent capacity gain, the ultimate axial resistance was estimated using typical unit side and base resistance for the Marl and the FB-Deep estimate for side resistance above the bearing layer. The 31 ft (9.4 m) of overburden material provides an estimated 59 kips (262 kN) of side resistance calculated from FB-Deep; therefore, the estimated ultimate resistance for a pile embedded 50 ft (15 m) is 283 kips (1,260 kN) with approximately 224 kips (997 kN) of side and base resistance from the Marl and approximately 59 kips (262 kN) of side resistance from the overburden material. The detailed capacity report from FB-Deep is presented in Appendix C. FB-Deep does not differentiate between concrete densities; therefore, the expected soil resistance presented is an estimate of all three concrete densities.

4.2.2 Pile Driveability

The piles were modeled in GRL WEAP to estimate driving stresses for initial driving, as well as ultimate restrike strength developed from the Cooper Marl. The maximum initial and ultimate driving tensile (TS_{max}) and compressive (CS_{max}) stresses are presented in Table 4.3.

Table 4.3 – Summary of GRL WEAP driving stresses

	NW		LW 50		LW 100	
	Drive	**Restrike**	**Drive**	**Restrike**	**Drive**	**Restrike**
TS_{max} (psi)	490	330	450	280	370	220
CS_{max} (psi)	1520	1900	1470	1840	1380	1740

Note: 1 psi = 0.0069 MPa

In addition to the maximum estimated stresses, the stress distribution with depth is also presented in Figure 4.5. The AASHTO (2010) TSL and CSL were calculated using Equation 2.1b and Equation 2.2 presented in Chapter 2, respectively. The TSL was taken as the effective prestress (f_{pe}) due to being driven in a severe corrosive environment. The f_{pe} was estimated by assuming the effective stress on strands after losses is 80% of the ultimate stress of a 270 ksi (1,863 MPa) Lolax strand which is 202.5 ksi (1,397 MPa). Four, ½ in. special Lolax strands were chosen based on conversations with the contractor which provides a prestressing steel area (A_{ps}) of 0.668in^2 (430 mm^2) (4 strands·0.167in^2/strand). The effective prestress on the gross cross-sectional area was estimated to be 940 psi (6.5 MPa) ([202.5 ksi·0.668in^2]/144in^2). Therefore, the TSL during driving was taken to be 940 psi (6.5 MPa).

The compressive stress limit is a function of the 28-day compressive strength (f'_c) of the concrete and the effective prestress. The compressive strength for all three trial mixtures was approximately 7,000 psi (41 MPa). Using ACI 318 (2011), the required average compressive strength (f'_{cr}) was taken as 7,000 psi (41 MPa); therefore, f'_c was determined to be 5,700 psi (39.3 MPa) using Equation 4.1 for a specified compressive strength greater than 5,000 psi (34.5 MPa) and not enough data to establish a standard deviation.

$$f'_{cr} = 1.10 \cdot f'_c + 700\,psi \tag{4.1}$$

The CSL was calculated to be 3,900 psi (28 MPa) for pre-driving modeling for each coarse aggregate replacement mix. The compressive stresses are presented with open markers below while the tensile stresses are presented with the darkened markers. The compressive and tensile stresses are presented as “drive” which represents during initial driving and “restrike” to represent ultimate restrike conditions with pile freeze.

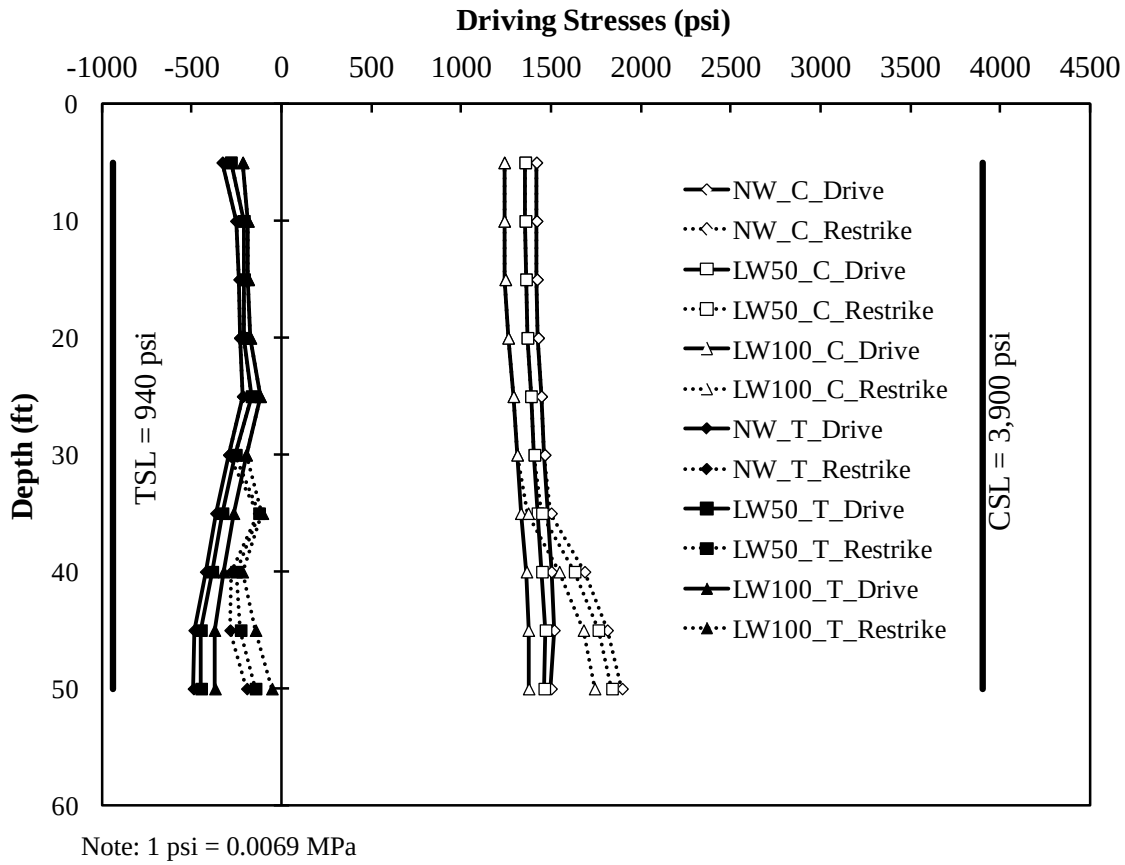

Note: 1 psi = 0.0069 MPa

Figure 4.5. GRL WEAP predicted driving stresses with depth

4.3 Field Work Results

4.3.1 Thermal Instrumentation Readings

Thermocouples placed within the piles themselves, as well as field and standard cured cylinders were used to measure the concrete temperature for up to seven days. The temperature profile for the NW, LW50, and LW100 pile are presented in Figure 4.6. The temperature readings within the pile at 10 ft (3 m), 25 ft (7.6 m), and 40 ft (12 m) were averaged and presented at one pile temperature profile with time. At the time the Datalogger was turned on, the NW, LW50, and LW100 concrete mix were already approximately 3.33 hr, 2.75 hr, and 1.33 hr old, respectively. Heat was applied approximately 3 hours after turning on the Datalogger. The gap in data presented in

Figure 4.6 corresponds to approximately 22 hours when the piles were removed from the forms and the thermocouples were temporarily disconnected to move the datalogger safely with the piles. Temperature was measured for 6 days, and then the thermocouples were disconnected so as to transport the piles for driving at 7 days after casting. Concrete cylinders were also prepared to measure the temperature development in the standard- and field-cured compressive cylinders. Cylinder thermocouple readings are presented in Figure 4.7.

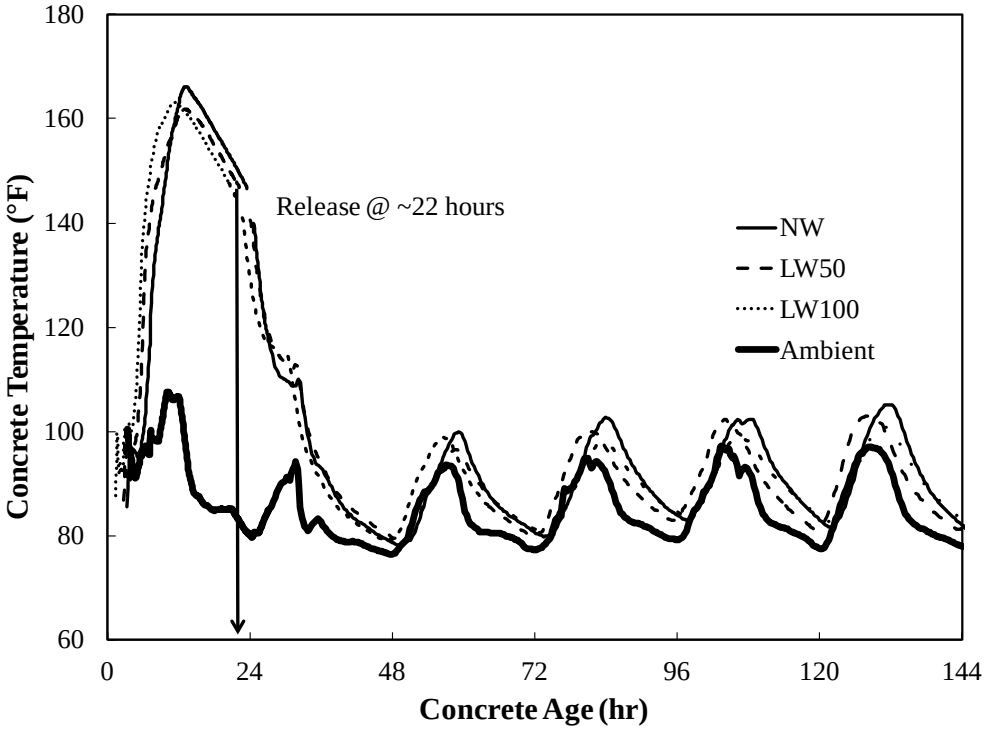

Figure 4.6. Temperature development within the piles

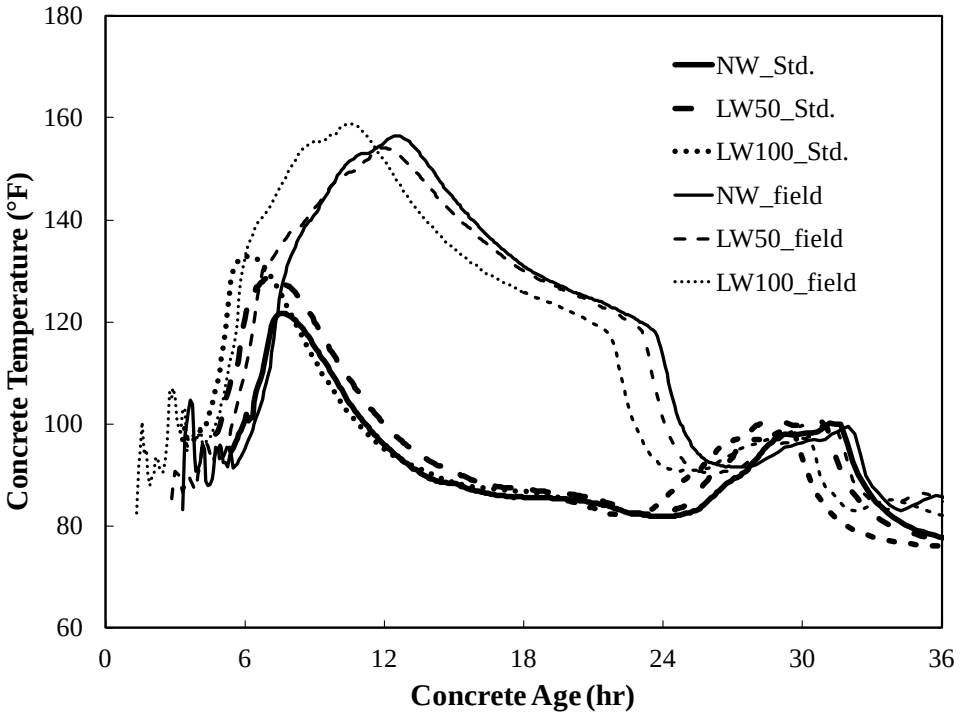

Figure 4.7. Temperature development within the compression cylinders

In addition to the thermocouples reading the internal concrete temperature, the heat was recorded coming from the boiler to the steaming beds. The supplied boiler temperature is presented in Figure 4.8. The actual readout is depicted in Appendix E as a circle graph. The final piles were cast at approximately 12:00 noon, and heat was applied at approximately 3:15 PM. Accelerated heating was supplied to the piles for approximately 15 hours.

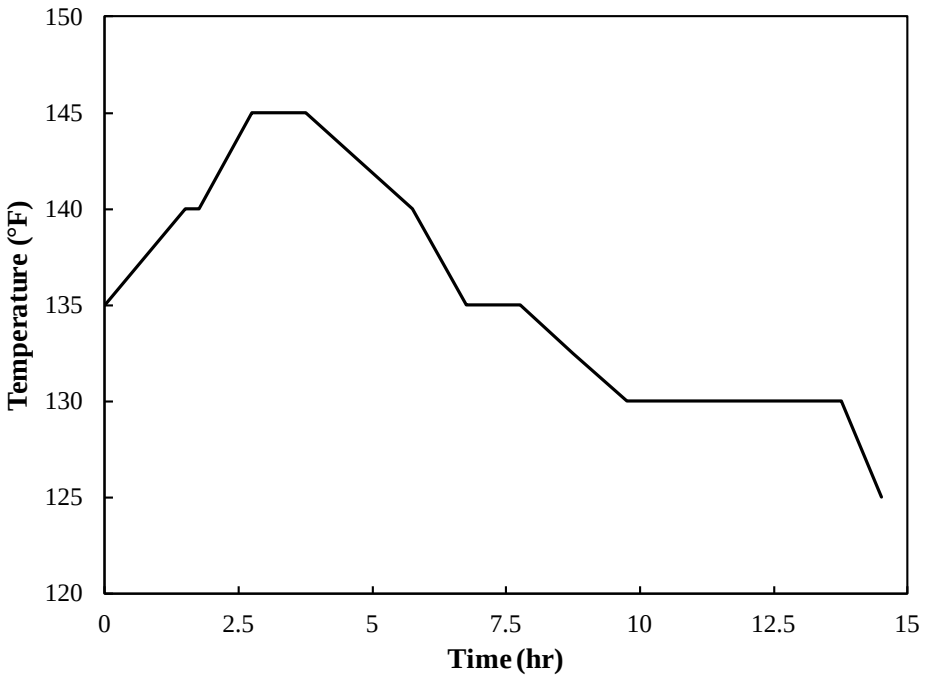

Note: 1 °F = 1.8°C +32

Figure 4.8. Applied heat profile

4.3.3 Concrete Pile Mixtures and Fresh Testing

Concrete was produced in 5 yd^3 (3.8 m^3) batches and brought to the pile yard in ready-mixed trucks. The concrete truck tickets are located in Appendix E which provides the batch numbers, as well as the time the concrete was batched. The tickets have a section for "water added" which differs from what was actually requested and added at the pile yard to increase workability. Table 4.4 presents the batching weights along with the actual additional water added to improve workability at the time of placement.

.

Table 4.4 – Concrete pile batching weights

Item	5 yd^3 Batches		
	NW	LW50	LW100
Cement Content (lb)	3565	3595	3580
Water Content (lb)	920	836	811
Normalweight Coarse Aggregate (lb)	9380	4540	0
Lightweight Coarse Aggregate (lb)	0	2320	5080
Fine Aggregate (lb)	6180	6980	7580
Daratard 17 (oz)	105	0	0
Darex II (oz)	21	0	0
WRDA 64 (oz)	0	180	177
Water Added (lb)	42	42	84

Note: 1 yd^3 = 0.76 m^3; 1lb = 0.45 kg

The free water (FW) is the amount of water above absorption capacity (AC) presented as a percentage. The aggregate moisture properties and SSD bulk specific gravities are presented in Table 4.5. The aggregate moisture content (MC) is the sum of AC and FW. The absorption capacity of the granite and sand were taken from the South Carolina DOT list of Qualified Products. Martin Marietta granite and Palmetto sand were used as presented in Table 3.2. The lightweight aggregate properties were provided from the supplier.

Table 4.5 – Concrete pile aggregate properties

Item	Absorption Capacity (%)	Free Water (%)	Aggregate Moisture (%)	SSD BSG
Normalweight Coarse Aggregate	0.5	0.3	0.8	2.67
Lightweight Coarse Aggregate	6	2	8	1.52
Fine Aggregate	0.1	5	5.1	2.65

The total weight of water when all aggregates are in the SSD moisture state (W_{water_total}) was needed to estimate the actual *w/c* of the concrete batches. W_{water_total} was calculated using Equation 4.2 where W_{water_batch} is the weight of water batched,

W_{water_added} is the weight of water added at the pile casting yard, and W_{water_NW}, W_{water_LW}, and W_{water_FA} is the difference in weight of water from batched aggregate weight to the SSD weight of the normalweight aggregates, lightweight aggregates, and fine aggregates.

$$W_{water\_total} = W_{water\_batch} + W_{water\_added} - \left(W_{water\_NW} + W_{water\_LW} + W_{water\_FA}\right) \quad (4.2)$$

The weight of the batched aggregate (W_{agg}) is the weight of either the normalweight, lightweight, or fine aggregates, respectively (W_{agg_NW}, W_{agg_LW}, or W_{agg_FA}). The weight of the oven dry aggregate (W_{OD_agg}) is the weight of either the normalweight, lightweight, or fine aggregates, respectively (W_{OD_NW}, W_{OD_LW}, or W_{OD_FA}) was determined using Equation 4.3. The weight of normalweight, lightweight, or fine aggregates in the SSD state (W_{SSD_agg}) was calculated using Equation 4.4. The difference in water from SSD and batched aggregate weights (W_{waer_agg}) as defined (W_{water_NW}, W_{water_LW}, or W_{water_FA}) was determined from Equation 4.5. The values computed are presented in Table 4.8 with the calculated *w/c* ratio. The SSD mixture proportions along with the fresh concrete testing data of slump, fresh density, fresh temperature, and total air content are presented in Table 4.7. The following equations may be found in Neville (2011).

$$W_{OD\_agg} = \frac{W_{agg}}{\left[1 + \left(AC + FW\right)/100\right]} \quad (4.3)$$

$$W_{SSD\_agg} = W_{OD\_agg} \cdot \left[1 + \left(\frac{AC}{100}\right)\right] \quad (4.4)$$

$$W_{water\_agg} = W_{SSD\_agg} - W_{agg} \quad (4.5)$$

Table 4.8 – Concrete pile estimated *w/c* as-batched

Weight (lb)	NW	LW50	LW100
$W_{water\_batch\ (lb)}$	920	836	811
$W_{water\_added\ (lb)}$	42	42	84
$W_{water\_NW\ (lb)}$	-28	-14	0
$W_{water\_LW\ (lb)}$	0	-43	-94
$W_{water\_FA\ (lb)}$	-294	-332	-361
$W_{water\_total\ (lb)}$	1284	1267	1350
$W_{cement\ (lb)}$	3565	3595	3580
w/c	0.36	0.35	0.38

Note: 1 lb = 0.45 kg

Table 4.7 – Fresh batch proportions and concrete testing values

Item	NW	LW50	LW100
Cement Content (pcy)	713	719	716
Water Content (pcy)	248	245	253
Normalweight Coarse Aggregate (pcy)	1870	905	0
Lightweight Coarse Aggregate (pcy)	0	455	997
Fine Aggregate (pcy)	1177	1330	1444
Daratard 17 (oz/yd^3)	21	0	0
Darex II (oz/yd^3)	4.2	0	0
WRDA 64 (oz/yd^3)	0	36	35.4
Water Added (pcy)	8.4	8.4	16.8
w/c	0.36	0.35	0.38
Slump (in.)	6	3.75	3
Fresh Density (pcf)	144	137	126
Fresh Temperature (°F)	96	100	94
Total Air Content (%)	3.75	2	3.25

Note: 1pcy = 0.6 kg/m^3; 1oz/yd^3 = 1.31 oz/m^3; 1 in. = 2.54 cm; 1 pcf = 16 kg/m^3; F° = 1.8C° + 32

4.3.4 Hardened Concrete Properties of Pile Concrete

As in the laboratory study, the modulus of elasticity and compressive strength were measured at multiple ages to monitor their development with time. The standard-

and field-cured compressive strength data are presented in Figure 4.9 and Figure 4.10, respectively. The predicted modulus of elasticity (E_c) from ACI 318 (2011) and Equation 2.10 is also presented with the measured static modulus of elasticity in Figure 4.11. The measured w_c of 144 pcf (2,304 kg/m^3) was used for the normalweight concrete; whereas, the calculated equilibrium density of 133 pcf (2,128 kg/m^3) and 123 pcf (1,968 kg/m^3) was used for the LW50 and LW100, respectively. The compressive strength and modulus of elasticity with respect to coarse aggregate replacement is presented in Figure 4.12 and Figure 4.13, respectively.

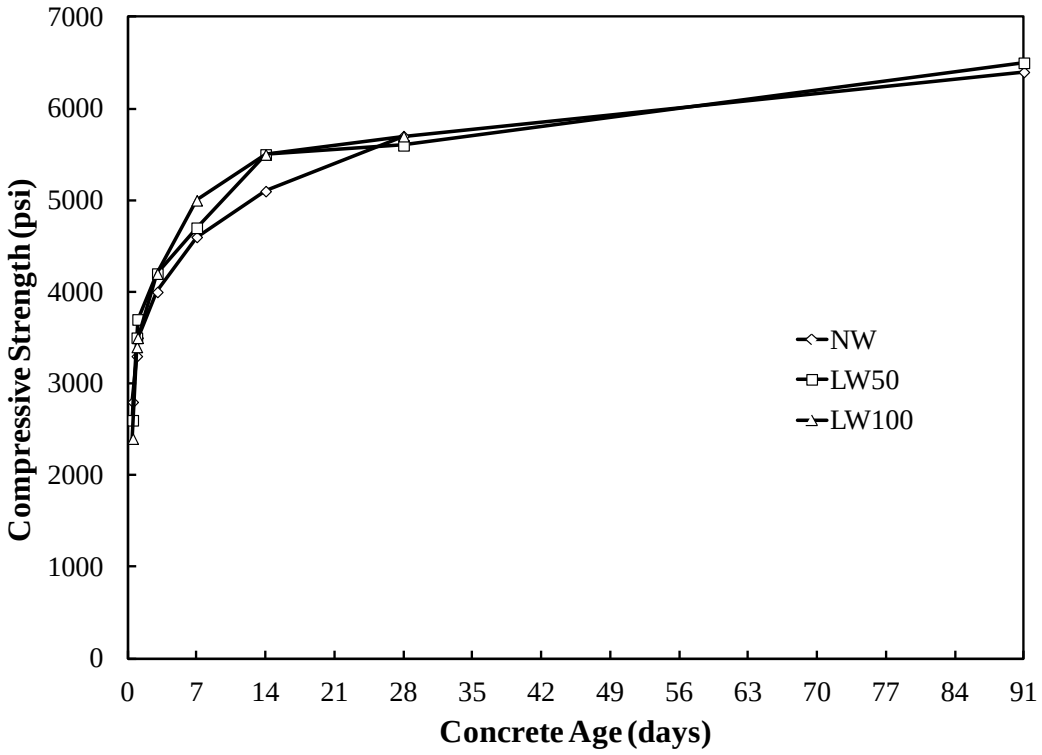

Note: 1 psi = 0.0069 MPa

Figure 4.9. Charleston standard-cured compressive strength versus concrete age

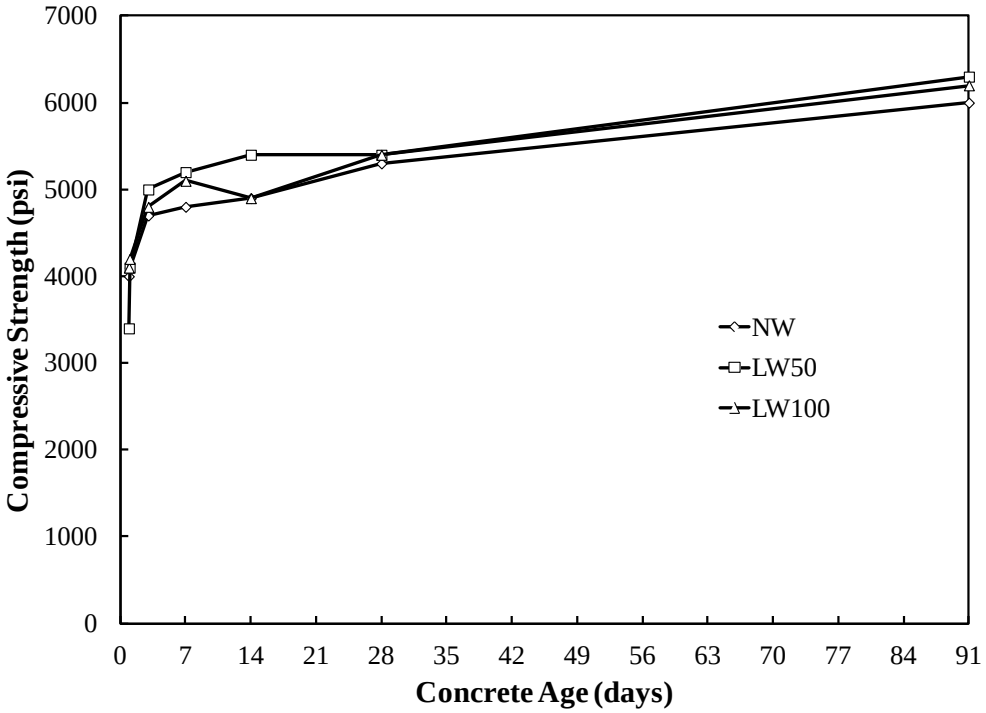

Note: 1 psi = 0.0069 MPa

Figure 4.10. Charleston field-cured compressive strength versus concrete age

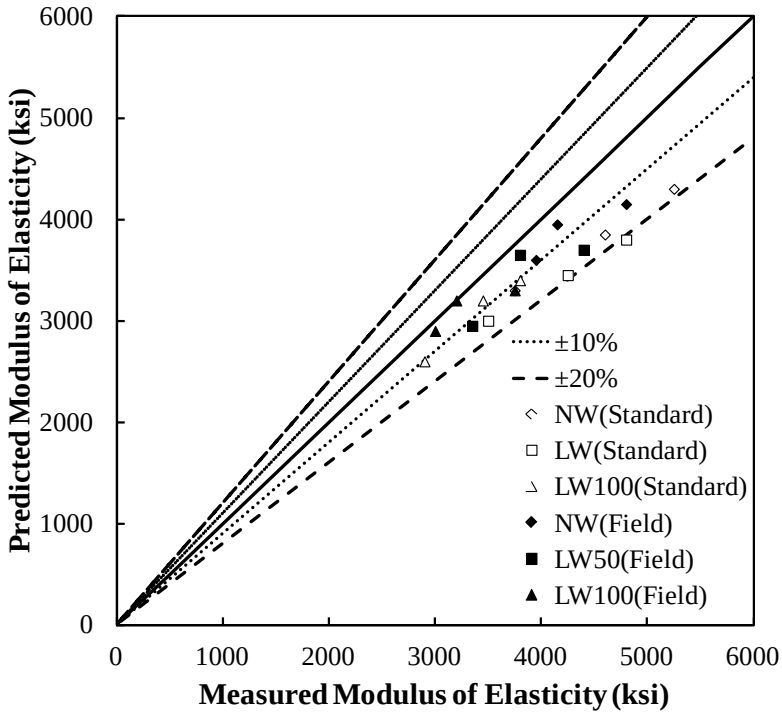

Note: 1 ksi = 0.0069 GPa

Figure 4.11. Field-scale predicted versus measured elastic modulus

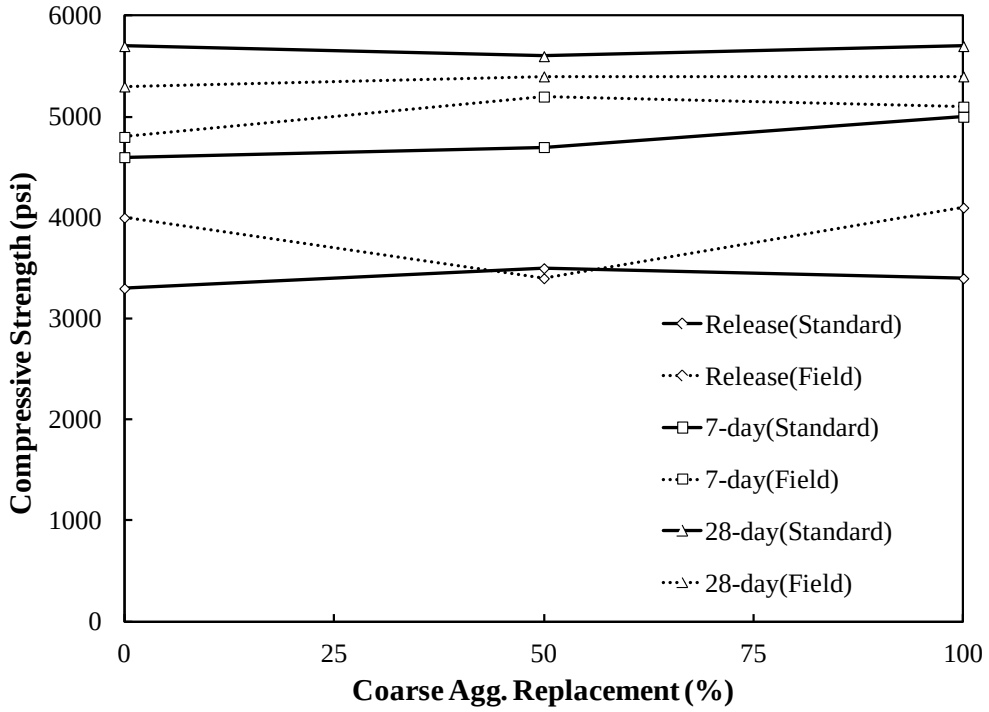

Note: 1 psi = 0.0069 MPa

Figure 4.12. Charleston compressive strength versus coarse aggregate replacement

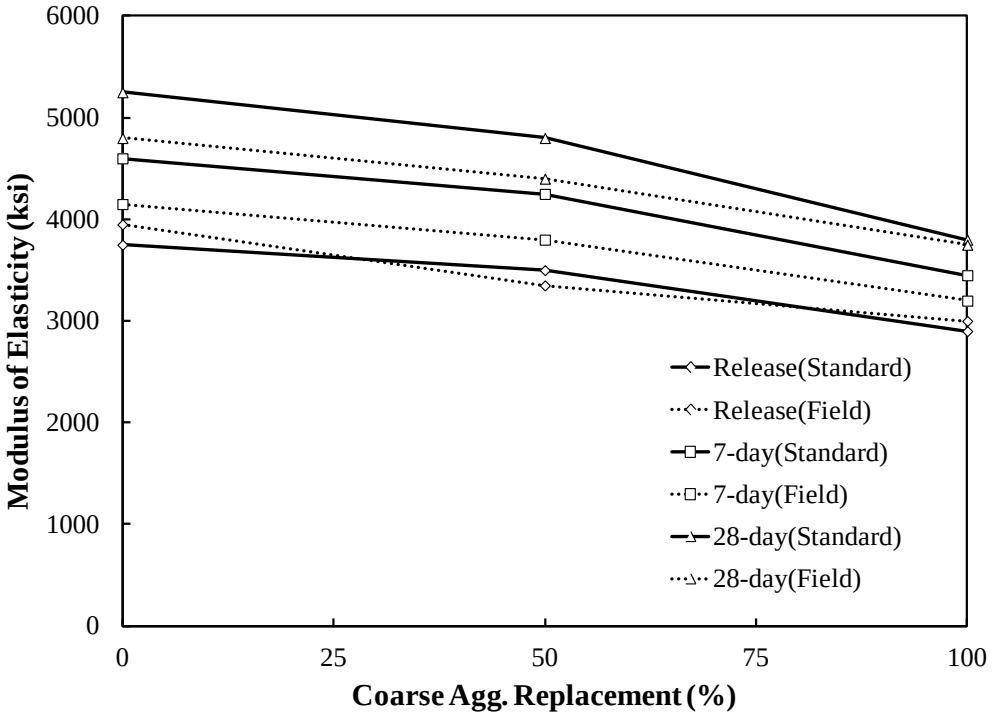

Note: 1 ksi = 0.0069 GPa

Figure 4.13. Charleston modulus of elasticity versus coarse aggregate replacement

The 28-day splitting tensile strengths of the NW and LW50 concrete are 400 psi (2.8 MPa) and 360 psi (2.5 MPa), respectively. The splitting tensile test data are presented in Appendix F.

The RCPT values at 91 days are presented in Table 4.8 along with their ASTM C 1202 (2010) designation for chloride ion penetrability.

Table 4.8 – Chloride ion penetrability of concrete pile mixtures

Concrete Mix	Charge Passed (Coulombs)	Cl^- Penetrability
NW	4364	High
LW 50	6372	High
LW 100	6119	High

4.3.5 Pile Driving Results

During pile driving, the hammer blows per foot (BPF) were recorded with pile depth. The driving logs for each pile are presented in Appendix G. Piles were denoted as Pile NW(A), Pile LW50, Pile NW(B), and Pile LW100. Pile LW50, Pile NW(B), and Pile LW100 were PDA tested.

PDA traces during initial driving at 15 ft (4.6 m), 30 ft (9.1 m), and 50 ft (15.2 m) embedment for the NW and LW50 piles are presented below along with traces at 50 ft (15.2 m) for LW100 pile. A broken gage on the LW100 pile was replaced after 35 ft of pile driving; therefore, only the trace at 50 ft (15.2 m) is presented. Figure 4.14 presents the PDA traces during driving for the NW pile, Figure 4.15 presents the PDA traces during driving for the LW50 pile, and Figure 4.16 presents the PDA trace for the LW100 pile during driving. The separation of the gray lines in the following figures represents a time of *2L/c*. The PDA traces at restrike and estimated CAPWAP capacities are presented Appendix G.

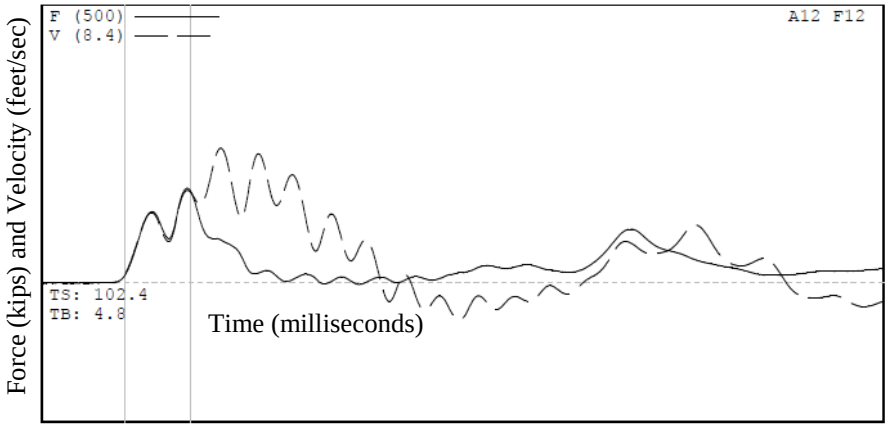

a

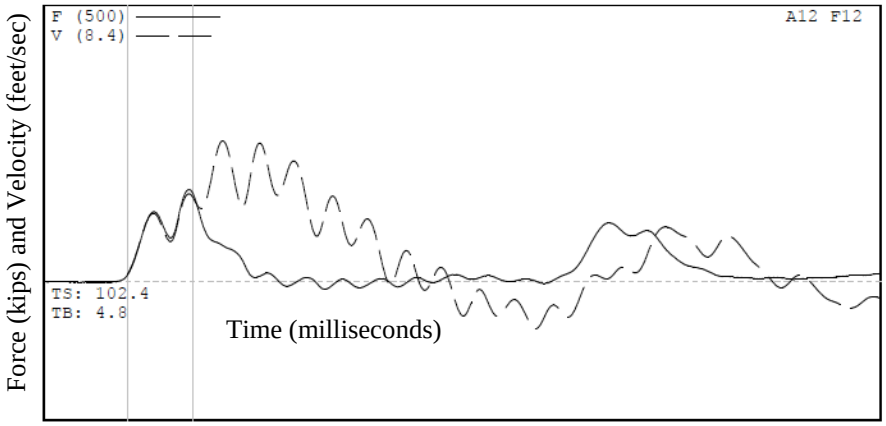

b

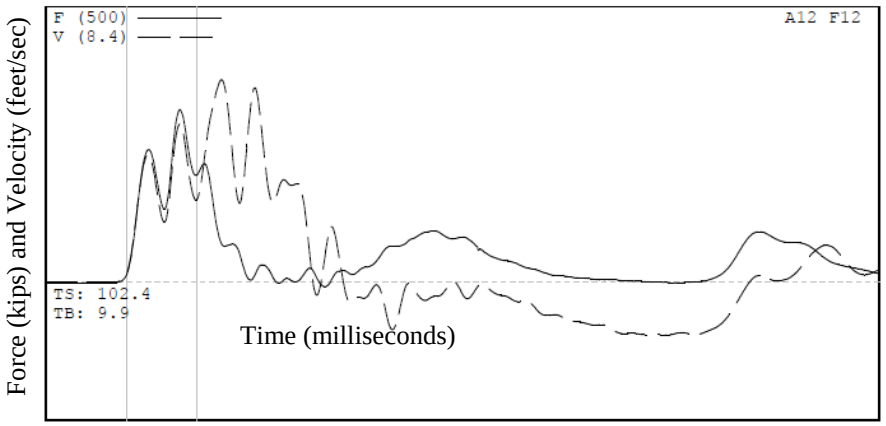

c

Figure 4.14. PDA traces during driving for NW pile a) 15 ft embedment b) 30 ft embedment c) 50 ft embedment

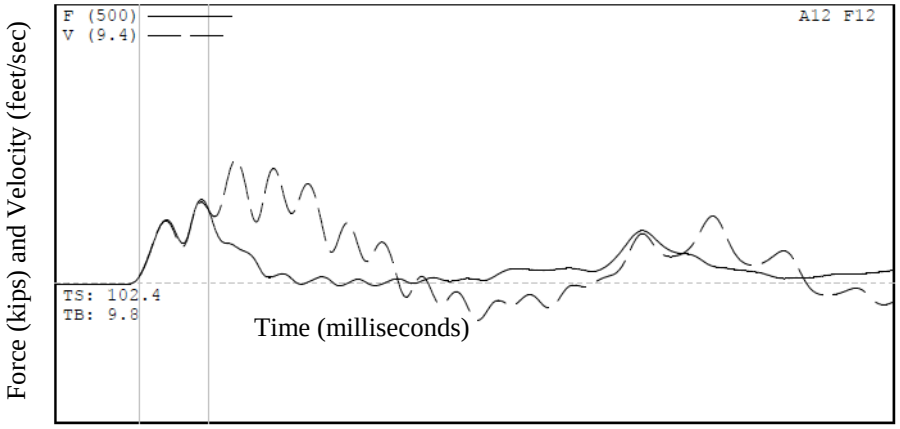

a

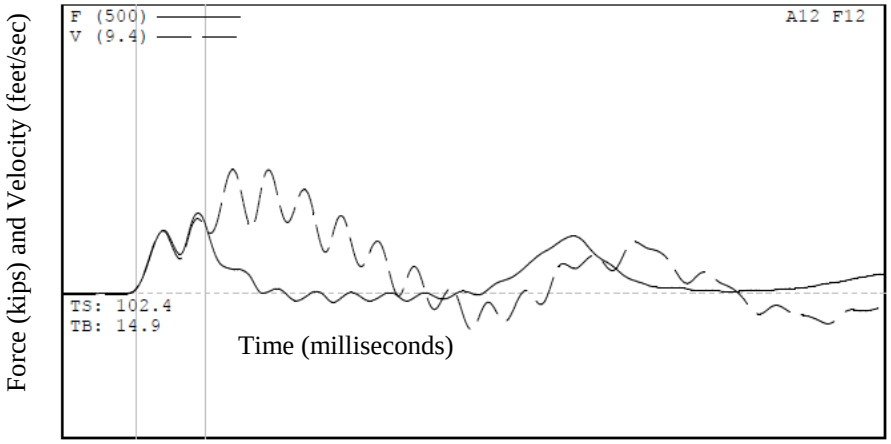

b

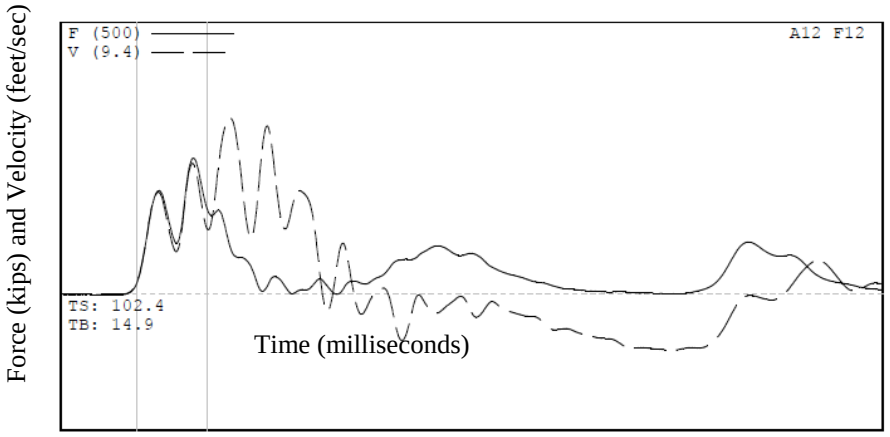

c

Figure 4.15. PDA traces during driving for LW50 pile a) 15 ft embedment b) 30 ft embedment c) 50 ft embedment

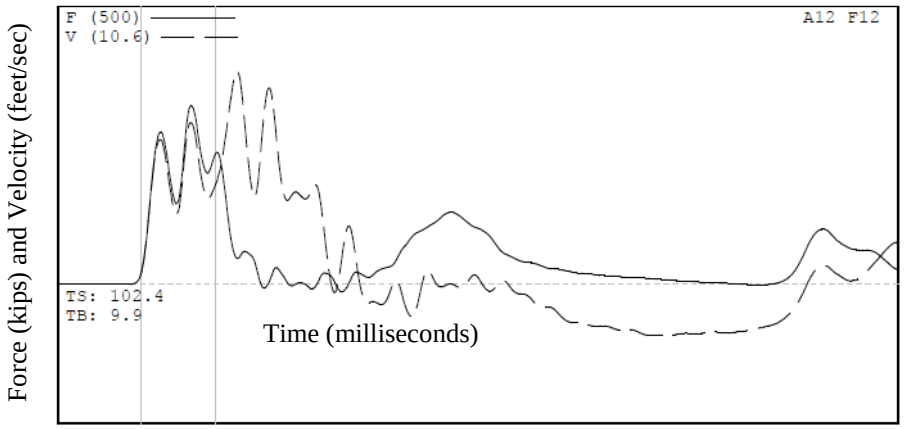

Figure 4.16. PDA trace during driving for the LW100 pile at 50 ft embedment

In addition to the force and velocity wave traces from the piles, the reflected wave up and displacement traces are presented for the NW and LW50 pile at 15 ft (4.6 m), 30 ft (9 m), and 50 ft (15.2 m) and at 50 ft (15.2 m) for the LW100 pile in Figure 4.17, 4.18, and 4.19, respectively.

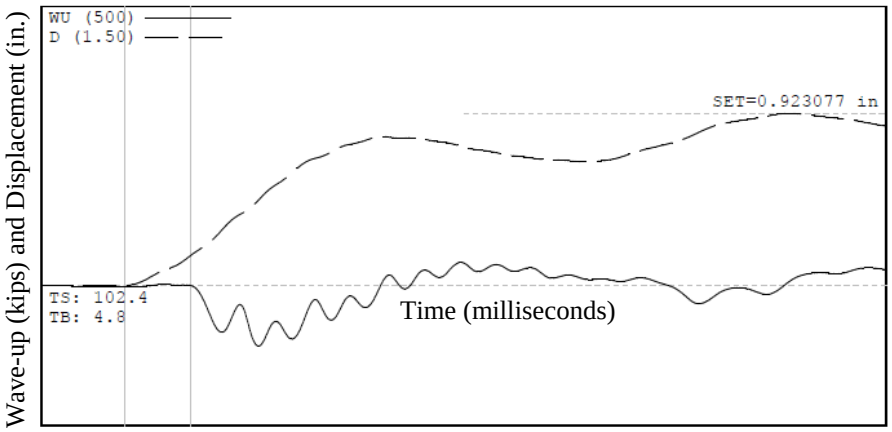

a

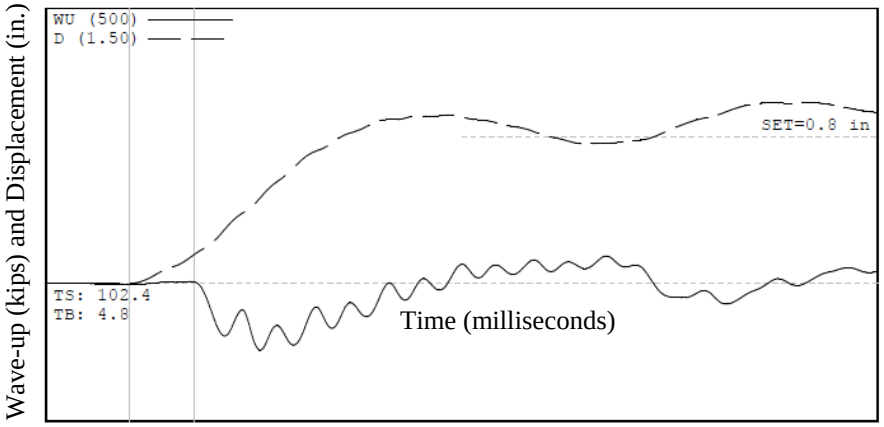

b

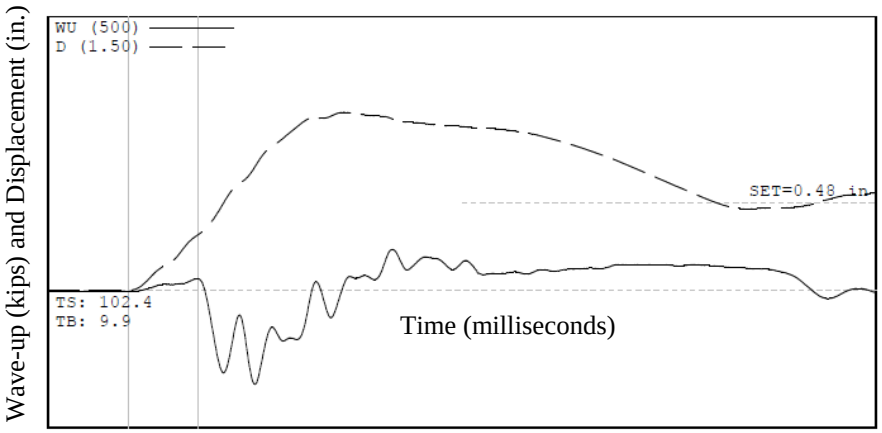

c

Figure 4.17. PDA traces of wave-up and displacement for the NW pile at a) 15 ft embedment b) 30 ft embedment and c) 50 ft embedment

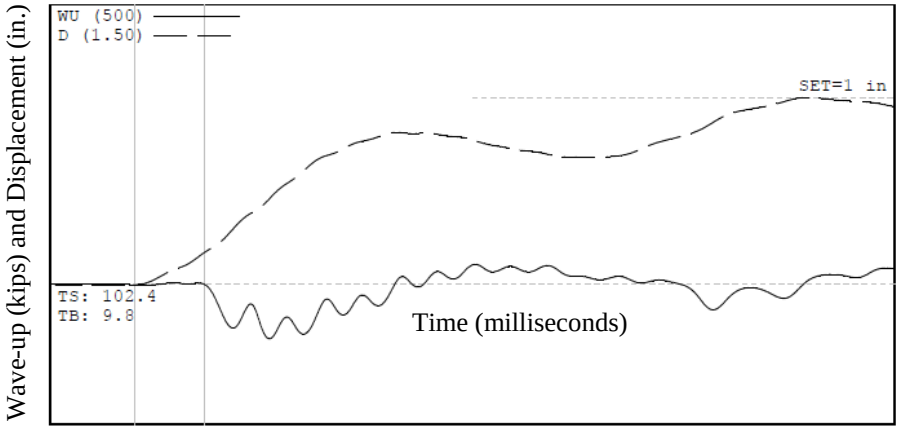

a

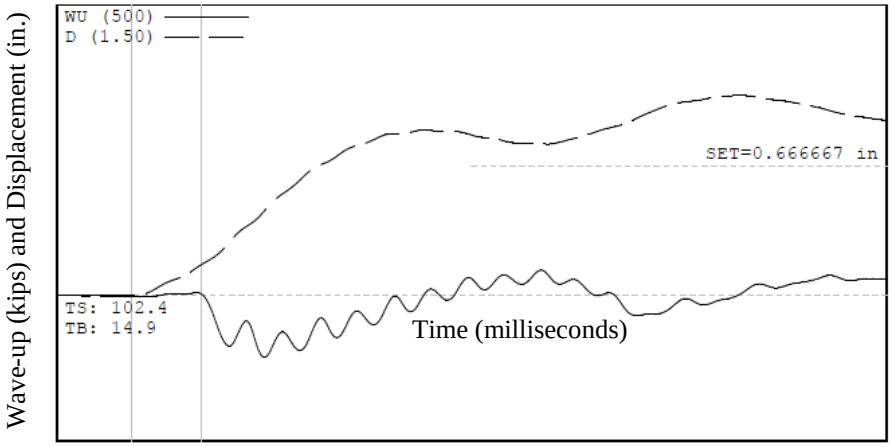

b

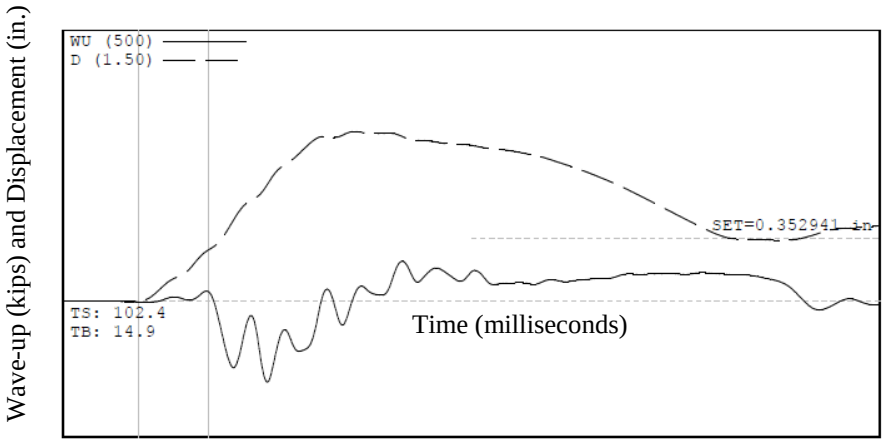

c

Figure 4.18. PDA traces of wave-up and displacement for the LW50 pile at a)15 ft embedment b) 30 ft embedment and c) 50 ft embedment

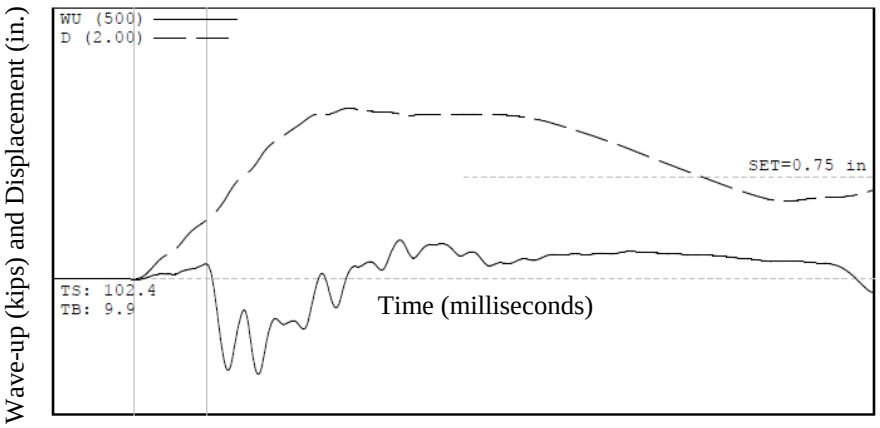

Figure 4.19. PDA trace of wave-up and displacement for the LW100 pile at 50 ft embedment

PDA testing also provided data with the depth of the pile which, most importantly, include the tensile and compressive stresses within the pile and is presented in Figure 4.20 for all piles at the end of driving. The CSL was decreased based on actual pile concrete strength. CAPWAP estimated resistance after 1 day of pile set up shows and an approximate resistance of 265 kips (1,178 kN), 202 kips (898 kN), and 213 kips (947 kN) for the NW, LW50, and LW100 piles, respectively. All PDA data provided by S&ME are summarized in Appendix G.

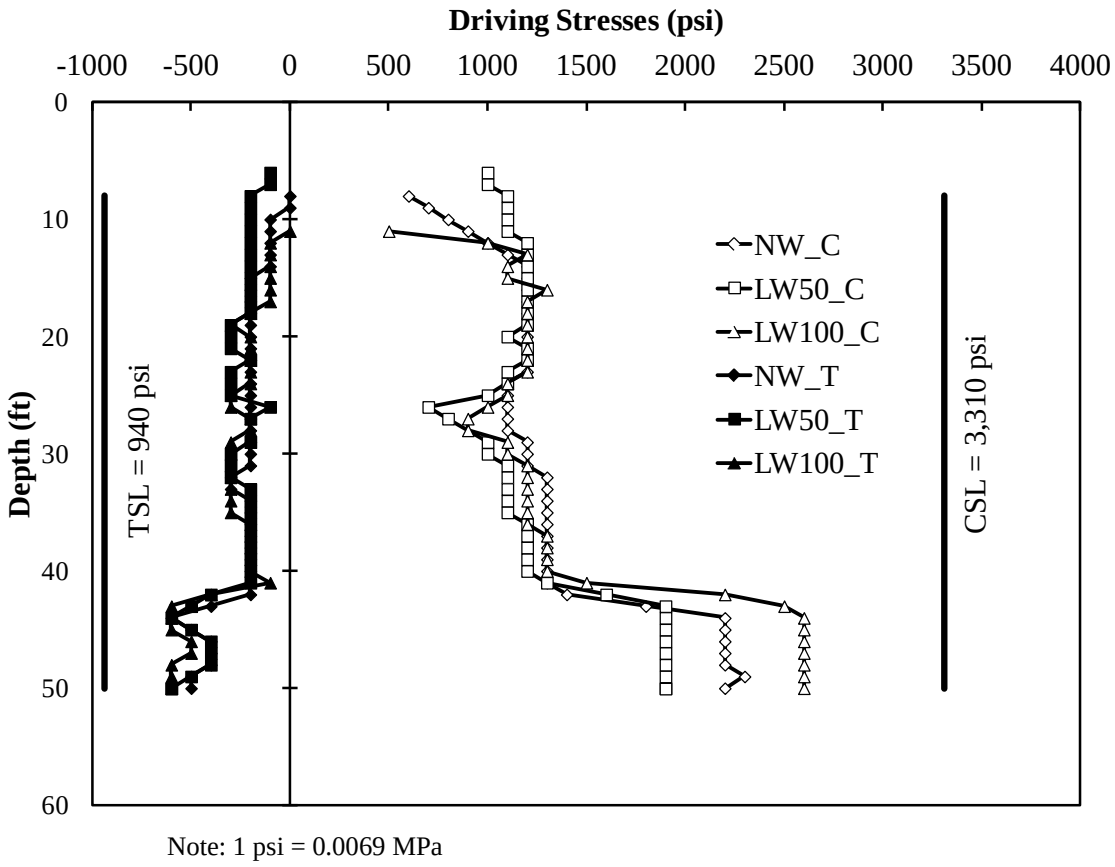

Note: 1 psi = 0.0069 MPa

Figure 4.18. PDA measured driving stresses with depth

The following morning restrike data are presented in Table 4.9 in which the hammer blows per inch (BPI) were recorded for a maximum penetration of 6 in. (15 cm). Piles were restuck beginning with Pile LW100 and ending with Pile LW50. The equivalent blows per foot (BPF) are presented to compare to initial driving data.

Table 4.9 – Restrike data on PDA tested piles

Restrike Pile LW50		**Restrike Pile NW(B)**		**Restrike Pile LW100**	
Penetration (in)	**BPI (BPF)**	**Penetration (in)**	**BPI (BPF)**	**Penetration (in)**	**BPI (BPF)**
1	6 (72)	1	9 (108)	1	4 (48)
2	4 (48)	2	6 (72)	2	n/a
3	4 (48)	3	7 (84)	3	4 (48)
4	3 (36)	4	6 (72)	4	4 (48)
5	3 (36)	5	6 (72)	5	4 (48)
6	4 (48)	6	6 (72)	6	4 (48)

4.4 Concrete Made to Simulate Charleston Temperature Conditions

4.4.1 Fresh Concrete Testing

Using essentially the same mixture as from the preliminary laboratory mixing, all materials were heated excluding the lightweight material. Table 4.10 presents the simulated hot mixtures with slight changes in the LW50 and LW100 from previous laboratory mixing due to a slight change in the fineness modulus used for the sand from 2.42 to 2.45. The 2.42 was used in early laboratory mixing due to a mix up not noticed until after mixing the heated NW mix. The fresh concrete testing data are presented in Table 4.11.

Table 4.10 – Mix proportions of heated lab mixtures

Item	NW	LW50	LW100
Cement Content (pcy)	717	717	717
Water Content (pcy)	290	290	284
SSD Normalweight Coarse Aggregate (pcy)	1703	886	0
SSD Lightweight Coarse Aggregate (pcy)	0	473	1031
SSD Fine Aggregate (pcy)	1361	1267	1149
Water-Reducing Admixture (oz/yd^3)	43	43	43
Total Air Content (%)	2	3	3.5
w/c	0.4	0.4	0.4

Note: 1 pcy = 0.6 kg/m^3; 1 oz/yd^3 = 1 oz/m^3

Table 4.11 – Fresh concrete testing values of heated lab mixtures

Fresh Test	NW	LW50	LW100
Slump (in.)	0.5	2.5	2.5
Fresh Density (pcf)	149	134	118
Fresh Temperature (°F)	91	93	92
Total Air Content (%)	3	3	3.25

Note: 1 in. = 2.54 cm; 1 pcf = 16 kg/m^3; F° = 1.8C° + 32

4.4.2 Compressive Strength Development

The only hardened concrete testing conducted on the hot mixtures was compressive strength testing for the simulated standard and field curing compressive cylinders. The concrete strength development for the standard- and-field curing is presented in Figure 4.21. The temperature with respect to time for each mixture is presented in Figure 4.22. The heat applied is an estimation of concrete temperature for the field cured specimens; however, the actual temperature was not measured for the simulated field curing.

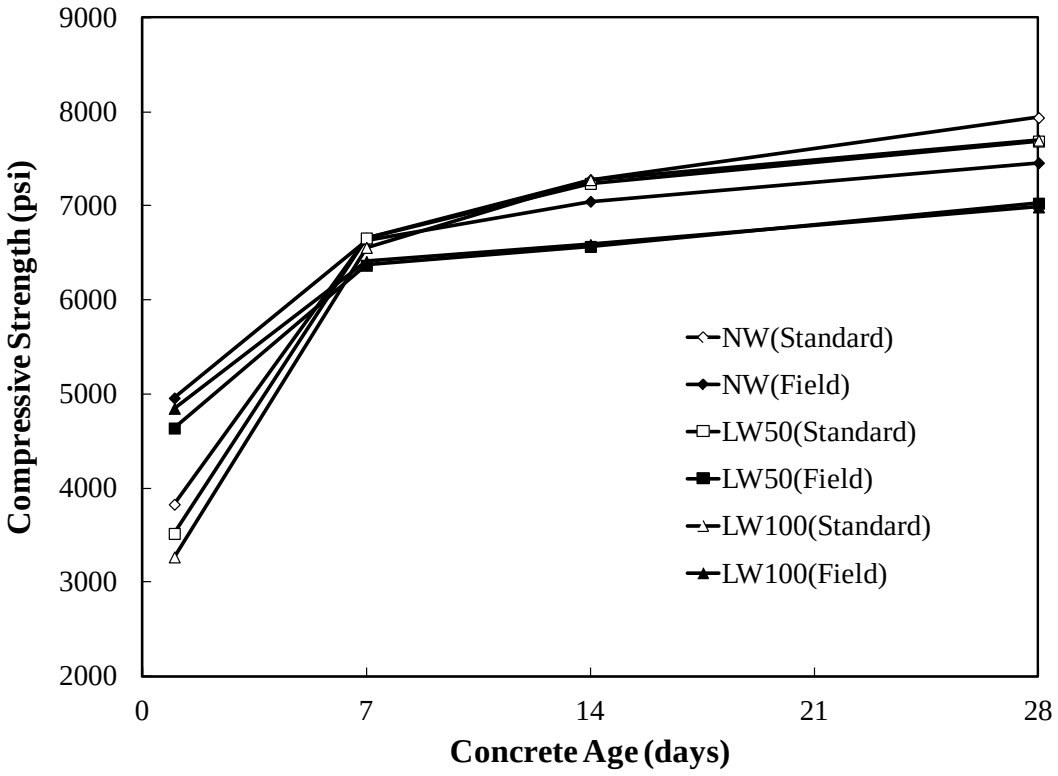

Note: 1 psi = 0.0069 MPa

Figure 4.21. Simulated curing compressive strength versus concrete age

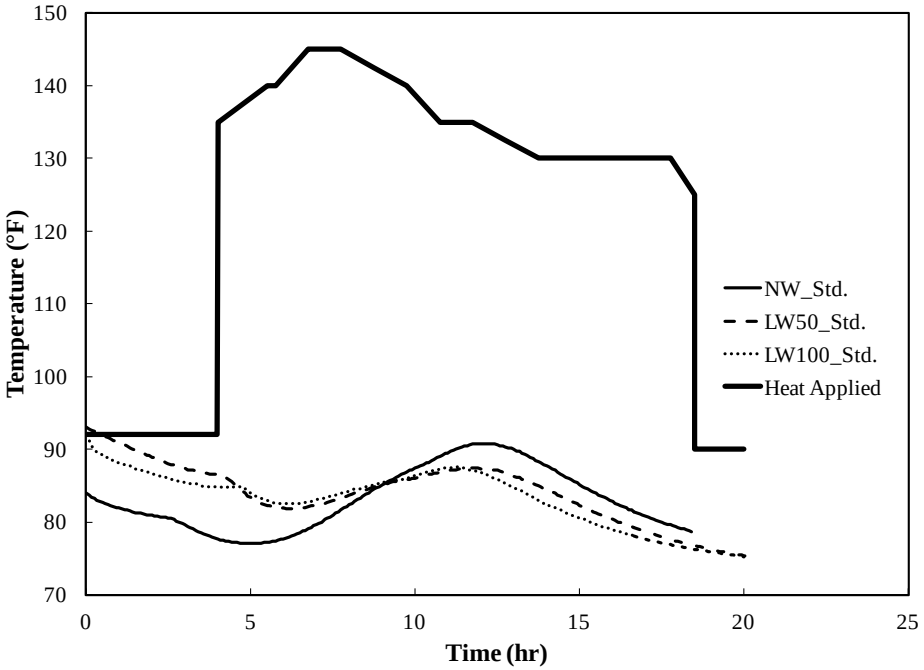

Note: F° = 1.8C° + 32

Figure 4.22. Temperature development of heated mixtures

4.5 Field-Calibrated Model Data

4.5.1 Axial Resistance Model Results

After pile driving, it was determined that the soil profile most resembled that of the 2002 SPT boring log found in Appendix B. The driving logs resembled the soil layering and SPT values more closely. In addition to a differing site condition, the pile was modeled without the first 10 ft (3 m) of overburden due to pre-drilling. The detailed capacity report is located in Appendix H. FB-Deep estimated 10 ft (3 m) of embedment into the Marl; therefore, there was approximately 30 ft (9 m) of overburden. The ultimate side resistance within the overburden was determined by FB-Deep to be 123 kips (547 kN). With 10 ft (3 m) of Marl embedment, the estimated side resistance and base resistance within the Marl was 17 kips (76 kN) and 4 kips (18 kN), respectively. The ultimate resistance at the end of driving was estimated to be 144 kips (641 kN). Using

the typical Charleston, SC, ultimate resistance values for the Marl, the ultimate resistance was predicted to be 267 kips (1,188 kN).

4.5.2 Pile Driveability Results

The GRL WEAP models were also adjusted to match the soil resistances from the 2002 SPT boring log. Figure 4.23 presents the blow counts with depth that were measured in the field along with the predicted blow counts from WEAP. The boring log N-values are also presented with depth. The maximum WEAP predicted and measured PDA tensile and compressive stresses within the pile are presented in Table 4.12.

Table 4.12 – Driving and restrike stresses

Stress	NW				LW50				LW100			
	Initial Drive		Restrike		Initial Drive		Restrike		Initial Drive		Restrike	
	WEAP	PDA	WEAP	PDA	WEAP	PDA	WEAP	PDA	WEAP	PDA	WEAP	PDA
TS_{max} (psi)	420	600	500	200	330	600	430	400	240	600	370	200
CS_{max} (psi)	1930	2300	2340	3100	1870	1900	2220	2800	1800	2600	2120	2600

Note: 1 psi = 0.0069 MPa

The maximum stresses from restrike are also presented. The tensile and compressive driving stresses with depth during initial driving are also presented in Figure 4.24, Figure 4.25, and Figure 4.26 for the NW, LW50, and LW100 mixes, respectively. The PDA measured wave speeds during pile driving for the NW, LW50, and LW100 piles were 13,250 ft/s (4,038 m/s), 12,500 ft/s (3,810 m/s), and 11,900 ft/s (3,627 m/s), respectively. These values of wave speeds are approximately 2,000 ft/s (610 m/s) faster than presented by Gerwick (1968) for the lightweight piles which was 9,800 ft/s (2,986 m/s). The dynamic modulus was calculated using Equation 3.1 and used within the WEAP models. The dynamic moduli used in the final models were 5,450 ksi (38 GPa), 4,450 ksi (31 GPa), and 3,750 ksi (26 GPa) for the NW, LW50, and LW100, respectively.

The values predicted based on the measured PDA wave speed were compared with methods for determining the dynamic modulus (Swamy and Bandyopadhyay 1975; Lydon and Balendran 1986) are presented in Table 4.13. The equation for Swamy and Bandyopadhyay (1975) utilizes units of GPa. The GPa units were converted to ksi units for comparison purposes.

Table 4.14 – Predicted dynamic modulus of pile concrete

Pile Mix	E_c (ksi)	E_d (ksi)		
		PDA Measured	Swamy and Bandyopadhyay (1975)	Lydon and Balendran (1986)
Charleston NW Field	4150	5450	4560	5000
Charleston LW50 Field	3800	4450	4200	4600
Charleston LW100 Field	3200	3750	3650	3850

Note: 1 ksi = 0.0069 GPa

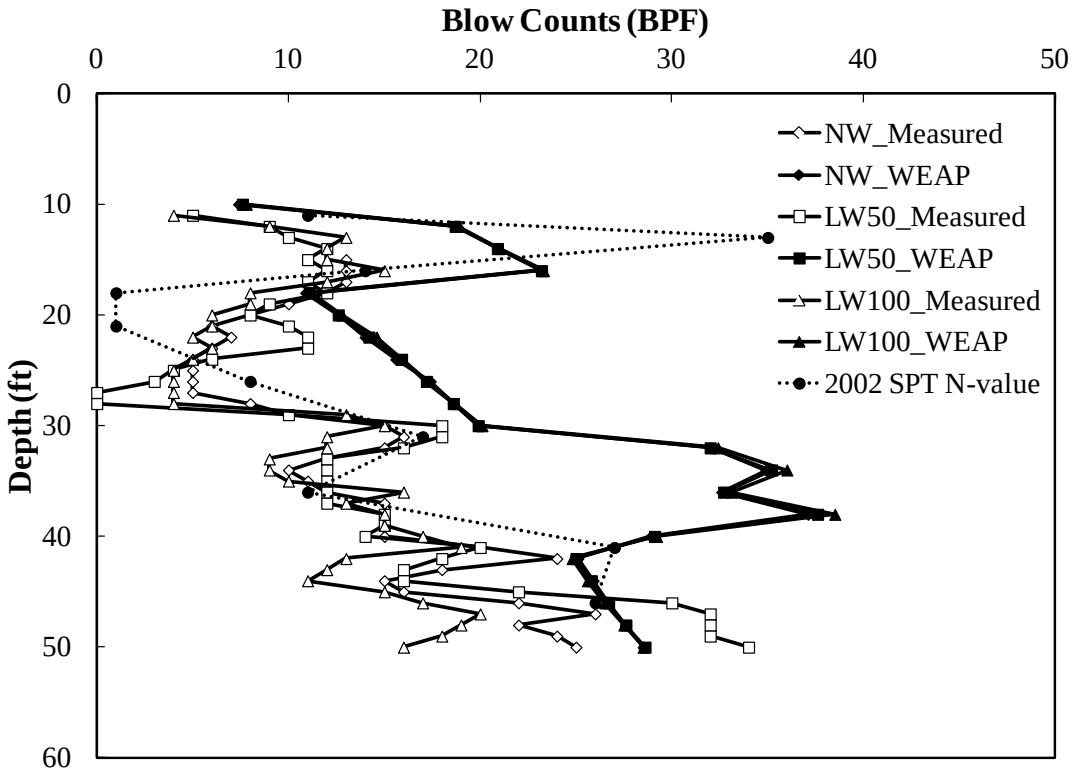

Note: 1 ft = 0.3028 m

Figure 4.23. Pile driving blows with depth

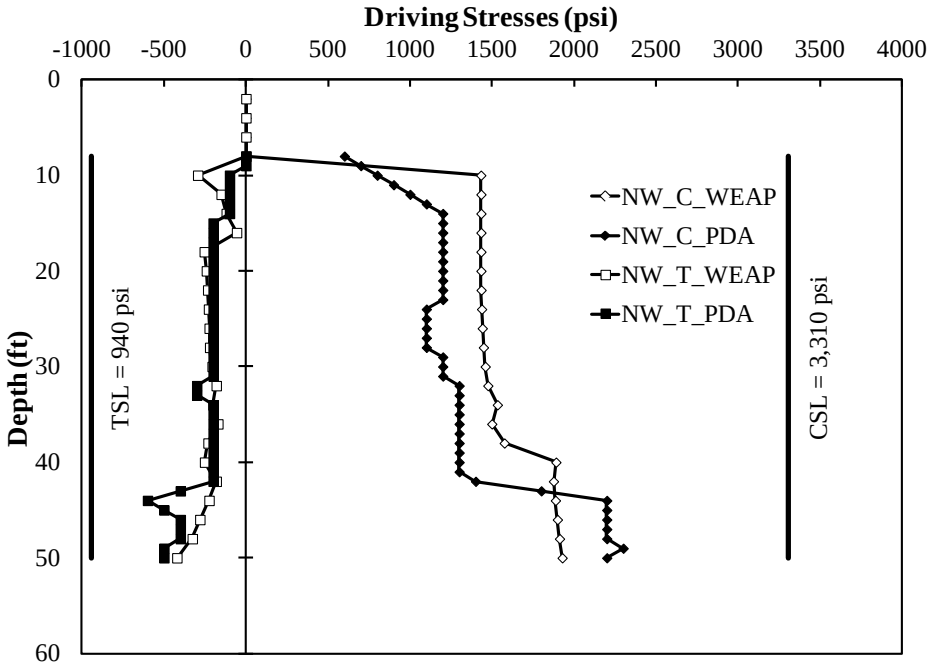

Note: 1 ft = 0.3028 m; 1 psi = 0.0069 MPa

Figure 4.24. NW driving stresses

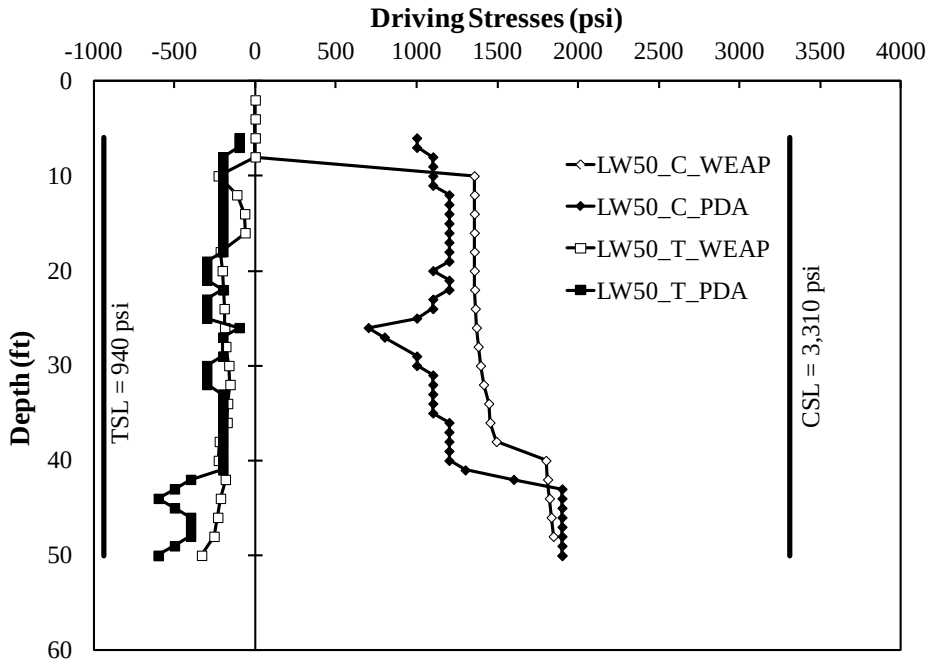

Note: 1 ft = 0.3028 m; 1 psi = 0.0069 MPa

Figure 4.25. LW50 driving stresses

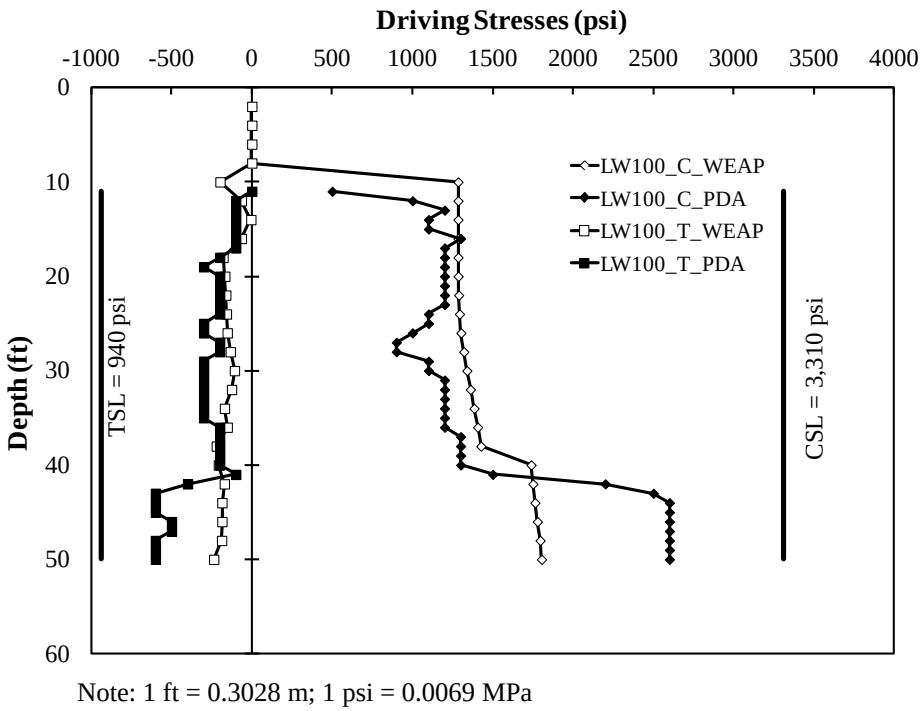

Note: 1 ft = 0.3028 m; 1 psi = 0.0069 MPa

Figure 4.26. LW100 driving stresses

5.0 DISCUSSION OF RESULTS

5.1 Concrete Behavior

5.1.1 Laboratory Concrete Behavior

Lab mixtures proved to be adequate for pile design and casting. The lightweight mixes had a slump that was within 2 to 4 in. (5 to 10 cm) as suggested by Kosmatka et al. (2002). The fresh density and air content for each mixture fell within an acceptable range of the batched proportions.

All three mixtures met the minimum release strength of 3,500 psi (24 MPa). These lab strengths are due to an accelerated curing regime. With the *w/c* = 0.4 for each mixture, the average 28-day compressive strength for non-air entrained concrete is approximately 6,100 psi (42 MPa) as linearly interpolated from ACI 211 (1991). Each mixture was in excess of 7,000 psi (48 MPa). All concrete mixtures had a static modulus of elasticity within the ±20% of the predicted modulus of elasticity which is within acceptable industry standards (ACI 318 2011). The lightweight concrete mixtures were also within ±20% of the predicted modulus of elasticity. All measured modulus values were greater than the predicted value; therefore, the ACI 318 (2011) estimation is conservative. The effect of lightweight coarse aggregate replacement showed no reduction in strength from either the LW50 or the LW100 at 18-hour release or at 28 days. There was a slight reduction at 7 days with the LW50. The modulus of elasticity decreases in a linear fashion as the coarse aggregate replacement percentage increases for all ages. This behavior was expected as seen in Holm and Ries (2006).

The splitting tensile strength of the laboratory NW concrete mixture was similar to the ACI 318 (2011) estimate of $7.5\lambda\sqrt{f'_c}$ where λ is 1 and 0.85 for normalweight and lightweight concrete, respectively. The splitting tensile values for the NW, LW50, and LW100 are $7.4\sqrt{f'_c}$, $6.5\sqrt{f'_c}$, and $6.6\sqrt{f'_c}$. The measured splitting tensile strengths for the lightweight mixtures are approximately 2 to 3 percent higher than the predicted $6.38\sqrt{f'_c}$; therefore, the ACI 318 (2011) prediction for splitting tensile strength is overly conservative for lightweight concrete.

The laboratory prepared RCPT specimens were cured under the same applied heat as the compression test cylinders with the maximum temperature reaching 160°F (71°C). These lab specimens showed to have moderate chloride ion penetrability. The NW had the lowest number of Coulombs; however, the two lightweight mixtures were within 79 Coulombs of one another. All these results fell in the "Moderate" chloride-ion penetrability classification in accordance with ASTM C 1202 (2010).

5.1.2 Pile Concrete Behavior

The concrete provided for the test piles had adequate workability; however, the fresh concrete density was higher than expected for the lightweight mixtures. The normalweight concrete had a significantly lower density than predicted from batch proportions. Batch proportions suggest the fresh density should be approximately 148 pcf (2,368 kg/m^3) and the measured density was 144 pcf (2,304 kg/m^3). When field specimens were cut, there were anomalies in the concrete materials. The predominant materials were visible; however, there were also aggregates that did not look like the others. The normalweight concrete had a few aggregates that were lighter in color which may have been a less dense limestone possibly from plant batching errors. The LW100

mixture contained some granite from the previous NW and LW50 mixtures which would have increased the fresh density; however, the measured fresh density was in accordance with the estimated density from the batch proportions.

The major effect of a decreased normalweight concrete density or an increased lightweight concrete density is the effect on the modulus of elasticity of a concrete specimen. The coarse aggregate content and its corresponding density within a concrete mixture have a significant effect on the overall concrete density. A lower density normalweight concrete will lower the modulus of elasticity. Conversely, a higher density lightweight concrete will increase the modulus of elasticity. The inclusion of different aggregates within the NW and LW100 concrete mixtures was not quantified at the time of this research. It should be noted that the measured modulus of elasticity values for these concrete mixtures may be lower or higher depending on the amount of different aggregates within the concrete and the actual type of aggregate that contaminated these concrete mixtures.

The placement temperature was also greater than 90°F (32°C) which falls within a range considered by ACI 305 (1999) to potentially cause adverse effects. The batch tickets indicated the concrete mixtures should have had 28-day strengths of 5,000 psi (34.5 MPa); however, the low *w/c* ratios for each mixture indicate that the strength should have been well over 6,000 (41 MPa) psi at 28 days based on ACI 211 (1991).

The compressive strength and static modulus of elasticity exhibited similar behavior as the laboratory mixtures in terms of coarse aggregate replacement percentage. The LW50 mixture within the field was harsh in spite of an adequate slump. The LW50 mixture cylinders were prepared approximately 1.5 hours after mixing due to inadequate

timing between ready-mixed trucks. The high temperature and low air content decreased the workability significantly. This may be the cause of the lower compressive strength for the field-cured specimen at the time of release due to a higher placement temperature of 100 °F, as well as accelerated field curing. The splitting tensile strength of the NW and the LW50 mixes were also lower than the ACI 318 (2011) allowable values. The NW concrete and LW50 concrete splitting tensile strength was $5.3\sqrt{f'_c}$ and $4.9\sqrt{f'_c}$, respectively. The measured compressive strength of the NW and LW50 concrete mixtures was 5,700 psi (39 MPa) and 5,600 psi (38.6 MPa), respectively.

The RCPT values at 91 days were greater than 4,000 Coulombs which means high Cl^- penetrability. ACI 318 (2011) specifies that a $w/c \leq 0.4$ should provide adequate resistance to Cl^- ions. The concrete pile mixtures were well below a $w/c = 0.4$.

5.1.3 Charleston Simulation Concreting

The high concrete placement temperatures are believed to the cause of the low compressive strengths and high permeability for all of the test pile concretes. The ambient temperature in mid-July was greater than 90°F (32°C) in Charleston, SC. The high ambient temperature coupled with the hot concrete is most likely the cause of the adverse concrete effects as presented by Neville (2011) and Mehta and Monteiro (2006).

Pile concrete was cured at over 125 °F (52 °C) for over 12 hours. The pile concrete temperature in conjunction with the high ambient temperatures showed a decrease in strength as presented in Mehta and Monteiro (2006), Brooks et al. (2007), and Verbeck and Helmuth (1968).

The fresh concrete tests of the Charleston simulated mixtures showed a lower workability than the same concrete mixed at room temperature [≈73 °F (23°C)]. The

only difference was the increased fresh concrete temperature, which was approximately 20 °F (11 °C) warmer than the mixtures batched at room temperature. This is similar to what Mehta and Monteiro (2006) present based on high ambient temperatures and slump loss with the use of ASTM C494 Type D admixtures. W.R. Grace WRDA 64 is classified as an ASTM C494 Type D admixture which was used in both laboratory and field concrete mixes.

Although the pile concrete in Charleston was workable (initial slump was greater than 2 in (5 cm).), the time to cast compressive cylinders for each mixture was already past one hour after mixing. The age of the LW50 mixture, which proved to be harshest during cylinder casting, was reaching 2 hours after mixing.

Comparing laboratory, field, and simulated field concrete compressive data, it is clear the difference in fresh concrete temperature, as well as the accelerated curing conditions significantly affect the long-term compressive strength. Figure 5.1 presents the compressive strength development of all NW mixtures while Figure 5.2 presents the temperature development of those same mixes. Likewise, Figure 5.3 and Figure 5.4 present the strength and temperature for all LW50 mixes, and Figure 5.5 and Figure 56 present the strength and temperature for all LW100 mixes. Strength comparative data are only presented up to 28 days. The heat applied is the same as the heat applied in Charleston; however, the SURE CURE^{TM} molds were held at the elevated fresh concrete temperature, and then increased, by the heat applied, as presented, after a holding period of 4 hours.

The Charleston simulated mixing and curing did not show a drastic reduction in compressive strength at 28 days; however, there are several factors that could not be

simulated fully. While the fresh concrete temperature was successfully elevated, the ambient temperature of the lab made it difficult to match conditions the standard-cured cylinders in Charleston experienced with an outdoor temperature of approximately 100 °F (38 °C). From the compressive strength comparisons, the simulated Charleston curing proved to have just as high if not higher 28-day strengths as the laboratory-cured specimens. Although the simulated mixes had 90 °F (32 °C) and higher fresh temperatures, the insulation boxes did not keep the temperature constant until set as expected. In addition, the internal cylinder temperature of the simulated standard-cured cylinders was approximately 40 °F (22 °C) less than Charleston standard cylinders after final set. When there is a drastic lack of workability, there exists a lack of consolidation thereby causing a decrease in strength. Field consolidation used hand rodding, while Charleston simulation placement in the lab used internal vibration overcoming this lack in workability.

The temperature difference between the fresh concrete and the ambient temperature was also a factor for the simulated field conditions. The concrete was placed in the SURE CURE ^{TM} system; the cylinders still needed to heat up to match the fresh temperature. After four hours, the temperature was increased and applied as in the field; however, at the time of heat application, the temperature was, at most, the fresh temperature. In the field, the concrete sat in the pile beds uncovered and exposed to the sun until steam heat was applied which would have accelerated the curing before steam heat was applied

Short of mixing and initially curing the concrete cylinders in an environmental chamber at an elevated temperature, complete simulation of curing conditions of

Charleston could not be achieved. Previous literature along with data presented show that the most likely factor causing lower than expected compressive strength breaks from Charleston was hot weather concreting not being properly addressed in the field.

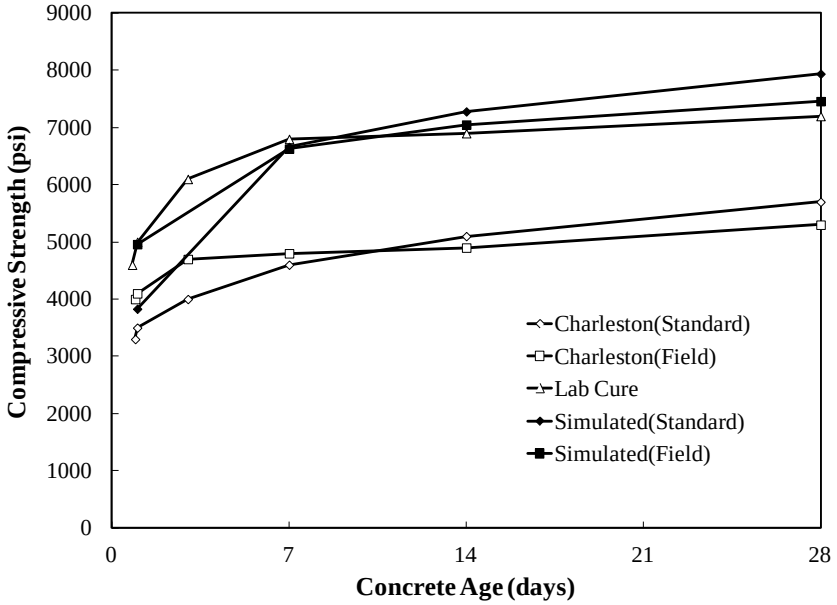

Note: 1 psi = 0.0069 MPa

Figure 5.1. Compressive strength development of all NW mixtures

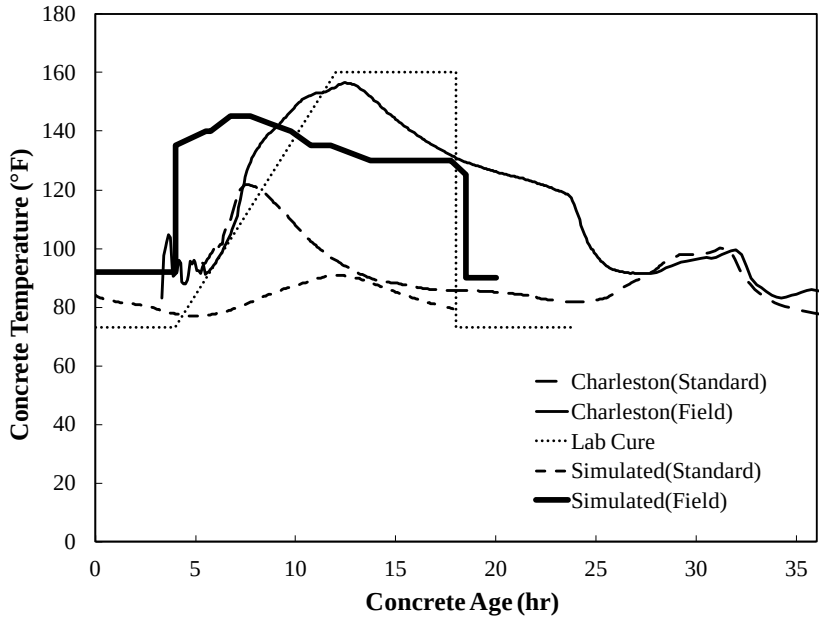

Note: F° = 1.8C° + 32

Figure 5.2. Temperature development of all NW mixtures

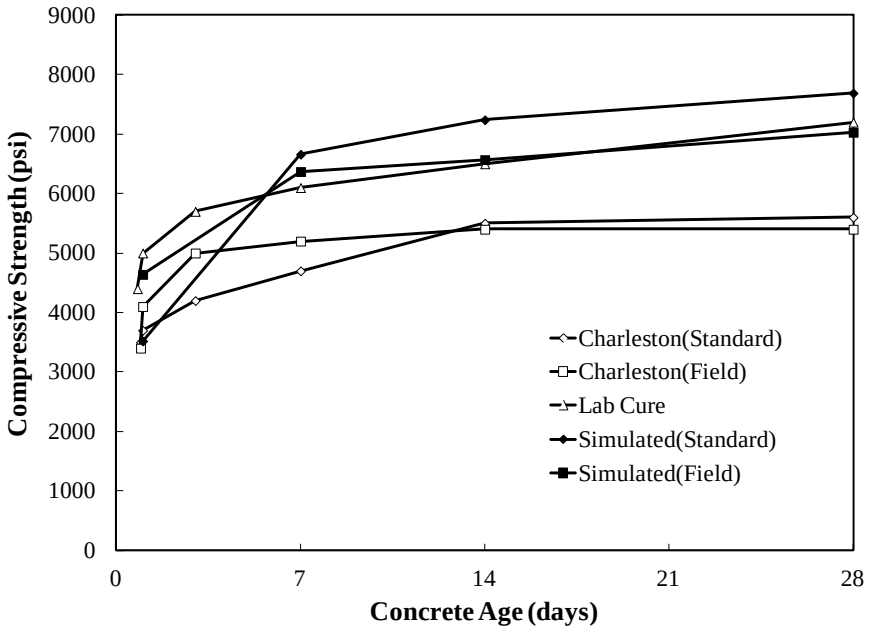

Note: 1 psi = 0.0069 MPa

Figure 5.3. Compressive strength development of all LW50 mixtures

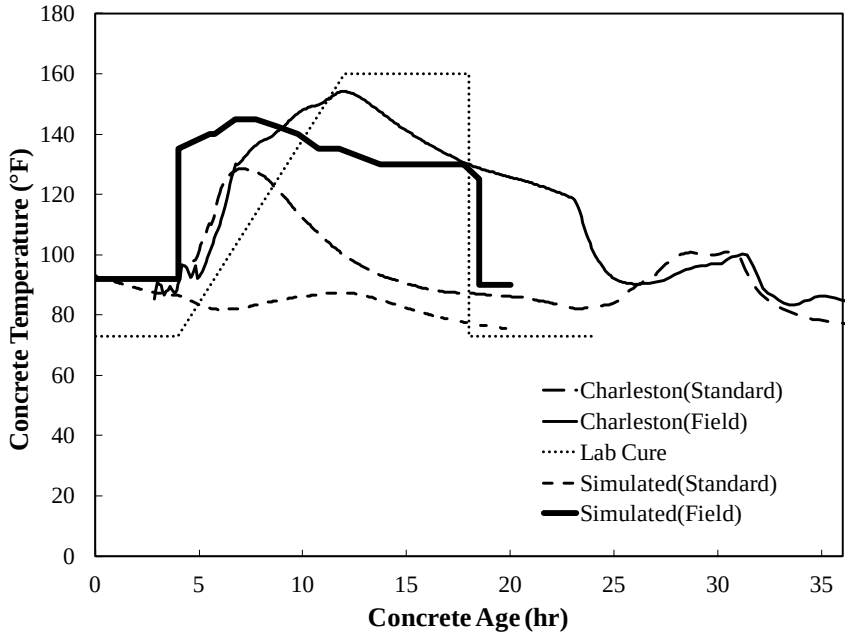

Note: F° = 1.8C° + 32

Figure 5.4. Temperature development of all LW50 mixtures

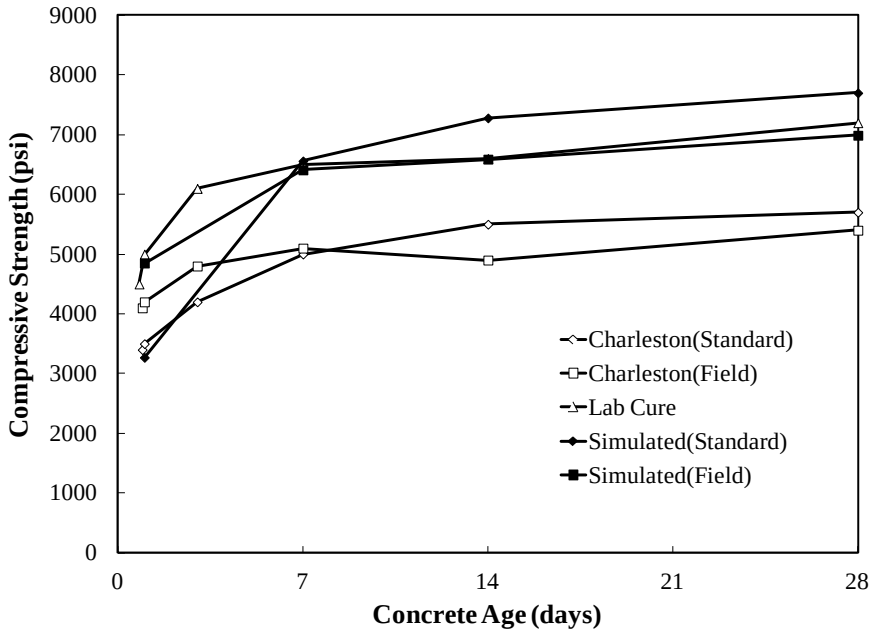

Note: 1 psi = 0.0069 MPa

Figure 5.5. Compressive strength development of all LW100 mixtures

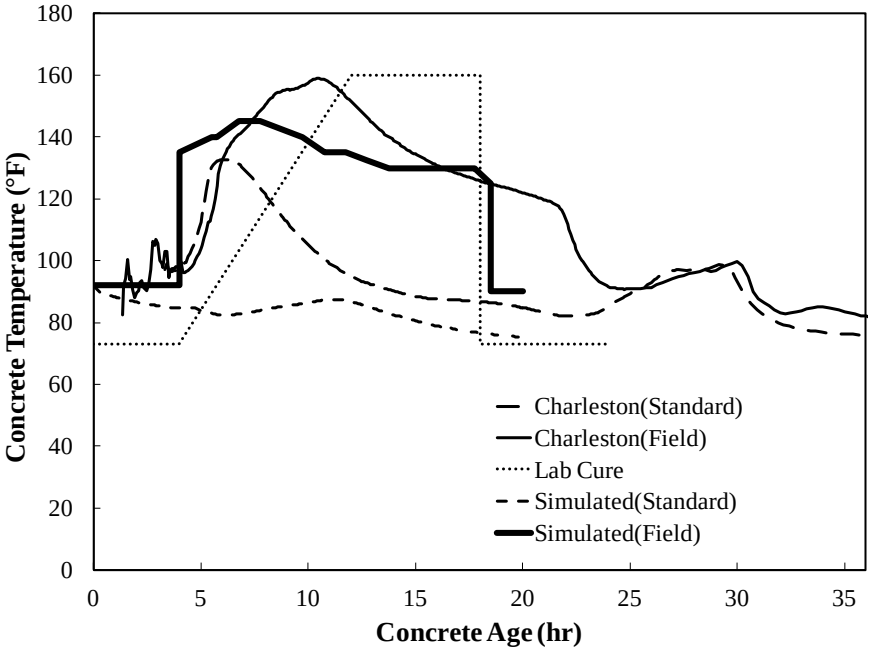

Note: F° = 1.8C° + 32

Figure 5.6. Temperature development of all LW100 mixtures

5.2 Pile Behavior

5.2.1 Pre-Driving Pile Driveability Model

The initial driveability analysis showed the concrete piles achieved adequate soil resistance and driveability with reasonable effort. The percentage difference was calculated using Equation 5.1 where TSL, TS_{max}, CSL, and CS_{max} are defined previously. The predicted driving and restrike stresses decreased as the coarse aggregate replacement increased. The differences are more pronounced in the tension stresses. The predicted stresses for the LW100 pile were approximately 12 percent less than the NW pile as presented in Table 5.1.

$$\%Diff = \left(\frac{TSL - TS_{\max}}{TSL}\right)\cdot 100 \; or \; \left(\frac{CSL - CS_{\max}}{CSL}\right)\cdot 100 \qquad (5.1)$$

Table 5.1 – Percent difference in predicted stresses relative to AASHTO

	AASHTO	NW		LW 50		LW 100	
	TSL/CSL(psi)	Driving	Restrike	Driving	Restrike	Driving	Restrike
TS_{max} (psi)	940	48%	65%	52%	70%	60%	77%
CS_{max} (psi)	3900	61%	51%	62%	53%	65%	55%

Note: 1 psi = 0.0069 MPa

As expected, when comparing initial driving with restrike stresses from Figure 4.4, the compressive strength increases upon restrike under ultimate strength conditions while the tensile stresses decrease due to increased resistance over time (pile set-up).

5.2.2 Pile Driving Behavior

PDA showed the tensile and compressive stresses are relatively similar profiles. The compressive stresses share a similar stress profile up to a depth of about 40 ft when the hammer stroke was increased from 1 ft (0.3 m) to 1.5 ft (0.46 m). The compressive

stresses decrease from the NW to the LW50 pile. The LW100 pile measured higher compressive stresses than both the NW and LW50. This was most likely due to a bad PDA gage that was replaced at approximately 40 ft (12 m) depth. During this time, it is believed that the Marl was already beginning to setup during driving and cause the LW100 pile to measure approximately 250 psi (1.7 MPa) more stress in compression than the NW pile.

Comparison of the driving record with the preliminary driveability model showed a differing site condition. The 2002 SPT boring indicated a more reasonable soil profile than the 2004 SPT profile due to similar shapes of N-values and measured blow counts during pile driving. The WEAP predicted blow counts show a general increase in blow counts with depth; however, at approximately 30 ft (9 m), WEAP predicted much higher blow counts than the measured and SPT N-values. Figure 4.23 shows the SPT N-values with depth are similar to that of the measured blow counts during pile driving. In addition to the measured blow counts, the WEAP estimated blow counts are also presented based on the model using the 2002 SPT boring log. This model shows reasonable agreement with the use of a dynamic modulus based on the PDA predicted value from the measured pile wave speed. The methods presented by Swamy and Bandyopadhyay (1975) and Lydon and Balendran (1986) also present reasonable estimates of the predicted dynamic modulus as compared to the modulus predicted from the wave speed.

The PDA showed low driving stresses which indicate there was no pile damage. The predicted WEAP and PDA measured stresses are all less than the AASHTO driving stress limits. A TSL of 940 psi (6.5 MPa) is the same as calculated previously. The

specified 28-day compressive strength based on the batch ticket was 5,000 psi (34.5 MPa); therefore, the CSL was determined to be 3,310 psi (22.8 MPa).

Table 5.7 – Final percentage difference of measured and predicted stresses

	AASHTO TSL/CSL(psi)	NW				LW 50				LW 100			
		Initial Drive		Restrike		Initial Drive		Restrike		Initial Drive		Restrike	
		WEAP	PDA	WEAP	PDA	WEAP	PDA	WEAP	PDA	WEAP	PDA	WEAP	PDA
TS_{max} (psi)	940	55%	36%	47%	79%	65%	36%	54%	57%	74%	36%	61%	79%
CS_{max} (psi)	3310	42%	31%	29%	6%	44%	43%	33%	15%	46%	21%	36%	21%

Note: 1 psi = 0.0069 psi

The predicted and measured tension stresses were between 36 and 79 percent less than the AASHTO (2010) tension stress limit; whereas, the predicted and measured compression stresses were between 6 and 46 percent less than the compression stress limit.

The percentage difference of the LW100 between the PDA at end of drive and restrike are similar. This indicates that the Marl set up as expected from theory while changing the PDA gage. This increased resistance during initial drive caused a higher stress to be recorded during driving as opposed to the NW and LW50 piles. It should also be noted that the restrike compressive stresses behaved as expected. As the coarse aggregate replacement percentage increases, the modulus decreases causing a decrease in compressive stresses. Figures 4.15 through Figure 4.17 also show that the compressive stresses with depth are less than WEAP predicted stresses to a depth of about 40 ft (12.2 m), but the stress profiles show similar trends with fairly uniform stresses through the overburden except for a depth of approximately 28 to 30 ft (8.5 to 9 m). The increase in stress at approximately 40 ft (12.2 m) in depth represents the increase in hammer stroke from 1 ft (0.3 m) to 1.5 ft (0.46 m) during initial driving.

It should be noted that based on the contamination of different aggregates within the NW and LW100 pile concrete, the measured stresses within the NW pile may be lower or higher depending on the type of aggregate and the amount of aggregate within the concrete. The driving stresses within LW100 pile may be skewed higher than expected based on the inclusion of a certain amount of granite within the mixture that was used for the NW and LW50 concrete mixtures.

Based on the PDA traces, there is no evidence of pile damage. At no point at 15 ft (4.6 m), 30 ft (9 m), or 50 ft (15.2 m) does the velocity curve any pile dip below the horizontal axis prior to a time of *2L/c* during initial driving nor at restrike as presented in Appendix H.

Driving performance of the piles may also be evaluated based on the displacement traces presented. Each pile showed similar trends at each embedment depth. Rebound is evident at 50 ft (15.2 m) when the velocity curve dips below the horizontal axis after a time of *2L/c*; however, this is only after the pile as set.

The axial resistance was estimated to be 265 kips (1,179 kN), 202 kips (898 kN), and 213 kips (947 kN) for the NW, LW50, and LW100 piles, respectively based on restrike data. The adjusted field-calibrated model predicted the ultimate resistance to be approximately 267 kips (1,188 kN) from FB-Deep and typical unit resistance values for the Cooper Marl. The NW pile achieved 99% of this value after one day while the LW50 and LW100 had reached approximately 75 and 80 %, respectively of the predicted ultimate resistance after one day when typical restrike occurs at 5 to 7 days after initial driving for piles driven in the Cooper Marl.

6.0 CONCLUSIONS AND RECOMMENDATIONS

Laboratory work, field work, and analytical modeling were used to evaluate the use of lightweight aggregate concrete piles. Those results were used to draw conclusions from the work, and recommendations are made to implement future research of lightweight aggregate concrete piles.

6.1 Summary of Work

Lightweight aggregate concrete was evaluated as suitable material to be used in precast, prestressed driven piles. Four primary research objectives were used to properly evaluate the material. Preliminary concrete mixes were prepared by replacing the normal weight coarse aggregate with commercially available Stalite (expanded slate). Fresh and hardened concrete properties were evaluated to verify their suitability as a pile concrete mix. The static modulus of elasticity, compressive strength, splitting tensile strength, and the chloride ion penetrability were determined for each mix.

Pre-driving axial resistance and driveability models were prepared based on subsurface data gathered previously at The Citadel Geotechnical Experimentation Site, local geology in Charleston, and concrete properties determined in the laboratory. Pre-driving models showed the concrete piles with a reduced modulus and unit weight (density) would survive both the initial driving conditions, as well as restrike after a significant increase in axial resistance.

Full scale test piles were cast, driven, and dynamically tested to monitor the behavior for the NW, LW50, and LW100 concrete piles. Thermocouples were placed in

the piles to measure the temperature of the concrete during initial curing. In addition to casting the piles, over 100 concrete compressive cylinders were prepared to evaluate the hardened concrete behavior. Half of the cylinders were used to evaluate standard field curing conditions, and the other half were used to evaluate the accelerated field curing conditions from the steam curing beds.

Finally, the pre-driving models were adjusted with the pile driving records and test data accordingly. The soil model was adjusted to more accurately represent the driving log, and the dynamic concrete modulus was used as opposed to the measured static modulus which is more indicative of pile driving.

6.2 Conclusions

Based on the research, the following conclusions can be made on the use of lightweight aggregate concrete in precast, prestressed driven piles.

- The ACI 318 (2011) prediction of modulus of elasticity provides a reasonable estimate of the static modulus of elasticity based on concrete density and compressive strength.
- The ACI 318 (2011) correction factor for lightweight concrete (λ) of 0.85 was shown to be overly conservative when used to predict the 28-day splitting tensile strengths for lightweight concrete prepared and cured according to the laboratory curing regime presented herein.
- The lab-cured lightweight concrete and normalweight concrete was classified as having moderate chloride ion penetrability using the Rapid Chloride Penetration Test in accordance with ASTM C 1202 (2010).

- The dynamic modulus estimated from the measured wave speed and concrete density for concrete provides a more accurate estimate of the driving stresses as opposed to using the measured static modulus of elasticity.
- The tension and compressive stresses within all of the piles were less than the AASHTO (2010) stress limits.
- A hydraulic hammer set with the same stroke settings drove each pile successfully without damage or excessive rebound regardless of the coarse aggregate replacement.
- There was no evidence of poor hammer performance or excessive rebound during initial driving or during restrike from the PDA wave traces. Piles did show slight rebound; however, this was only after they set from the hammer blow.
- Lightweight aggregate concrete can be cast, handled, and driven successfully when used in precast, prestressed piles.

6.3 Recommendations for Future Research

There are several recommendations for future research with lightweight aggregate concrete piles.

1. Additional test piles should be cast and/or driven to verify concrete and pile behavior presented herein. These additional piles should be PDA tested to provide more data when evaluating driving stress limits for lightweight concrete piles.
2. The temperature effects on the concrete should be evaluated for the summer placement and fall/spring placement temperatures.

3. The splitting tensile strength and RCPT values for the standard-cured concrete field specimens indicates they may not be representative of the concrete placed in the piles due to a severe loss in workability from the time of fresh concrete testing to molding of the concrete cylinders. Concrete cores should be taken from the additional LW50 and LW100 piles to measure the in-place splitting tensile strength and chloride ion penetrability.
4. In addition to placement temperatures, precast, prestressed pile curing should be evaluated based on the time of year and ambient temperatures.
5. Cores should be taken from additional piles to verify field-cured values instead of attempting to simulate hot weather concreting.
6. Other lightweight aggregates sources should be evaluated in driven pile applications which include other expanded aggregates.
7. Static axial and lateral load tests should be performed on the LW50 and LW100 piles, respectively. Load tests will verify the ultimate resistance provided by the Cooper Marl, as well as measure internal concrete behavior to address AASHTO design stress limits.

REFERENCES

AASHTO. 2010. *AASHTO LRFD Bridge Design Specifications.* Washington, DC.

ACI 211. 1991. *Standard Practice for Selecting Proportions for Normal, Heavyweight and Mass Concrete.* Committee Report, Farmington Hills, MI: American Concrete Institute.

ACI 213. 2003. *Guide for Structural Lightweight-Aggregate Concrete.* Committee Report, Farmington Hills, MI: American Concrete Institute.

ACI 305. 1999. *Hot Weather Concreting*. Committee Report, Farmington Hills, MI: American Concrete Institute.

ACI 318. 2011. *Building Code Requirements for Structural Concrete and Commentary.* Committee Report. Farmington Hills, MI: American Concrete Institute.

ACI 543. 2005. *Design, Manufacture, and Installation of Concrete Piles.* Committee Report, Farmington Hills, MI: American Concrete Institute.

Al-Khaiat, H., and M.N. Haque. 1998. "Effect of Initial Curing on Early Strength and Physical Properties of a Lightweight Concrete." *Cement and Concrete Research* 28, no. 6: 859-866.

Al-Khaiat, Husain, and Naseer Haque. 1999. "Strength and Durability of Lightweight and Normal Weight Concrete." *Journal of Materials in Civil Engineering*, August: 231-235.

ASTM C1202. 2010. "Standard Test Method for Electrical Indication of Concrete's Ability to Resist Chloride Ion Penetration." West Conshohocken, PA: ASTM International.

ASTM C1231/C1231M. 2012. "Standard Practice for Use of Unbonded Caps in Determination of Compressive Strength of Hardened Concrete Cylinders." West Conshohocken, PA: ASTM International.

ASTM C1260. 2007. "Standard Test Method for Potential Alkali Reactivity of Aggregates (Mortar-Bar Method)." West Conshohocken, PA: ASTM International.

ASTM C138/C138M. 2009. "Standard Test Method for Density (Unit Weight), Yield, and Air Content (Gravimetric) of Concrete." West Conshohocken, PA: ASTM International.=ASTM C143/C143M. 2010. "Standard Test Method for Slump of Hydraulic-Cement Concrete." West Conshohocken, PA: ASTM International.

ASTM C1543. 2010. "Standard Test Method for Determining the Penetration of Chloride Ion into Concrete by Ponding." West Conshohocken, PA: ASTM International.

ASTM C173/C173M. 2010. "Standard Test Method for Air Content of Freshly Mixed Concrete by the Volumetric Method." West Conshohocken, PA: ASTM International.

ASTM C192/C192M. 2002. "Standard Practice for Making and Curing Concrete Test Specimens in the Laboratory." West Conshohocken, PA: ASTM International.

ASTM C289. 2007. "Standard Test Method for Potential Alkali-Silica Reactivity of Aggregates (Chemical Method)." West Conshohocken, PA: ASTM International.

ASTM C330/C330M. 2009. "Standard Specification for Lightweight Aggregates for Structural Concrete." West Conshohocken, PA: ASTM International.

ASTM C39. 2009. "Standard Test Method for Compressive Strength of Cylindrical Concrete Specimens." West Conshohocken, PA, PA: ASTM International.

ASTM C469. 2002. "Standard Test Method for Static Modulus of Elasticity and Poisson's Ratio of Concrete in Compression." West Conshohocken, PA, PA: ASTM International.

ASTM C494/C494M. 2012. "Standard Specification for Chemical Admixtures for Concrete." West Conshohocken, PA: ASTM International.

ASTM C496/C496M. 2004. "Standard Test Method for Splitting Tensile Strength of Cylindrical Concrete Specimens." West Conshohocken, PA: ASTM International.

ASTM C567. 2005. "Standard Test Method for Determining Density of Structural Lightweight Concrete." West Conshohocken, PA, PA: ASTM International.

ASTM C666/C666M. 2008. "Standard Test Method for Resistance of Concrete to Rapid Freezing and Thawing." West Conshohocken, PA: ASTM International.

ASTM D1143. 1994. "Standard Test Method for Piles Under Static Axial Compressive Load." West Conshohocken, PA: ASTM International.

ASTM D4945. 2008. "Standard Test Method for High-Strain Dynamic Testing of Deep Foundations." West Conshohocken, PA: ASTM International.

Bamforth, P.B. 1987. "The Relationship Between Permeability Coefficients for Concrete Obtained Using Liquid and Gas." *Magazine of Concrete Research* 39, no. 138: 3-11.

Basset, R., and S.M. Uzumeri. 1986. "Effect of confinement on the behaviour of high-strength lightweight concrete columns." *Canadian Journal of Civil Engineering* 13: 741-751.

Bentur, A., S. Igarashi, and K. Kovler. 2001. "Prevention of Autogenous Shrinkage in High-Strength Concrete by Internal Curing Using Wet Lightweight Aggregates." *Cement and Concrete Research*: 1587-1591.

Bremner, T.W., and T.A. Holm. 1986. "Elastic Compatibility and the Behavior of Concrete." *ACI Journal* 83, no. 2: 244-250.

Brooks, A.G., A.K. Schindler, and R.W. Barnes. 2007. "Maturity Method Evaluated for Various Cementitious Materials." *Journal of Materials in Civil Engineering* 19, no. 12: 1017-1025.

Camp, III, W.M. 2004. "Drilled and Driven Foundation Behavior in a Calcareous Clay." Edited by J.P. Turner and P.W. Mayne. *GeoSupport 2004: Drilled Shafts, Micropiling, Deep Mixing, Remedial Methods, and Specialty Foundation Systems, GSP 124.* Orlando: ASCE. 1-18.

Camp, W.M., and H.S. Parmar. 1999. "Characterization of Pile Capacity with Time in Cooper Marl: Study of Applicability of a Past Approach to Predict Long-Term Pile Capacity." *Transportation Research Record 1663* Paper No. 99-1381: 16-24.

Campbell, R.H., and R.E. Tobin. 1967. "Core and Cylinder Strengths of Natural and Lightweight Concrete." *ACI Journal*, April: 190-195.

Chen, H - J, C - H Huang, and C - W Tang. 2010. "Dynamic Properties of Lightweight Concrete Beams Made by Sedimentary Lightweight Aggregate." *Journal of Materials in Civil Engineering* 22, no. 6: 599-606.

Chi, J.M., R. Huang, C.C. Yang, and J.J. Chang. 2003. "Effect of Aggregate Properties on the Strength and Stiffness of Lightweight Concrete." *Cement and Concrete Composites* 25: 197-205.

Chia, K.S., and M. Zhang. 2002. "Water Permeability and Chloride Penetrability of High-Strength Lightweight Aggregate Concrete." *Cement and Concrete Research* 32: 639-645.

Cleary, John, and Norbert Delatte. 2008. "Implementation of Internal Curing in Transportation Concrete." *Transportation Research Record: Journal of the Transportation Research Board* 2070: 1-7.

Collins, R.J., and P.D. Bareham. 1987. "Alkali-Silica Reaction: Supression of Expansion Using Porous Aggregate." *Cement and Concrete Research* 17: 89-96.

Das, B.M. 2011. *Principles of Foundation Engineering.* 7th. Pacific Grove: Brooks/Cole - Thomson Learning.

Davidson, J., J. Maultsby, and K. Spoor. 1999. *Standard Penetration Test Energy Calibrations.* Contract No. BB261, Florida Department of Transportation.

Day, R.L. 1994. "Strength Measurement of Concrete Using Different Cylinder Sizes: A Statistical Analysis." *Cement, Concrete, and Aggregates* 16, no. 1: 21-30.

Emiko, L., T.H. Wee, and T. Tamilselvan. 2010. "Penetrability of Lightweight Aggregate Concrete." *Magazine of Concrete Research* 62, no. 3: 201-209.

Fellenius, B.H., P.A. Goudreault. 2002. *UniPile User Manual: A Program for the Analysis of Piles and Groups Considering Capacity, Settlement, and Negative Skin Friction*. User Manual, Calgary: Unisoft Ltd.

Florida Bridge Software Institute. 2002. "FB-Deep Version 2.02." Gainesville, Florida: Florida Department of Transportation.

Gao, X. F., Y. T. Lo, and C. M. Tam. 2002. "Investigation of micro-cracks and microstructure of high performance lightweight aggregate concrete." *Building and Enviroment* 37: 485-489.

Geokon. 2012. "Installation Manual: Models 4911A/4911 VW Rebar Strain Meters." Lebanon, NH: Geokon.

Gerwick, Jr, B.C. 1968. "Prestressed Concrete Piles." *PCI Journal* 13, no. 5: 66-93.

Gjorv, O. E., Kefeng Tan, and P. J.M. Monteiro. 1994. "Effect of Elevated Curing Temperature on the Chloride Permeability of High-Strength Lightweight Concrete." *Cement, Concrete, and Aggregates* 16, no. 1: 57-62.

Hannigan, P. 2011. "Pile Types." *PDCA Professor's Driven Pile Institute 2011*.

Hannigan, P.J., G.G. Goble, G.E. Likens, and F. Rausche. 2006. *Design and Construction of Driven Pile Foundations.* Reference Manual, Washington, D.C.: FHWA.

Haque, M. N., H. Al-Khaiat, and O. Kayali. 2004. "Strength and Durability of Lightweight Concrete." *Cement and Concrete Composites*: 307-314.

Holm, T.A. 1983. "Structural Lightweight Concrete." Chap. 7 in *Handbook of Structural Concrete*, by F. Kong and R.H. Evans, 1-34. New York: McGraw-Hill.

Holm, T.A., and J.P. Ries. 2006. "Lightweight Concrete and Aggregates." *ASTM International STP 169 D-EB*: 548-560.

Holm, T.A., and J.P. Ries. 2005. "Specified Density Concrete: A Transition for the Concrete Industry." Expanded Shale, Clay and Slate Institute. 1-10.

Hussein, M.H., and G.G. Goble. 1987. "Qualitative Evaluation of Force and Velocity Measurements During Pile Driving." *Dynamic Response of Pile Foundations* GSP 11: 166-183.

Hussein, M.H., and G.G. Goble. 2000. "Structural Failure of Pile Foundations During Installation." *ASCE Construction Congress VI: Orlando, FL.* Orlando: ASCE. 799-807.

Hussein, M.H., and F. Rausche. 1991. "Determination of Driving Induced Pile Damage." *Fondations Profondes:* Paris, France. 455-462.

IBC. 2006. "International Building Code." Country Club Hills, IL: International Code Council.

Iwanami, M., E. Kato, H. Yokota, and H. Ito. 2005. "Structural Performance of Lightweight Concrete Columns Subject to Reversed Cyclic Loading." *Concrete for Transportation Infrastructure; Proceedings of the International Conference Held at the University of Dundee*: 205-214.

Jensen, J. J., and K. Hoiseth. 1983. "Impact of Dropped Objects on Lightweight Concrete." *Nordic Concrete Research*: 102-113.

Kahn, L. F., and M. Lopez. 2005. "Prestress Losses in High Performance Lightweight Concrete Pretensioned Bridge Girders." *PCI Journal*, Sept./Oct.: 84-94.

Kayali, O., and B. Zhu. 2005. "Chloride induced reinforcement corrosion in lightweight aggregate high-strength fly ash concrete." *Construction and Building Materials* 19: 327-336.

Ke, Y., A.L. Beaucour, S. Ortola, H. Dumontet, and R. Cabrillac. 2009. "Influence of volume fraction and characteristics of lightweight aggregates on the mechanical properties of concrete." *Construction and Building Materials* 23: 2821-2828.

Keeton, J.R.1970. *Permeability Studies of Reinforced Thin-Shell Concrete.* Technical Report, Port Hueneme, CA: Naval Facilities Engineering Command.

Ke-feng, T., and O. Gjorv. 2003. "The Accelerated Test of Chloride Permeability of Concrete." *Journal of Wuhan University of Technology - Materials Science Ed.* 18, no. 2: 57-60.

Kohno, K., T. Okamoto, Y. Isikawa, T. Sibata, and H. Mori. 1999. "Effects of Artificial Lightweight Aggregate on Autogenous Shrinkage of Concrete." *Cement and Concrete Research* 29: 611-614.

Kosmatka, S. H., B. Kerkhoff, and W. C. Panarese. 2002. *Design and Control of Concrete Mixtures.* Engineering Bulletin, Skokie, IL: Portland Cement Association.

Likins, G. 2011. "CAPWAP." *PDCA Professor's Driven Pile Institute 2011.*

Likins, G. 2011. "Dynamic Pile Testing." *PDCA Professor's Driven Pile Institute 2011*.

Likins, G. 2005. "Pile Driving Equipment." *PDCA Professor's Driven Pile Institute 2005*.

Lo, T. Y., and H. Z. Cui. 2004. "Effect of porous lightweight aggregate on strength of concrete." *Materials Letters* 58: 916-919.

Lo, T. Y., H. Z. Cui, A. Nadeem, and Z. G. Li. 2006. "The Effects of Air Content Permeability of Lightweight Concrete." *Cement and Concrete Research*: 1874-1878.

Lo, T.Y., W.C. Tang, and H.Z. Cui. 2007. "The Effects of Aggregate Propertes on Lightweight Concrete." *Building and Environment* 42: 3025-3029.

Lo, Y., X.F. Gao, and A.P. Jeary. 1999. "Microstructure of pre-wetted aggregate on lightweight concrete." *Building and Environment*: 759-764.

Lura, P., O. M. Jensen, and S. Igarashi. 2007. "Experimental Observation of Internal Water Curing of Concrete." *Materials and Structures*: 211-220.

Lydon, F.D., and R.V. Balendran. 1986. "Some observations on elastic properties of plain concrete." *Cement and Concrete Research*: 314-324.

Maltais, Yannick, Eric Ouellet, Jacques Marchand, Eric Samson, and Douglas Burke. 2006. "Prediction of the long-term durability of lightweight aggregate concrete mixtures under severe marine environment." *Materials and Structures* 39: 911-918.

Mao, J., and K. Ayuta. 2008. "Freeze-Thaw Resistance of Lightweight Concrete and Aggregate at Different Freezing Rates." *Journal of Materials in Civil Engineering*: 78-84.

Mathias, D., and M. Cribbs. 1998. *Driven 1.0: A Microsoft Windows Based Program for Determining Ultimate Vertical Static Pile Capacity.* User's Manual, FHWA.

McCarthy, David F. 2002. *Essentials of Soil Mechanics and Foundations: Basic Geotechnics.* 6th. Upper Saddle River: Prentice-Hall.

Mehta, P.K., and P. J.M. Monteiro. 2006. *Concrete: Microstructure, Properties, and Materials.* 3rd. New York: McGraw-Hill.

Mladenovic, A., J. S. Suput, V. Ducman, and A. S. Skapin. 2004. "Alkali-Silica Reactivity of Some Frequently Used Lightweight Aggregates." *Cement and Concrete Research*: 1809-1816.

Morgan, M.H. 1960. *Vitruvius: The Ten Books of Architecture.* New York: Dover Publications, Inc.

Neville, A.M. 2011. *Properties of Concrete.* 5th. London: Pearson.

PCI Committee on Prestressed Concrete Piling. 1993. *Recommended Practice for Design, Manufacture and Installation of Prestressed Concrete Piling.* Chicago, IL: Precast/Prestressed Concrete Institute, 14-42.

Pile Dynamics Incorporated. 2010. *GRL WEAP Procedures and Models.* Background Report, Cleveland, OH: Pile Dynamics Incorporated.

Ronne, M., and T.A. Hammer. 1999. "Delayed Ettringite Formation in Structural Lightweight Aggregate Concrete: Effect of Curing Temperature, Moisture, and Silica Fume Content." *Cement, Concrete, and Aggregates* 21, no. 2: 202-211.

Rossignolo, J.A., M.V.C. Agnesini, and J.A. Morais. 2003. "Properties of High-Performance LWAC for Precast Structures with Brazilian Lightweight Aggregates." *Cement and Concrete Composites* 25: 77-82.

Sandvik, M., and O.E. Gjorv. 1992. "High Curing Temperatures in Lightweight High-Strength Concrete." *Concrete International*: 40-42.

Schmertmann, J.H. 1967. *Guidelines for Use in the Soils Investigation and Design of Foundations for Bridge Structures in the State of Florida.* Research Bulletin No. 121, Florida State Road Department: Division of Materials, Research and Training.

Soil Consultants Inc. 2004. *Log of Boring B-1: Geotechnical Investigation of the Citadel Property, Dunneman Avenue.* January 1, 2004. Charleston, SC.

Soil Consultants Inc. 2002. *Log of Boring B-1: Proposed Building, Dunneman Avenue*. June 21, 2002. Charleston, SC.

Shah, S.P., A.E. Naaman, and J. Moreno. 1983. "Effect of confinement on the ductility of lightweight concrete." *The International Journal of Cement Composites and Lightweight Concrete* 5, no. 1: 15-25.

Sin, L., W. Huan, M. Islam, and M. Mansur. 2011. "Reinforced Lightweight Concrete Beams in Flexure." *ACI Structural Journal*, Jan/Feb: 3-12.

Smith, E.A.L. 1960. "Pile Driving Analysis by the Wave Equation." *Journal of the Soil Mechanics and Foundations Division* 86, no. 4: 35-61.

Suleiman, M.T., T. Vande Voort, and S. Sritharan. 2010. "Behavior of Driven Ultrahigh-Performance Concrete H-Piles Subjected to Vertical and Lateral Loadings." *Journal of Geotechnical and Geoenvironmental Engineering* 136, no. 10: 1403-1413.

Swamy, R.N., and A.K. Bandyopadhyay. 1975. "The elastic properties of structural lightweight concrete." *Proceedings of the Institute of Civil Engineers:* 381-394.

Tomlinson, M.J. 1994. *Pile Design and Construction Practice.* 4th. New York: Champman and Hall.

US Bureau of Reclamation. 1975. "Concrete Manual."

Vande Voort, T., M.T. Suleiman, and S. Sritharan. 2008. *Design and performance verifcation of ultra-high performance concrete piles for deep foundations.* Final Report; IHRB Project TR-558, CTRE Project 06-264, Ames, IA: Iowa Dept. of Transportation.

Verbeck, G.J., and R.H. Helmuth. 1968. "Structure and Physical Properties of Cement Pastes." *Proceedings, Fifth International Symposium on the Chemistry of Cement* III: 1-32.

Waldron, C.J., T.E. Cousins, A.J. Nassar, and J.P. Gomez, 2005. "Demonstration of Use of High Performance Lightweight Concrete Bridge Superstructure in Virginia." *Journal of Performance of Constructed Facilities* 19, no. 2: 146-154.

Wasserman, R., and A. Bentur. 1996. "Interfacial Interactions in Lightweight Aggregate Concretes and their Influence on the Concrete Strength." *Cement and Concrete Composites* (18): 67-76.

Weber, S., and H.W. Reinhardt. 1997. "A New Generation of High Performance Concrete: Concrete with Autogenous Curing." *Advanced Cement Based Materials*

6, no. 2: 59-68. *Proceedings of the Fifth International Conference on the Application of Stress-wave Theory to Piles 1996*: Orlando, FL: 980-990.

Webster,S. and W. Teferra. 1996. "Pile Damage Assessments Using the Pile Driving Analyzer." *Proceedings of the Fifth International Conference on the Application of Stress-wave Theory to Piles 1996*. Orlando, FL: 980-990.

Zhang, M-H, and O.E. Gjorv, 1990. "Microstructure of the Interfacial Zone Between Lightweight Aggregate and Cement Paste." *Cement and Concrete Research* 20, no. 4: 610-618.

Zhutovsky, S., K. Kovler, and A. Bentur. 2002. "Efficiency of Lightweight Aggregates for Internal Curing of High Strength Concrete to Eliminate Autogenous Shrinkage." *Materials and Structures*: 97-101.

APPENDIX A: STALITE DATA SHEETS

STALITE Lightweight Aggregate
Properties and Gradations for Structural Applications

	3/4" (18mm)		1/2" (12.5mm)		3/8" (9.5mm)		Fines (#4 - 0)	
Typical Density (Unit Weight)	lbs/cf	kg/m^3	lbs/cf	kg/m^3	lbs/cf	kg/m^3	lbs/cf	kg/m^3
Dry Loose (ASTM C 29)	48	768	50	800	52	832	60	960
Dry Rodded (ASTM C 29)	55	880	56	896	58	928	65	1040
Saturated Surface Dry Loose (ASTM C 29)	50	800	52	832	53	848	55	880
Maximum Dry Density (ASTM D 4253)	60	960	-		-		-	
Damp Loose (ASTM C 29)	48 - 52	768-832	50 - 54	800-864	51 - 55	816-880	53 - 57	848-912
Typical Relative Density (Specific Gravity)								
Dry (ASTM C 127)	1.46		1.47		1.54		1.69	
Saturated Surface Dry (ASTM C 127)	1.52		1.53		1.60		1.75	
Range in Saturated Surface Dry (ASTM C 127)	1.47 - 1.54		1.49 - 1.55		1.57 - 1.64		1.70 - 1.80	
Sieve Size	% Passing		% Passing		% Passing		% Passing	
1" (25mm)	100		100		100		100	
3/4" (19mm)	90-100		100		100		100	
1/2" (12.5mm)	-		90-100		100		100	
3/8" (9.5mm)	10-50		40-80		80-100		100	
#4 (4.75mm)	0-15		0-20		5-40		91-96	
#8 (2.36mm)	-		0-10		0-20		59-75	
#16 (1.18mm)	-		-		0-10		39-55	
#30 (600um)	-		-		-		23-38	
#50 (300um)	-		-		-		15-27	
#100 (150um)	-		-		-		9-19	

APPENDIX B: CGES SOIL SPT BORINGS

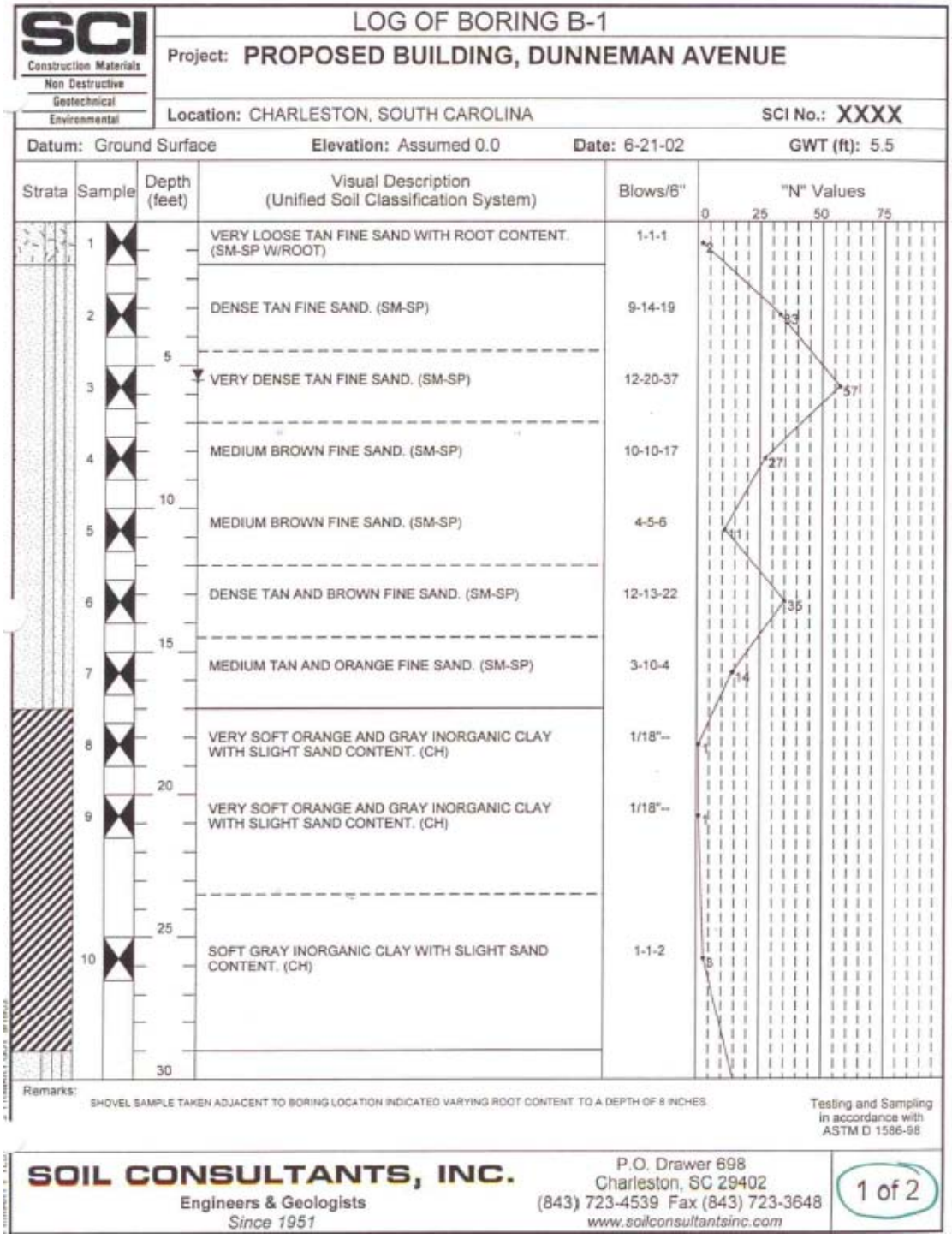

SCI Construction Materials
Non Destructive
Geotechnical
Environmental

LOG OF BORING B-1

Project: PROPOSED BUILDING, DUNNEMAN AVENUE

Location: CHARLESTON, SOUTH CAROLINA SCI No.: XXXX

Datum: Ground Surface Elevation: Assumed 0.0 Date: 6-21-02 GWT (ft): 5.5

Strata	Sample	Depth (feet)	Visual Description (Unified Soil Classification System)	Blows/6"
	1		VERY LOOSE TAN FINE SAND WITH ROOT CONTENT. (SM-SP W/ROOT)	1-1-1
	2		DENSE TAN FINE SAND. (SM-SP)	9-14-19
	3	5	VERY DENSE TAN FINE SAND. (SM-SP)	12-20-37
	4		MEDIUM BROWN FINE SAND. (SM-SP)	10-10-17
	5	10	MEDIUM BROWN FINE SAND. (SM-SP)	4-5-6
	6		DENSE TAN AND BROWN FINE SAND. (SM-SP)	12-13-22
	7	15	MEDIUM TAN AND ORANGE FINE SAND. (SM-SP)	3-10-4
	8		VERY SOFT ORANGE AND GRAY INORGANIC CLAY WITH SLIGHT SAND CONTENT. (CH)	1/18"--
	9	20	VERY SOFT ORANGE AND GRAY INORGANIC CLAY WITH SLIGHT SAND CONTENT. (CH)	1/18"--
	10	25	SOFT GRAY INORGANIC CLAY WITH SLIGHT SAND CONTENT. (CH)	1-1-2
		30		

"N" Values: 0 25 50 75

Remarks: SHOVEL SAMPLE TAKEN ADJACENT TO BORING LOCATION INDICATED VARYING ROOT CONTENT TO A DEPTH OF 8 INCHES.

Testing and Sampling in accordance with ASTM D 1586-98

SOIL CONSULTANTS, INC.
Engineers & Geologists
Since 1951

P.O. Drawer 698
Charleston, SC 29402
(843) 723-4539 Fax (843) 723-3648
www.soilconsultantsinc.com

1 of 2

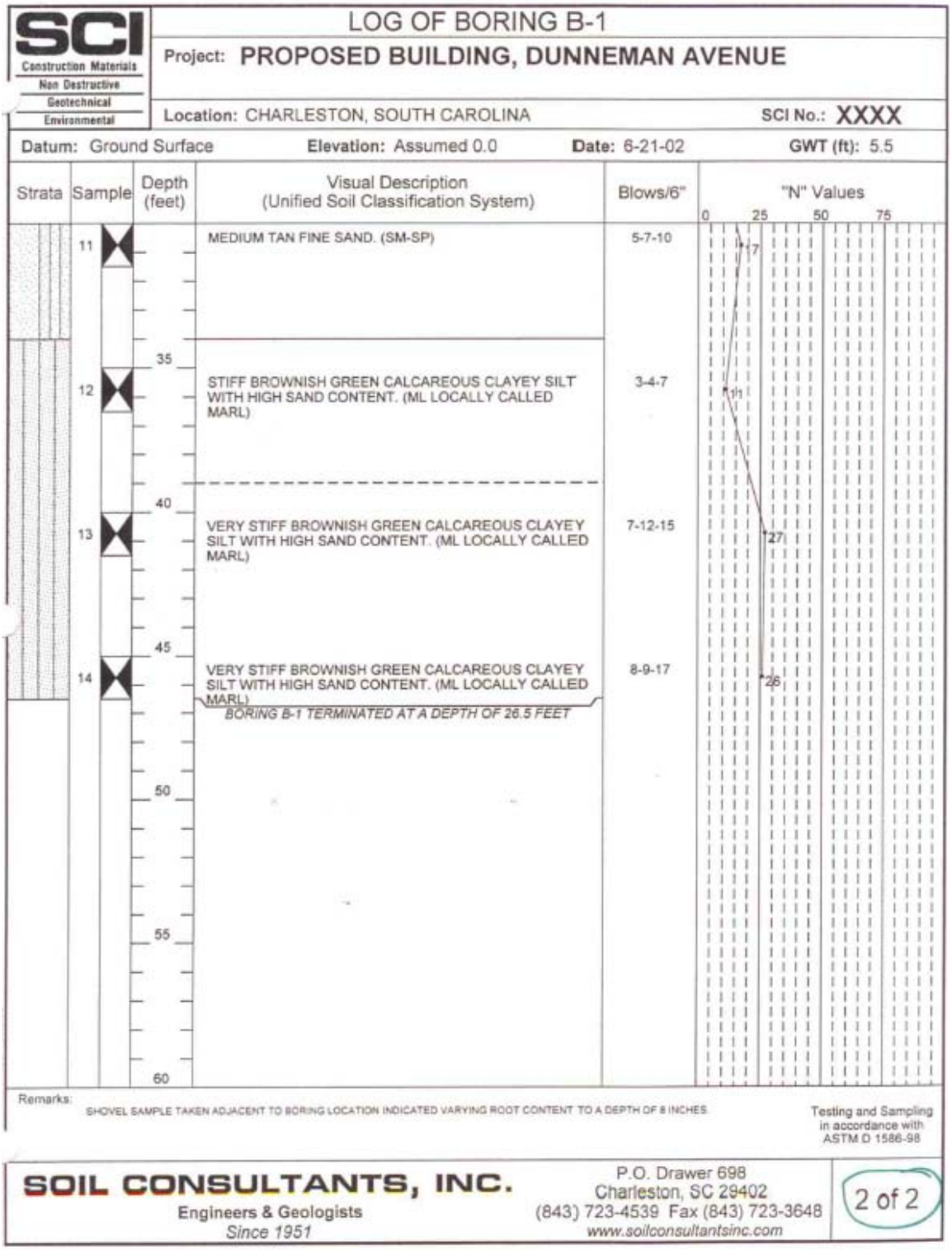

Figure B1. 2002 CGES SPT soil boring

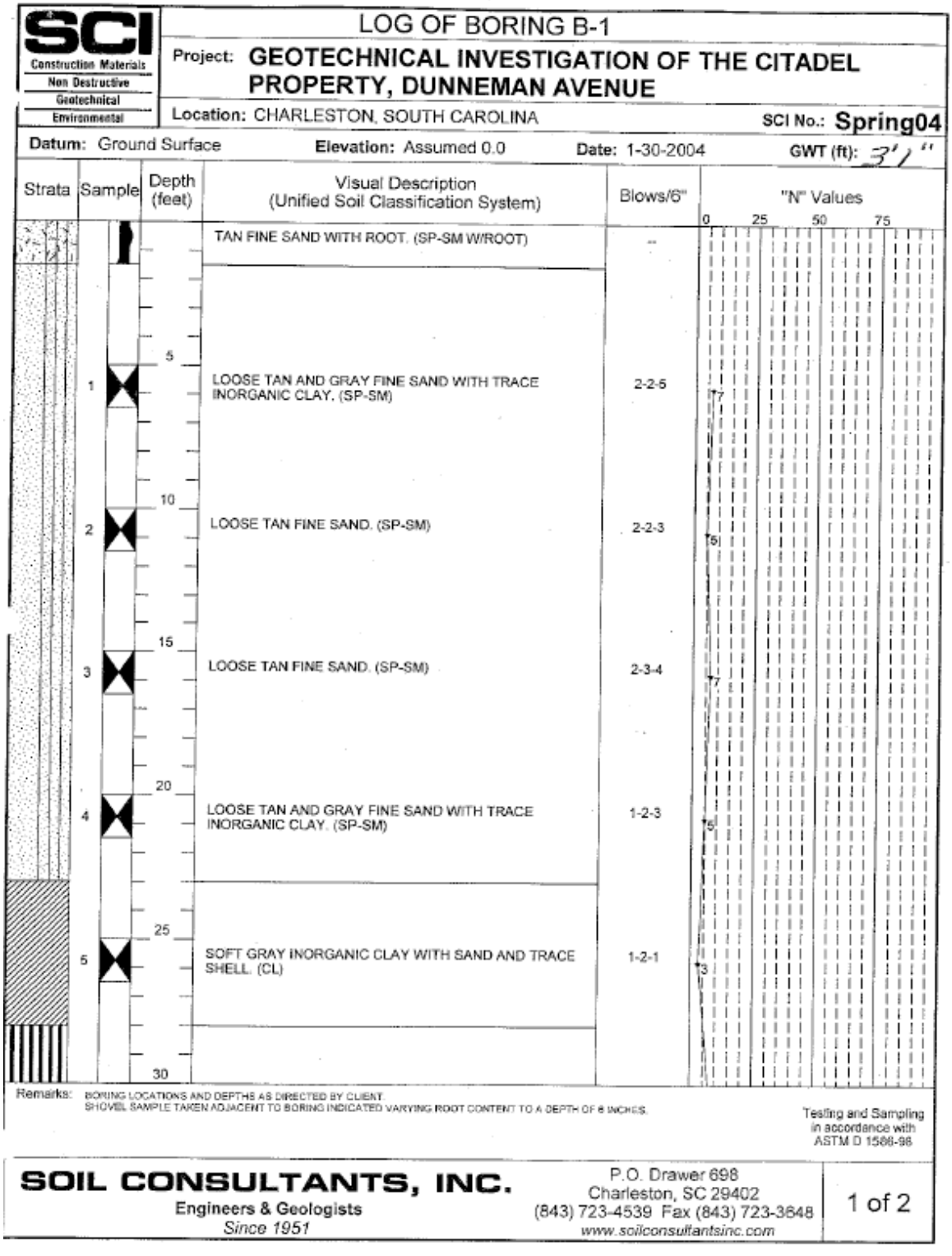
SCI
Construction Materials
Non Destructive
Geotechnical
Environmental
LOG OF BORING B-1
Project: GEOTECHNICAL INVESTIGATION OF THE CITADEL PROPERTY, DUNNEMAN AVENUE
Location: CHARLESTON, SOUTH CAROLINA
SCI No.: Spring04
Datum: Ground Surface
Elevation: Assumed 0.0
Date: 1-30-2004
GWT (ft): 3' 1"
Strata
Sample
Depth (feet)
Visual Description (Unified Soil Classification System)
Blows/6"
"N" Values
0
25
50
75
TAN FINE SAND WITH ROOT. (SP-SM W/ROOT)
LOOSE TAN AND GRAY FINE SAND WITH TRACE INORGANIC CLAY. (SP-SM)
2-2-5
7
LOOSE TAN FINE SAND. (SP-SM)
2-2-3
5
LOOSE TAN FINE SAND. (SP-SM)
2-3-4
7
LOOSE TAN AND GRAY FINE SAND WITH TRACE INORGANIC CLAY. (SP-SM)
1-2-3
5
SOFT GRAY INORGANIC CLAY WITH SAND AND TRACE SHELL. (CL)
1-2-1
3
5
10
15
20
25
30
1
2
3
4
5
Remarks: BORING LOCATIONS AND DEPTHS AS DIRECTED BY CLIENT.
SHOVEL SAMPLE TAKEN ADJACENT TO BORING INDICATED VARYING ROOT CONTENT TO A DEPTH OF 6 INCHES.
Testing and Sampling in accordance with ASTM D 1586-98
SOIL CONSULTANTS, INC.
Engineers & Geologists
Since 1951
P.O. Drawer 698
Charleston, SC 29402
(843) 723-4539 Fax (843) 723-3648
www.soilconsultantsinc.com
1 of 2

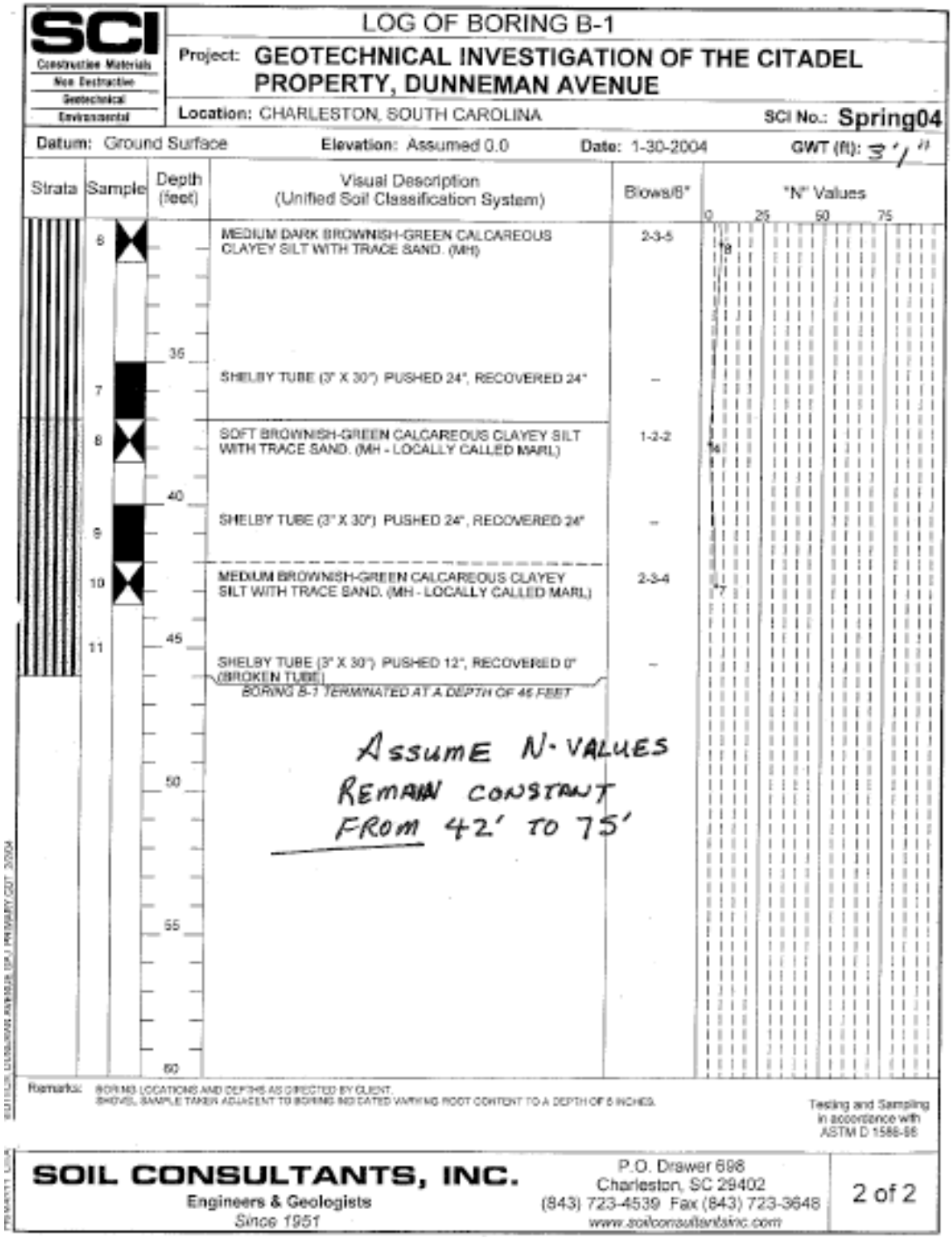

Figure B2. 2004 CGES SPT soil boring

APPENDIX C: 2004 CGES FB-DEEP PILE CAPACITY

Florida Bridge Software Institute Date: January 22, 2013
Shaft and Pile Analysis (FB-Deep v.2.02) Time: 11:47:23

General Information:
==========
Input file: .....RN\Documents\Dissertation\Charleston\CGES\Models\CGES_2004.spc
Project number:
Job name:
Engineer:
Units: English

Analysis Information:
==========
Analysis Type: SPT

Soil Information:
==========
Boring date: , Boring Number:
Station number: Offset:

Ground Elevation: 0.000(ft)

Hammer type: Safety Hammer

ID	Depth (ft)	No. of Blows (Blows/ft)	Soil Type
1	0.00	7.00	2- Clay and silty sand
2	6.00	7.00	2- Clay and silty sand
3	11.00	5.00	2- Clay and silty sand
4	16.00	7.00	2- Clay and silty sand
5	21.00	5.00	2- Clay and silty sand
6	26.00	3.00	1- Plastic Clay
7	31.00	8.00	2- Clay and silty sand

8	38.00	4.00	2- Clay and silty sand
9	42.00	7.00	2- Clay and silty sand
10	65.00	7.00	2- Clay and silty sand

PILE INFORMATION (Pile Length = 50.00 (ft))
==========

Section Type: Square, Width = 12.00(in)
Length = 50.00(ft), Tip Elevation = -50.00(ft)
Unit Weight of Pile = 126.00(pcf), Weight of pile = 3.15(tons)

Skin friction capacity

Soil Layer Num.	Bottom Elev. (ft)	Average SPT Blows (Blows/ft)	Ult. Skin Friction (Tons)	Thick. (ft)	Soil Type
1	-26.00	5.85	26.15	26.00	2- Clay and silty sand
2	-31.00	5.50	3.56	5.00	1- Plastic Clay
3	-65.00	6.62	0.00	34.00	2- Clay and silty sand

(* IN LAYERS ABOVE BEARING LAYER)

Ultimate skin friction in layers above bearing layer = 29.71(tons)
Average SPT in Bearing layer above tip = 6.32(blow/ft)
Ultimate skin friction in bearing layer = 17.57(tons)
Corrected Ultimate skin friction in bearing layer = 17.57(tons)
Total Skin Friction = 47.28(tons)

End bearing capacity

ELEVATION (ft)	SPT Blows (Blows/ft)	UNIT E. B. (tsf)	
-42.00	7.00	3.73	<-- 8B above pile tip
-50.00	7.00	3.73	<-- Pile tip elevation
-53.50	7.00	3.73	<-- 3.5B below pile tip

Average unit end bearing above pile tip = 3.73(tsf)
Average unit end bearing below pile tip = 3.73(tsf)
Average unit end bearing in vicinity of pile tip = 3.73(tsf)

Critical depth of embedment in bearing layer = 4.00(ft)
Actual depth of embedment = 19.00(ft)

Maximum mobilized end bearing capacity = 3.73(tons)
Corrected mobilized end bearing capacity = 3.73(tons)

Pile Capacity

Estimated Davisson capacity = 51.02(tons)
Allowable pile capacity = 25.51(tons)
Ultimate pile capacity = 58.48(tons)

APPENDIX D: LOAD TEST INSTRUMENTATION

Load test instrumentation included the strain gages cast into the LW 50 pile and the inclinometer casing placed into the LW 100 pile. Vibrating wire strain gages measure the frequency and convert it to "Digits" as outlined in the Model 4911 installation manual using Equation 1 where *f* is the measured frequency (Geokon 2012). The apparent strain ($\varepsilon_{apparent}$) was determined using Equation 2 where D_{inst} is the initial reading in digits taken after casting, D_t is the reading in digits at the desired time, and C is the supplied gage factor (Geokon 2012). Calibration data sheets are presented in Figure D1 through Figure D6.

$$Digits = \frac{f^2}{1000} \tag{1}$$

$$\varepsilon_{apparent} = \left(D_t - D_{inst}\right) \times C \tag{2}$$

The apparent strain is presented in Table D1. The depth is presented with respect to the top of the pile (T.O.P.) and not the top of embedment. Embedment of the strain gages within the ground is approximately 2.5 ft (0.76 m) less the depth from the T.O.P. "Near" and "Far" refer to the strand on which the strain gage is attached from the side of the person tying the gages. "Near" refers to the closest strand, and "Far" is the strand furthest away.

Table D1 – Apparent strain measurements

Depth (ft) (T.O.P.)	Location	ε_{2d} ($\mu\varepsilon$)	ε_{6d} ($\mu\varepsilon$)	ε_{drive} ($\mu\varepsilon$)
25	Far	-324	-363	-522
	Near	-389	-427	-333
40	Far	-363	-402	-607
	Near	-391	-428	-392
48	Far	-357	-371	-563
	Near	-341	-375	-206

Note: 1 ft = 0.3028 m

Upon restrike on the LW 100 pile, baseline readings were taken using the inclinometer to set up a "zero" deflection profile before load testing. Baseline inclinometer readings are presented in Table D2.

GEOKON 48 Spencer St, Lebanon, NH 03766 USA

Sister Bar Calibration Report

Model Number: 4911-4 Date of Calibration: June 14, 2012

Serial Number: 1215105 Cable Length: 65 feet

Prestress: 35,000 psi Regression Zero: 7148

Temperature: 23.8 °C Technician:

Calibration Instruction: CI-VW Rebar

Applied Load (pounds)	Readings				Linearity % Max. Load
	Cycle #1	Cycle #2	Average	Change	
100	7200	7199	7200		
1500	7852	7855	7854	654	-0.13
3000	8563	8563	8563	709	-0.12
4500	9278	9278	9278	715	0.09
6000	9985	9986	9986	708	0.03
100	7199	7201	7200		

For conversion factor, load to strain, refer to table C-2 of the Installation Manual

Gage Factor: 0.354 microstrain/ digit (GK-401 Pos. "B")

Calculated Strain = Gage Factor(Current Reading - Zero Reading)

Note: The above calibration uses the linear regression method.

Users are advised to establish their own zero conditions.

Linearity: ((Calculated Load - Applied Load)/Max. Applied Load) X 100 percent

The above instrument was found to be in tolerance in all operating ranges.
The above named instrument has been calibrated by comparison with standards traceable to the NIST, in compliance with ANSI Z540-1.

Figure D1. Far gage at 48 ft (14.6 m) from top of pile

GEOKON 48 Spencer St, Lebanon, NH 03766 USA

Sister Bar Calibration Report

Model Number: 4911-4 Date of Calibration: June 14, 2012

Serial Number: 1215106 Cable Length: 65 feet

Prestress: 35,000 psi Regression Zero: 7238

Temperature: 23.8 °C Technician:

Calibration Instruction: CI-VW Rebar

Applied Load (pounds)	Readings				Linearity % Max. Load
	Cycle #1	Cycle #2	Average	Change	
100	7293	7295	7294		
1500	7942	7946	7944	650	-0.29
3000	8661	8660	8661	717	-0.22
4500	9376	9386	9381	720	-0.01
6000	10098	10101	10100	719	0.13
100	7295	7295	7295		

For conversion factor, load to strain, refer to table C-2 of the Installation Manual

Gage Factor: 0.352 microstrain/ digit (GK-401 Pos. "B")

Calculated Strain = Gage Factor(Current Reading - Zero Reading)

Note: The above calibration uses the linear regression method.

Users are advised to establish their own zero conditions.

Linearity: ((Calculated Load - Applied Load)/Max. Applied Load) X 100 percent

The above instrument was found to be in tolerance in all operating ranges.
The above named instrument has been calibrated by comparison with standards traceable to the NIST, in compliance with ANSI Z540-1.

Figure D2. Near gage at 48 ft (14.6 m) from top of pile

GEOKON 48 Spencer St, Lebanon, NH 03766 USA

Sister Bar Calibration Report

Model Number: 4911-4 Date of Calibration: June 14, 2012

Serial Number: 1215107 Cable Length: 50 feet

Prestress: 35,000 psi Regression Zero: 7051

Temperature: 23.8 °C Technician:

Calibration Instruction: CI-VW Rebar

Applied Load (pounds)	Readings				Linearity % Max. Load
	Cycle #1	Cycle #2	Average	Change	
100	7109	7111	7110		
1500	7764	7769	7767	657	-0.38
3000	8498	8499	8499	732	-0.19
4500	9232	9234	9233	734	0.09
6000	9960	9960	9960	727	0.11
100	7111	7110	7111		

For conversion factor, load to strain, refer to table C-2 of the Installation Manual

Gage Factor: 0.348 microstrain/ digit (GK-401 Pos. "B")

Calculated Strain = Gage Factor(Current Reading - Zero Reading)

Note: The above calibration uses the linear regression method.

Users are advised to establish their own zero conditions.

Linearity: ((Calculated Load - Applied Load)/Max. Applied Load) X 100 percent

The above instrument was found to be in tolerance in all operating ranges
The above named instrument has been calibrated by comparison with standards traceable to the NIST, in compliance with ANSI Z540-1.

Figure D3. Near gage at 40 ft (12 m) from top of pile

GEOKON 48 Spencer St. Lebanon, NH 03766 USA

Sister Bar Calibration Report

Model Number: 4911-4 Date of Calibration: June 14, 2012

Serial Number: 1215108 Cable Length: 50 feet

Prestress: 35,000 psi Regression Zero: 6998

Temperature: 23.8 °C Technician:

Calibration Instruction: CI-VW Rebar

Applied Load (pounds)	Readings				Linearity % Max. Load
	Cycle #1	Cycle #2	Average	Change	
100	7046	7048	7047		
1500	7700	7701	7701	654	-0.03
3000	8403	8404	8404	703	-0.05
4500	9109	9108	9109	705	0.01
6000	9813	9813	9813	704	0.05
100	7048	7052	7050		

For conversion factor, load to strain, refer to table C-2 of the Installation Manual

Gage Factor: 0.356 microstrain/ digit (GK-401 Pos. "B")

Calculated Strain = Gage Factor(Current Reading - Zero Reading)

Note: The above calibration uses the linear regression method.

Users are advised to establish their own zero conditions.

Linearity: ((Calculated Load - Applied Load)/Max. Applied Load) X 100 percent

The above instrument was found to be in tolerance in all operating ranges
The above named instrument has been calibrated by comparison with standards traceable to the NIST, in compliance with ANSI Z540-1

Figure D4. Far gage at 40 ft (12 m) from top of pile

GEOKON 48 Spencer St. Lebanon, NH 03766 USA

Sister Bar Calibration Report

Model Number: 4911-4 Date of Calibration: June 14, 2012

Serial Number: 1215109 Cable Length: 35 feet

Prestress: 35,000 psi Regression Zero: 6978

Temperature: 23.8 °C Technician:

Calibration Instruction: CI-VW Rebar

Applied Load (pounds)	Readings				Linearity % Max. Load
	Cycle #1	Cycle #2	Average	Change	
100	7033	7031	7032		
1500	7671	7671	7671	639	-0.29
3000	8379	8378	8379	708	-0.05
4500	9085	9079	9082	703	0.03
6000	9785	9784	9785	703	0.09
100	7031	7030	7031		

For conversion factor, load to strain, refer to table C-2 of the Installation Manual

Gage Factor: 0.357 microstrain/ digit (GK-401 Pos. "B")

Calculated Strain = Gage Factor(Current Reading - Zero Reading)

Note: The above calibration uses the linear regression method.

Users are advised to establish their own zero conditions.

Linearity: ((Calculated Load - Applied Load)/Max. Applied Load) X 100 percent

The above instrument was found to be in tolerance in all operating ranges
The above named instrument has been calibrated by comparison with standards traceable to the NIST, in compliance with ANSI Z540-1.

Figure D5. Near gage at 25 ft (7.6 m) from top of pile

GEOKON 48 Spencer St. Lebanon, NH 03766 USA

Sister Bar Calibration Report

Model Number: 4911-4 Date of Calibration: June 14, 2012

Serial Number: 1215110 Cable Length: 35 feet

Prestress: 35,000 psi Regression Zero: 7208

Temperature: 23.8 °C Technician:

Calibration Instruction: CI-VW Rebar

Applied Load (pounds)	Readings				Linearity % Max. Load
	Cycle #1	Cycle #2	Average	Change	
100	7268	7263	7266		
1500	7909	7910	7910	644	-0.32
3000	8623	8621	8622	712	-0.24
4500	9342	9339	9341	719	0.04
6000	10058	10051	10055	714	0.16
100	7263	7261	7262		

For conversion factor, load to strain, refer to table C-2 of the Installation Manual

Gage Factor: 0.354 microstrain/ digit (GK-401 Pos. "B")

Calculated Strain = Gage Factor(Current Reading - Zero Reading)

Note: The above calibration uses the linear regression method.

Users are advised to establish their own zero conditions.

Linearity: ((Calculated Load - Applied Load)/Max. Applied Load) X 100 percent

The above instrument was found to be in tolerance in all operating ranges.
The above named instrument has been calibrated by comparison with standards traceable to the NIST, in compliance with ANSI Z540-1.

Figure D6. Far gage at 25 ft (7.6 m) from top of pile

Table D2 – Inclinometer baseline readings (Geokon Model 603)

FLEVEL	A+	A-	B+	B-
-48	-111	63	-68	-15
-46	-38	-23	-95	25
-44	35	-83	-123	63
-42	58	-105	-7	-64
-40	25	-72	123	-189
-38	-14	-48	220	-276
-36	-23	-41	242	-306
-34	84	-130	316	-373
-32	89	-135	307	-362
-30	30	-78	325	-388
-28	110	-158	282	-357
-26	174	-218	238	-310
-24	78	-126	284	-363
-22	52	-104	241	-317
-20	114	-163	277	-352
-18	167	-214	320	-386
-16	198	-223	219	-297
-14	227	-276	155	-215
-12	222	-270	234	-289
-10	172	-219	264	-324
-8	53	-98	339	-389
-6	-88	48	487	-572
-4	-85	32	771	-838
-2	116	-165	841	-909

APPENDIX E: APPLIED HEAT AND CONCRETE TICKETS

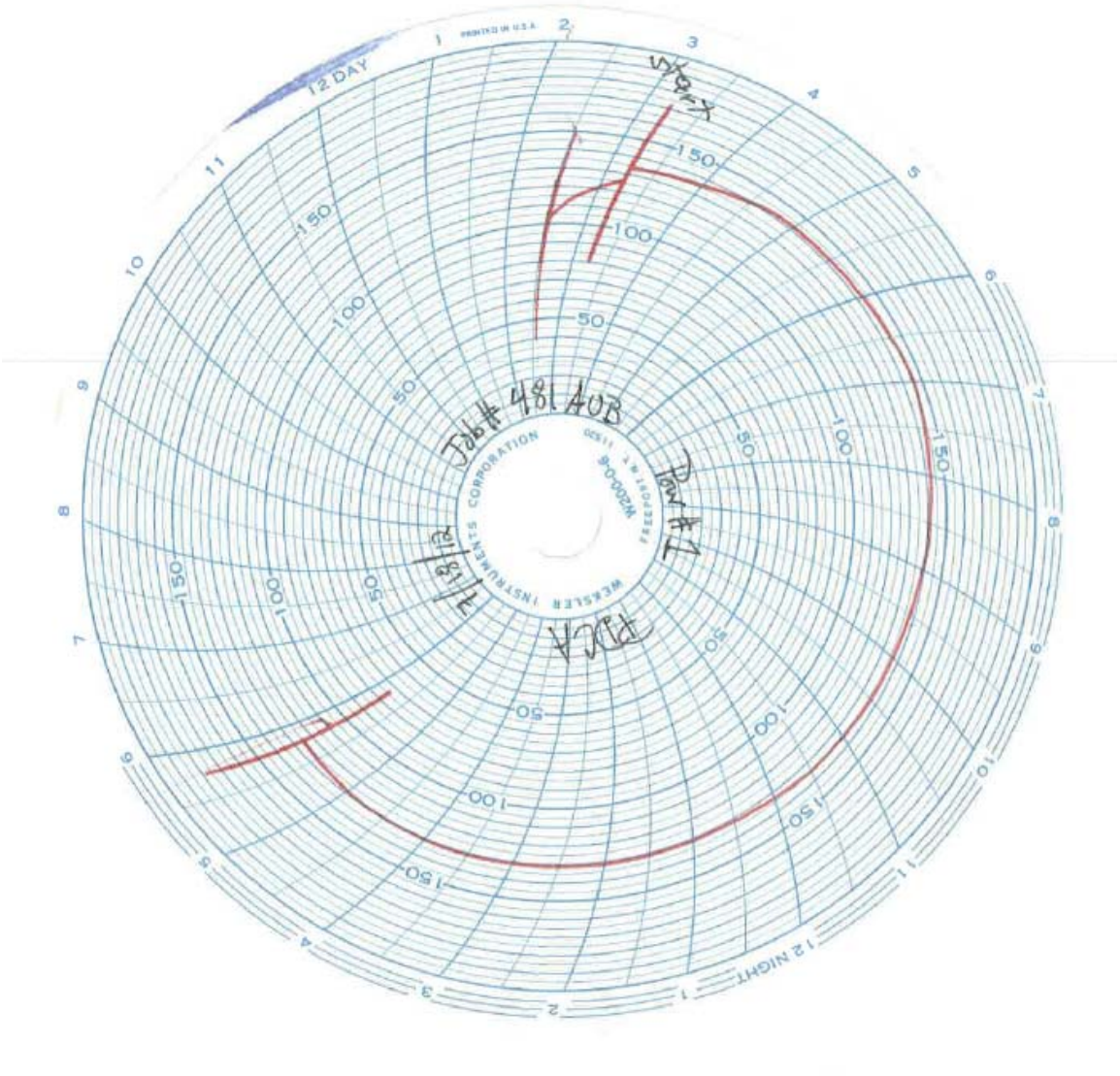

Figure E1. Applied steam curing heat profile

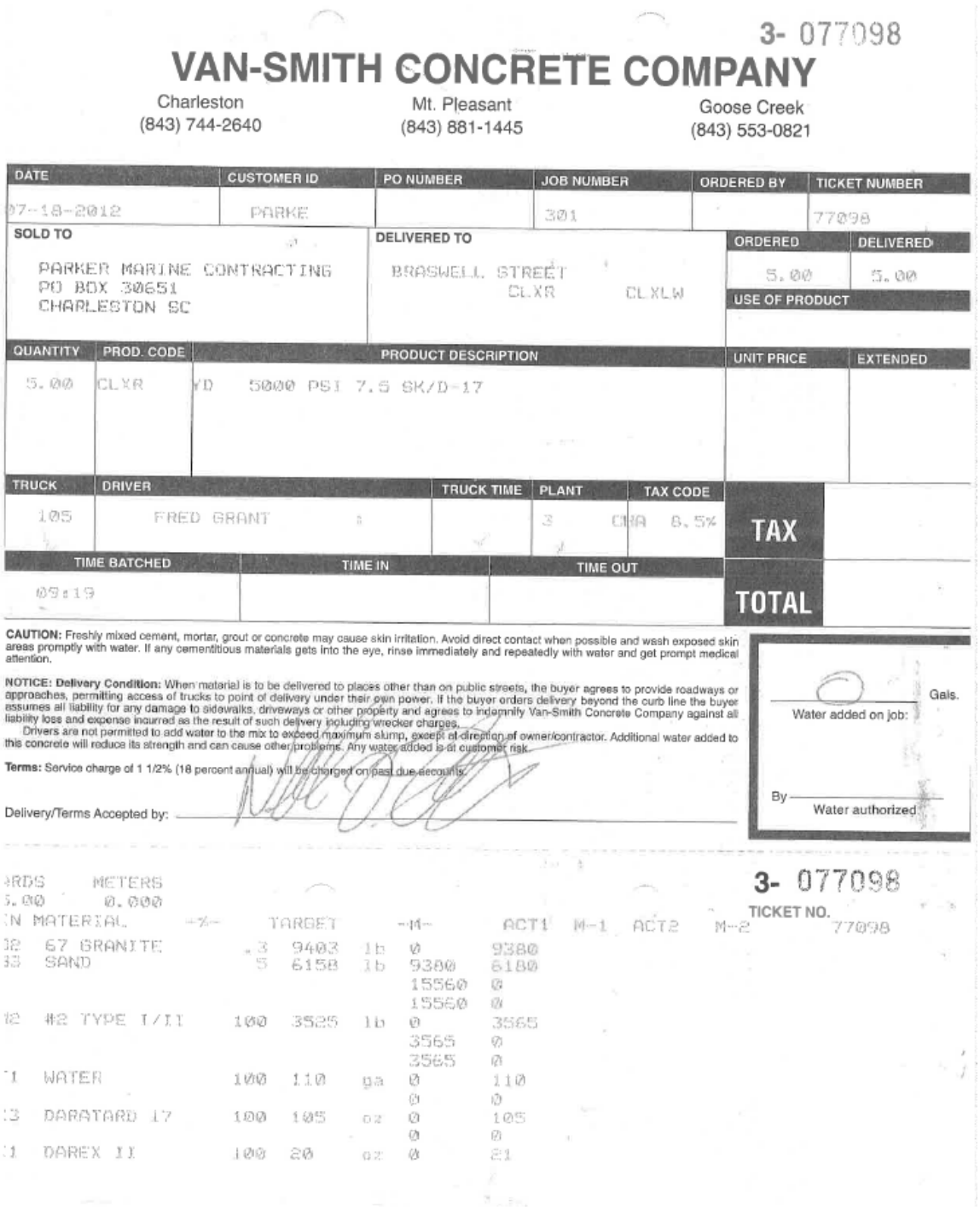

3- 077098

VAN-SMITH CONCRETE COMPANY

Charleston (843) 744-2640 | Mt. Pleasant (843) 881-1445 | Goose Creek (843) 553-0821

DATE	CUSTOMER ID	PO NUMBER	JOB NUMBER	ORDERED BY	TICKET NUMBER
07-18-2012	PARKE		301		77098

SOLD TO	DELIVERED TO	ORDERED	DELIVERED
PARKER MARINE CONTRACTING PO BOX 30651 CHARLESTON SC	BRASWELL STREET CLXR CLXLW	5.00	5.00
		USE OF PRODUCT	

QUANTITY	PROD. CODE	PRODUCT DESCRIPTION	UNIT PRICE	EXTENDED
5.00	CLXR	YD 5000 PSI 7.5 SK/D-17		

TRUCK	DRIVER	TRUCK TIME	PLANT	TAX CODE	
105	FRED GRANT		3	CHA 8.5%	TAX

TIME BATCHED	TIME IN	TIME OUT	
09:19			TOTAL

CAUTION: Freshly mixed cement, mortar, grout or concrete may cause skin irritation. Avoid direct contact when possible and wash exposed skin areas promptly with water. If any cementitious materials gets into the eye, rinse immediately and repeatedly with water and get prompt medical attention.

NOTICE: Delivery Condition: When material is to be delivered to places other than on public streets, the buyer agrees to provide roadways or approaches, permitting access of trucks to point of delivery under their own power. If the buyer orders delivery beyond the curb line the buyer assumes all liability for any damage to sidewalks, driveways or other property and agrees to indemnify Van-Smith Concrete Company against all liability loss and expense incurred as the result of such delivery including wrecker charges.

Drivers are not permitted to add water to the mix to exceed maximum slump, except at direction of owner/contractor. Additional water added to this concrete will reduce its strength and can cause other problems. Any water added is at customer risk.

Terms: Service charge of 1 1/2% (18 percent annual) will be charged on past due accounts.

Delivery/Terms Accepted by: _____

_____ Gals.
Water added on job:

By _____
Water authorized

RDS METERS
5.00 0.000

3- 077098
TICKET NO. 77098

N	MATERIAL	-%-	TARGET		-M-	ACT1	M-1	ACT2	M-2
2	67 GRANITE	3	9403	lb	0	9380			
3	SAND	5	6158	lb	9380	6180			
					15560	0			
					15560	0			
2	#2 TYPE I/II	100	3525	lb	0	3565			
					3565	0			
					3565	0			
1	WATER	100	110	ga	0	110			
					0	0			
3	DARATARD 17	100	105	oz	0	105			
					0	0			
1	DAREX II	100	20	oz	0	21			

Figure E2. NW concrete truck ticket

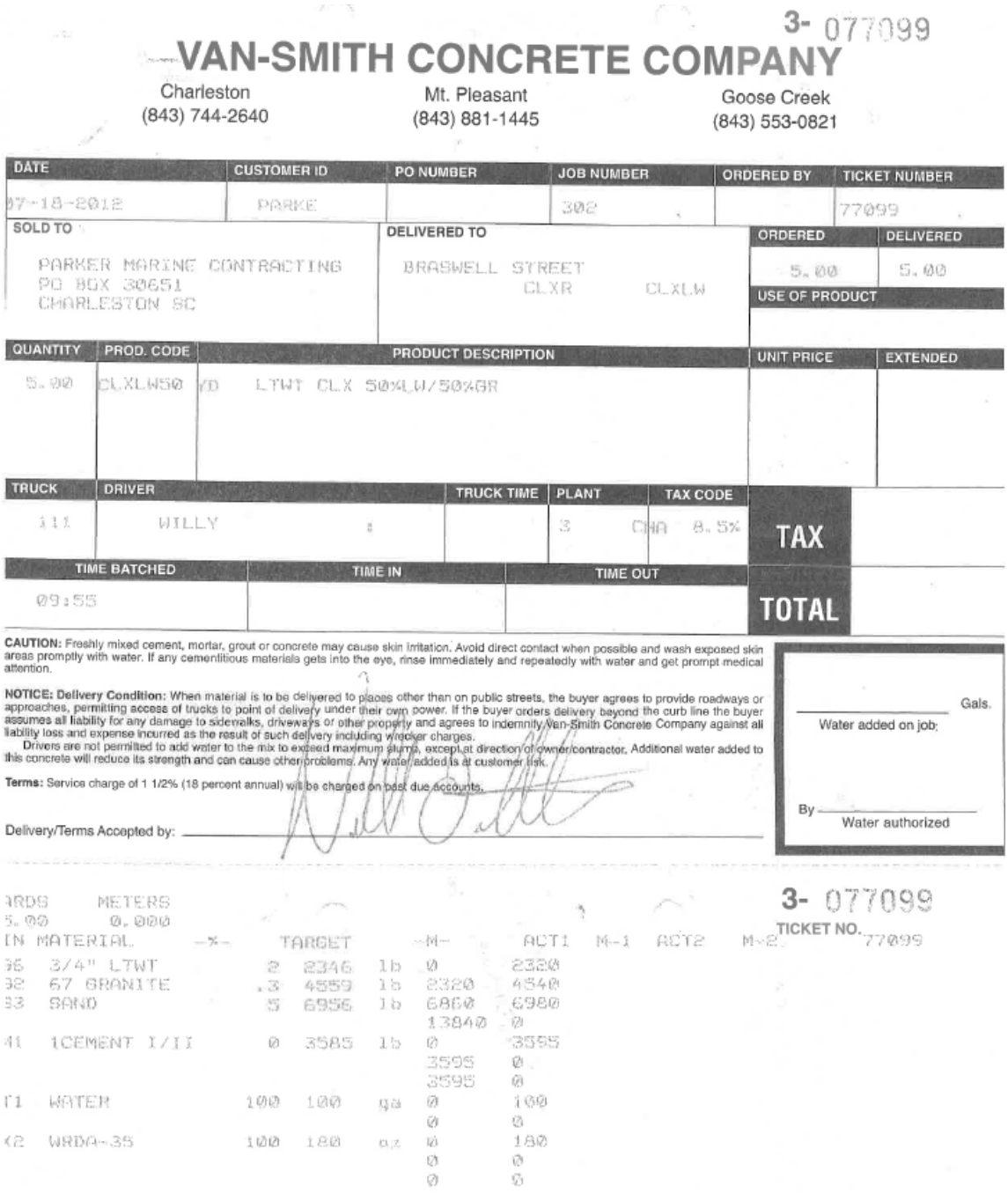

3- 077099

VAN-SMITH CONCRETE COMPANY

Charleston (843) 744-2640 | Mt. Pleasant (843) 881-1445 | Goose Creek (843) 553-0821

DATE	CUSTOMER ID	PO NUMBER	JOB NUMBER	ORDERED BY	TICKET NUMBER
07-18-2012	PARKE		302		77099

SOLD TO	DELIVERED TO	ORDERED	DELIVERED
PARKER MARINE CONTRACTING PO BOX 30651 CHARLESTON SC	BRASWELL STREET CLXR CLXLW	5.00	5.00

USE OF PRODUCT

QUANTITY	PROD. CODE	PRODUCT DESCRIPTION	UNIT PRICE	EXTENDED
5.00	CLXLW50	YD LTWT CLX 50%LW/50%GR		

TRUCK	DRIVER	TRUCK TIME	PLANT	TAX CODE	TAX
111	WILLY		3	CHA 8.5%	

TIME BATCHED	TIME IN	TIME OUT	TOTAL
09:55			

CAUTION: Freshly mixed cement, mortar, grout or concrete may cause skin irritation. Avoid direct contact when possible and wash exposed skin areas promptly with water. If any cementitious materials gets into the eye, rinse immediately and repeatedly with water and get prompt medical attention.

NOTICE: Delivery Condition: When material is to be delivered to places other than on public streets, the buyer agrees to provide roadways or approaches, permitting access of trucks to point of delivery under their own power. If the buyer orders delivery beyond the curb line the buyer assumes all liability for any damage to sidewalks, driveways or other property and agrees to indemnify Van-Smith Concrete Company against all liability loss and expense incurred as the result of such delivery including wrecker charges.

Drivers are not permitted to add water to the mix to exceed maximum slump, except at direction of owner/contractor. Additional water added to this concrete will reduce its strength and can cause other problems. Any water added is at customer risk.

Terms: Service charge of 1 1/2% (18 percent annual) will be charged on past due accounts.

Delivery/Terms Accepted by: _____

_____ Gals.
Water added on job:

By _____
Water authorized

3- 077099
TICKET NO. 77099

WRDS METERS
5.00 0.000

IN	MATERIAL	-%-	TARGET		-M-	ACT1	M-1	ACT2	M-2
36	3/4" LTWT	2	2346	lb	0	2320			
32	67 GRANITE	3	4559	lb	2320	4540			
33	SAND	5	6956	lb	6860	6980			
					13840	0			
41	1CEMENT I/II	0	3585	lb	0	3595			
					3595	0			
					3595	0			
71	WATER	100	100	ga	0	100			
					0	0			
42	WRDA-35	100	180	oz	0	180			
					0	0			
					0	0			

Figure E3. LW50 concrete truck ticket

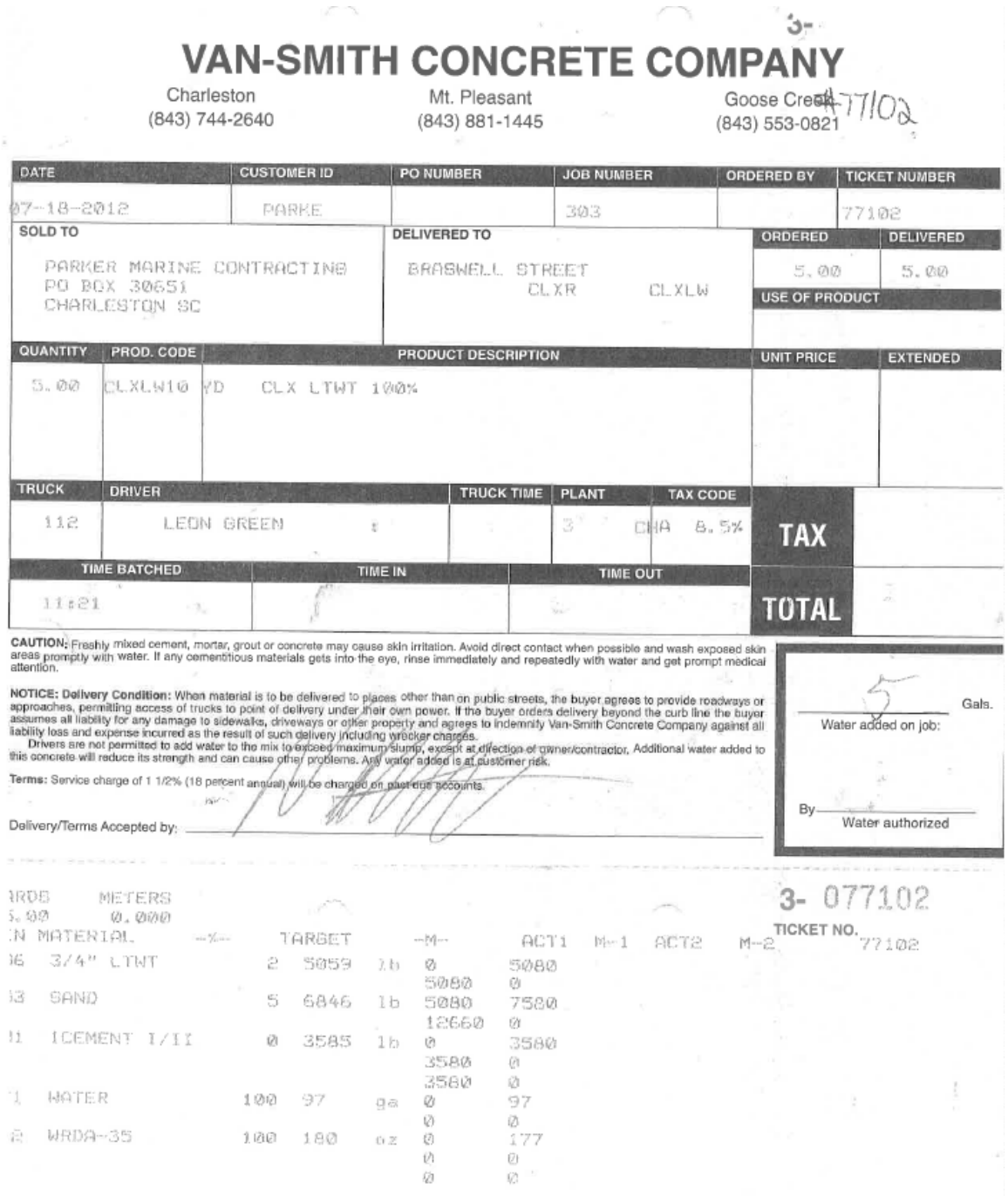

VAN-SMITH CONCRETE COMPANY

Charleston (843) 744-2640 | Mt. Pleasant (843) 881-1445 | Goose Creek (843) 553-0821

3- 077102

DATE	CUSTOMER ID	PO NUMBER	JOB NUMBER	ORDERED BY	TICKET NUMBER
07-18-2012	PARKE		303		77102

SOLD TO
PARKER MARINE CONTRACTING
PO BOX 30651
CHARLESTON SC

DELIVERED TO
BRASWELL STREET
CLXR CLXLW

ORDERED	DELIVERED
5.00	5.00

USE OF PRODUCT

QUANTITY	PROD. CODE	PRODUCT DESCRIPTION	UNIT PRICE	EXTENDED
5.00	CLXLW10	YD CLX LTWT 100%		

TRUCK	DRIVER	TRUCK TIME	PLANT	TAX CODE
112	LEON GREEN		3	CHA 8.5%

TIME BATCHED	TIME IN	TIME OUT
11:21		

TAX

TOTAL

CAUTION: Freshly mixed cement, mortar, grout or concrete may cause skin irritation. Avoid direct contact when possible and wash exposed skin areas promptly with water. If any cementitious materials gets into the eye, rinse immediately and repeatedly with water and get prompt medical attention.

NOTICE: Delivery Condition: When material is to be delivered to places other than on public streets, the buyer agrees to provide roadways or approaches, permitting access of trucks to point of delivery under their own power. If the buyer orders delivery beyond the curb line the buyer assumes all liability for any damage to sidewalks, driveways or other property and agrees to indemnify Van-Smith Concrete Company against all liability loss and expense incurred as the result of such delivery including wrecker charges.

Drivers are not permitted to add water to the mix to exceed maximum slump, except at direction of owner/contractor. Additional water added to this concrete will reduce its strength and can cause other problems. Any water added is at customer risk.

Terms: Service charge of 1 1/2% (18 percent annual) will be charged on past due accounts.

Delivery/Terms Accepted by: _____

5 Gals.
Water added on job:

By _____
Water authorized

WRDS METERS
5.00 0.000

3- 077102
TICKET NO. 77102

N	MATERIAL	-%-	TARGET		-M-	ACT1	M-1	ACT2	M-2
6	3/4" LTWT	2	5059	lb	0	5080			
					5080	0			
3	SAND	5	6846	lb	5080	7580			
					12660	0			
1	CEMENT I/II	0	3585	lb	0	3580			
					3580	0			
					3580	0			
1	WATER	100	97	ga	0	97			
					0	0			
2	WRDA-35	100	180	oz	0	177			
					0	0			
					0	0			

Figure E4. LW100 concrete truck ticket

APPENDIX F: CONCRETE MECHANICAL PROPERTIES

Table F1 – Compressive strength results

Compressive Strength (psi)									
Concrete Mix	Concrete Age (days)								
	0.5	Release	1	3	7	14	28	56	91
Lab NW	-	4610	4970	6050	6810	6860	7230	8520	-
Lab LW50	-	4390	4970	5650	6110	6450	7160	8610	-
Lab LW100	-	4530	4990	6030	6460	6630	7200	8200	-
Charleston NW Std.	2820	3280	3460	4000	4570	5130	5680	-	6390
Charleston LW50 Std.	2640	3500	3660	4220	4650	5480	5590	-	6450
Charleston LW100 Std.	2400	3350	3470	4190	5000	5470	5730	-	-
Charleston NW Field	-	3980	4110	4660	4830	4900	5300	-	6010
Charleston LW50 Field	-	3440	4140	5030	5220	5370	5360	-	6310
Charleston LW100 Field	-	4060	4170	4810	5070	4930	5380	-	6240
Simulated NW Std.	-	-	3830	-	6660	7280	7940	-	-
Simulated LW50 Std.	-	-	3520	-	6660	7240	7690	-	-
Simulated LW100 Std.	-	-	3270	-	6560	7280	7700	-	-
Simulated NW Field	-	-	4960	-	6630	7050	7460	-	-
Simulated LW50 Field	-	-	4640	-	6370	6570	7030	-	-
Simulated LW100 Field	-	-	4850	-	6410	6590	6990	-	-

Note: 1 psi = 0.0069 MPa

Table F2 – Splitting tensile strength results

Splitting Tensile Strength (psi)	
Concrete Mix	Concrete Age (days)
	28
Lab NW	630
Lab LW50	585
Lab LW100	590
Charleston NW Std.	400
Charleston LW50 Std.	365
Charleston LW100 Std.	314*

*One field-cured cylinder tested

Note: 1 psi = 0.0069 MPa

Table F3 – Static modulus of elasticity results

Modulus of Elasticity (ksi)								
Concrete Mix	**Concrete Age (days)**							
	0.5	**Release**	**1**	**3**	**7**	**14**	**28**	**56**
Lab NW	-	5050	5450	5750	5950	6200	6450	6800
Lab LW50	-	3950	4050	4200	4450	4550	4700	5400
Lab LW100	-	3000	3250	3350	3400	3750	3550	4000
Charleston NW Std.	-	3750	-	-	4600	-	5250	-
Charleston LW50 Std.	-	3500	-	-	4250	-	4800	-
Charleston LW100 Std.	-	2900	-	-	3450	-	3800	-
Charleston NW Field	-	3950	-	-	4150	-	4800	-
Charleston LW50 Field	-	3350	-	-	3800	-	4400	-
Charleston LW100 Field	-	3000	-	-	3200	-	3750	-

Note: 1 psi = 0.0069 MPa

APPENDIX G: PILE DRIVING LOGS

Table G1 – Pile 1 driving log (NW)

Depth (ft)	BPF	Depth (ft)	BPF	Depth (ft)	BPF	Depth (ft)	BPF	Depth (ft)	BPF
1	-	11	6	21	9	31	18	41	22
2	-	12	11	22	12	32	20	42	30
3	-	13	10	23	7	33	14	43	30
4	-	14	12	24	4	34	15	44	32
5	-	15	13	25	6	35	14	45	38
6	-	16	10	26	5	36	16	46	23
7	-	17	13	27	6	37	16	47	25
8	-	18	14	28	7	38	18	48	28
9	-	19	12	29	12	39	18	49	24
10	begin	20	10	30	18	40*	19	50	30

* Stroke changed to 1.5 ft
Note: 1 ft = 0.3028 m

Table G2 – Pile 2 driving log (LW50)

Depth (ft)	BPF	Depth (ft)	BPF	Depth (ft)	BPF	Depth (ft)	BPF	Depth (ft)	BPF
1	-	11	5	21	10	31	18	41*	20
2	-	12	9	22	11	32	16	42	18
3	-	13	10	23	11	33	12	43	16
4	-	14	12	24	6	34	12	44	16
5	begin	15	11	25	4	35	12	45	22
6	2	16	12	26	3	36	12	46	30
7	3	17	11	27	ran	37	12	47	32
8	ran	18	12	28	ran	38	15	48	32
9	ran	19	9	29	10	39	15	49	32
10	ran	20	8	30	18	40	14	50	34

* Stroke changed to 1.5 ft
Note: 1 ft = 0.3028 m

Table G3 – Pile 3 driving log (NW)

Depth (ft)	BPF	Depth (ft)	BPF	Depth (ft)	BPF	Depth (ft)	BPF	Depth (ft)	BPF
1	-	11	lost	21	6	31	16	41	20
2	-	12	lost	22	7	32	15	42*	24
3	-	13	lost	23	6	33	12	43	18
4	-	14	lost	24	5	34	10	44	15
5	ran	15	13	25	5	35	11	45	16
6	ran	16	13	26	5	36	12	46	22
7	ran	17	13	27	5	37	15	47	26
8	ran	18	12	28	8	38	15	48	22
9	ran	19	10	29	10	39	15	49	24
10	ran	20	8	30	15	40	15	50	25

* Stroke changed to 1.5 ft
Note: 1 ft = 0.3028 m

Table G4 – Pile 4 driving log (LW100)

Depth (ft)	BPF	Depth (ft)	BPF	Depth (ft)	BPF	Depth (ft)	BPF	Depth (ft)	BPF
1	-	11	4	21	6	31	12	41	19
2	-	12	9	22	5	32	12	42	13
3	-	13	13	23	6	33	9	43	12
4	-	14†	12	24	5	34	9	44	11
5	-	15	12	25	4	35	10	45	15
6	pushed	16	15	26	4	36	16	46	17
7	ran	17	12	27	4	37	13	47	20
8	ran	18	8	28	4	38	15	48	19
9	ran	19	8	29	13	39	15	49	18
10	ran	20	6	30	15	40*‡	17	50	16

* Stroke changed to 1.5 ft
† PDA strain gage stopped working
‡ PDA continued with replacement gage
Note: 1 ft = 0.3028 m

APPENDIX H: PDA TESTING REPORT

S&ME, Inc. - Case Method Results

PDIPLOT Ver. 2010.2 - Printed: 9-Oct-2012

Test date: 25-Jul-2012

Auburn Research Piles - Pile 2 (50% Replacement) - Installation

55-ft, 12-in. Square PSC

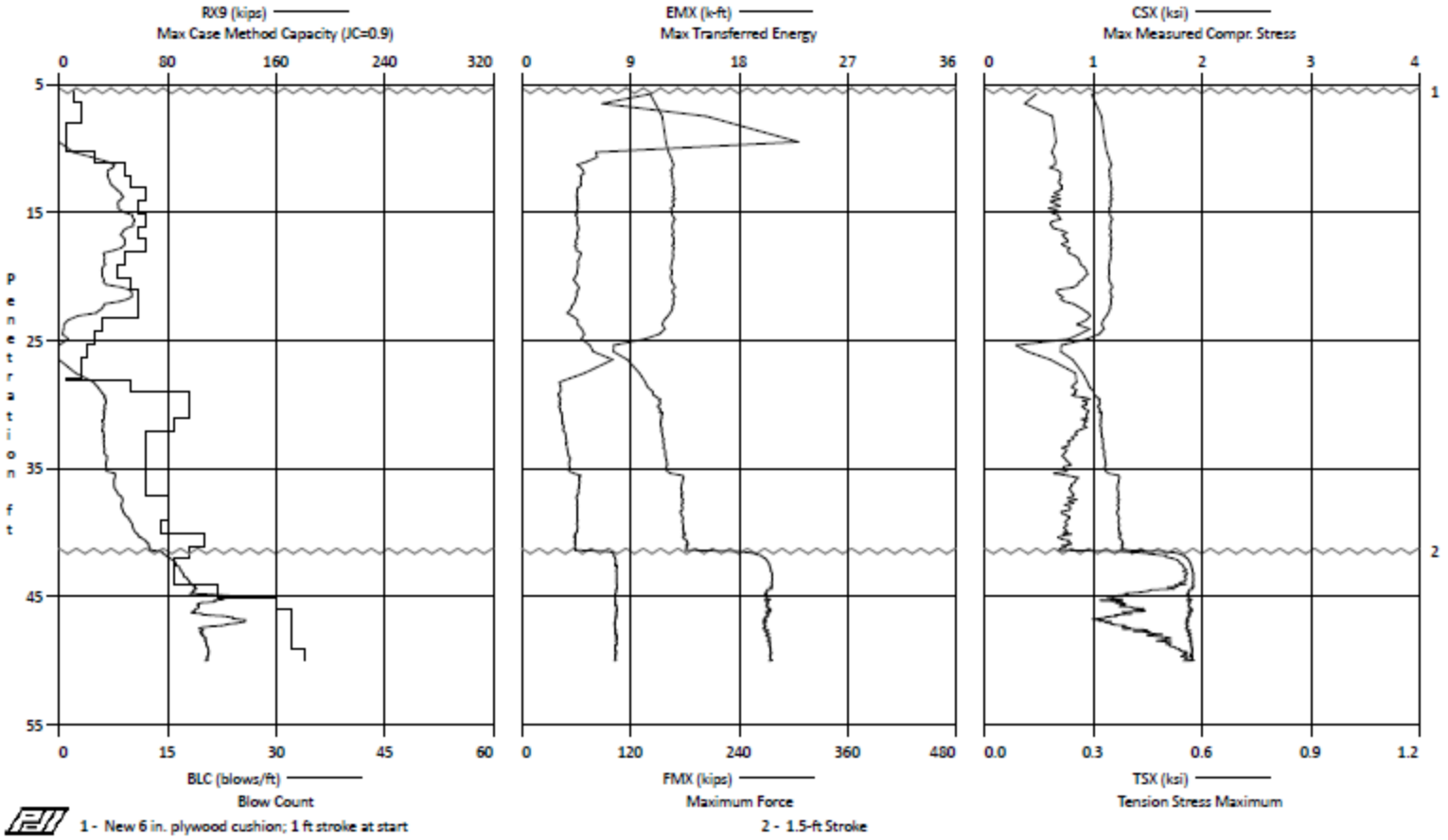

Auburn Research Piles - Pile 2 (50% Replacement) - Installation
OP: RHF
55-ft, 12-in. Square PSC
Test date: 25-Jul-2012

AR: 144.00 in^2
LE: 53.00 ft
WS: 12,500.0 f/s
SP: 0.150 k/ft3
EM: 5,059 ksi
JC: 0.90

RX9: Max Case Method Capacity (JC=0.9)
EMX: Max Transferred Energy
FMX: Maximum Force
VMX: Maximum Velocity
BPM: Blows per Minute
CSX: Max Measured Compr. Stress
TSX: Tension Stress Maximum
DFN: Final Displacement
FVP: Force/Velocity proportionality

BL# end	depth ft	BLC bl/ft	TYPE	RX9 kips	EMX k-ft	FMX kips	VMX f/s	BPM ""	CSX ksi	TSX ksi	DFN in	FVP []
2	6.00	2	AV2	0	10.7	142	4.7	20.1	1.0	0.1	6.00	1.00
			MAX	0	11.3	153	5.1	38.3	1.1	0.2	6.00	1.01
5	7.00	3	AV3	0	7.0	149	4.3	25.8	1.0	0.1	4.00	1.01
			MAX	0	7.6	153	4.4	50.4	1.1	0.2	4.00	1.01
6	8.00	1	AV1	0	22.9	157	9.7	49.5	1.1	0.2	12.01	1.00
			MAX	0	22.9	157	9.7	49.5	1.1	0.2	12.01	1.00
7	9.00	1	AV1	0	23.0	159	10.1	49.6	1.1	0.2	12.01	1.00
			MAX	0	23.0	159	10.1	49.6	1.1	0.2	12.01	1.00
8	10.00	1	AV1	0	22.8	159	9.6	49.5	1.1	0.2	12.01	1.00
			MAX	0	22.8	159	9.6	49.5	1.1	0.2	12.01	1.00
13	11.00	5	AV5	20	6.2	164	4.3	49.5	1.1	0.2	2.40	1.00
			MAX	30	6.2	166	4.3	49.7	1.2	0.2	2.40	1.01
22	12.00	9	AV9	38	4.9	166	4.1	93.0	1.2	0.2	1.33	1.01
			MAX	41	5.2	169	4.2	134.4	1.2	0.2	1.33	1.01
32	13.00	10	AV10	37	4.9	166	4.1	134.1	1.2	0.2	1.20	1.01
			MAX	41	5.0	168	4.1	134.7	1.2	0.2	1.20	1.01
44	14.00	12	AV12	45	4.6	168	4.1	135.2	1.2	0.2	1.00	1.01
			MAX	48	4.6	169	4.1	135.7	1.2	0.2	1.00	1.01
55	15.00	11	AV11	44	4.6	166	4.1	134.6	1.2	0.2	1.09	1.01
			MAX	48	4.7	168	4.2	134.8	1.2	0.2	1.09	1.02
67	16.00	12	AV12	54	4.5	167	4.2	136.5	1.2	0.2	1.00	1.01
			MAX	59	4.6	169	4.2	137.5	1.2	0.2	1.00	1.02
78	17.00	11	AV11	48	4.6	167	4.2	135.1	1.2	0.2	1.09	1.01
			MAX	54	4.7	169	4.2	136.8	1.2	0.3	1.09	1.02
90	18.00	12	AV12	47	4.5	167	4.2	134.4	1.2	0.2	1.00	1.01
			MAX	49	4.6	168	4.2	135.1	1.2	0.2	1.00	1.02
99	19.00	9	AV9	33	4.8	166	4.2	129.8	1.2	0.3	1.33	1.02
			MAX	35	5.0	168	4.2	132.9	1.2	0.3	1.33	1.03
107	20.00	8	AV8	32	4.6	165	4.3	126.0	1.1	0.3	1.50	1.01
			MAX	33	4.8	165	4.4	126.3	1.1	0.3	1.50	1.03
117	21.00	10	AV10	38	4.5	167	4.3	129.0	1.2	0.3	1.20	1.02
			MAX	51	4.8	169	4.3	133.8	1.2	0.3	1.20	1.02
128	22.00	11	AV11	51	4.5	167	4.2	135.1	1.2	0.2	1.09	1.02
			MAX	54	4.6	169	4.2	136.8	1.2	0.2	1.09	1.03
139	23.00	11	AV11	30	4.0	165	4.2	128.7	1.1	0.3	1.09	1.00
			MAX	36	4.4	168	4.3	133.3	1.2	0.3	1.09	1.02
145	24.00	6	AV6	6	4.6	157	4.3	137.8	1.1	0.3	2.00	1.01
			MAX	8	4.7	162	4.4	139.4	1.1	0.3	2.00	1.01
150	25.00	5	AV5	4	5.1	147	4.0	141.2	1.0	0.3	2.40	1.01
			MAX	8	5.3	159	4.4	146.0	1.1	0.3	2.40	1.02
154	26.00	4	AV4	0	5.8	101	3.0	98.6	0.7	0.1	3.00	1.02
			MAX	0	6.0	110	3.2	158.1	0.8	0.1	3.00	1.02
157	27.00	3	AV3	0	7.5	120	3.5	147.3	0.8	0.2	4.00	1.01
			MAX	1	7.7	127	3.7	150.9	0.9	0.2	4.00	1.01
168	29.00	10	AV10	28	3.2	139	3.9	138.0	1.0	0.2	1.20	1.00
			MAX	31	3.3	145	4.1	140.2	1.0	0.3	1.20	1.01
186	30.00	18	AV18	34	3.1	150	4.0	134.6	1.0	0.3	0.67	0.99
			MAX	35	3.3	154	4.2	135.6	1.1	0.3	0.67	1.00
204	31.00	18	AV18	33	3.2	153	4.1	132.7	1.1	0.3	0.67	1.00
			MAX	34	3.4	155	4.2	136.2	1.1	0.3	0.67	1.00
220	32.00	16	AV16	33	3.4	154	4.2	130.4	1.1	0.3	0.75	0.99
			MAX	33	3.5	155	4.2	132.2	1.1	0.3	0.75	1.00

Auburn Research Piles - Pile 2 (50% Replacement) - Installation
OP: RHF
55-ft, 12-in. Square PSC
Test date: 25-Jul-2012

BL# end	depth ft	BLC bl/ft	TYPE	RX9 kips	EMX k-ft	FMX kips	VMX f/s	BPM ""	CSX ksi	TSX ksi	DFN in	FVP []
232	33.00	12	AV12	33	3.6	155	4.3	130.3	1.1	0.2	1.00	0.98
			MAX	33	3.7	158	4.3	132.3	1.1	0.3	1.00	1.00
244	34.00	12	AV12	33	3.8	157	4.3	125.3	1.1	0.2	1.00	0.96
			MAX	35	3.8	159	4.3	130.0	1.1	0.2	1.00	1.00
256	35.00	12	AV12	35	4.0	160	4.4	126.2	1.1	0.2	1.00	0.98
			MAX	36	4.0	162	4.4	127.5	1.1	0.3	1.00	1.00
268	36.00	12	AV12	39	4.5	171	4.6	115.8	1.2	0.2	1.00	0.99
			MAX	47	4.9	179	4.9	127.3	1.2	0.3	1.00	1.00
280	37.00	12	AV12	42	4.7	176	4.7	125.9	1.2	0.2	1.00	0.99
			MAX	44	4.8	178	4.8	128.1	1.2	0.3	1.00	1.00
295	38.00	15	AV15	46	4.6	177	4.7	126.9	1.2	0.2	0.80	0.99
			MAX	47	4.6	179	4.7	128.5	1.2	0.3	0.80	1.00
310	39.00	15	AV15	49	4.6	177	4.6	126.8	1.2	0.2	0.80	0.99
			MAX	52	4.7	179	4.7	127.8	1.2	0.3	0.80	1.00
324	40.00	14	AV14	54	4.6	178	4.6	128.3	1.2	0.2	0.86	1.00
			MAX	56	4.6	180	4.6	130.3	1.3	0.2	0.86	1.01
344	41.00	20	AV20	62	4.4	181	4.6	130.0	1.3	0.2	0.60	0.99
			MAX	66	4.4	184	4.6	131.6	1.3	0.2	0.60	1.00
362	42.00	18	AV18	74	6.3	228	5.7	103.2	1.6	0.4	0.67	0.99
			MAX	81	7.7	268	6.6	131.9	1.9	0.5	0.67	1.00
378	43.00	16	AV16	87	7.8	273	6.5	85.1	1.9	0.5	0.75	1.00
			MAX	90	7.9	276	6.5	85.4	1.9	0.6	0.75	1.01
394	44.00	16	AV16	94	7.8	276	6.4	85.7	1.9	0.6	0.75	1.01
			MAX	98	7.9	277	6.5	86.2	1.9	0.6	0.75	1.01
416	45.00	22	AV22	104	7.8	272	6.2	87.6	1.9	0.5	0.55	1.01
			MAX	129	7.9	278	6.4	89.7	1.9	0.6	0.55	1.01
446	46.00	30	AV30	110	7.8	271	6.0	89.4	1.9	0.4	0.40	1.01
			MAX	128	7.9	276	6.1	90.0	1.9	0.4	0.40	1.01
478	47.00	32	AV32	117	7.8	270	5.8	89.5	1.9	0.4	0.38	1.01
			MAX	138	7.9	275	6.0	90.5	1.9	0.4	0.38	1.01
510	48.00	32	AV32	111	7.7	269	5.9	89.2	1.9	0.4	0.38	1.01
			MAX	133	7.8	273	6.0	90.3	1.9	0.5	0.38	1.02
542	49.00	32	AV32	108	7.8	273	5.9	88.3	1.9	0.5	0.38	1.01
			MAX	110	7.9	275	6.0	89.0	1.9	0.5	0.38	1.02
576	50.00	34	AV34	110	7.8	274	6.1	88.3	1.9	0.6	0.35	1.02
			MAX	111	7.8	277	6.1	88.8	1.9	0.6	0.35	1.02
577	50.03	34	AV1	108	7.6	273	6.0	88.0	1.9	0.6	0.35	1.01
			MAX	108	7.6	273	6.0	88.0	1.9	0.6	0.35	1.02
			Average	65	5.8	206	5.0	111.2	1.4	0.3	0.92	1.00
			Maximum	138	23.0	278	10.1	158.1	1.9	0.6	12.01	1.03

Total number of blows analyzed: 576

BL#	depth (ft)	Comments
1	5.50	New 6 in. plywood cushion; 1 ft stroke at start
352	41.44	1.5-ft Stroke

Time Summary

Drive 5 minutes 51 seconds 12:29:24 PM - 12:35:15 PM (7/25/2012) BN 1 - 577

S&ME, Inc. - Case Method Results

PDIPLOT Ver. 2010.2 - Printed: 9-Oct-2012

Test date: 26-Jul-2012

Auburn Research Piles - Pile 2 (50% Repacement) - Restrike

55-ft, 12-in. Square PSC

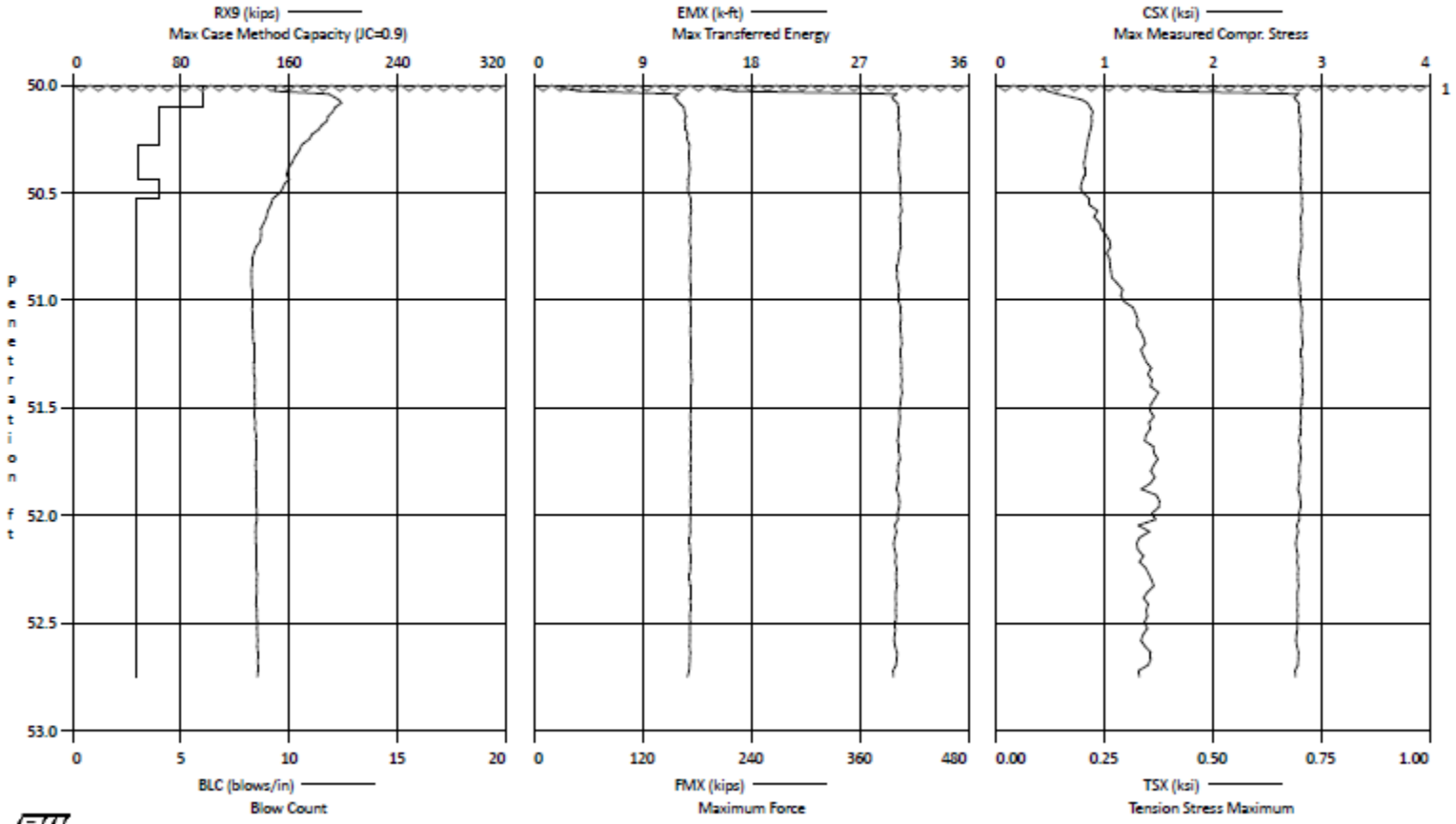

1 - Used 6 in. plywood cushion; 1.5 ft stroke during restrike

Auburn Research Piles - Pile 2 (50% Repacement) - Restrike
OP: RHF
55-ft, 12-in. Square PSC
Test date: 26-Jul-2012

AR: 144.00 in^2
LE: 53.00 ft
WS: 12,500.0 f/s
SP: 0.150 k/ft3
EM: 5,059 ksi
JC: 0.90

RX9: Max Case Method Capacity (JC=0.9)
EMX: Max Transferred Energy
FMX: Maximum Force
VMX: Maximum Velocity
BPM: Blows per Minute
CSX: Max Measured Compr. Stress
TSX: Tension Stress Maximum
DFN: Final Displacement
FVP: Force/Velocity proportionality

BL#	depth	BLC	RX9	EMX	FMX	VMX	BPM	CSX	TSX	DFN	FVP
	ft	bl/in	kips	k-ft	kips	f/s	**	ksi	ksi	in	[]
1	50.01	6	150	2.2	201	1.8	1.9	1.4	0.1	0.17	1.26
2	50.03	6	149	3.8	223	2.8	12.5	1.5	0.1	0.17	1.10
3	50.04	6	189	12.0	401	5.6	16.9	2.8	0.1	0.16	1.07
4	50.06	6	193	11.6	396	5.7	72.6	2.7	0.2	0.17	1.08
5	50.07	6	196	11.8	397	5.8	73.3	2.8	0.2	0.17	1.08
6	50.08	6	198	12.0	402	5.9	73.0	2.8	0.2	0.16	1.07
7	50.10	4	194	12.4	402	6.0	72.9	2.8	0.2	0.25	1.08
8	50.13	4	192	12.5	402	6.0	72.9	2.8	0.2	0.25	1.08
9	50.15	4	188	12.6	403	6.1	72.9	2.8	0.2	0.26	1.08
10	50.17	4	188	12.5	402	6.0	72.9	2.8	0.2	0.25	1.08
11	50.19	4	184	12.6	403	6.1	72.9	2.8	0.2	0.25	1.08
12	50.21	4	181	12.6	404	6.1	72.9	2.8	0.2	0.25	1.08
13	50.23	4	177	12.7	405	6.1	72.8	2.8	0.2	0.25	1.08
14	50.25	4	175	12.7	404	6.1	72.9	2.8	0.2	0.26	1.08
15	50.28	3	169	12.9	404	6.2	72.8	2.8	0.2	0.33	1.08
16	50.31	3	167	12.8	403	6.1	72.8	2.8	0.2	0.33	1.08
17	50.33	3	164	12.8	403	6.2	72.8	2.8	0.2	0.34	1.08
18	50.36	3	162	12.9	404	6.2	72.7	2.8	0.2	0.34	1.08
19	50.39	3	159	12.9	403	6.2	72.7	2.8	0.2	0.33	1.08
20	50.42	3	158	12.8	404	6.2	72.6	2.8	0.2	0.34	1.08
21	50.44	4	160	12.7	405	6.1	72.6	2.8	0.2	0.25	1.08
22	50.46	4	156	12.8	404	6.1	72.6	2.8	0.2	0.25	1.08
23	50.48	4	155	12.7	404	6.1	72.6	2.8	0.2	0.25	1.08
24	50.50	4	153	12.8	405	6.2	72.6	2.8	0.2	0.25	1.08
25	50.53	3	148	13.0	406	6.3	72.5	2.8	0.2	0.34	1.08
26	50.56	3	146	12.9	405	6.3	72.5	2.8	0.2	0.34	1.08
27	50.58	3	144	13.0	406	6.4	72.5	2.8	0.2	0.34	1.08
28	50.61	3	143	12.9	404	6.3	72.4	2.8	0.2	0.34	1.08
29	50.64	3	141	12.9	405	6.4	72.4	2.8	0.2	0.34	1.08
30	50.67	3	139	13.0	405	6.4	72.4	2.8	0.2	0.34	1.08
31	50.70	3	139	12.9	405	6.4	72.4	2.8	0.3	0.34	1.08
32	50.73	3	139	12.9	405	6.4	72.5	2.8	0.3	0.34	1.08
33	50.75	3	135	13.0	405	6.4	72.4	2.8	0.3	0.34	1.08
34	50.78	3	134	12.9	403	6.4	72.4	2.8	0.3	0.34	1.08
35	50.81	3	132	13.0	403	6.5	72.4	2.8	0.3	0.34	1.08
36	50.84	3	132	12.9	402	6.5	72.3	2.8	0.3	0.34	1.08
37	50.87	3	132	12.9	402	6.5	72.3	2.8	0.3	0.34	1.08
38	50.89	3	132	12.9	401	6.5	72.4	2.8	0.3	0.34	1.08
39	50.92	3	132	12.9	403	6.5	72.3	2.8	0.3	0.34	1.08
40	50.95	3	132	13.0	403	6.5	72.3	2.8	0.3	0.34	1.08
41	50.98	3	132	13.0	403	6.6	72.3	2.8	0.3	0.34	1.08
42	51.01	3	132	12.9	403	6.5	72.3	2.8	0.3	0.35	1.08
43	51.03	3	132	13.0	405	6.6	72.3	2.8	0.3	0.34	1.08
44	51.06	3	133	13.0	406	6.6	72.3	2.8	0.3	0.34	1.08
45	51.09	3	133	12.9	405	6.6	72.3	2.8	0.3	0.34	1.08
46	51.12	3	133	13.0	405	6.6	72.3	2.8	0.3	0.34	1.08
47	51.15	3	133	12.9	405	6.6	72.2	2.8	0.3	0.34	1.08
48	51.18	3	133	13.0	406	6.7	72.2	2.8	0.3	0.34	1.09
49	51.20	3	134	13.0	407	6.7	72.2	2.8	0.3	0.34	1.08
50	51.23	3	134	13.0	405	6.7	72.2	2.8	0.3	0.34	1.08
51	51.26	3	134	13.0	405	6.7	72.2	2.8	0.3	0.34	1.08
52	51.29	3	134	12.9	405	6.7	72.2	2.8	0.3	0.34	1.09
53	51.32	3	134	13.0	406	6.7	72.2	2.8	0.4	0.34	1.08
54	51.34	3	134	13.0	406	6.7	72.2	2.8	0.3	0.34	1.08
55	51.37	3	135	13.0	407	6.8	72.2	2.8	0.4	0.34	1.08
56	51.40	3	134	13.0	406	6.7	72.2	2.8	0.4	0.34	1.09
57	51.43	3	134	13.0	407	6.8	72.1	2.8	0.4	0.34	1.08
58	51.46	3	135	13.0	405	6.8	72.1	2.8	0.4	0.34	1.09
59	51.48	3	135	13.0	405	6.7	72.1	2.8	0.4	0.34	1.09
60	51.51	3	134	13.0	404	6.8	72.2	2.8	0.4	0.34	1.09
61	51.54	3	134	12.9	404	6.8	72.0	2.8	0.4	0.34	1.09
62	51.57	3	135	13.0	404	6.7	72.0	2.8	0.4	0.34	1.09
63	51.60	3	134	12.9	403	6.8	72.0	2.8	0.4	0.34	1.08
64	51.63	3	136	13.0	403	6.7	72.0	2.8	0.3	0.34	1.09
65	51.65	3	135	12.9	402	6.8	72.0	2.8	0.3	0.34	1.09

Auburn Research Piles - Pile 2 (50% Repacement) - Restrike
55-ft, 12-in. Square PSC
OP: RHF
Test date: 26-Jul-2012

BL#	depth ft	BLC bl/in	RX9 kips	EMX k-ft	FMX kips	VMX ft/s	BPM **	CSX ksi	TSX ksi	DFN in	FVP []
66	51.68	3	135	13.0	404	6.8	72.0	2.8	0.4	0.34	1.09
67	51.71	3	135	12.9	403	6.8	72.0	2.8	0.4	0.34	1.09
68	51.74	3	135	13.0	405	6.8	72.0	2.8	0.4	0.34	1.09
69	51.77	3	135	12.9	402	6.8	72.1	2.8	0.4	0.34	1.08
70	51.79	3	135	12.9	402	6.8	72.1	2.8	0.4	0.34	1.09
71	51.82	3	135	12.9	403	6.8	72.1	2.8	0.4	0.34	1.09
72	51.85	3	136	13.0	402	6.8	72.1	2.8	0.4	0.34	1.09
73	51.88	3	135	12.9	400	6.7	72.1	2.8	0.3	0.34	1.09
74	51.91	3	136	13.0	403	6.8	72.0	2.8	0.4	0.34	1.09
75	51.93	3	136	13.0	404	6.8	72.0	2.8	0.4	0.34	1.09
76	51.96	3	136	12.9	404	6.8	72.0	2.8	0.4	0.34	1.09
77	51.99	3	136	12.9	402	6.8	72.0	2.8	0.4	0.34	1.09
78	52.02	3	136	13.0	402	6.8	72.0	2.8	0.4	0.34	1.09
79	52.05	3	135	12.9	399	6.7	72.0	2.8	0.3	0.34	1.09
80	52.08	3	135	12.9	401	6.7	71.9	2.8	0.4	0.34	1.09
81	52.10	3	135	12.9	399	6.7	72.0	2.8	0.3	0.34	1.09
82	52.13	3	135	12.9	397	6.7	72.0	2.8	0.3	0.34	1.09
83	52.16	3	136	12.9	399	6.7	72.1	2.8	0.3	0.34	1.09
84	52.19	3	136	12.9	400	6.7	71.9	2.8	0.3	0.34	1.09
85	52.22	3	136	12.9	399	6.7	72.1	2.8	0.3	0.34	1.09
86	52.24	3	135	13.0	401	6.7	72.0	2.8	0.3	0.34	1.09
87	52.27	3	136	12.9	400	6.7	72.0	2.8	0.4	0.34	1.09
88	52.30	3	136	12.9	400	6.8	72.0	2.8	0.4	0.34	1.09
89	52.33	3	136	12.9	401	6.8	72.0	2.8	0.4	0.34	1.09
90	52.36	3	136	12.9	400	6.7	72.0	2.8	0.3	0.34	1.09
91	52.38	3	136	12.9	399	6.7	72.1	2.8	0.3	0.34	1.09
92	52.41	3	135	12.9	400	6.7	72.0	2.8	0.4	0.34	1.09
93	52.44	3	136	12.9	400	6.7	71.9	2.8	0.3	0.34	1.09
94	52.47	3	136	12.9	400	6.7	72.0	2.8	0.3	0.34	1.09
95	52.50	3	136	12.9	399	6.7	71.9	2.8	0.3	0.34	1.09
96	52.53	3	136	12.9	400	6.7	72.0	2.8	0.3	0.34	1.09
97	52.55	3	136	12.9	398	6.7	71.9	2.8	0.3	0.34	1.09
98	52.58	3	137	12.9	398	6.7	72.0	2.8	0.3	0.34	1.09
99	52.61	3	136	12.9	399	6.7	72.0	2.8	0.3	0.34	1.09
100	52.64	3	137	12.9	401	6.7	72.0	2.8	0.4	0.34	1.09
101	52.67	3	137	12.9	401	6.7	71.9	2.8	0.4	0.34	1.10
102	52.69	3	137	12.9	400	6.7	72.0	2.8	0.4	0.34	1.09
103	52.72	3	137	12.8	397	6.6	72.1	2.8	0.3	0.34	1.09
104	52.75	3	136	12.7	397	6.6	72.1	2.8	0.3	0.34	1.09
		Average	144	12.7	399	6.4	70.5	2.8	0.3	0.32	1.09
		Maximum	198	13.0	407	6.8	73.3	2.8	0.4	0.35	1.26

Total number of blows analyzed: 104

BL#	depth (ft)	Comments
1	50.01	Used 6 in. plywood cushion; 1.5 ft stroke during restrike

Time Summary

Drive 1 minute 32 seconds 7:48:08 AM - 7:49:40 AM (7/26/2012) BN 1 - 104

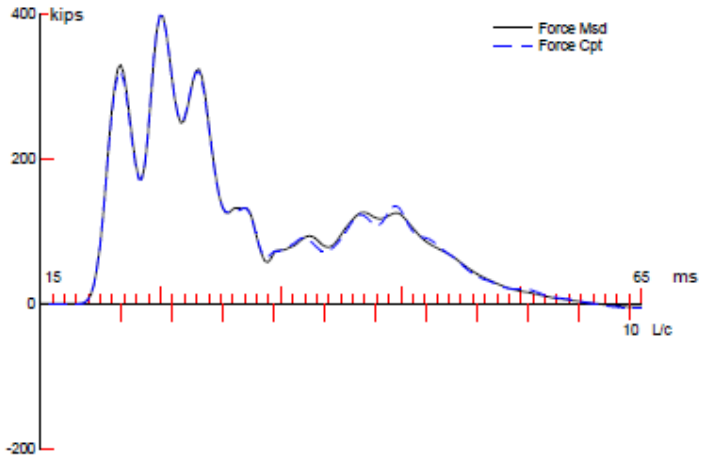
400
kips
200
0
-200
15
65
ms
10
L/c
Force Msd
Force Cpt

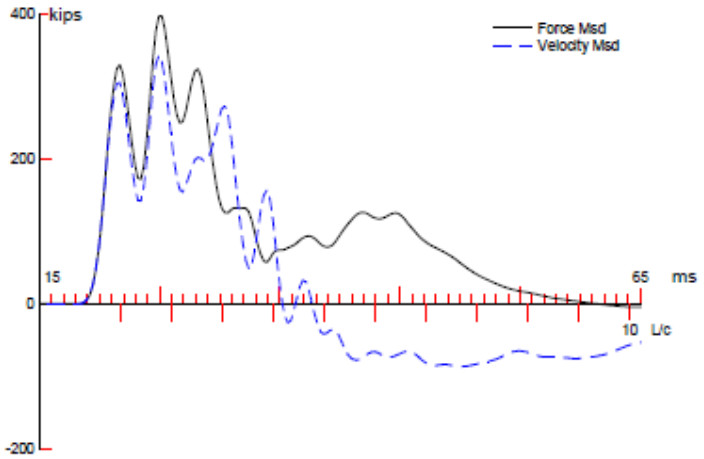
400
kips
200
0
-200
15
65
ms
10
L/c
Force Msd
Velocity Msd

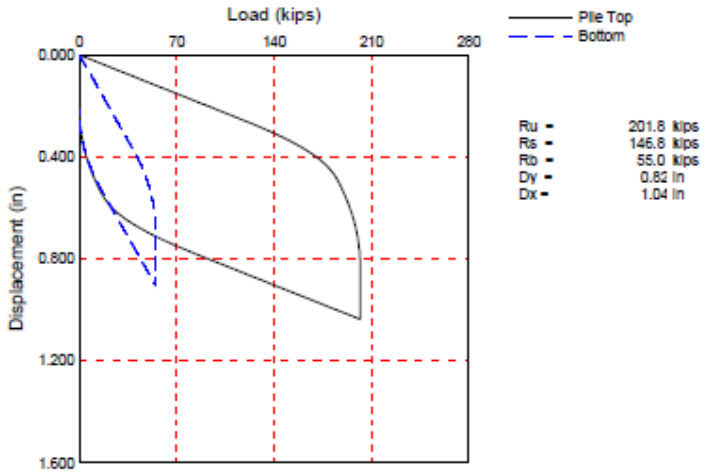
Load (kips)
0
70
140
210
280
0.000
0.400
0.800
1.200
1.600
Displacement (in)
Pile Top
Bottom
Ru = 201.8 kips
Rs = 146.8 kips
Rb = 55.0 kips
Dy = 0.82 in
Dx = 1.04 in

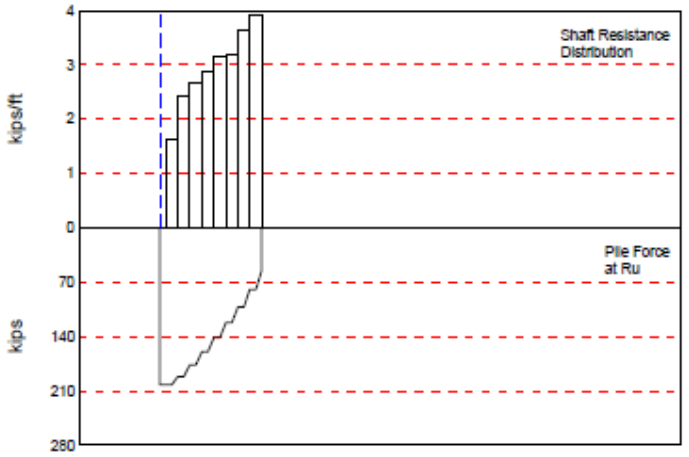
4
3
2
1
0
kips/ft
Shaft Resistance
Distribution
70
140
210
280
kips
Pile Force
at Ru

Auburn Research Piles; Pile: Pile 2 (50% Repacement) - Restrike Test: 26-Jul-2012 07:48:
55-ft, 12-in. Square PSC; Blow: 6 CAPWAP(R) 2006-2
S&ME, Inc. OP: RHF

CAPWAP SUMMARY RESULTS

Total CAPWAP Capacity: 201.8; along Shaft 146.8; at Toe 55.0 kips

Soil Sgmnt No.	Dist. Below Gages ft	Depth Below Grade ft	Ru kips	Force in Pile kips	Sum of Ru kips	Unit Resist. (Depth) kips/ft	Unit Resist. (Area) ksf	Smith Damping Factor s/ft
				201.8				
1	9.4	6.4	10.2	191.7	10.2	1.60	0.40	0.204
2	15.6	12.6	15.2	176.5	25.4	2.44	0.61	0.204
3	21.8	18.8	16.7	159.8	42.1	2.68	0.67	0.204
4	28.1	25.1	18.0	141.8	60.0	2.88	0.72	0.204
5	34.3	31.3	19.7	122.1	79.8	3.16	0.79	0.204
6	40.5	37.5	20.0	102.1	99.7	3.20	0.80	0.204
7	46.8	43.8	22.7	79.4	122.4	3.64	0.91	0.204
8	53.0	50.0	24.4	55.0	146.8	3.92	0.98	0.204
Avg. Shaft			18.4			2.94	0.73	0.204
Toe			55.0				55.00	0.070

Soil Model Parameters/Extensions		Shaft	Toe
Quake	(in)	0.302	0.529
Case Damping Factor		0.513	0.066
Damping Type			Smith
Unloading Quake	(% of loading quake)	118	44
Reloading Level	(% of Ru)	100	100
Unloading Level	(% of Ru)	50	
Resistance Gap (included in Toe Quake)	(in)		0.196
Soil Plug Weight	(kips)		0.29

CAPWAP match quality = 1.39 (Wave Up Match) ; RSA = 0
Observed: final set = 0.218 in; blow count = 55 b/ft
Computed: final set = 0.216 in; blow count = 55 b/ft

max. Top Comp. Stress = 2.80 ksi (T= 25.4 ms, max= 1.031 x Top)
max. Comp. Stress = 2.88 ksi (Z= 9.4 ft, T= 26.2 ms)
max. Tens. Stress = -0.46 ksi (Z= 43.6 ft, T= 27.2 ms)
max. Energy (EMX) = 12.1 kip-ft; max. Measured Top Displ. (DMX)= 0.61 in

EXTREMA TABLE

Pile Sgmnt No.	Dist. Below Gages ft	max. Force kips	min. Force kips	max. Comp. Stress ksi	max. Tens. Stress ksi	max. Trnsfd. Energy kip-ft	max. Veloc. ft/s	max. Displ. in
1	3.1	402.6	-9.2	2.80	-0.06	12.11	5.8	0.611
2	6.2	408.3	-10.8	2.83	-0.08	12.08	5.7	0.605
3	9.4	415.2	-12.5	2.88	-0.09	12.05	5.6	0.600
4	12.5	403.4	-11.3	2.80	-0.08	11.27	5.7	0.596
5	15.6	408.7	-12.7	2.84	-0.09	11.26	5.7	0.593
6	18.7	383.8	-10.3	2.66	-0.07	10.12	5.4	0.590
7	21.8	375.0	-11.6	2.60	-0.08	10.11	5.6	0.586
8	24.9	317.2	-9.1	2.20	-0.06	8.86	6.3	0.582
9	28.1	309.0	-10.2	2.14	-0.07	8.85	7.0	0.579
10	31.2	293.4	-7.6	2.04	-0.05	7.51	7.6	0.575
11	34.3	298.6	-8.5	2.07	-0.06	7.49	7.7	0.571
12	37.4	279.3	-5.9	1.94	-0.04	6.01	7.3	0.567
13	40.5	273.8	-21.3	1.90	-0.15	5.98	6.6	0.561
14	43.6	237.9	-66.1	1.65	-0.46	4.53	5.7	0.556
15	46.8	223.6	-52.3	1.55	-0.36	4.52	6.2	0.553
16	49.9	151.5	-49.3	1.05	-0.34	2.89	7.0	0.550
17	53.0	102.8	-4.7	0.71	-0.03	1.04	7.4	0.547
Absolute	9.4			2.88			(T =	26.2 ms)
	43.6				-0.46		(T =	27.2 ms)

CASE METHOD

J =	0.0	0.1	0.2	0.3	0.4	0.5	0.6	0.7	0.8	0.9
RP	256.8	218.5	180.2	142.0	103.7	65.4	27.1	0.0	0.0	0.0
RX	343.9	306.6	270.7	237.5	212.7	199.9	199.8	199.8	199.8	199.8
RU	256.8	218.5	180.2	142.0	103.7	65.4	27.1	0.0	0.0	0.0

RAU = 183.1 (kips); RA2 = 194.2 (kips)

Current CAPWAP Ru = 201.8 (kips); Corresponding J(RP)= 0.14; J(RX) = 0.48

VMX ft/s	TVP ms	VT1*E kips	FT1 kips	FMX kips	DMX in	DFN in	SET in	EMX kip-ft	QUS kips
5.93	21.95	309.0	330.7	401.6	0.612	0.218	0.218	12.1	351.0

Auburn Research Piles; Pile: Pile 2 (50% Repacement) - Restrike Test: 26-Jul-2012 07:48:
55-ft, 12-in. Square PSC; Blow: 6 CAPWAP(R) 2006-2
S&ME, Inc. OP: RHF

PILE PROFILE AND PILE MODEL

Depth ft	Area in^2	E-Modulus ksi	Spec. Weight lb/ft^3	Perim. ft
0.00	144.00	5057.4	150.000	4.000
53.00	144.00	5057.4	150.000	4.000

Toe Area 1.000 ft^2

Top Segment Length 3.12 ft, Top Impedance 58.28 kips/ft/s

Pile Damping 2.0 %, Time Incr 0.249 ms, Wave Speed 12500.0 ft/s, 2L/c 8.5 ms

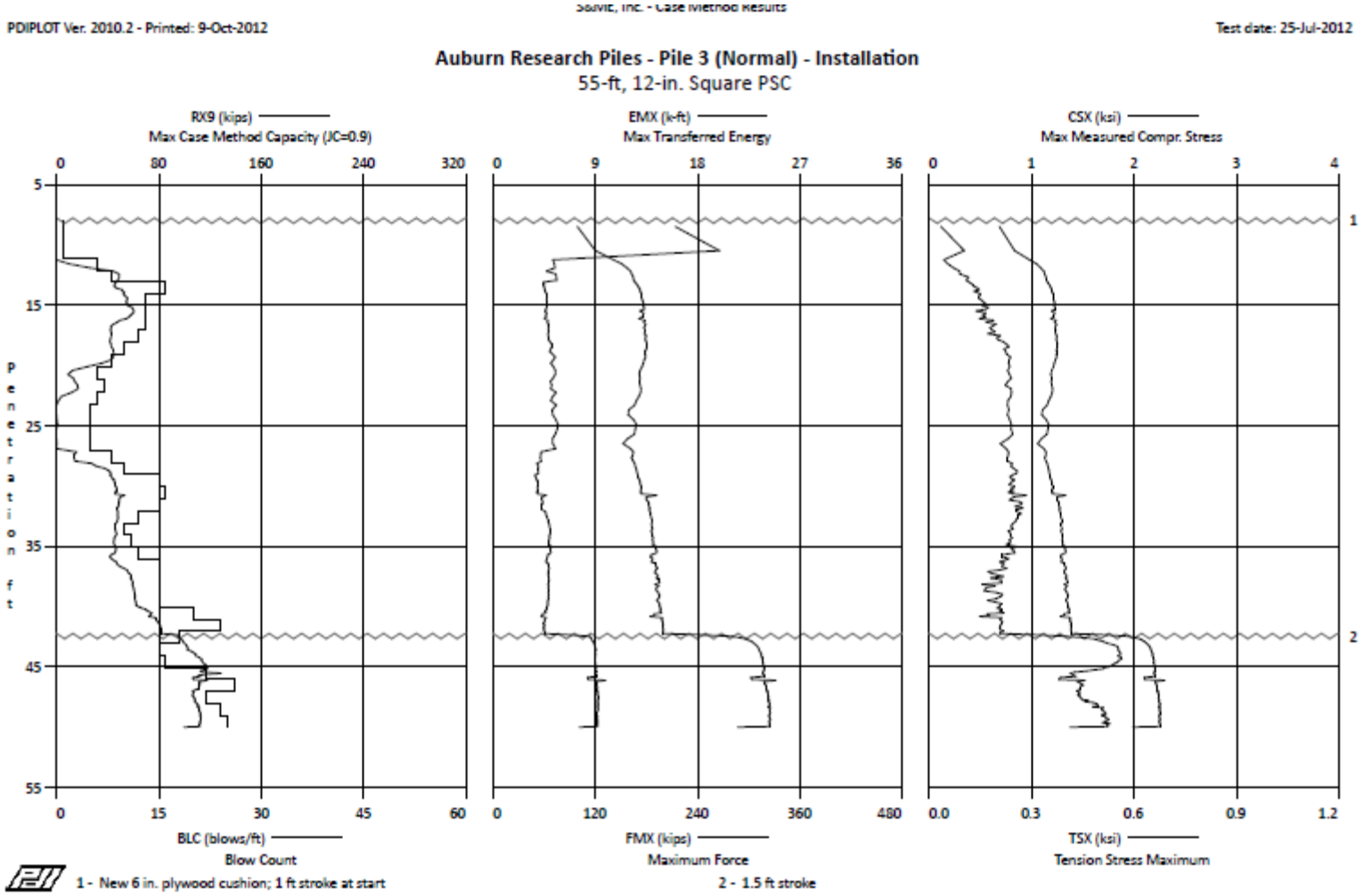
Saivis, Inc. - Case Method Results
PDIPLOT Ver. 2010.2 - Printed: 9-Oct-2012
Test date: 25-Jul-2012
Auburn Research Piles - Pile 3 (Normal) - Installation
55-ft, 12-in. Square PSC
RX9 (kips)
Max Case Method Capacity (JC=0.9)
EMX (k-ft)
Max Transferred Energy
CSX (ksi)
Max Measured Compr. Stress
Penetration ft
BLC (blows/ft)
Blow Count
FMX (kips)
Maximum Force
TSX (ksi)
Tension Stress Maximum
1 - New 6 in. plywood cushion; 1 ft stroke at start
2 - 1.5 ft stroke

Auburn Research Piles - Pile 3 (Normal) - Installation
OP: RHF
55-ft, 12-in. Square PSC
Test date: 25-Jul-2012

AR: 144.00 in^2
LE: 53.00 ft
WS: 13,250.0 f/s
SP: 0.150 k/ft3
EM: 5,684 ksi
JC: 0.90

RX9: Max Case Method Capacity (JC=0.9)
EMX: Max Transferred Energy
FMX: Maximum Force
VMX: Maximum Velocity
BPM: Blows per Minute
CSX: Max Measured Compr. Stress
TSX: Tension Stress Maximum
DFN: Final Displacement
FVP: Force/Velocity proportionality

BL# end	depth ft	BLC bl/ft	TYPE	RX9 kips	EMX k-ft	FMX kips	VMX f/s	BPM "	CSX ksi	TSX ksi	DFN in	FVP []
1	8.00	1	AV1	0	13.9	93	9.4	1.9	0.6	0.0	12.01	1.11
			MAX	0	13.9	93	9.4	1.9	0.6	0.0	12.01	1.11
2	9.00	1	AV1	0	18.2	105	9.2	12.6	0.7	0.0	12.01	1.03
			MAX	0	18.2	105	9.2	12.6	0.7	0.0	12.01	1.03
3	10.00	1	AV1	0	17.5	113	9.5	53.0	0.8	0.1	12.01	1.01
			MAX	0	17.5	113	9.5	53.0	0.8	0.1	12.01	1.02
4	11.00	1	AV1	0	22.3	128	9.2	52.2	0.9	0.1	12.01	1.01
			MAX	0	22.3	128	9.2	52.2	0.9	0.1	12.01	1.01
10	12.00	6	AV6	12	5.4	150	4.0	44.2	1.0	0.1	2.00	1.02
			MAX	30	5.5	158	4.1	49.6	1.1	0.1	2.00	1.02
18	13.00	8	AV8	47	5.4	163	4.0	102.1	1.1	0.1	1.50	1.02
			MAX	49	5.6	165	4.0	134.4	1.1	0.1	1.50	1.03
34	14.00	16	AV16	48	4.5	171	3.9	135.4	1.2	0.1	0.75	1.03
			MAX	55	4.7	174	3.9	137.0	1.2	0.1	0.75	1.03
47	15.00	13	AV13	54	4.7	175	4.0	136.6	1.2	0.2	0.92	1.03
			MAX	56	4.8	177	4.1	137.3	1.2	0.2	0.92	1.04
60	16.00	13	AV13	59	4.7	176	4.0	136.9	1.2	0.2	0.92	1.03
			MAX	61	4.8	178	4.1	138.7	1.2	0.2	0.92	1.03
73	17.00	13	AV13	46	4.8	177	4.1	134.4	1.2	0.2	0.92	1.03
			MAX	55	4.9	179	4.1	135.6	1.2	0.2	0.92	1.04
85	18.00	12	AV12	42	4.9	179	4.1	133.6	1.2	0.2	1.00	1.03
			MAX	44	5.0	180	4.2	134.2	1.3	0.2	1.00	1.04
95	19.00	10	AV10	44	5.1	180	4.2	131.4	1.2	0.2	1.20	1.03
			MAX	45	5.2	181	4.2	134.2	1.3	0.2	1.20	1.04
103	20.00	8	AV8	40	5.3	177	4.2	128.1	1.2	0.2	1.50	1.04
			MAX	45	5.5	179	4.2	128.9	1.2	0.2	1.50	1.05
109	21.00	6	AV6	13	5.5	172	4.2	131.1	1.2	0.2	2.00	1.04
			MAX	20	5.7	175	4.3	133.0	1.2	0.3	2.00	1.05
116	22.00	7	AV7	16	5.1	173	4.2	132.0	1.2	0.2	1.71	1.04
			MAX	18	5.2	174	4.3	133.0	1.2	0.3	1.71	1.04
122	23.00	6	AV6	6	5.3	171	4.3	133.6	1.2	0.2	2.00	1.04
			MAX	12	5.7	174	4.3	136.2	1.2	0.3	2.00	1.04
127	24.00	5	AV5	0	5.4	161	4.1	145.5	1.1	0.2	2.40	1.04
			MAX	0	5.7	168	4.3	152.9	1.2	0.2	2.40	1.04
132	25.00	5	AV5	0	5.6	165	4.2	142.5	1.1	0.2	2.40	1.04
			MAX	2	5.7	169	4.3	148.9	1.2	0.2	2.40	1.04
137	26.00	5	AV5	0	5.5	165	4.2	139.9	1.1	0.2	2.40	1.04
			MAX	0	5.7	168	4.3	145.5	1.2	0.3	2.40	1.04
142	27.00	5	AV5	0	5.4	156	4.0	147.6	1.1	0.2	2.40	1.03
			MAX	1	5.6	163	4.2	152.3	1.1	0.2	2.40	1.04
150	28.00	8	AV8	14	4.2	164	4.1	139.6	1.1	0.2	1.50	1.03
			MAX	17	4.3	166	4.3	140.7	1.2	0.2	1.50	1.03
160	29.00	10	AV10	36	4.0	168	4.2	133.8	1.2	0.2	1.20	1.03
			MAX	43	4.0	170	4.3	135.6	1.2	0.3	1.20	1.04
175	30.00	15	AV15	44	3.9	172	4.2	130.0	1.2	0.2	0.80	1.03
			MAX	47	4.0	174	4.3	132.3	1.2	0.3	0.80	1.04
191	31.00	16	AV16	48	4.1	177	4.3	125.7	1.2	0.2	0.75	1.03
			MAX	57	5.0	204	5.1	128.5	1.4	0.3	0.75	1.04
206	32.00	15	AV15	48	4.3	182	4.4	122.3	1.3	0.3	0.80	1.03
			MAX	50	4.4	184	4.4	123.1	1.3	0.3	0.80	1.04
218	33.00	12	AV12	48	4.7	185	4.5	122.7	1.3	0.3	1.00	1.03
			MAX	49	4.8	188	4.5	123.3	1.3	0.3	1.00	1.03

Auburn Research Piles - Pile 3 (Normal) - Installation
OP: RHF
55-ft, 12-in. Square PSC
Test date: 25-Jul-2012

BL# end	depth ft	BLC bl/ft	TYPE	RX9 kips	EMX k-ft	FMX kips	VMX f/s	BPM **	CSX ksi	TSX ksi	DFN in	FVP []
228	34.00	10	AV10	46	5.0	186	4.4	121.6	1.3	0.2	1.20	1.03
			MAX	48	5.1	188	4.4	125.3	1.3	0.3	1.20	1.03
239	35.00	11	AV11	45	5.0	188	4.4	123.9	1.3	0.2	1.09	1.03
			MAX	47	5.1	192	4.5	126.4	1.3	0.3	1.09	1.04
251	36.00	12	AV12	45	5.0	189	4.4	127.5	1.3	0.2	1.00	1.03
			MAX	47	5.2	193	4.5	130.9	1.3	0.3	1.00	1.04
266	37.00	15	AV15	49	4.8	190	4.4	129.3	1.3	0.2	0.80	1.03
			MAX	56	5.0	194	4.4	131.1	1.3	0.2	0.80	1.04
281	38.00	15	AV15	58	4.9	192	4.4	131.1	1.3	0.2	0.80	1.04
			MAX	60	5.0	195	4.4	131.9	1.4	0.2	0.80	1.04
296	39.00	15	AV15	60	4.9	193	4.3	131.4	1.3	0.2	0.80	1.04
			MAX	61	4.9	195	4.4	131.9	1.4	0.2	0.80	1.04
311	40.00	15	AV15	62	4.9	194	4.4	132.0	1.3	0.2	0.80	1.03
			MAX	63	4.9	196	4.4	132.6	1.4	0.2	0.80	1.04
331	41.00	20	AV20	72	4.6	194	4.3	133.7	1.3	0.2	0.60	1.03
			MAX	77	4.7	199	4.5	135.7	1.4	0.2	0.60	1.04
355	42.00	24	AV24	80	4.5	199	4.4	134.9	1.4	0.2	0.50	1.03
			MAX	82	4.6	200	4.4	136.5	1.4	0.2	0.50	1.04
373	43.00	18	AV18	93	7.3	263	5.8	99.0	1.8	0.4	0.67	1.02
			MAX	100	8.9	304	6.5	136.8	2.1	0.5	0.67	1.03
388	44.00	15	AV15	104	9.0	311	6.4	82.4	2.2	0.6	0.80	1.02
			MAX	109	9.1	315	6.5	82.7	2.2	0.6	0.80	1.03
404	45.00	16	AV16	114	9.0	316	6.4	83.1	2.2	0.5	0.75	1.03
			MAX	118	9.1	317	6.5	83.6	2.2	0.6	0.75	1.03
426	46.00	22	AV22	114	8.9	314	6.1	86.0	2.2	0.4	0.55	1.03
			MAX	130	9.1	318	6.3	91.7	2.2	0.5	0.55	1.03
452	47.00	26	AV26	111	9.1	319	6.1	85.0	2.2	0.4	0.46	1.03
			MAX	123	10.9	349	6.8	91.5	2.4	0.5	0.46	1.04
474	48.00	22	AV22	107	9.2	323	6.1	84.6	2.2	0.4	0.55	1.04
			MAX	109	9.3	324	6.1	84.9	2.3	0.5	0.55	1.04
498	49.00	24	AV24	111	9.2	324	6.1	84.1	2.3	0.5	0.50	1.04
			MAX	113	9.3	326	6.2	84.3	2.3	0.5	0.50	1.05
523	50.00	25	AV25	112	9.1	323	6.1	84.8	2.2	0.5	0.48	1.05
			MAX	113	9.2	326	6.2	96.2	2.3	0.5	0.48	1.05
			Average	66	6.2	223	4.9	114.8	1.5	0.3	0.99	1.03
			Maximum	130	22.3	349	9.5	152.9	2.4	0.6	12.01	1.11

Total number of blows analyzed: 523

BL#	depth (ft)	Comments
1	8.00	New 6 in. plywood cushion; 1 ft stroke at start
363	42.44	1.5 ft stroke

Time Summary

Drive 4 minutes 54 seconds 1:09:31 PM - 1:14:25 PM (7/25/2012) BN 1 - 523

S&ME, Inc. - Case Method Results

PDIPLOT Ver. 2010.2 - Printed: 9-Oct-2012

Test date: 26-Jul-2012

Auburn Research Piles - Pile 3 (Normal) - Restrike
55-ft, 12-in. Square PSC

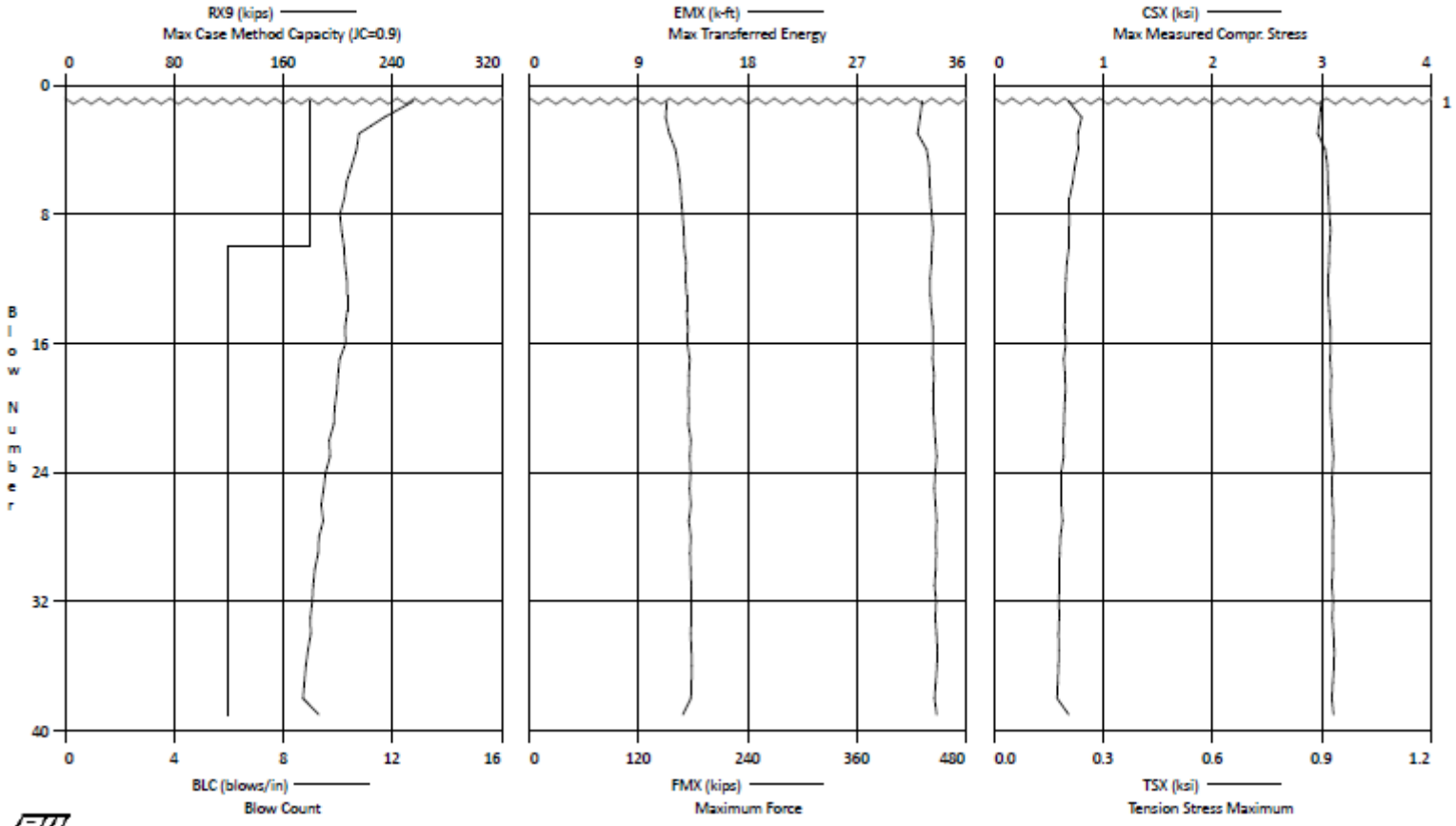

1 - Used 6 in. plywood cushion; 1.5 ft stroke during restrike

Auburn Research Piles - Pile 3 (Normal) - Restrike
55-ft, 12-in. Square PSC
OP: RHF
Test date: 26-Jul-2012

AR: 144.00 in^2
SP: 0.150 k/ft3
LE: 53.00 ft
EM: 5,684 ksi
WS: 13,250.0 f/s
JC: 0.90

RX9: Max Case Method Capacity (JC=0.9)
CSX: Max Measured Compr. Stress
EMX: Max Transferred Energy
TSX: Tension Stress Maximum
FMX: Maximum Force
DFN: Final Displacement
VMX: Maximum Velocity
FVP: Force/Velocity proportionality
BPM: Blows per Minute

BL#	depth ft	BLC bl/in	RX9 kips	EMX k-ft	FMX kips	VMX f/s	BPM ""	CSX ksi	TSX ksi	DFN in	FVP []
1	50.01	9	255	11.3	431	4.7	4.4	3.0	0.2	0.11	1.16
2	50.02	9	234	11.2	429	5.0	73.4	3.0	0.2	0.11	1.16
3	50.03	9	215	11.5	426	5.2	74.0	3.0	0.2	0.11	1.16
4	50.04	9	214	12.0	436	5.4	73.9	3.0	0.2	0.11	1.15
5	50.05	9	210	12.2	439	5.5	73.8	3.0	0.2	0.11	1.15
6	50.06	9	206	12.4	440	5.5	73.8	3.1	0.2	0.11	1.15
7	50.07	9	205	12.5	441	5.6	73.8	3.1	0.2	0.11	1.15
8	50.07	9	202	12.6	442	5.6	73.7	3.1	0.2	0.11	1.15
9	50.08	9	203	12.7	444	5.7	73.7	3.1	0.2	0.11	1.15
10	50.10	6	204	12.7	442	5.7	73.7	3.1	0.2	0.17	1.14
11	50.11	6	205	12.9	441	5.7	73.6	3.1	0.2	0.17	1.15
12	50.13	6	207	12.8	440	5.7	73.7	3.1	0.2	0.17	1.15
13	50.14	6	207	12.9	440	5.7	73.7	3.1	0.2	0.17	1.15
14	50.15	6	207	12.9	441	5.8	73.6	3.1	0.2	0.17	1.15
15	50.17	6	205	13.0	443	5.8	73.6	3.1	0.2	0.17	1.14
16	50.18	6	206	13.0	443	5.8	73.6	3.1	0.2	0.17	1.14
17	50.19	6	201	13.2	443	5.8	73.6	3.1	0.2	0.17	1.14
18	50.21	6	200	13.1	444	5.8	73.6	3.1	0.2	0.17	1.14
19	50.22	6	199	13.1	443	5.8	73.4	3.1	0.2	0.17	1.15
20	50.24	6	198	13.1	443	5.8	73.4	3.1	0.2	0.17	1.14
21	50.25	6	197	13.1	445	5.8	73.4	3.1	0.2	0.17	1.14
22	50.26	6	194	13.3	446	5.9	73.4	3.1	0.2	0.17	1.14
23	50.28	6	194	13.2	447	5.9	73.3	3.1	0.2	0.17	1.14
24	50.29	6	191	13.3	446	5.9	73.3	3.1	0.2	0.17	1.15
25	50.31	6	190	13.2	445	5.9	73.4	3.1	0.2	0.17	1.14
26	50.32	6	188	13.3	446	5.9	73.4	3.1	0.2	0.17	1.14
27	50.33	6	189	13.1	447	5.8	73.3	3.1	0.2	0.17	1.14
28	50.35	6	186	13.3	446	5.9	73.3	3.1	0.2	0.17	1.14
29	50.36	6	186	13.2	447	5.9	73.3	3.1	0.2	0.17	1.14
30	50.38	6	183	13.3	446	5.9	73.3	3.1	0.2	0.17	1.15
31	50.39	6	182	13.3	445	5.9	73.3	3.1	0.2	0.17	1.15
32	50.40	6	181	13.3	447	5.9	73.3	3.1	0.2	0.17	1.15
33	50.42	6	180	13.3	446	5.9	73.2	3.1	0.2	0.17	1.15
34	50.43	6	180	13.3	447	5.9	73.2	3.1	0.2	0.17	1.15
35	50.44	6	178	13.3	448	5.9	73.3	3.1	0.2	0.17	1.15
36	50.46	6	177	13.4	448	5.9	73.2	3.1	0.2	0.17	1.14
37	50.47	6	175	13.3	446	5.9	73.2	3.1	0.2	0.17	1.14
38	50.49	6	174	13.3	445	5.8	73.2	3.1	0.2	0.17	1.15
39	50.50	6	186	12.6	447	5.6	73.3	3.1	0.2	0.17	1.14
		Average	197	12.9	443	5.7	71.7	3.1	0.2	0.16	1.15
		Maximum	255	13.4	448	5.9	74.0	3.1	0.2	0.17	1.16

Total number of blows analyzed: 39

BL#	depth (ft)	Comments
1	50.01	Used 6 in. plywood cushion; 1.5 ft stroke during restrike

Time Summary

Drive 31 seconds 7:37:39 AM - 7:38:10 AM (7/26/2012) BN 1 - 39

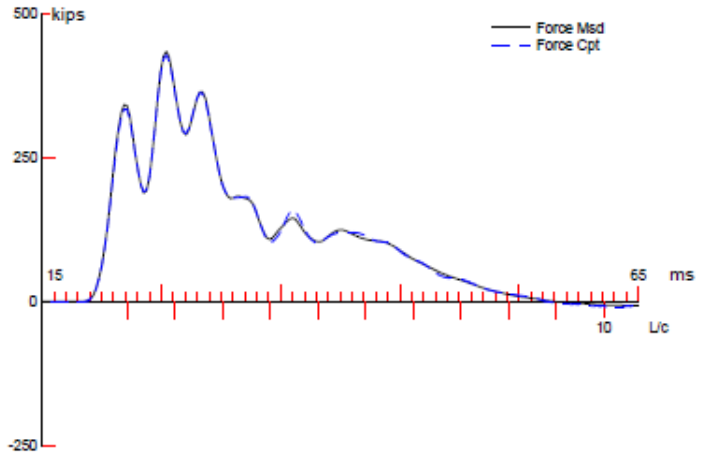
500
kips
250
0
-250
Force Msd
Force Cpt
15
65
ms
10
L/c

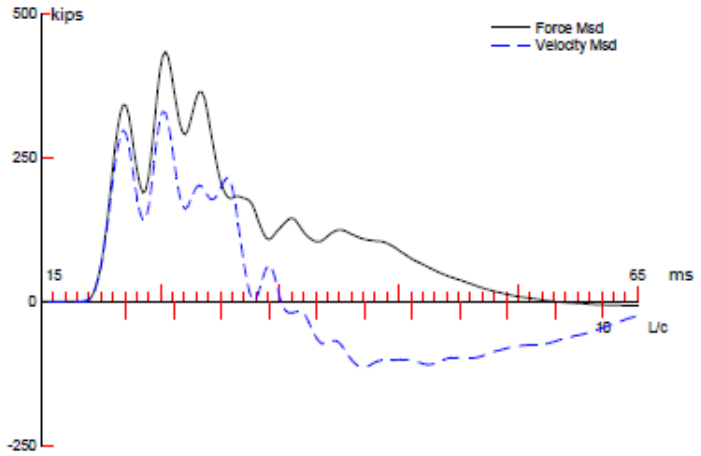
500
kips
250
0
-250
Force Msd
Velocity Msd
15
65
ms
48
L/c

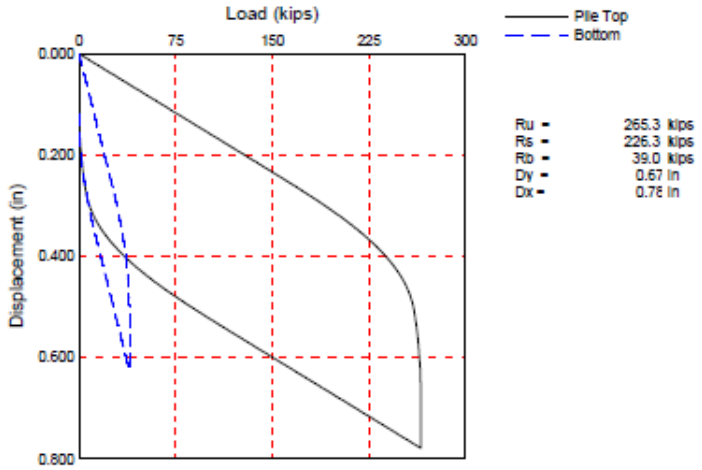
Load (kips)
0
75
150
225
300
0.000
0.200
0.400
0.600
0.800
Displacement (in)
Pile Top
Bottom
Ru = 265.3 kips
Rs = 226.3 kips
Rb = 39.0 kips
Dy = 0.67 in
Dx = 0.78 in

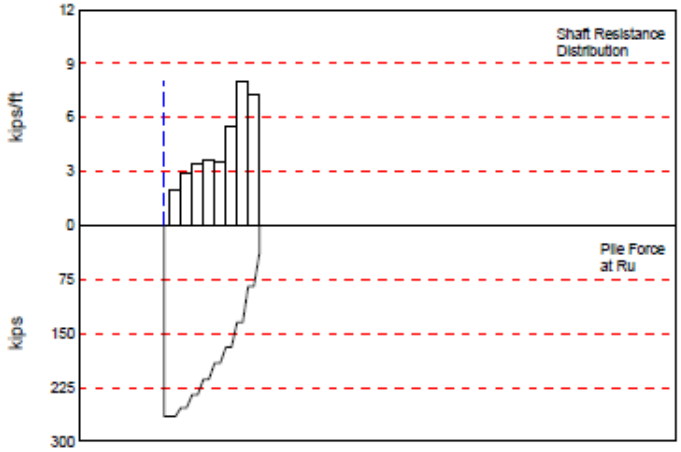
12
9
6
3
0
kips/ft
Shaft Resistance Distribution
75
150
225
300
kips
Pile Force at Ru

Auburn Research Piles; Pile: Pile 3 (Normal) - Restrike — Test: 26-Jul-2012 07:37:
55-ft, 12-in. Square PSC; Blow: 4 — CAPWAP(R) 2006-2
S&ME, Inc. — OP: RHF

CAPWAP SUMMARY RESULTS

Total CAPWAP Capacity: 265.3; along Shaft 226.3; at Toe 39.0 kips

Soil Sgmnt No.	Dist. Below Gages ft	Depth Below Grade ft	Ru kips	Force in Pile kips	Sum of Ru kips	Unit Resist. (Depth) kips/ft	Unit Resist. (Area) ksf	Smith Damping Factor s/ft
				265.3				
1	9.4	6.4	12.0	253.2	12.0	1.88	0.47	0.193
2	15.6	12.6	18.2	235.0	30.2	2.92	0.73	0.193
3	21.8	18.9	21.4	213.6	51.7	3.44	0.86	0.193
4	28.1	25.1	22.4	191.1	74.1	3.60	0.90	0.193
5	34.3	31.3	21.9	169.2	96.1	3.52	0.88	0.193
6	40.5	37.6	34.4	134.8	130.5	5.52	1.38	0.193
7	46.8	43.8	50.1	84.6	180.6	8.04	2.01	0.193
8	53.0	50.0	45.6	39.0	226.3	7.32	1.83	0.193
Avg. Shaft			28.3			4.52	1.13	0.193
Toe			39.0				39.00	0.171

Soil Model Parameters/Extensions		Shaft	Toe
Quake	(in)	0.283	0.396
Case Damping Factor		0.706	0.108
Damping Type			Smith
Unloading Quake	(% of loading quake)	120	33
Reloading Level	(% of Ru)	100	100
Unloading Level	(% of Ru)	49	
Resistance Gap (included in Toe Quake)	(in)		0.174
Soil Plug Weight	(kips)		0.28

CAPWAP match quality = 1.10 (Wave Up Match) ; RSA = 0
Observed: final set = 0.111 in; blow count = 108 b/ft
Computed: final set = 0.115 in; blow count = 104 b/ft

max. Top Comp. Stress = 3.03 ksi (T= 25.9 ms, max= 1.031 x Top)
max. Comp. Stress = 3.12 ksi (Z= 9.4 ft, T= 26.4 ms)
max. Tens. Stress = -0.23 ksi (Z= 49.9 ft, T= 27.5 ms)
max. Energy (EMX) = 12.0 kip-ft; max. Measured Top Displ. (DMX)= 0.50 in

EXTREMA TABLE

Pile Sgmnt No.	Dist. Below Gages ft	max. Force kips	min. Force kips	max. Comp. Stress ksi	max. Tens. Stress ksi	max. Trnsfd. Energy kip-ft	max. Veloc. ft/s	max. Displ. in
1	3.1	436.1	-10.4	3.03	-0.07	11.97	5.3	0.502
2	6.2	441.6	-12.0	3.07	-0.08	11.93	5.2	0.495
3	9.4	449.5	-13.8	3.12	-0.10	11.86	5.1	0.487
4	12.5	437.5	-12.2	3.04	-0.08	11.15	5.0	0.480
5	15.6	445.5	-13.9	3.09	-0.10	11.11	4.8	0.473
6	18.7	419.5	-11.2	2.91	-0.08	10.11	4.8	0.467
7	21.8	413.0	-12.6	2.87	-0.09	10.06	4.9	0.460
8	24.9	357.8	-9.7	2.48	-0.07	8.94	5.4	0.454
9	28.1	325.3	-10.9	2.26	-0.08	8.91	5.9	0.448
10	31.2	308.1	-8.4	2.14	-0.06	7.79	6.3	0.444
11	34.3	314.5	-9.7	2.18	-0.07	7.76	6.3	0.440
12	37.4	298.2	-8.6	2.07	-0.06	6.67	6.0	0.435
13	40.5	300.0	-10.0	2.08	-0.07	6.64	5.3	0.431
14	43.6	269.7	-23.1	1.87	-0.16	5.04	4.5	0.427
15	46.8	271.1	-11.0	1.88	-0.08	5.03	5.1	0.423
16	49.9	167.8	-33.2	1.17	-0.23	2.80	5.7	0.421
17	53.0	123.2	-6.9	0.86	-0.05	0.70	6.1	0.418
Absolute	9.4			3.12			(T =	26.4 ms)
	49.9				-0.23		(T =	27.5 ms)

CASE METHOD

J =	0.0	0.1	0.2	0.3	0.4	0.5	0.6	0.7	0.8	0.9
RP	79.3	84.7	90.1	95.6	101.0	106.4	111.8	117.2	122.6	128.1
RX	445.5	414.4	384.0	354.2	325.0	296.7	268.9	242.2	216.0	204.0
RU	333.6	302.6	271.6	240.5	209.5	178.5	147.4	116.4	85.4	54.4

RAU = 204.0 (kips); RA2 = 244.4 (kips)

Current CAPWAP Ru = 265.3 (kips); Corresponding J(RP)= 0.00; J(RX) = 0.61

VMX ft/s	TVP ms	VT1*E kips	FT1 kips	FMX kips	DMX in	DFN in	SET in	EMX kip-ft	QUS kips
5.40	22.35	12.1	13.0	436.2	0.502	0.113	0.111	12.0	469.8

PILE PROFILE AND PILE MODEL

Depth ft	Area in^2	E-Modulus ksi	Spec. Weight lb/ft^3	Perim. ft
0.00	144.00	5682.5	150.000	4.000
53.00	144.00	5682.5	150.000	4.000

Toe Area 1.000 ft^2

Auburn Research Piles; Pile: Pile 3 (Normal) - Restrike Test: 26-Jul-2012 07:37:
55-ft, 12-in. Square PSC; Blow: 4 CAPWAP(R) 2006-2
S&ME, Inc. OP: RHF

Segmnt Number	Dist. B.G. ft	Impedance kips/ft/s	Imped. Change %	Tension Slack in	Tension Eff.	Compression Slack in	Compression Eff.	Perim. ft	Soil Plug kips
1	3.12	61.77	0.00	0.000	0.000	-0.000	0.000	4.000	0.00
2	6.24	61.77	0.00	0.000	0.000	-0.000	0.000	4.000	0.05
17	53.00	61.77	0.00	0.000	0.000	-0.000	0.000	4.000	0.05

Pile Damping 2.0 %, Time Incr 0.235 ms, Wave Speed 13250.0 ft/s, 2L/c 8.0 ms

S&ME, Inc. - Case Method Results

PDIPLOT Ver. 2010.2 - Printed: 9-Oct-2012

Test date: 25-Jul-2012

Auburn Research Piles - Pile 4 (100% Replacement) - Installation

55-ft, 12-in. Square PSC

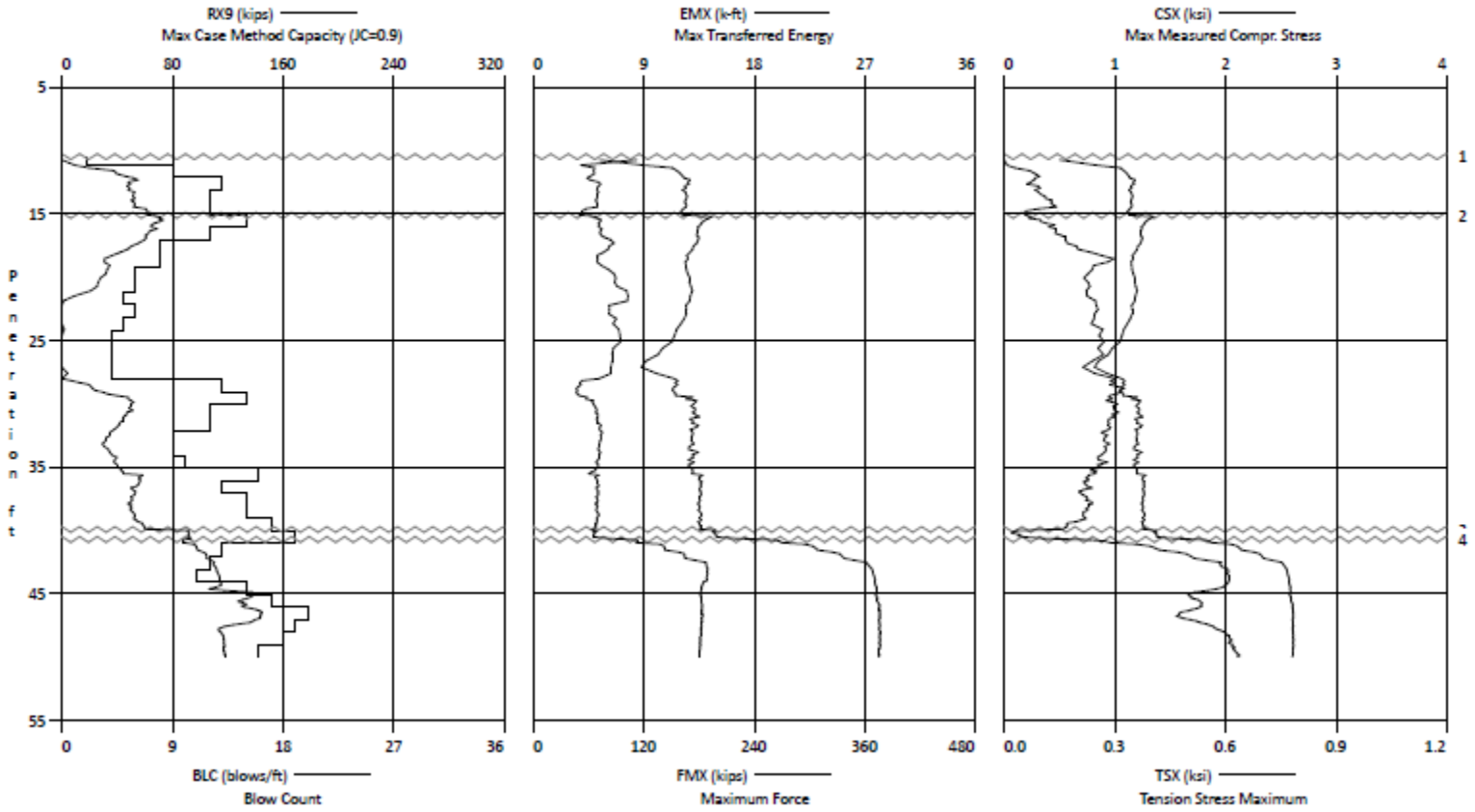

1 - New 6 in. plywood cushion; 1 ft stroke at start

2 - Force gage malfunctioning - no access to pile top to replace gage;

3 - Stopped to replace force gage.

4 - 1.5 ft stroke

Auburn Research Piles - Pile 4 (100% Replacement) - Installation
OP: RHF
55-ft, 12-in. Square PSC
Test date: 25-Jul-2012

AR: 144.00 in^2
LE: 53.00 ft
WS: 11,900.0 f/s
SP: 0.150 k/ft3
EM: 4,585 ksi
JC: 0.90

RX9: Max Case Method Capacity (JC=0.9)
EMX: Max Transferred Energy
FMX: Maximum Force
VMX: Maximum Velocity
BPM: Blows per Minute
CSX: Max Measured Compr. Stress
TSX: Tension Stress Maximum
DFN: Final Displacement
FVP: Force/Velocity proportionality

BL# end	depth ft	BLC bl/ft	TYPE	RX9 kips	EMX k-ft	FMX kips	VMX f/s	BPM ""	CSX ksi	TSX ksi	DFN in	FVP []
2	11.00	2	AV2	0	8.4	72	4.8	27.8	0.5	0.0	6.00	1.05
			MAX	0	9.1	86	4.9	53.6	0.6	0.0	6.00	1.09
11	12.00	9	AV9	28	4.7	148	4.1	45.3	1.0	0.1	1.33	1.04
			MAX	43	5.1	161	4.5	60.9	1.1	0.1	1.33	1.04
24	13.00	13	AV13	50	5.0	167	4.2	97.1	1.2	0.1	0.92	1.24
			MAX	56	5.5	170	4.3	138.2	1.2	0.1	0.92	1.34
36	14.00	12	AV12	51	5.2	165	4.2	138.2	1.1	0.1	1.00	1.29
			MAX	54	5.4	167	4.2	138.6	1.2	0.1	1.00	1.30
48	15.00	12	AV12	57	4.7	164	4.0	97.4	1.1	0.1	1.00	1.29
			MAX	63	5.4	168	4.3	138.1	1.2	0.2	1.00	1.30
63	16.00	15	AV15	68	5.1	183	4.3	100.6	1.3	0.1	0.80	1.28
			MAX	74	5.6	196	4.4	140.7	1.4	0.2	0.80	1.30
75	17.00	12	AV12	63	5.6	179	4.4	137.8	1.2	0.1	1.00	1.28
			MAX	71	5.9	181	4.5	140.0	1.3	0.2	1.00	1.30
83	18.00	8	AV8	51	6.3	175	4.5	134.4	1.2	0.2	1.50	1.27
			MAX	59	6.6	180	4.6	135.7	1.2	0.2	1.50	1.28
91	19.00	8	AV8	34	5.3	167	4.5	130.2	1.2	0.3	1.50	1.27
			MAX	41	5.7	169	4.6	133.3	1.2	0.3	1.50	1.29
97	20.00	6	AV6	31	6.3	167	4.5	130.4	1.2	0.2	2.00	1.29
			MAX	34	6.7	170	4.6	133.5	1.2	0.2	2.00	1.30
103	21.00	6	AV6	26	6.8	171	4.6	128.4	1.2	0.2	2.00	1.29
			MAX	27	7.1	172	4.6	128.6	1.2	0.2	2.00	1.30
108	22.00	5	AV5	7	7.8	171	4.6	127.8	1.2	0.2	2.40	1.28
			MAX	16	8.2	173	4.6	128.5	1.2	0.3	2.40	1.29
114	23.00	6	AV6	0	6.2	166	4.5	127.3	1.2	0.2	2.00	1.29
			MAX	0	6.4	167	4.6	128.8	1.2	0.3	2.00	1.30
119	24.00	5	AV5	0	6.6	161	4.4	137.7	1.1	0.2	2.40	1.28
			MAX	0	7.0	164	4.5	164.8	1.1	0.3	2.40	1.28
123	25.00	4	AV4	1	7.1	154	4.2	112.9	1.1	0.3	3.00	1.28
			MAX	3	7.3	155	4.5	142.9	1.1	0.3	3.00	1.37
127	26.00	4	AV4	0	6.6	141	4.0	154.8	1.0	0.3	3.00	1.22
			MAX	0	7.0	147	4.2	159.4	1.0	0.3	3.00	1.23
131	27.00	4	AV4	0	6.5	126	3.6	156.6	0.9	0.2	3.00	1.23
			MAX	0	6.7	137	3.9	160.6	1.0	0.3	3.00	1.24
135	28.00	4	AV4	2	6.4	133	3.8	154.1	0.9	0.2	3.00	1.23
			MAX	8	6.8	150	4.4	161.3	1.0	0.3	3.00	1.24
148	29.00	13	AV13	16	3.8	154	4.5	133.4	1.1	0.3	0.92	1.22
			MAX	25	4.1	159	4.6	140.5	1.1	0.3	0.92	1.25
163	30.00	15	AV15	43	4.2	165	4.7	126.2	1.1	0.3	0.80	1.20
			MAX	53	4.9	178	4.9	131.7	1.2	0.3	0.80	1.23
175	31.00	12	AV12	48	5.1	175	5.0	125.0	1.2	0.3	1.00	1.18
			MAX	51	5.3	181	5.0	125.5	1.3	0.3	1.00	1.19
187	32.00	12	AV12	42	5.3	175	4.9	124.3	1.2	0.3	1.00	1.18
			MAX	45	5.6	184	5.0	124.5	1.3	0.3	1.00	1.20
196	33.00	9	AV9	34	5.5	172	4.9	123.9	1.2	0.3	1.33	1.18
			MAX	36	5.7	174	4.9	125.3	1.2	0.3	1.33	1.21
205	34.00	9	AV9	32	5.4	173	4.9	122.5	1.2	0.3	1.33	1.18
			MAX	37	5.7	184	4.9	123.7	1.3	0.3	1.33	1.19
215	35.00	10	AV10	39	5.3	171	4.8	122.9	1.2	0.3	1.20	1.18
			MAX	42	5.5	181	4.9	124.1	1.3	0.3	1.20	1.19
231	36.00	16	AV16	49	5.0	176	4.7	118.7	1.2	0.2	0.75	1.18
			MAX	59	5.4	186	4.9	130.7	1.3	0.3	0.75	1.21

Auburn Research Piles - Pile 4 (100% Replacement) - Installation
OP: RHF

55-ft, 12-in. Square PSC
Test date: 25-Jul-2012

BL# end	depth ft	BLC bl/ft	TYPE	RX9 kips	EMX k-ft	FMX kips	VMX f/s	BPM ""	CSX ksi	TSX ksi	DFN in	FVP []
244	37.00	13	AV13	54	5.2	181	4.7	129.7	1.3	0.2	0.92	1.20
			MAX	57	5.5	185	4.7	131.6	1.3	0.2	0.92	1.22
259	38.00	15	AV15	51	5.2	180	4.6	130.1	1.3	0.2	0.80	1.20
			MAX	53	5.4	183	4.7	131.6	1.3	0.2	0.80	1.22
274	39.00	15	AV15	51	5.2	181	4.6	130.0	1.3	0.2	0.80	1.21
			MAX	55	5.4	185	4.7	131.7	1.3	0.2	0.80	1.22
291	40.00	17	AV17	59	5.1	182	4.6	122.9	1.3	0.2	0.71	1.19
			MAX	92	5.4	200	4.7	131.4	1.4	0.2	0.71	1.22
310	41.00	19	AV19	90	6.2	222	4.8	119.8	1.5	0.1	0.63	1.04
			MAX	96	8.5	269	5.9	138.4	1.9	0.3	0.63	1.04
323	42.00	13	AV13	99	11.2	314	6.9	71.3	2.2	0.4	0.92	1.04
			MAX	105	12.6	334	7.5	76.3	2.3	0.5	0.92	1.04
335	43.00	12	AV12	108	13.5	354	7.8	64.6	2.5	0.6	1.00	1.03
			MAX	111	14.2	367	8.1	69.4	2.5	0.6	1.00	1.04
346	44.00	11	AV11	113	14.2	369	8.1	62.1	2.6	0.6	1.09	1.03
			MAX	114	14.2	371	8.2	62.2	2.6	0.6	1.09	1.04
361	45.00	15	AV15	118	13.7	372	8.2	62.6	2.6	0.6	0.80	1.03
			MAX	139	13.8	373	8.2	63.3	2.6	0.6	0.80	1.04
378	46.00	17	AV17	133	13.7	374	8.1	63.3	2.6	0.5	0.71	1.04
			MAX	138	13.8	376	8.2	63.7	2.6	0.5	0.71	1.04
398	47.00	20	AV20	141	13.7	376	8.1	63.6	2.6	0.5	0.60	1.04
			MAX	145	13.8	377	8.1	63.8	2.6	0.5	0.60	1.04
417	48.00	19	AV19	124	13.7	375	8.1	63.2	2.6	0.6	0.63	1.04
			MAX	140	13.8	377	8.2	63.6	2.6	0.6	0.63	1.04
435	49.00	18	AV18	117	13.6	376	8.2	62.9	2.6	0.6	0.67	1.04
			MAX	117	13.7	377	8.2	63.0	2.6	0.6	0.67	1.04
451	50.00	16	AV16	117	13.5	376	8.1	62.8	2.6	0.6	0.75	1.04
			MAX	118	13.6	377	8.2	62.9	2.6	0.6	0.75	1.04
			Average	68	7.9	233	5.6	103.6	1.6	0.3	1.06	1.16
			Maximum	145	14.2	377	8.2	164.8	2.6	0.6	6.00	1.37

Total number of blows analyzed: 451

BL#	depth (ft)	Comments
1	10.50	New 6 in. plywood cushion; 1 ft stroke at start
50	15.13	Force gage malfunctioning - no access to pile top to replace gage;
290	39.94	Stopped to replace force gage.
305	40.74	1.5 ft stroke

Time Summary

Drive 19 minutes 43 seconds 1:36:03 PM - 1:55:46 PM (7/25/2012) BN 1 - 451

S&ME, Inc. - Case Method Results

PDIPLOT Ver. 2010.2 - Printed: 9-Oct-2012

Test date: 26-Jul-2012

Auburn Research Piles - Pile 4 (100% Replacement) - Restrike

55-ft, 12-in. Square PSC

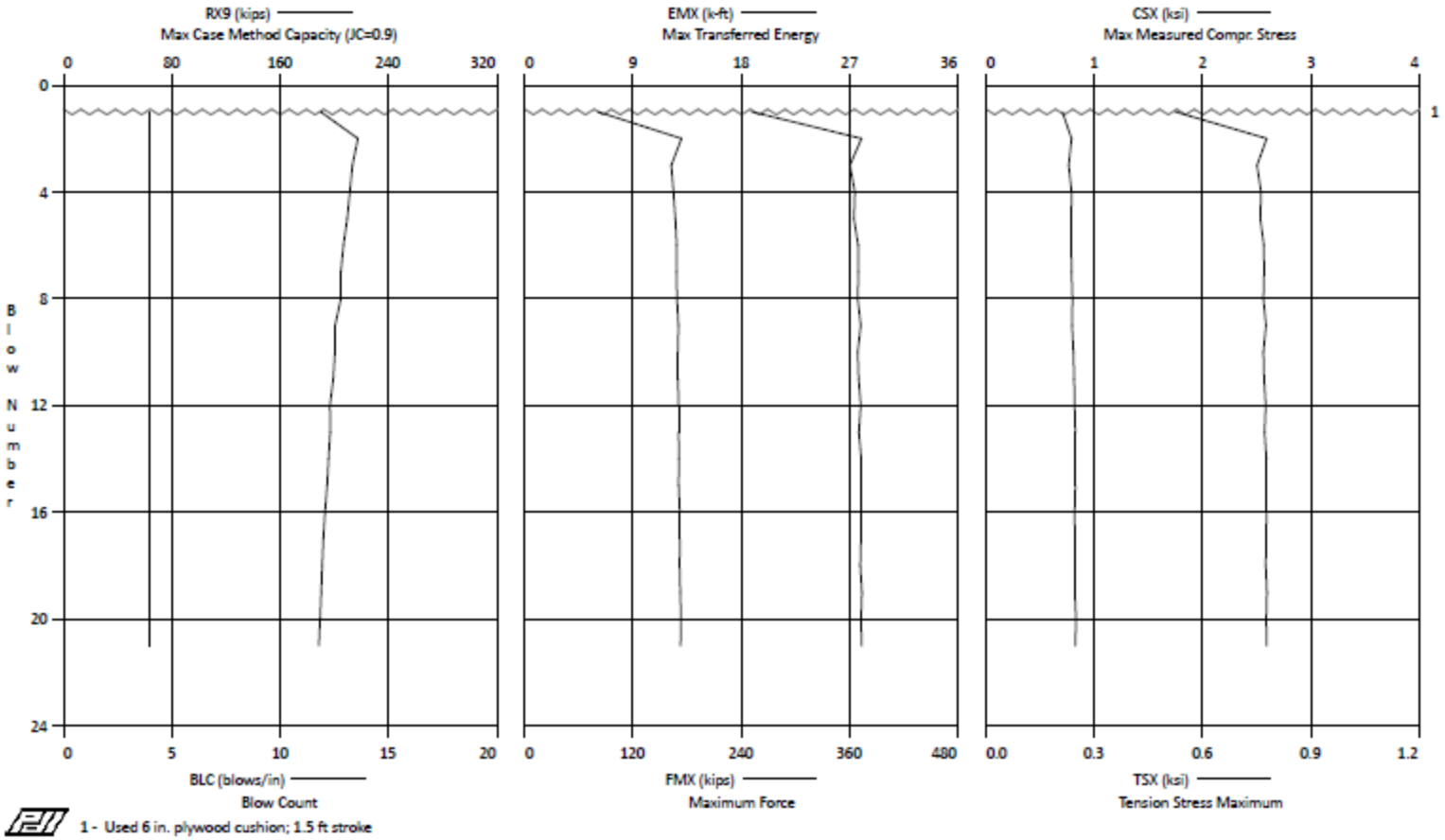

1 - Used 6 in. plywood cushion; 1.5 ft stroke

Case Method Results PDIPLOT Ver. 2010.2 - Printed: 9-Oct-2012

Auburn Research Piles - Pile 4 (100% Replacement) - Restrike 55-ft, 12-in. Square PSC
OP: RHF Test date: 26-Jul-2012

AR: 144.00 in^2 SP: 0.150 k/ft3
LE: 53.00 ft EM: 4,470 ksi
WS: 11,750.0 f/s JC: 0.90

RX9: Max Case Method Capacity (JC=0.9)
EMX: Max Transferred Energy
FMX: Maximum Force
VMX: Maximum Velocity
BPM: Blows per Minute
CSX: Max Measured Compr. Stress
TSX: Tension Stress Maximum
DFN: Final Displacement
FVP: Force/Velocity proportionality

BL#	depth ft	BLC bl/in	RX9 kips	EMX k-ft	FMX kips	VMX f/s	BPM **	CSX ksi	TSX ksi	DFN in	FVP []
1	50.02	4	190	6.1	252	3.8	1.9	1.7	0.2	0.24	1.03
2	50.04	4	217	13.0	373	6.2	13.0	2.6	0.2	0.25	1.02
3	50.06	4	213	12.2	360	5.9	73.2	2.5	0.2	0.25	1.02
4	50.08	4	211	12.3	366	6.0	73.0	2.5	0.2	0.25	1.02
5	50.10	4	209	12.5	365	6.0	72.9	2.5	0.2	0.25	1.02
6	50.13	4	207	12.6	369	6.1	72.8	2.6	0.2	0.25	1.02
7	50.15	4	205	12.6	370	6.1	72.8	2.6	0.2	0.25	1.02
8	50.17	4	205	12.6	369	6.1	72.7	2.6	0.2	0.25	1.02
9	50.19	4	201	12.8	372	6.2	72.6	2.6	0.2	0.25	1.02
10	50.21	4	201	12.7	369	6.1	72.6	2.6	0.2	0.25	1.03
11	50.23	4	199	12.7	370	6.2	72.6	2.6	0.2	0.25	1.03
12	50.25	4	197	12.8	372	6.2	72.6	2.6	0.2	0.25	1.02
13	50.27	4	197	12.8	370	6.2	72.6	2.6	0.2	0.25	1.03
14	50.29	4	196	12.8	373	6.2	72.6	2.6	0.2	0.25	1.02
15	50.31	4	195	12.8	373	6.2	72.4	2.6	0.2	0.25	1.02
16	50.33	4	193	12.9	372	6.2	72.5	2.6	0.2	0.25	1.02
17	50.35	4	192	12.9	372	6.2	72.6	2.6	0.2	0.25	1.02
18	50.38	4	191	12.9	372	6.2	72.5	2.6	0.2	0.25	1.02
19	50.40	4	190	12.9	373	6.2	72.6	2.6	0.2	0.25	1.02
20	50.42	4	189	13.0	372	6.2	72.4	2.6	0.2	0.25	1.03
21	50.44	4	189	12.9	373	6.2	72.4	2.6	0.2	0.25	1.02
		Average	199	12.4	365	6.0	66.4	2.5	0.2	0.25	1.02
		Maximum	217	13.0	373	6.2	73.2	2.6	0.2	0.25	1.03

Total number of blows analyzed: 21

BL#	depth (ft)	Comments
1	50.02	Used 6 in. plywood cushion; 1.5 ft stroke

Time Summary

Drive 20 seconds 7:28:56 AM - 7:29:16 AM (7/26/2012) BN 1 - 21

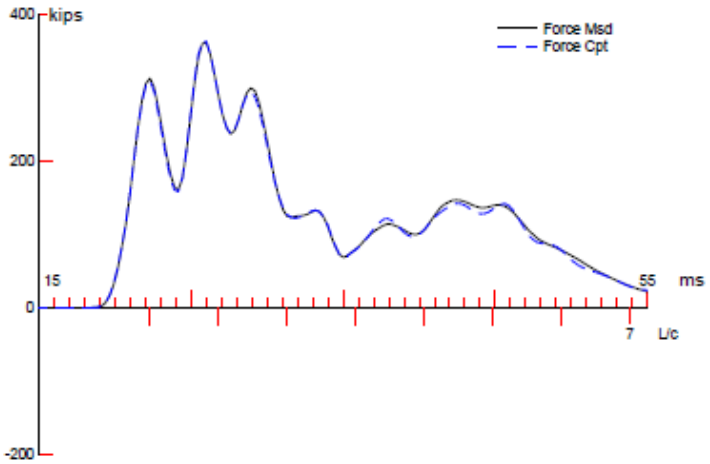
400
kips
200
0
-200
15
55
ms
7
L/c
Force Msd
Force Cpt

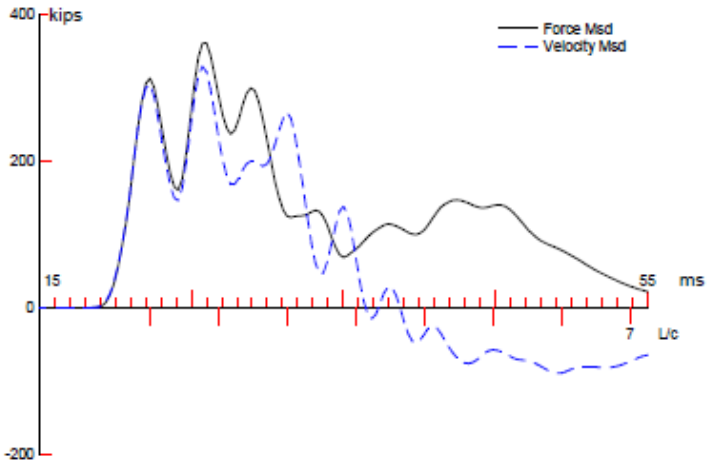
400
kips
200
0
-200
15
55
ms
7
L/c
Force Msd
Velocity Msd

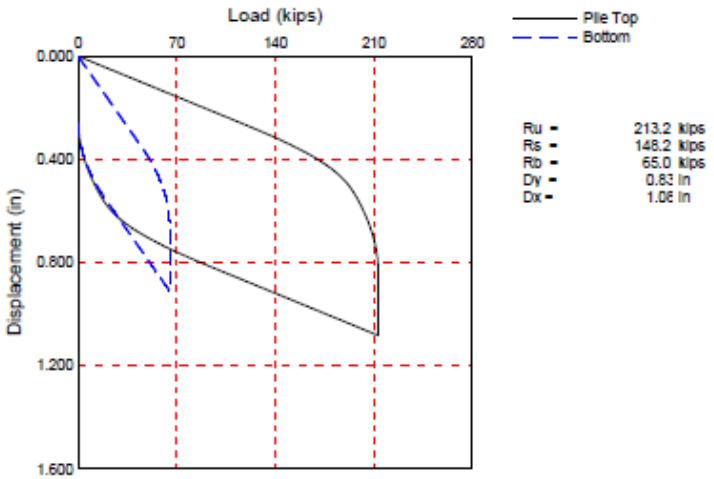
Load (kips)
0
70
140
210
280
0.000
0.400
0.800
1.200
1.600
Displacement (in)
Pile Top
Bottom
Ru = 213.2 kips
Rs = 148.2 kips
Rb = 65.0 kips
Dy = 0.83 in
Dx = 1.06 in

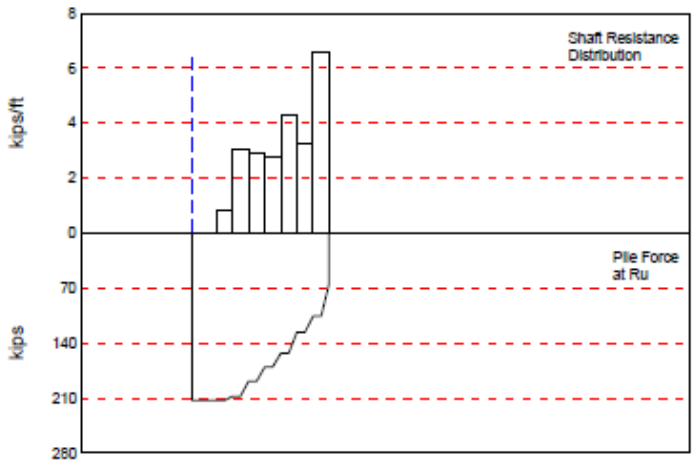
8
6
4
2
0
kips/ft
Shaft Resistance Distribution
70
140
210
280
kips
Pile Force at Ru

Auburn Research Piles; Pile: Pile 4 (100% Replacement) - RestrikeTest: 26-Jul-2012 07:29:
55-ft, 12-in. Square PSC; Blow: 5 CAPWAP(R) 2006-2
S&MB, Inc. OP: RHF

CAPWAP SUMMARY RESULTS

Total CAPWAP Capacity: 213.2; along Shaft 148.2; at Toe 65.0 kips

Soil Sgmnt No.	Dist. Below Gages ft	Depth Below Grade ft	Ru kips	Force in Pile kips	Sum of Ru kips	Unit Resist. (Depth) kips/ft	Unit Resist. (Area) ksf	Smith Damping Factor s/ft
				213.2				
1	9.4	6.5	0.0	213.2	0.0	0.00	0.00	0.000
2	15.6	12.7	5.2	207.9	5.2	0.84	0.21	0.186
3	21.8	18.9	19.2	188.7	24.4	3.08	0.77	0.186
4	28.1	25.2	18.2	170.5	42.6	2.92	0.73	0.186
5	34.3	31.4	17.5	153.0	60.1	2.80	0.70	0.186
6	40.5	37.6	26.9	126.1	87.0	4.32	1.08	0.186
7	46.8	43.9	20.2	105.9	107.2	3.24	0.81	0.186
8	53.0	50.1	40.9	65.0	148.2	6.56	1.64	0.186
Avg. Shaft			18.5			2.96	0.74	0.186
Toe			65.0				65.00	0.102

Soil Model Parameters/Extensions		Shaft	Toe
Quake	(in)	0.295	0.507
Case Damping Factor		0.502	0.120
Damping Type			Smith
Unloading Quake	(% of loading quake)	100	47
Reloading Level	(% of Ru)	100	100
Unloading Level	(% of Ru)	12	
Resistance Gap (included in Toe Quake)	(in)		0.298
Soil Plug Weight	(kips)		0.15

CAPWAP match quality = 1.86 (Wave Up Match) ; RSA = 0
Observed: final set = 0.250 in; blow count = 48 b/ft
Computed: final set = 0.271 in; blow count = 44 b/ft

max. Top Comp. Stress = 2.56 ksi (T= 26.3 ms, max= 1.050 x Top)
max. Comp. Stress = 2.69 ksi (Z= 15.6 ft, T= 27.3 ms)
max. Tens. Stress = -0.30 ksi (Z= 43.6 ft, T= 28.1 ms)
max. Energy (EMX) = 12.4 kip-ft; max. Measured Top Displ. (DMX)= 0.67 in

EXTREMA TABLE

Pile Sgmnt No.	Dist. Below Gages ft	max. Force kips	min. Force kips	max. Comp. Stress ksi	max. Tens. Stress ksi	max. Trnsfd. Energy kip-ft	max. Veloc. ft/s	max. Displ. in
1	3.1	368.2	-16.6	2.56	-0.12	12.44	5.9	0.664
2	6.2	372.2	-17.8	2.58	-0.12	12.40	5.8	0.656
3	9.4	376.7	-18.9	2.62	-0.13	12.36	5.7	0.649
4	12.5	382.6	-19.9	2.66	-0.14	12.33	5.8	0.643
5	15.6	386.8	-21.1	2.69	-0.15	12.30	5.8	0.636
6	18.7	377.1	-21.2	2.62	-0.15	11.85	5.5	0.630
7	21.8	365.5	-22.3	2.54	-0.16	11.80	5.8	0.622
8	24.9	305.2	-19.5	2.12	-0.14	10.29	6.4	0.615
9	28.1	310.5	-20.9	2.16	-0.14	10.25	7.1	0.608
10	31.2	294.8	-18.1	2.05	-0.13	8.83	7.5	0.601
11	34.3	300.2	-19.1	2.08	-0.13	8.79	7.5	0.594
12	37.4	282.1	-16.3	1.96	-0.11	7.45	7.0	0.587
13	40.5	272.5	-17.1	1.89	-0.12	7.40	6.1	0.579
14	43.6	226.1	-43.4	1.57	-0.30	5.47	5.6	0.573
15	46.8	220.5	-21.3	1.53	-0.15	5.45	6.4	0.568
16	49.9	149.5	-9.2	1.04	-0.06	4.01	7.1	0.564
17	53.0	134.6	-9.7	0.93	-0.07	1.06	7.5	0.558
Absolute	15.6			2.69			(T =	27.3 ms)
	43.6				-0.30		(T =	28.1 ms)

CASE METHOD

J =	0.0	0.1	0.2	0.3	0.4	0.5	0.6	0.7	0.8	0.9
RP	241.6	203.8	166.1	128.3	90.6	52.8	15.0	0.0	0.0	0.0
RX	318.5	282.6	252.1	233.5	221.4	209.2	206.9	206.9	206.9	206.9
RU	241.6	203.8	166.1	128.3	90.6	52.8	15.0	0.0	0.0	0.0

RAU = 200.0 (kips); RA2 = 208.8 (kips)

Current CAPWAP Ru = 213.2 (kips); Corresponding J(RP)= 0.08; J(RX) = 0.47

VMX ft/s	TVP ms	VT1*E kips	FT1 kips	FMX kips	DMX in	DFN in	SET in	EMX kip-ft	QUS kips
6.04	22.55	306.5	312.8	364.7	0.669	0.250	0.250	12.5	326.5

Auburn Research Piles; Pile: Pile 4 (100% Replacement) - RestrikeTest: 26-Jul-2012 07:29:
55-ft, 12-in. Square PSC; Blow: 5 CAPWAP(R) 2006-2
S&ME, Inc. OP: RHF

PILE PROFILE AND PILE MODEL

Depth ft	Area in^2	E-Modulus ksi	Spec. Weight lb/ft^3	Perim. ft
0.00	144.00	4468.7	150.000	4.000
53.00	144.00	4468.7	150.000	4.000

Toe Area 1.000 ft^2

Top Segment Length 3.12 ft, Top Impedance 54.78 kips/ft/s

Pile Damping 2.0 %, Time Incr 0.265 ms, Wave Speed 11750.0 ft/s, 2L/c 9.0 ms

APPENDIX I: 2002 CGES FB-DEEP PILE CAPACITY

Florida Bridge Software Institute Date: August 08, 2012
Shaft and Pile Analysis (FB-Deep v.2.02) Time: 11:03:18

General Information:
==========
Input file: .....AUBURN\Documents\Dissertation\Charleston\CGES\Models\CGES.spc
Project number:
Job name:
Engineer:
Units: English

Analysis Information:
==========
Analysis Type: SPT

Soil Information:
==========
Boring date: , Boring Number:
Station number: Offset:

Ground Elevation: 0.000(ft)

Hammer type: Safety Hammer

ID	Depth (ft)	No. of Blows (Blows/ft)	Soil Type
1	0.00	11.00	2- Clay and silty sand
2	2.00	34.00	2- Clay and silty sand
3	5.00	14.00	2- Clay and silty sand
4	7.00	1.00	1- Plastic Clay
5	10.00	1.00	1- Plastic Clay
6	15.00	8.00	1- Plastic Clay
7	20.00	17.00	2- Clay and silty sand

8	25.00	11.00	1- Plastic Clay
9	30.00	27.00	2- Clay and silty sand
10	35.00	26.00	2- Clay and silty sand
11	65.00	26.00	2- Clay and silty sand

PILE INFORMATION (Pile Length = 40.00 (ft))

Section Type: Square, Width = 12.00(in)
Length = 40.00(ft), Tip Elevation = -40.00(ft)
Unit Weight of Pile = 126.00(pcf), Weight of pile = 2.52(tons)

Skin friction capacity

Soil Layer Num.	Bottom Elev. (ft)	Average SPT Blows (Blows/ft)	Ult. Skin Friction (Tons)	Thick. (ft)	Soil Type
1	-7.00	18.86	19.04	7.00	2- Clay and silty sand
2	-20.00	6.77	15.05	13.00	1- Plastic Clay
3	-25.00	14.00	12.33	5.00	2- Clay and silty sand
4	-30.00	19.00	15.22	5.00	1- Plastic Clay
5	-65.00	26.07	0.00	35.00	2- Clay and silty sand

(* IN LAYERS ABOVE BEARING LAYER)

Ultimate skin friction in layers above bearing layer = 61.64(tons)
Average SPT in Bearing layer above tip = 26.25(blow/ft)
Ultimate skin friction in bearing layer = 38.37(tons)
Corrected Ultimate skin friction in bearing layer = 37.00(tons)
Total Skin Friction = 98.64(tons)

End bearing capacity

ELEVATION (ft)	SPT Blows (Blows/ft)	UNIT E. B. (tsf)	
-32.00	26.60	14.19	<-- 8B above pile tip
-35.00	26.00	13.87	
-40.00	26.00	13.87	<-- Pile tip elevation
-43.50	26.00	13.87	<-- 3.5B below pile tip

Average unit end bearing above pile tip = 13.93(tsf)
Average unit end bearing below pile tip = 13.87(tsf)
Average unit end bearing in vicinity of pile tip = 13.90(tsf)

Critical depth of embedment in bearing layer = 4.00(ft)

Actual depth of embedment = 10.00(ft)

Maximum mobilized end bearing capacity = 13.90(tons)
Corrected mobilized end bearing capacity = 13.90(tons)

Pile Capacity

Estimated Davisson capacity = 112.54(tons)
Allowable pile capacity = 56.27(tons)
Ultimate pile capacity = 140.33(tons)